An Adaptive Modeling and Simulation Environment for Combined-Cycle Data Reconciliation and Degradation Estimation

A Thesis
Presented to
The Academic Faculty

by

TsungPo Lin

In Partial Fulfillment
of the Requirements for the Degree
Doctor of Philosophy

Aerospace Engineering
Georgia Institute of Technology
August 2008

An Adaptive Modeling and Simulation Environment for Combined-Cycle Data Reconciliation and Degradation Estimation

Approved by:

Dr. Dimitri Mavris, Advisor
School of Aerospace Engineering
Georgia Institute of Technology

Dr. Hongmei Chen
School of Aerospace Engineering
Georgia Institute of Technology

Dr. Vitali Volovoi
School of Aerospace Engineering
Georgia Institute of Technology

Mr. Mark Waters
School of Aerospace Engineering
California Polytechnic State University

Mr. Erwing Calleros
EED ESE Gas Apps CC Performance
GE Energy

Date Approved: June 2008

ACKNOWLEDGEMENTS

This research work would not have been accomplished without the support and help from others. Above all others, I would like to thank my advisor, Dr. Dimitri Mavris, for his confidence, encouragement and support throughout my thesis work. I also must thank him for giving me the opportunity of being exposed to many research projects where I had learned tremendous knowledge and skills to achieve this task.

My advisory committee, including Mr. Erwing Calleros, Dr. Hongmei Chen, Dr. Vitali Volovoi, and Mr. Mark Waters, provided many useful suggestions which enhanced the quality of this work. Erwing has been mentoring me many invaluable knowledge about combined cycle modeling and simulation, and helping me to consolidate the thesis work. Mark has being sharing his invaluable experience in power generation with me and helped tremendously in my thesis editing. Dr. Hongmei and Dr. Vitali also provided invaluable suggestions, feedback, and guidance. Funding supplied by GE and ASDL helped make the research possible.

Finally, I would like to express my deepest gratitude to my parents and my younger brother, for their understanding and patience during the span of this work. Without the support and encouragement from them, I would not have come such a long way. Of course, they may be even happier to see this day coming than anybody. Also, I would like to thank Ana Sierra, who came into my life at just the right time to support me and enrich my life.

TABLE OF CONTENTS

Page

LIST OF TABLES

LIST OF FIGURES

NOMENCLATURE

$\dot{Q}$: Heat Transfer

$\dot{m}$: Mass flow rate

$\dot{W}$: Shaft Power

σ : Standard Deviation

χ^2 : The value of Least Squares Function

ε: Heat or mass balance error.

h: Enthalpy

DP: Pressure Drop

HP: High Pressure

HPEC1: 1st High Pressure Economizer

HPEC2: 2nd High Pressure Economizer

HPEVP: High Pressure Evaporator

HPSHT: High Pressure Superheater

HRSG: Heat Recovery Steam Generator

HTC: Heat Transfer Correction

LP: Low Pressure

LPEC: Low Pressure Economizer

LPEVP: Low Pressure Evaporator

LPSHT: Low Pressure Superheater

M&S: Modeling and Simulation

NLP: Nonlinear Programming

N&C: New and Clean

O&M: Operation and Maintain

P: Pressure

p: Probability

SDRMC: Simultaneous Data Reconciliation and Model Calibration

T: Temperature

U: Measurement Uncertainty

Subscripts

evp: evaporator

fdw: feed water

g/gi/go: gas/inlet gas/outlet gas

i, j: measured parameter index

s/si/so: steam/inlet steam/outlet steam

sat: saturation

sph: superheater

Superscripts

*: reconciled valu

SUMMARY

Performance engineers face the major challenge in modeling and simulation for the after-market power system due to the fact the system has undergone some degradation and estimating degradation is based on the data that are subject to measurement errors. They often have to rely on the data from the on-site monitoring system, which usually have larger uncertainties and more biases than the data from precision test, to carry out model calibration and performance simulation. Currently, the majority in power generation industries utilizes the deterministic data matching method to calibrate the model and cascade system degradation, which causes significant calibration uncertainty and also the risk when providing performance guarantees. In this research work, a maximum-likelihood based simultaneous data reconciliation and model calibration (SDRMC) is used for power system modeling and simulation. By replacing the current deterministic data matching with SDRMC one can reduce the calibration uncertainty and mitigate the error propagation to the performance simulation.

A modeling and simulation environment for a complex power system with certain degradation has been developed. In this environment multiple data sets are imported when carrying out simultaneous data reconciliation and model calibration. Calibration uncertainties are estimated through error analyses and populated to performance simulation by using principle of error propagation. System degradation is then quantified by performance comparison between the calibrated model and its expected new & clean status.

To mitigate smearing effects caused by gross errors, gross error detection (GED) is carried out in two stages. The first stage is a screening stage, in which serious gross errors are eliminated in advance. The GED techniques used in the screening stage are based on multivariate data analysis (MDA), including multivariate data visualization and

principal component analysis (PCA). Subtle gross errors are treated at the second stage, in which the serial bias compensation or robust M-estimator is engaged. To achieve a better efficiency in the combined scheme of the least squares based data reconciliation and the GED technique based on hypotheses testing, the Levenberg-Marquardt (LM) algorithm is utilized as the optimizer.

To reduce the computation time and stabilize the problem solving for a complex power system such as a combined cycle power plant, meta-modeling using the response surface equation (RSE) and system/process decomposition are incorporated with the simultaneous scheme of SDRMC. The goal of this research work is to reduce the calibration uncertainties and, thus, the risks of providing performance guarantees arisen from uncertainties in performance simulation.

CHAPTER 1

COMBINED CYCLE PERFORMANCE EVALUATION

1.1. Introduction

The major change in the global electricity power market from regulated to deregulated has brought drastic competition among power suppliers. The objective of deregulation in the electric power market was to introduce competition and reduce the price of electricity. Competition in the electricity market has also driven major changes in power generation industry and led to two facts: the fact that power plant operations depend on demand and market prices; and that power demand and market prices have been changing rapidly in the past decades. To be more adaptive in the rapidly changed market, power systems that have the capability of operating at a wide range of output levels with high efficiency are more favored.

The combined cycle power system utilizes the Brayton Cycle (gas turbine) and the Rankine Cycle (heat recovery steam generator -- HRSG and steam turbine), with air and water as working fluids, respectively. The combined cycle power plant has been proven to generate efficient, reliable, and economic power. It provides many aspects of flexibility that satisfies both utility-power generation and industrial-cogeneration applications. A plant thermal efficiency in the range of 50~55% LHV has been achieved by a typical combined cycle system commercially available in the industry. Additional developments in the high-temperature material and surface cooling technologies for the gas turbine hot gas path will enable combined cycle systems to reach a plant thermal efficiency of 60% or greater in the near future. In addition, with the small capacity increments of gas turbine generators designed and manufactured in discrete frame sizes, the gas turbine product line can cover an output range of approximately 37 MW to 250

MW. These gas turbine products with a wide range of output levels can then be applied to combined cycle systems with single or multiple trains of HRSGs and provide from 50 MW to several thousand megawatts of power at constant plant thermal efficiencies.

These favored features such as high thermal efficiency and the wide range of output levels has lead to a rapid growth in the use of gas turbine based combine cycle systems. In general, combined cycle systems provide operational flexibilities and have the following features: high thermal efficiency, low installed cost, fuel flexibility, flexible duty cycle, short-installation cycle, high reliability/availability, and low overhaul and maintenance O&M costs, which make them more adaptive than other power plant systems in the rapidly changing power market.

1.2. Status of Plant Degradation

Features such as high efficiency, low maintenance cost, and good availability make the combined cycle power systems strong competitors in the dynamic electric market. To remain competitively strong, plant availability plays an important role in lowering the O&M cost. Reducing the plant outage period is one of the ways to yield improved availability. Prior knowledge about the plant degradation status can facilitate the layout of maintenance plans before the outage, and, thus, reduce the downtime. It is, therefore, important to identify the current plant status and understand how the plant performance changes as plant components are degraded.

By using an on-line monitoring system, plant performance and flow parameters are measured and data are sent to the control room for inspection. This is the only way for the plant operator to know the current plant running condition. To identify the current plant status without shutting down the plant, the measurements need to be investigated. By knowing how the fault of each plant component affects the corresponding flow parameters and overall plant performance, the cause of performance change can be pinpointed and the degradation located.

Due to operational flexibilities in the combined cycle system, not only the degradation effects but also the changing operating conditions can cause variations in overall plant performance and flow conditions (temperature, pressure, and flow rate). Thus, it is difficult to distinguish the causes of the performance shift between changing operating conditions and plant degradation.

In the traditional way of degradation estimation, the "expected" performance is first obtained by carrying out a heat balance analysis based on measured data. The "measured" performance is then "corrected" to the value at the ISO condition and compared to the "rated" performance. In this method, only the overall degradation can be estimated and the fault of an individual plant component cannot be identified.

1.3. Performance Monitoring

Continuously evaluating the plant performance through the monitoring system can help the plant operators know the current plant degradation (decrease in performance). This information is necessary for the operators to identify the problems, search for the potential of performance improvement, and make economic decisions about scheduling maintenance and optimizing operations. A successful performance monitoring and evaluation system can give plant operators a clear view of how much the plant performance has degraded and how much each subsystem in the plant has contributed to that degradation. Based on this information plant operators can pinpoint the causes of the performance problems in the power plant and estimate the operational cost incurred due to the degradation.

Degradation is defined as the performance deteriorations in the plant equipments caused by mechanical problems (such as corrosion, fouling, and oxidation). The change of plant performance due to the shift of set points controlled by the operators is excluded from the definition of degradation. Following the evaluation of plant degradation is the process of economic optimization, the objective of which is to determine a plant

operation mode and the control set points that maximize plant profits and meet all operation constraints (such as equipment operation limits and emission regulations). The optimization analysis needs the current plant degradation status as a crucial input while the current plant control set points are also key inputs to the degradation analysis.

Through the plant performance monitoring system, the production capability and efficiency of a power plant and its subsystems are continuously evaluated over time using the measured plant data. Repeated performance monitoring and evaluations over regular time intervals are made by the on-line instrumentation, which is the only of information that enables plant operators to know the current plant status. This differs from the one-time precision test that relies on the instrumentation installed specifically for that test.

A precision test is a one-time performance evaluation of plant equipment that utilizes precision instrumentation installed specifically for that test. Since the tests are often done for the purpose of verifying vender guarantees on new & clean or upgraded equipment, the operating conditions of the equipment being tested are set as close to design (or guarantee) points as possible. The objective of a precision performance test is to measure the absolute production or efficiency capability of the equipment [1]. On the other hand, performance monitoring is done over time intervals, and its objective is to detect deviations of performance mainly caused by degradation effects. Following detection, actions of equipment upgrade and/or maintenance for the correction are often made. The goal of performance monitoring is not necessarily to obtain the absolute capability of the plant; instead, repeatable measured results, by which the changes of performance over time can be evaluated, are most important [2]. Repeatability is the long-term variation in gross error (bias), and, as defined by ASME Performance Test Code Committee, it is estimated as one-half the total instrument uncertainty [3]. The repeatability of the monitoring data enables performance monitoring to track changes in plant performance. However, the data is usually not accurate enough for vender guarantees. It is the

repeatable characteristic of performance monitoring that helps the engineers to exclude results that are not consistent with long-term trends.

In the current on-line monitoring and data reduction technique, measurements believed to have higher accuracies are chosen as model inputs and used to close the heat balance. The selection of input measured data is sometimes subjective and the heat balance analysis is carried out in a deterministic way without considering the measurement uncertainties and biases.

1.4. Performance Analysis

1.4.1. Physics-Based Performance Analysis

The objective of a physical-based performance analysis is to apply thermodynamic principles, which include energy and mass balance equations, to the combined cycle system. In order to differentiate the performance of each major subsystem from others, the heat and mass balances are applied to the control volume specified for each of the three major parts in the combined cycle system: gas turbine, heat recovery steam generator (HRSG), and steam turbine. Each subsystem is composed of several thermal components as well, and they can be further divided into smaller control volumes. By applying the heat and mass balances to the specified control volumes, unmeasured flow parameters and/or performance factors can be estimated. During the performance analysis the measured data are taken as inputs to the balance equations, and a complete set of thermodynamic data for each flow stream is calculated. The heat balance analysis is not aimed to predict the plant or equipment performance. Instead, it is a process of determining detailed thermodynamic properties of the operating system.

The number of heat balance equations increases significantly when more control volumes are used in a complex combined cycle system. The interactions between subsystems make the closure of equation-based heat balances (balances inside and among

the control volumes of subsystems) more difficult without using a solver. Fortunately, commercial heat balance software such as GateCycleTM and GTPRO has a built-in solver [4] making the modeling of very complex combined cycle systems easier for system engineers. With the aid of the heat balance solver, the current procedure of physical-based performance analysis involves most of the following steps:

1. Build a computer model for the combined cycle plant or its subsystems being investigated based on its configuration and operation condition. The procedure of building the plant heat balance model differs from one heat balance solver to another. But once the heat balance model is built, it represents a thermal system with balanced energy and mass equations regardless of the way of building it. The geometry information such as surface areas of tube bundles inside the HRSG is obtained from the vendor and is input to the heat balance model at the design mode. The heat transfer coefficients of the heat exchangers inside the HRSG are then adjusted to match the vendor-provided rating specification.
2. Run the heat balance model at the prediction mode (off-design mode), which has fixed HRSG surface areas, and size the gas turbine and steam turbine. Test the model by comparing the model predicted values to the vendor guarantee data over a wide range of operating conditions (if available). Calibrate the model if the predicted performance does not match vendor-provided data closely at different operation conditions. The model is tuned at the design mode and rerun at an off-design mode when comparing the predicted performance to the measured data.
3. Run the model at the current operating condition where the measurements were made, and obtain the expected performance data.
4. Compare the expected performance (obtained from the model) to the measured data. The “measured” performance is then “corrected” to the value at the ISO condition and compared to the “rated” performance. The degradation is then

evaluated by looking at the difference between the rated and corrected performance values.

The traditional way of combined cycle modeling and simulation is shown by the flow chart in Fig. 1-1.

1.4.2. Measurement Redundancy

A measured variable is said to be redundant if it is observable even when its measurement is removed [5]. Redundancy classification of variables can be carried out as part of the data reconciliation problem [6]. When performing the heat balance analysis at the design mode, a set of measured data is input to the computer heat balance model, and a complete set of performance data is obtained by closing the heat and mass balances. Sometimes the number of available measurements is larger than needed to close the heat and mass balance, and in this situation the heat balance is over specified. For example if the feed water flow into the HRSG is measured as well as the main steam flow, the heat balance will state that these two measured data for flow rate should be equal if there is no blow-down at the evaporator. If these two measured values are not equal due to the measurement uncertainties, the heat balance analysis leads to no solution. The current way to deal with this problem is to believe one of the redundant measurements, take that as an input, and throw away the others. The selection is usually based on the prior knowledge about the uncertainties of the measurements. In this case, the measurement uncertainty of the steam flow is higher than the measurement of the water flow, and, thus, the measurement of the feed water flow is selected as the model input while the measured steam flow is thrown away.

On the other hand, when the available measurements are less than needed, a reasonable performance factor is assumed for the component for which the data was measured. In this situation the heat balance analysis is under specified. The traditional deterministic calibration of the design mode heat balance model is given in Fig. 1-2.

1.5. Importance of Good Data

The online performance monitoring system typically extracts the data from existing data source in the plant, such as the plant DCS systems. The causes to performance changes due to the "natural" factors such like the ambient conditions should be distinguished from actual system degradation. Deriving performance parameters from measurements in the turbine control system or plant control system without correcting for ambient and load effects would produce practically useless information. Instead, a performance monitoring system must be capable of not only accepting the necessary data inputs, but of also containing the detailed thermodynamic models that allow "correction" of the raw data for all relevant effects of operation. In some cases, the necessary data may not be available, or perhaps more commonly, the quality of the measurement may be insufficient for performance monitoring purposes, necessitating the need for additional sensors. The quality of the incoming measurements is very important. Because many performance calculations are derived using mathematical relationships that involve exponents, small inaccuracies in one measured variable can result in very large inaccuracies or uncertainties in a derived result. For this reason, a necessary part of any performance monitoring endeavor must be to review all data inputs for sufficiency during initial system installation and design, and regularly thereafter to ensure that input quality is not degrading over time. Proper pre-processing and range-checking of the data by the online system prior to the performance analysis also helps to detect erroneous sensor readings. Failure to observe this will result in poor accuracy and inconclusive information at best, or at worst, false assumptions and forced outages due to performance problems that are not detected by the system.

1.6. Summary

Combined cycle system engineers utilize a commercial heat balance solver, e.g., GateCycleTM, to predict plant performance and provide performance guarantees. Heat balance analysis needs the measured data from the site as model inputs and, thus, is subject to uncertainties and biases from the measurements. In addition, performance predictions will not be accurate if degradation effects are not taken into account. In the traditional way of combined cycle plant modeling, the measured data believed to have higher accuracies are chosen as inputs to the heat balance analysis while the others are discarded. As the plant detailed geometries are available, the performance multipliers, which represent the degradation status, are calibrated to match the selected measured data in a deterministic way. Therefore, the current combined cycle performance guarantees are based on deterministic modeling and simulation without considering the uncertainties. To avoid the subjective decision making on what data to believe and what to discard, a probabilistic methodology that takes into account the measurement uncertainties and gross errors when carrying out model calibration is needed. By introducing the probabilistic method for model calibration, one can reduce the uncertainties in performance simulation and the risks in providing performance guarantees.

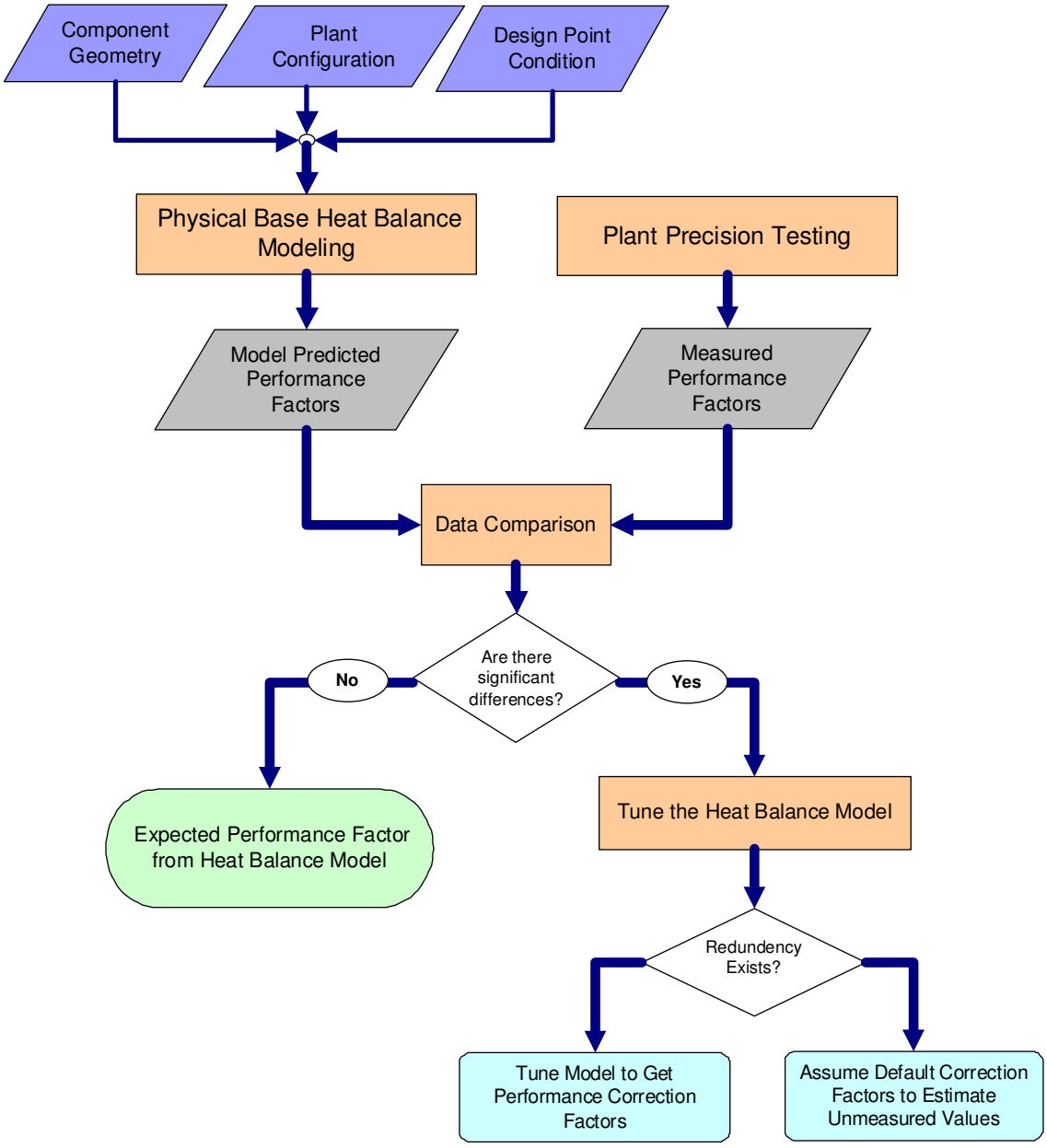

Figure 1-1: Traditional combined cycle M&S procedure

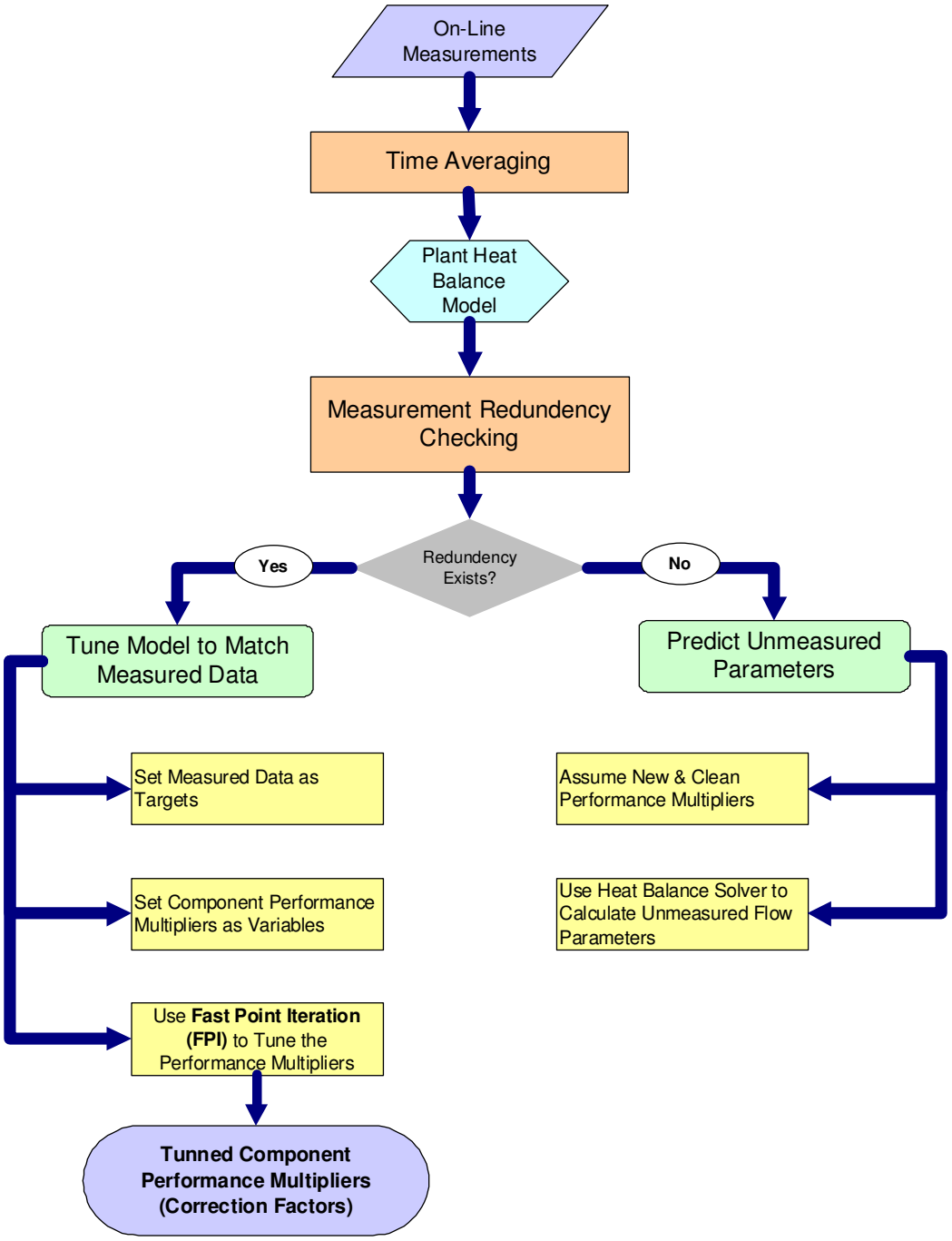

Figure 1-2: Deterministic model calibration procedure

CHAPTER 2

PROBLEM STATEMENT

Modeling and simulation for a complex system that has undergone a certain degree of degradation face a major challenge in estimating degradation and predicting performance while subject to measurement uncertainties. From the modeling & simulation point of view, degradation estimation can be conducted by model calibration based on the measurement data and by a performance comparison between the calibrated and expected new-and-clean models. By running two models, i.e., degraded and new-and-clean, at the same operation condition, one can quantify the overall degradation and break it down into portions contributed by different system components. A performance simulation of the degraded system is then carried out by running the calibrated model in an off-design mode, in which the system size and configuration are frozen, and, therefore, the performance is only dependent on the degradation status and operation conditions.

The challenge arises from the fact that all measurements are corrupted with random errors caused by instrument uncertainties, and, with small probabilities, are contaminated with gross errors due to instrument failures. These errors are propagated through the calibration process, which is usually a nonlinear inference process. Therefore, any physical-based model that is calibrated to the measured data is subject to uncertainties and biases. These uncertainties need to be addressed, quantified, and populated to the performance simulation while the model calibration should be performed without the contamination effects caused by gross errors.

Currently in the power generation industry, calibration uncertainties and their propagation to performance simulation are not adequately addressed, i.e., measurement errors are not populated to the modeling and simulation environment with the uncertainties associated with both model calibration and performance simulation. In

addition, the majority of calibration processes follow the data-matching type, a deterministic procedure often based on subjective decisions on what data to match and what to ignore. The deterministic calibration process is subject to larger uncertainties from measurement errors since there is no suppression mechanism on error propagation during the calibration process. In addition, miss-calibration often happens when gross errors occur in measurement data. A miss-calibrated model can lead to serious bias in performance simulation. These motivating observations lead to a summarizing research question that guides this research work.

Research Question 1: *How can the performance engineer estimate system degradation based on the measurement data that are subject to errors?*

This research work is motivated to answer the research questions outlined above, and to present a guide to develop a modeling and simulation environment that addresses the problems of uncertainties in model calibration and their propagation through the performance simulation. The following hypothesis presents a testable answer to the research question.

Hypothesis 1: *By performing data reconciliation and model calibration simultaneously, i.e., simultaneous data reconciliation and model calibration (SDRMC), one can estimate system degradation based on the error-free data, i.e., the reconciled data, while the measurement uncertainties are taken into account as well.*

The hypothesis given above is a testable answer to the guiding research question. To demonstrate the hypothesis, a modeling & simulation environment that enables the system engineer to perform simultaneous data reconciliation and model calibration is developed. A combined cycle system, which represents a typical complex energy system, is modeled and used in this environment to test the proposed methodology.

The main advantage of the data reduction method currently used in the majority of calibration processes is its fast execution due to the fact that a subjective decision on the data to be matched is made in advance and the fact that the deterministic process does

not require an optimization scheme. Introducing data reconciliation into model calibration, however, makes the calibration process become an iteration process, and therefore more computation time is required due to the optimization scheme involved. These two facts lead to the second research question.

Research Question 2: *What is the major benefit that the performance engineer can get by using SDRMC instead of a deterministic data reduction method which needs less computation time?*

Obviously, the SDRMC method eliminates the subjective decision making process of selecting "good" data to match. A more important benefit is, however, related to the reduction of calibration uncertainties. The answer to this research question is the following hypothesis which can be tested in the developed modeling and simulation environment for a combined cycle SDRMC.

Hypothesis 2: *If one carries out SDRMC instead of utilizing data reduction for model calibration, the calibration uncertainties and, therefore, the uncertainties of performance simulation can be reduced.*

The reduction of uncertainties in performance simulations also means the mitigation in the risk of issuing performance guarantees, by which the performance engineer can provide more aggressive quotes of performance benefits so as to be competitive.

The implementation of SDRMC to a complex combined cycle system faces two major challenges: the smearing effect caused by gross errors, and the computational expense incurred by a complex system. These challenges lead to the following research questions and the corresponding answers by testable hypotheses.

Research Question 3: *How can one perform SDRMC properly when the measurement data are subject to gross errors?*

Introducing data reconciliation means all the measurement data are taken into account in model calibration, whereas no subjective decisions are made for "good" data.

There is, however, a challenge in every data reconciliation scheme to face and tackle -- the smearing effects caused by the gross errors, i.e., biases in the measurement data. The occurrence of measurement biases does not disprove the usability of data reconciliation. Instead, applying the gross error detection (GED) techniques into the simultaneous data reconciliation and parameter estimation scheme can suppress the smearing effects.

Hypothesis 3: *The occurrence of gross errors can be tested. Once it is confirmed, one can apply gross error detection techniques to mitigate the smearing effects and identify locations and magnitude of gross errors while performing SDRMC.*

As the GED techniques are incorporated to the simultaneous schemes used for model calibration and data reconciliation, more system level iterations are required, especially when the hypotheses-testing based method is utilized. Combination of the high fidelity performance simulator and the GED scheme could lead to tremendous computation costs for a complex system.

Research Question 4: *How can one reduce the computation time in SDRMC for a complex system?*

To ease the cumbersome computation requirements, rapid system modeling is required. It can be achieved by utilizing meta-modeling, which provides for the efficient approximation of arbitrarily complex functions.

Hypothesis 4: *For a complex system, one can incorporate the meta-modeling into the SDRMC scheme to reduce the computation time.*

In this research work, the above hypotheses are to be tested in a developed modeling and simulation environment where the performance engineer can create meta-modeling for a complex thermodynamic system and incorporate the gross error detection techniques into a simultaneous scheme for data reconciliation and model calibration. This modeling and simulation environment (M&S) is aimed to aid the performance engineers to perform model calibration in a probabilistic manner such that all measurements that are subject to random and gross errors are taken into account, while making no subjective

decisions for the “good data” to be used. The estimation uncertainty for system degradation is also provided in this developed M&S environment, by which the performance engineer can populate the calibration uncertainty to the uncertainty in performance simulation. The ultimate goals of this project are to reduce the uncertainties in performance simulation for degraded thermodynamic systems and to aid the performance engineer to build confidence levels on the predicted system performance. The application of this new M&S environment can then be used to provide more reliable and accurate performance guarantees for combined cycle power plant systems.

CHAPTER 3

BACKGROUND

3.1. Combined Cycle Basics

The combined cycle power plant has become the most commonly built type of power generation system in recent years due to its high efficiency, relatively low installed investment costs and on-line availability once installed. The technology of its components, developed to improve the efficiency, has matured and makes its overall plant efficiency much higher than a traditional Rankine-cycle power plant.

The thermodynamic characteristics of different type combined cycle power systems have been studied by Horlock and Crane[7, 8]. Detailed descriptions of system principles, design considerations, and the component behavior at off-design condition were covered by Kehlhofer[9]. Recent advances and prospects have also been reported by Horlock[10] and Frutchi[11]. Combined cycle off-design performance, which has been studied in a lesser degree, can be found in the work done by Fantozzi and Desideri[12].

In the combined cycle system, the three major parts – gas turbine, HRSG, and steam turbine, are operated in an interactive way. The gas turbine not only generates the power but also provides the hot exhaust gas to the heat recovery steam generator (or HRSG). The HRSG then transforms the gas turbine exhaust heat into usable steam energy. The hot, hig- pressure steam is sent to the steam turbine to generate extra power or to serve as a source of process steam that can be utilized as heat input. In this latter mode, the plant would be called a “Cogeneration” plant. Inside the HRSG there are a series of heat exchangers: superheaters, evaporators, economizers and feed water heaters at different pressure levels. The hot exhaust gas of the gas turbine passes through these heat exchangers and the energy is transferred from the exhaust gas into water and steam inside

the tubes via heat convection on both sides of the tube and conduction through the tube wall. Additional equipment like duct burners and bypass ducts may be added to the gas path section in the HRSG. The combined cycle system can be represented with a temperature gradient diagram given in Fig. 3-1.

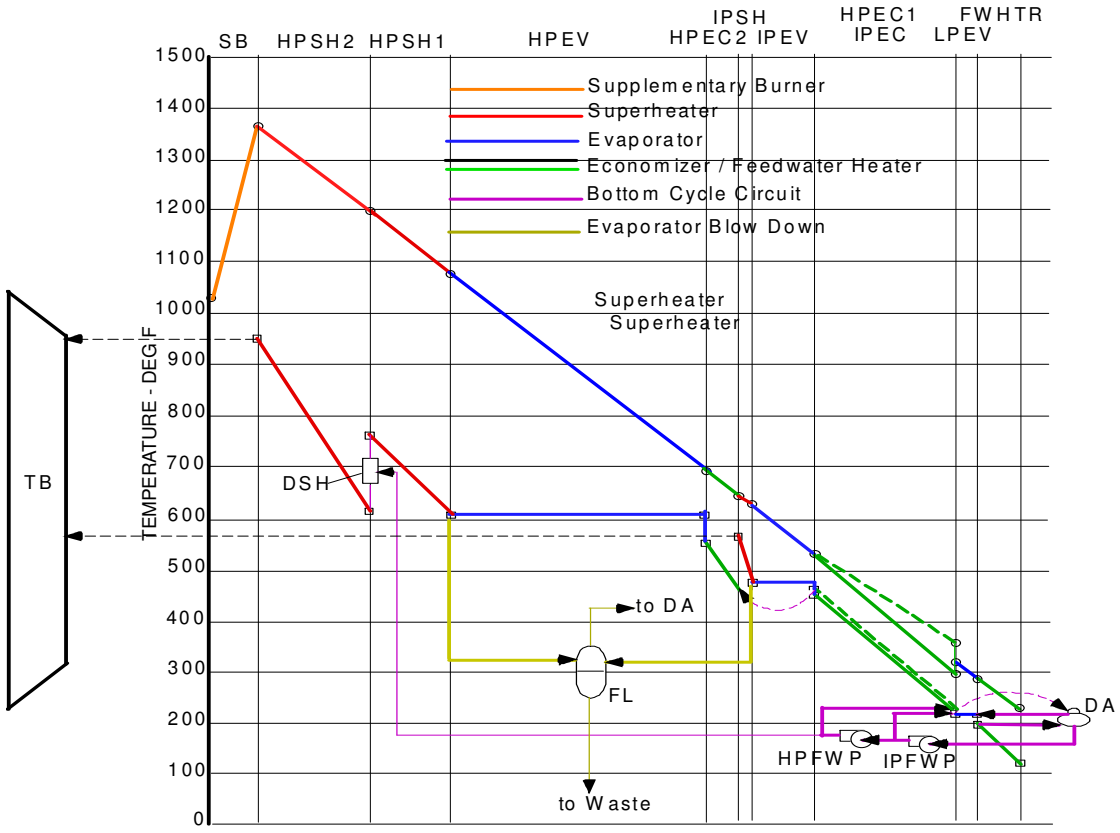

Figure 3-1: Temperature gradient diagram for a typical combined cycle system

The ordinate of the figure is temperature showing both the gas and water/steam side temperatures. The abscissa simply represents the length of the HRSG in a qualitative way. The different types of heat exchangers - economizers/feedwater heaters, evaporators and superheaters are color coded as defined on the figure. The gas temperature drops uniformly through the HRSG, but this is not the case for the water/steam temperatures. Note that water from an economizer enters an evaporator below saturation temperature. This is a typical situation to avoid any boiling in the economizer that may take place in some off-design case. The thermal efficiency of the combined cycle system increases with the number of pressure levels. There is, however, a trade-off between the plant efficiency and the cost of building a more complex multiple-pressure system.

3.2. Performance Monitoring – Where are we now?

Performance monitoring is the process by which the efficiency and production capability of plant equipment is continuously evaluated. The evaluation of performance implies a comparison to some standard that defines good performance. For example, does good performance mean that the plant would pass its original acceptance test? Does it mean that the plant is better than it was last year, or last month?

Performance monitoring and diagnosis for combined cycle power plants have become more important in recent years due to the need for continuously evaluating the performance and operating costs of the plants and their subsystems. This need has been revealed by many available commercial monitoring packages being utilized in the power generation industry. These commercial packages are designed to achieve various goals such as instrument fault detection, energy and cost accounting, or production and maintenance scheduling among others.

A compilation of analytic methods utilized in typical monitoring systems to evaluate power plant performance and determine the degradation status can be seen in the

textbook of Gay [2]. The method presented in this literature utilizes the measurements with repeatable precision to perform the heat balance analysis, which gives the corrected plant performance. The degradation is then estimated by a comparison between the corrected and rated performances. Similar studies on the performance monitoring can also be found in Haub [13] and Rickli [14].

A typical combined cycle monitoring system utilizes the first law of thermodynamics to perform the heat balance analysis and to estimate the system degradation. Performance monitoring and diagnosis using exergy analysis methodology, which is based on the second law of thermodynamics, has also been developed. These thermodynamic analysis methods are then typically combined with an economic analysis of the plant investment and operation, e.g., Lozano uses a thermo-economic analysis to diagnose the operation deficiencies in an existing combined cycle power plant [15]. Diagnosis of plant performance based on Structural Theory has been theoretically developed by Valero[16][17][18][19]. Application of Structure Theory to the combined cycle performance monitoring and diagnosis was done by Correas[20]. Similar studies of thermal system performance monitoring and component malfunction diagnosis based on Structure Theory and thermo-economic analyses have also been published (e.g., Stoppato and Lazzaretto [21], Arena and Borchielini [22], Lerch et al. [23], and Lazzaretto et al. [24]). Zaleta proposed a diagnosis methodology based on both energy and exergy analyses using heat rate and total power as thermodynamic indices [25].

In the studies based on exergy analysis and Structure Theory, the thermal energy system is transformed into a productive structure, which is built according to the exergy usage in each component. The process is very similar to setting up control volumes for the thermal system based on the first law of thermodynamics. Any type of performance diagnostic technique (first law or second law) carries out diagnosis based on the measured data. Before the measured data can be utilized, a reconciliation process needs

to be done to eliminate the errors caused by measurement uncertainties or faulty sensors. Otherwise the results of the diagnosis will not be valid.

Currently in the power generation industry, the performance monitoring flows three basic steps:

Step 1: Range and Reasonableness of Inputs

Incoming measured data that serve as inputs to the performance calculations are checked for validity, compared to physical limits, and – if necessary – substituted with reasonable default values in order to guarantee proper online operation of the systems.

Step 2: Component Heat Balance

A heat balance around the gas turbine produces additional information on the conditions of the ingoing and outgoing streams and also adds information on certain parameters that cannot be measured directly. It is important to note that the heat balance calculation is not designed to measure performance, but to create detailed information about the current operating point that is consistent with mass and energy balances around the equipment. If the monitoring system covers the entire plant, the redundancy of information between the individual equipment even allows reconciliation of plant measurements and advisories regarding current sensor conditions.

Step 3: Performance Analysis

Once a consistent set of data on the current operating point has been generated, the performance analysis itself can be conducted, comparing current performance against expected performance calculated from detailed equipment models based on design and test information. In order to make performance data comparable over time, the current performance degradation is corrected to reference

conditions, e.g., ISO or acceptance test conditions, so that it is easy for the operator or performance engineer to evaluate trends of equipment performance.

3.3. Degradation Effects

The term "degradation," as used in this research work, refers to a change in equipment performance over time compared to that of the "new and clean" equipment at equivalent operating conditions.

Deviation of combined cycle performance from its expected value is primarily caused by two reasons:

1. Changes in ambient and operating conditions.
2. Changes in fluid path component configurations due to degradation.

When evaluating performance degradation, two types of degradations are typically considered:

- **Recoverable Degradation** is the performance loss that can be recovered by operational procedures such as keeping the inlet and outlet pressures low, or online and offline water washing of the compressor.
- **Non-Recoverable Degradation** is the performance loss that cannot be recovered without repair or replacement of affected gas turbine components. Examples of non-recoverable degradation include: loss of surface finish on blades, increases in blade tip clearances, packing leakage of both the compressor and turbine, and combustion system component corrosion/erosion leading to flame instabilities or increased thermal stress on the subsequent turbine sections.

Degradation usually results in performance shortfalls, and it is difficult to prevent. The causes of degradation are related to many correlated parameters. In the Rankine cycle, fouling has the biggest impact on the performance downgrade and is the most common cause of degradation in the HRSG. According to ref. [26], fouling of the power plant heat exchangers results in huge economic losses. Von Nostrand [27] estimated the total cost

caused by heat exchanger fouling for petroleum refining in the non-Communist countries as high as $4.41 billion per year.

Degradation of gas turbine hot gas path components (e.g. compressor and turbine) were studied and presented in [28~32]. A complete discussion of the degradation mechanism can be examined in [30, 32]. According to ref. [30], the faults that occur in a combustion chamber that affect overall performance are rare compared to those that occur in a compressor and turbine. Thus, those faults occurring in combustion systems are usually excluded from the gas turbine degradation studies.

The performance shortfalls caused by degradation can be reflected in the measured data such as a decrease in the measured power output or increase in the measured heat rate. Or, the performance metric can be defined in a small scale such as the heat exchanger outlet temperature or turbine exit pressure, and degradation of the performance in this scale can be identified by the change in flow parameters such as pressure and temperature. In this paper, attention is focused on including degradation effects, both large scale and small scale, as part of combined cycle modeling and simulation.

Degradation effects have a crucial impact on the performance prediction, and if the degradation is not included in the plant modeling and simulation, the performance prediction will not be valid. To identify the degradation, measured data from the site must be relied upon. The measured data, however, are always subject to uncertainties and biases, which will affect the reliability of degradation identification. Measurement errors not only bias the degradation estimation, but also cause errors in plant modeling and simulation. Figure 3-2 shows the shift of a heat release diagram for a combined cycle HRSG due to measurement errors. Errors in the heat rate and HRSG surface area predictions caused by inaccurate data are also given in Fig. 3-3. Studies on combined cycle degradation identification based on measurements are very rare. So far in the power

generation industry, there is no formal technique used to identify current plant degradation status by analyzing the measurements in a probabilistic way.

.

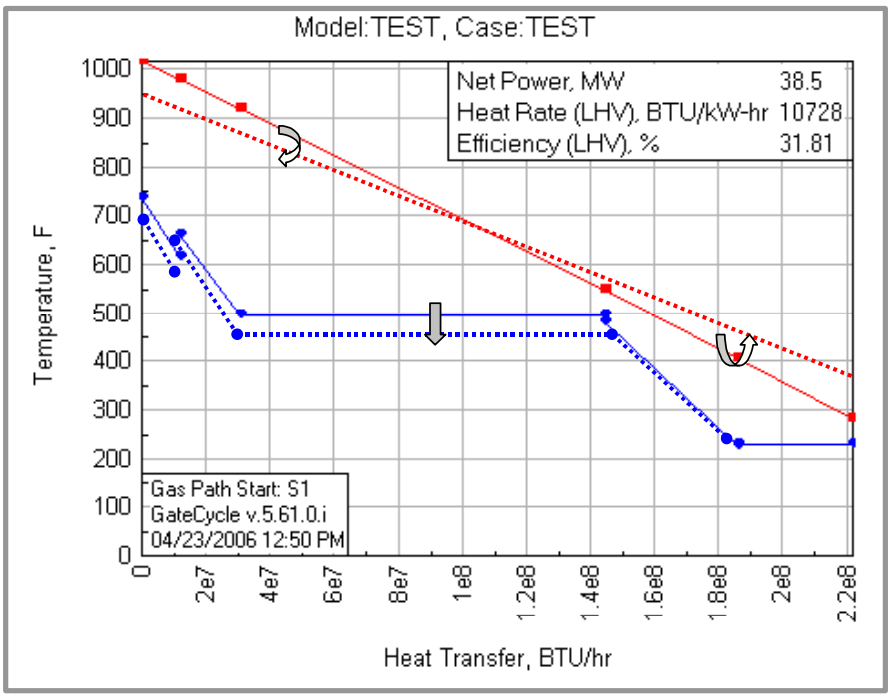

Figure 3-2: Shift of HRSG heat release diagram due to measurement errors

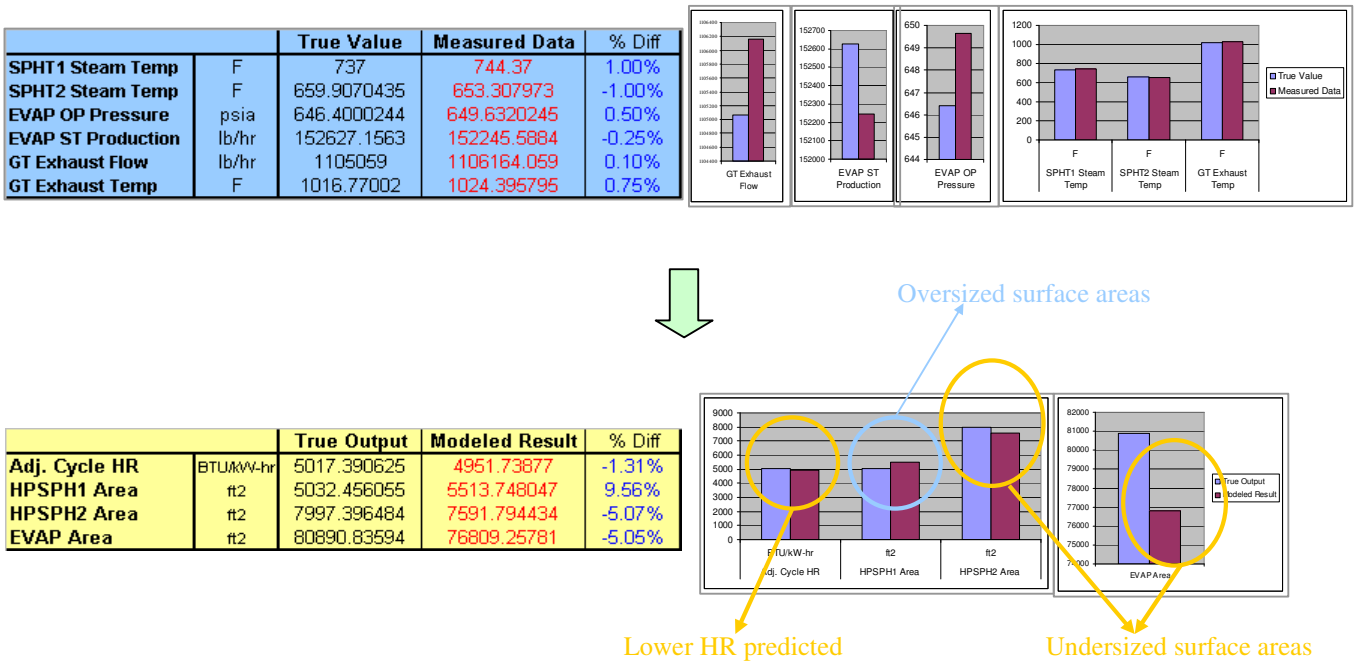

		True Value	Measured Data	% Diff
SPHT1 Steam Temp	F	737	744.37	1.00%
SPHT2 Steam Temp	F	659.9070435	653.307973	-1.00%
EVAP OP Pressure	psia	646.4000244	649.6320245	0.50%
EVAP ST Production	lb/hr	152627.1563	152245.5884	-0.25%
GT Exhaust Flow	lb/hr	1105059	1106164.059	0.10%
GT Exhaust Temp	F	1016.77002	1024.395795	0.75%

		True Output	Modeled Result	% Diff
Adj. Cycle HR	BTU/kW-hr	5017.390625	4951.73877	-1.31%
HPSPH1 Area	ft2	5032.456055	5513.748047	9.56%
HPSPH2 Area	ft2	7997.396484	7591.794434	-5.07%
EVAP Area	ft2	80890.83594	76809.25781	-5.05%

Figure 3-3: Errors in predicted CC heat rate and HRSG surface area due to inaccurate data

3.4. Degradation Estimation by Model Calibration

Model calibration for a power system is the process of modifying the input parameters to a heat balance model until the output from the model matches an observed set of data. Once the model is calibrated, it can be used to predict the system performance in off-design conditions. To be able to quantify degradation in the power system, a detailed combined cycle heat balance model is required instead of simplified energy and mass balance equations for two reasons. First is the capability of the commercial heat balance solver to carry out detailed modeling of geometries and configurations for each plant component. This capability enables the utilization of the performance correction factors to simulate the degradation effects based upon the input geometry and design point specifications. Second is the capability of the commercial heat balance software to handle the interactions between subsystems inside the combined cycle power plant, and, most importantly, close the heat and mass balances.

These features provide flexibilities to the whole plant or subsystem modeling and simulation based on the available information. For example, selection of the subsystem (or control volume) in the heat balance modeling is adjustable depending on the measurement availability. If measurements of flow parameters are available and redundant for each section of the plant, the subsystems can be defined at a small scale. In this situation we are able to determine the degradation status of each section. If the available measurements are limited, the selection of subsystems has to be tailored such that measurement redundancies exist. No matter how we define subsystems based on the availability of information, the heat balance solver is able to close the energy and mass balances all the time.

Having the capability of the off-design performance simulation from the heat balance solver, the performance engineers are able to create the model that represents the current status by tuning the performance correction factors of system components to

match the measurement data. The system degradation then can be quantified by comparing the predicted performance from the calibrated model with that obtained from the new and clean. Currently, the majority in the power generation industry relies on the deterministic data matching method to calibrate the model. In the deterministic model calibration, the model is tuned to match the selected data based on the prior belief while the rest of data are ignored. The decision making on what data to match and what to ignore itself is often subjective.

3.5. Measurement Uncertainty

A measurement uncertainty is defined by the document, *Guide to the Expression of Uncertainty in Measurement* [33], as "*a parameter, associated with a result of a measurement, that characterizes the dispersion of the values that could reasonably be attributed to a given particular quantity being measured.*" Due to the occurrence of uncertainties, every measurement should be expressed by the true value of the quantity being measured plus a measurement error. Measurement errors are deviations of the measured data from their "true" values, which are either caused by fluctuations in measurements or associated with the theoretical description of the results.

The source of measurement uncertainties mainly comes from two categories: random errors and systematic errors (gross errors). In a typical on-line monitoring system, the measurement of a flow parameter is taken from a computer-based data acquisition system as a single value or an average of measured data over a short period of time. Measurement uncertainties caused by random errors can be estimated by calculating the standard deviation of a set of repeated measurements. A gross error, however, represents a large scale of deviation from the true value that constantly occurs during the measurement. Unless the information of likely gross errors for a given sensor is provided, systematic errors cannot be estimated by inspecting the scattering of repeated

measurements. They must be estimated by either engineering judgment or through the gross error detection techniques.

By quantifying measurement uncertainties of sensors, we are able to estimate the mother population of measured data, which is a key input to the model-based data reconciliation process. The method of defining and quantifying measurement uncertainties can be found in ASME PTC 19.1-1998, Test Uncertainty [3], which serves as a guideline for quantifying measurement uncertainties in this paper.

3.6. Data Reconciliation, Gross Error Detection, and Parameter Estimation

In the combined cycle power plant, hundreds or even thousands of variables such as pressures, temperatures, flow rates, etc. are routinely measured and recorded by data acquisition systems for the purpose of performance monitoring. The use of computers in the modern data acquisition systems not only facilitates collection and processing of a large amount of data but also eliminates errors caused by manual recording. Measured data are always corrupted by errors during the measuring, processing and transmission of the measured signals. These errors lead to deviations of measured data from the true values of the flow parameters being measured. The total error in a measurement primarily comes from two sources– random errors and gross error (systematic errors).

Random errors arise from different sources of noise such as power supply fluctuations, signal conversion noise, changes in ambient conditions, etc, which are beyond the control of the design engineer. Neither the magnitudes nor the signs of random errors can be predicted. Therefore, the only possible way these errors can be characterized is by the use of probability distributions.

Gross errors, on the other hand, are caused by non-random events such as instrument malfunctioning (due to improper installation of measuring devices), miss-calibration, wear or corrosion of sensors, etc [33]. Due to its non-random nature, a gross error has a constant magnitude and sign at any given time in a given sensor. Thus, the

contribution of a gross error to a measured value remains the same as the measurement is repeated with the same instrument at the same condition. Although gross errors occur less frequently, their magnitudes are typically much larger than those of random errors.

Plant engineers rely on measurements from the site to monitor the plant performance and decide the best operating strategy. The plant operating conditions are adjusted by the control system to maintain the optimized power output or heat rate. Measurement errors lead to significant deterioration in controlling and monitoring plant performance. In some cases, erroneous data can also drive the process into an uneconomic operating regime [34]. The problems related to measurement errors are magnified because vendors utilize measurements for plant modeling and simulation to provide customers the performance guarantees. Using measured data that have errors as the model inputs during modeling can cause the predicted performance to deviate from what it should be, and they may cause the penalties to the vendors for the underachievement of a performance guarantee. It is therefore important to reduce the error effects in the process of a performance guarantee.

Data reconciliation is a technique developed to reduce the effect of random errors and improve the measurement accuracies. What differentiates data reconciliation from other data filtering techniques is that data reconciliation utilizes process model constraints and estimates process variables by adjusting the measurements so that the estimates satisfy the model constraints [34]. The reconciled true value estimates are expected to be more accurate than the measurements and, most importantly, satisfy the physical constraints such as conservation of energy and mass. The results of data reconciliation, however, may be invalid due to the contamination effects of gross errors. In order for data reconciliation to be effective, the gross errors need to be excluded during the process. Gross error detection is a companion technique to data reconciliation that has been developed to identify and eliminate gross errors. Therefore, data reconciliation and

gross error detection are carried out together either in a parallel or serial way to improve the accuracy of measured data.

Data reconciliation has been widely implemented in the chemical industries during the past 35 years. There is a large volume of literature available addressing related topics. A detailed description of the underlying concepts and application examples can be found in Romagnoli and Sanchez [35]. Data reconciliation for linear models is also well studied. Crowe et al. [36] used a matrix projection method to decompose the model constraints and solve for the measured and unmeasured parameters sequentially. Pai and Fisher [36] use Crowe's matrix projection method to decompose the linearized sub-problems and Broyden's method to update the Jacobian. Swartz [37] also uses Crowe's method along with a QR matrix factorization to eliminate the unmeasured parameters.

On the other hand, various nonlinear programming (NLP) techniques, such as generalized reduced gradient algorithm (GRG2), sequential linearization programming (SLP), sequential quadratic programming (SQP), etc., can be applied directly to solve nonlinear data reconciliation problems. Studies have shown that the NLP technique is more robust, but at the expense of computing time. A hybrid SQP method modified to fit a least square object function was developed by Tjoa and Biegler[38], and the demonstration showed a significant saving in computing time.

The use of a least squares objective function in data reconciliation is based on the assumption that all the measurements are normally distributed due to random errors. In the data reconciliation process, data being reconciled are adjusted not only to minimize the least squares objective function but also to satisfy all the nonlinear physical constraints. The presence of gross errors can contaminate the results of data reconciliation. This is because the weighting factors defined based on uncertainties of random errors are applied to the measurements found to have gross errors. As gross errors are found during the process, they should be pulled out and the data reconciliation process performed again after removing the found gross errors. To avoid the

contamination effect of an iterative process due to gross errors during data reconciliation, Tjoa and Biegler [39] utilized a bi-variant distribution function (contamination normal function), which takes into account both random and gross errors, and constructed a new objective function based on the maximum likelihood principle. Minimizing this newly constructed objective function gives unbiased estimates in the presence of gross errors, and a simultaneous gross error detection test can therefore be carried out based on their distribution functions. In the study by Ozyurt, D. B. and R. W. Pike [41], six different *M*-estimators derived from robust statistics for simultaneous data reconciliation and gross error detection were investigated along with weighted least squares and a modified iterative measurement test method (MIMT) for nonlinear models. These *M*-estimators all reduce the gross error effect during data reconciliation. Their performances were compared and investigated through the applications to two industrial cases, and the comparison shows that the Cauchy distribution and Hampel's redescending M-estimator give promising results for simultaneous data reconciliation and gross error detection with less computation time.

A gross error is statistically an error whose occurrence as the result of a random variable is highly unlikely. The presence of a gross error is usually detected by statistical tests generally based on linear or nonlinear models. Rejection of gross errors can be performed using confidence level or α values when the underlying distribution function for the measurement is available. A measurement value with a probability of occurrence less than ($\alpha \times 100\%$) can be detected as a gross error. Some of these tests can be found in Tamhane and Mah [41], Rosenberg et al. [42] and Narasimhan and Mah [43]. The occurrence of gross errors could invalidate the results of reconciled measured data that are from good sensors. The use of a robust estimator can reduce the contamination effects caused by gross errors and avoid the use of an iterative scheme during data reconciliation. Parameter estimation is a crucial step to realize the underlying physical phenomena in modeling and simulation. It is directly linked to model calibration. In the traditional least-

squares method used for parameter estimation, it is assumed that the parameters being estimated are not subject to measurement errors. In reality, random and gross errors occur in measurements and can bias the process of parameter estimation. Duever et al. [44] proposed the error-in-variables (EIV) approach for parameter estimation, which assumes all measurements have errors. Thus, in solving the EIV problem, not only the model parameters are estimated, but data reconciliation is also carried out. A deterministic EIV method that guarantees global optimality was proposed by Esposito and Floudas[45], who reformulated the optimization problem in terms of convex underestimating functions and then utilized a branch-and-bound procedure. Arora and Biegler suggested re-descending estimators for simultaneous data reconciliation and parameter estimation. The advantage to re-descending estimators is its easy identification of outliers without any extra data analysis on the residuals of regression.

Application of data reconciliation in the power generation industry is not as widespread as in the chemical industry. However, there have been significant contributions: An equation-based data validation technique proposed by Cheng et al. was implemented to the gas turbine performance monitoring system [46]. Hartner et al. [47] suggested a model-based data reconciliation method and applied it to a fossil boiler plant. In this model, a commercial heat balance solver was utilized instead of a set of nonlinear physical constraints to perform the plant data reconciliation. Most of these studies have been done for simple cycle gas turbine plants (gas turbine only with no HRSG or steam turbine), and very few studies have been done for the combined cycle data reconciliation. Gotz and Reisacher [48] performed equation-based data reconciliation for a combined cycle system represented by a set of simplified energy and mass balance equations. The residuals, which are caused by the measurement uncertainties or biases, were approximated by the 1st order Taylor series, and the estimates were obtained by solving a linear algebra problem. Gulen and Smith [49] developed analytical solutions to the data reconciliation problem based on the concept of the Kalman filter. The method was

applied to a single-shaft combined-cycle system to separate the total power distribution. In this method the residuals were also linearized using a 1st Taylor Series, and the reconciled values were obtained by solving a differential equation that minimizes the uncertainties of the estimates. In these two combined cycle-related literatures, measurements were assumed only subject to random errors, and gross errors were assumed not to exist. The occurrence of gross errors will invalidate the results since in both methods the residuals are linearized by a 1st order Taylor series, which is only valid when deviations of the measurements from true values are small and under the scope of random errors. This assumption is invalid even if gross errors occur.

3.7. Post Market Combined Cycle Performance Guarantees

Performance guarantees for the upgraded after-market combined-cycle power plants cannot be done properly without establishing the current plant status correctly. Underestimating the current degradation status could result in providing the over-predicted power and heat rate as the performance guarantees, which leads to the financial penalties for the EPC (Engineering, Procurement, Construction) contractors. Overestimating the shortfalls of the current plant performance, on the contrary, results in conservative performance guarantees, which could cause a less competitive contract. Performance guarantees of plant upgrades for the current degraded plant present a unique challenge due to the fact that the plant is not at the new and clean condition whose performance guarantees. For a new plant, the status is new and clean, and guarantees can be provided by the design-point heat balance analysis and confirmed by the precision test. However, for the degraded plant, the new and clean heat balance analysis is no longer valid and a model calibration is necessary. The calibration reference is, however, based on the on-site measured data, which are subject to higher uncertainties than the precision test.

The process of performance guarantee is the EPC contractor's proprietary information, and, thus, it is usually not available to the public. However, based on the information obtained from the interviews with engineers of EPC contractors and the related website [50], it is known that in most of the performance guarantee processes a heat balance analysis is utilized, and the margined point estimation is provided. In the heat balance analysis, the plant measurements are input to the design-point model and the point estimation of the upgraded plant performance is obtained by running the off-design heat balance heat balance model. The model predicted performance is the engineering expected value. It is margined by a factor (between 0 and 1) to take into account the model accuracy and other uncertainties. A risk analysis is then carried out and the final guaranteed performance is obtained with a certain confidence level.

3.8. From Deterministic to Probabilistic

From the above literature reviews, the following facts have been found:

1. Techniques used in the chemical industry for data reconciliation and gross error detections are equation-based. While dealing with systems that have nonlinear processes such as heat transfer and chemical reaction, it is inevitable that nonlinear constrained optimization problems must be solved. In these techniques, the optimization problem is solved either by linearization or traditional nonlinear programming methods such as SQP (sequential quadratic programming) and SLP (sequential linearization programming). Almost all of the references to these techniques are being utilized in the chemical industry; there are very few literature citations showing applications of these techniques in the power generation industry. A combined cycle system has complex mass and energy transport among small components such as heat exchangers and subsystems such as a gas turbine, HRSG, or steam turbine. This makes it difficult to implement equation-based data reconciliation without simplifying the problem such as treating a

whole HRSG as a black box. In the previous works of combined cycle data reconciliation, simplified model equations were utilized. Simplified model equations, however, are less representative of real combined cycle plants, plants which have differing configurations and whose degradation status varies from plant to plant. Therefore, there is a need for a technique that can carry out concurrent data reconciliation and gross error detection and is able to handle the complexity of a combined cycle system.

2. Very few references have been found that consider the estimation of combined cycle degradation effects. The available literature exhibits the impact of system component degradation, but techniques for estimating current degradation status are not available. However, in chemical industry there are techniques available for concurrent data reconciliation and parameter estimation. In these techniques, the robust maximum likelihood estimators (*M*-estimators) are employed to mitigate the gross error effects. These methods, however, mainly target the process parameters, and, most importantly, they are equation-based meaning that certain simplifications are necessary. In a combined cycle power system, degradation deteriorates the heat transfer capabilities of the system components and thus has a crucial impact on the energy terms in the model equations. It also makes the model-predicted plant performance deviate from the real value. Without taking degradation effects into account, the data reconciliation would be biased as well. Therefore, there is a need for a technique that not only can reconcile the measurements but also is able to evaluate the hidden degradation status in a combined cycle system.

An integrated methodology utilizing the heat balance solver for carrying out simultaneous data reconciliation and model calibration (*SDRMC*) is proposed and has been implemented to an adaptive modeling and simulation environment for the combined cycle system. In this integrated environment, the performance engineer first builds the

plant-specific heat balance model using the commercial software such like GateCycle^{TM}, and specifies the subsystem boundaries according to the measurement availability and redundancy. Once determine the measurement uncertainties from the prior belief, the integrated modeling and simulation is then engaged to perform simultaneous data reconciliation and model calibration. By doing so, the model is calibrated in a probabilistic way, from which one can get the tuned performance correction factors based on the reconciled data. The gross error detection techniques are engaged when the test statistics for the first run of *SDRMC* indicates the occurrence of gross errors. The gross error detection scheme ensures the model is calibrated with the least smearing effects caused by gross errors. Figure 3-4 shows the process map of the integrated modeling and simulation environment. The flow chart of the *SDRMC* process is given in Fig. 3-5.

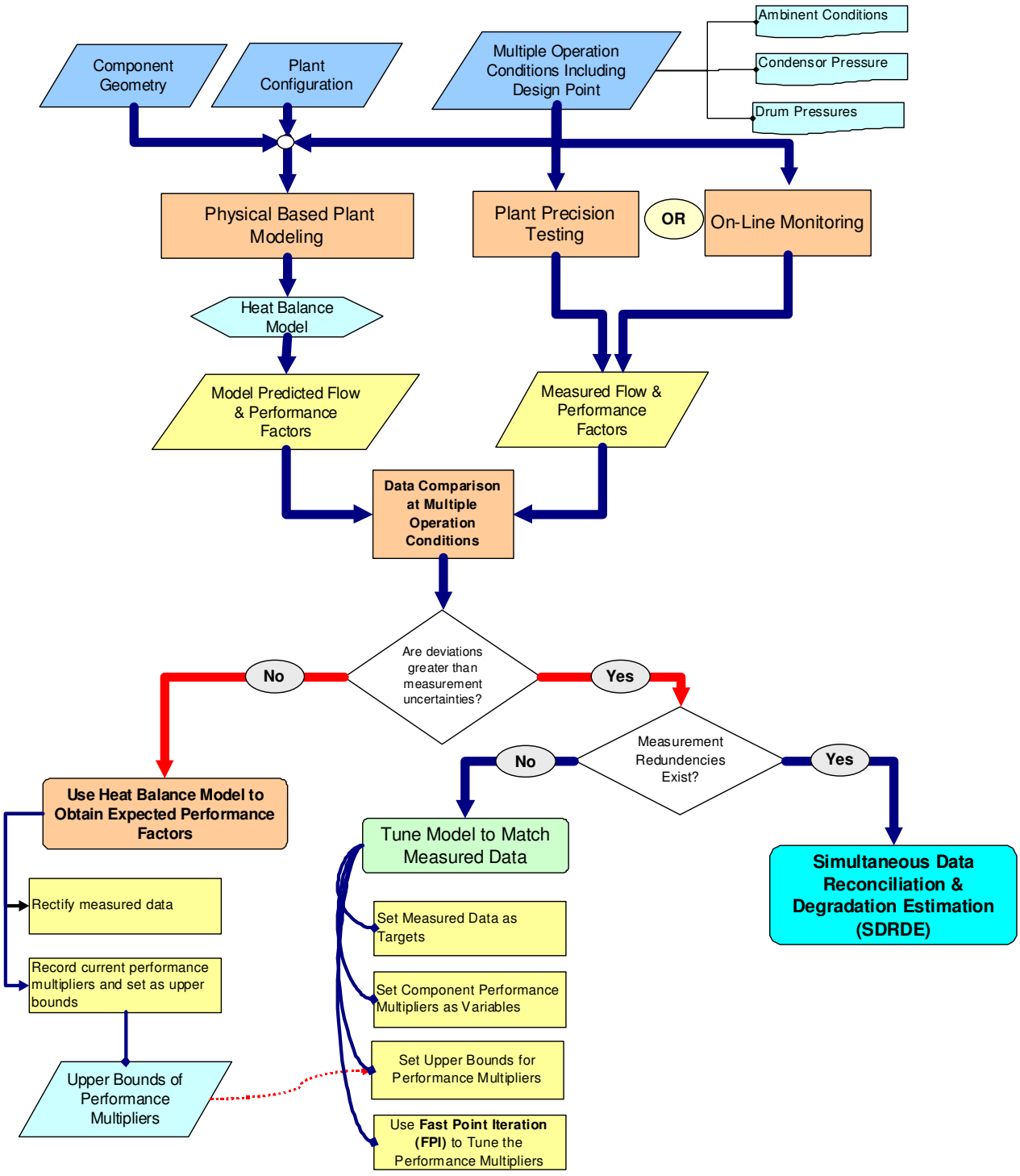

Figure 3-4: Integrated M&S environment for a complex system

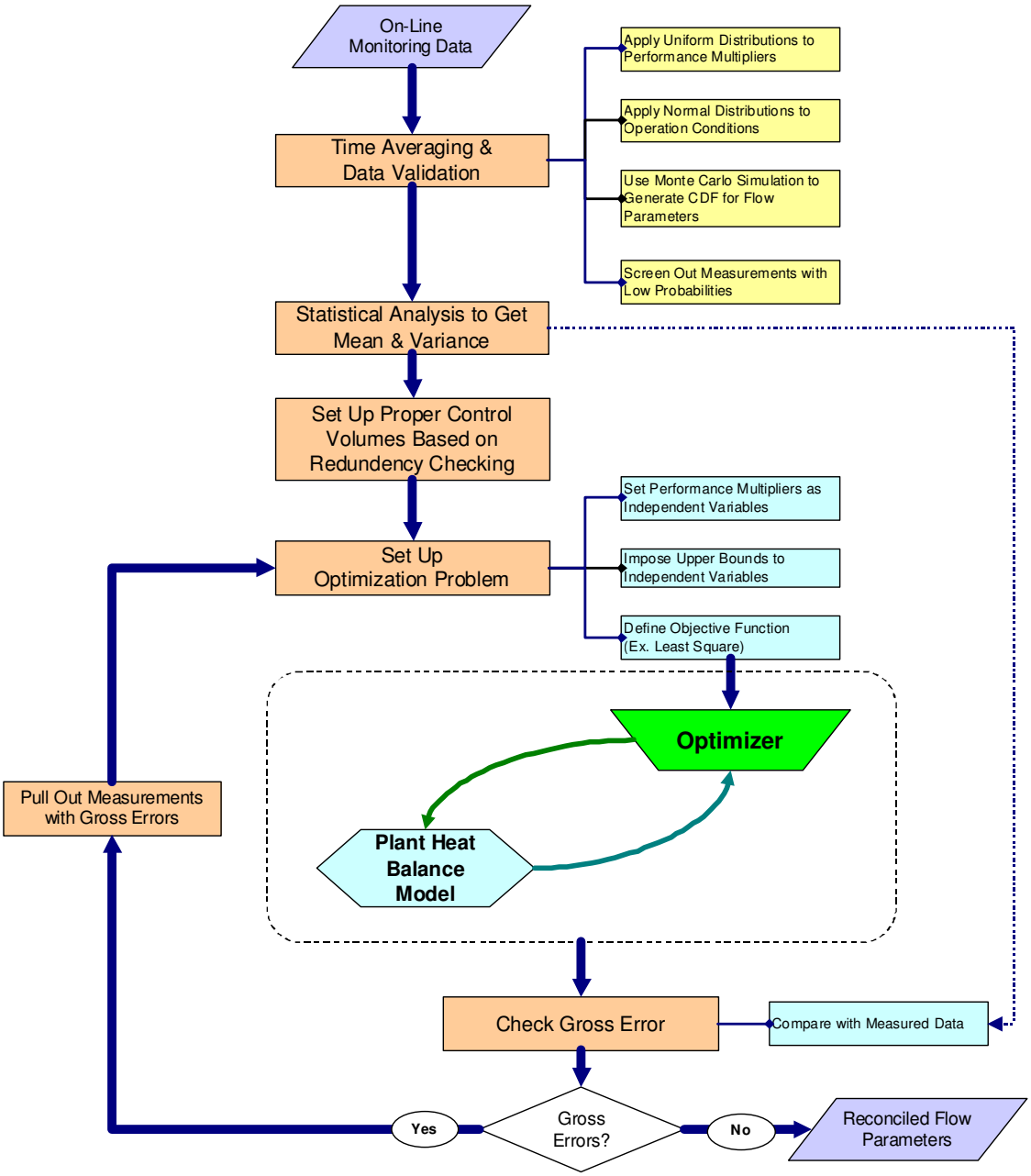

Figure 3-5: SDRMC process map

CHAPTER 4

MODEL BASED DATA RECONCILIATION

The quality of measurement data is crucial to the inference of model parameters as well as to the model based on-line optimization of power system performance. Apart from on-line monitoring and optimization for power system performance, the off-line power system degradation estimation and root-cause-analysis (RCA) also rely on the quality of measurement data. Measurement data always contain both random errors and gross errors due to uncertainties and instrument failure. The random errors are mainly from instrument inaccuracies caused by uncertainties on the part of the manufacturers of the equipment, and they are often tabulated by vendors or estimated through statistical analysis based on historical measured data. The cause of gross errors can be from different reasons such as the wrongly chosen sensor locations or miss-calibration of instruments.

Data reconciliation is a process of filtering out the random errors by either non model-based or model-based techniques. The most widely used techniques for data reconciliation are model-based types, in which the adjustments to the measured data lead to residual-free material and energy balances. In this type of data reconciliation, the measured data are optimally adjusted so that the conservation laws and other physical constraints are satisfied [51]. In chemical engineering, the analysis of model-based data reconciliation was first published by Kuehn and Davidson [52]. The application of data reconciliation to industry processes has also been reported [53~56].

The other type of model-based data reconciliation utilizes the performance simulation model, which generates simulated data sets that automatically satisfy the material and energy balances at off-design conditions for any specific system status. In this type of data reconciliation process, the model parameters are adjusted such that the

likelihood of observing the measurements is maximized, and, therefore, data reconciliation and model parameter estimation, i.e., model calibration, are carried out simultaneously. This type of data reconciliation is similar to Error-in-Variables Estimation (EVM). The application of EVM to industry process has been published in past decades [57~59]. The occurrence of gross errors is much less frequent than random errors, but they cause smearing effects on data reconciliation and model calibration. To mitigate smearing effects, gross error detection and elimination can be performed simultaneously with data reconciliation and model calibration or carried out as an outer loop process with data reconciliation and model calibration executed in an inner loop.

4.1. Maximum Likelihood Principle

The maximum likelihood method was introduced by Fisher [60]. It has been used in a wide range of applications such as regression analysis, model discrimination, and parameter estimation. The maximum likelihood principle states that the model parameters should be chosen so as to make the likelihood of observing the experimental data appear to be the highest. A specific form of the probability density function that represents the parent population of experimental observations is required in the application of the maximum likelihood principle. The Gaussian distribution, or normal distribution, has been known to be the form that closely approximates the parent population for most types of measurements. For a Gaussian distribution the corresponding multivariate joint probability density function is given by:

$$P_i(x'_i - x_i) = \frac{1}{\sqrt{2\pi}\left|\sigma_i\right|^{1/2}} \exp\left\{-\frac{1}{2}(x'_i - x_i)^T \beta_i^{-1}(x'_i - x_i)\right\} \tag{4-1}$$

The function P_i gives the probability of making an observation x'_i for a given mean x_i and σ_i. The mean x_i represents the true value for a target to be measured and is an unknown variable, which is to be estimated during the maximum likelihood application. σ_i is a $M \times M$ variance-covariance matrix for the measured data, which is categorized by

the measurement instruments and is provided initially by manufactures or through the multivariate analysis on the data. The off-diagonal element of σ_i is the covariance of a pair of measurement variables. Most of the time the correlations between pairs of measurements are zero, and, thus, the off-diagonal elements of σ_i are assumed to be zero in most applications.

If the experimental observations are made independently, the likelihood function for all experimental observations can be formulated as the product of their corresponding probability density functions:

$$L(\mathbf{X}', \mathbf{X}, \theta) = \prod_{i=1}^{N} P_i(x'_i, x_i) \tag{4-2}$$

$\boldsymbol{L}$ is the likelihood function, i.e., the probability of observing all the measurement data $\mathbf{X}'$ for the unknown means $\mathbf{X}$ of parent populations, which is determined by the model parameters θ. It is obvious that the likelihood function reaches the maximum when the estimated mean x_i coincides with the measured value x_i'. But this is usually not the solution since the measurements are, most of the time, not able to satisfy the model constraints, i.e., thermodynamic consistency. The search of the solution, i.e., the model parameters, is, therefore, an optimization procedure with $\boldsymbol{L}$ as an objective function subject to model constraints. The basic assumption of the maximum likelihood principle says that the set of measurements observed is the most likely set. Thus, the best estimates of the model parameters and the true values, which are functions of the estimated parameters, are those maximizing the likelihood function subject to the model constraints.

By taking the natural logarithm of equation (4-2) and then substituting the probability density function assumed in equation (4-1), one obtains a form of objective function that is more conveniently solved:

$$\ln L = \ln\left[\frac{1}{\sqrt{2\pi}^{NM}}\prod_{i=1}^{N}\left(\frac{1}{\left|\sigma_i\right|^{1/2}}\right)\right] - \frac{1}{2}\sum_{i=1}^{N}(x'_i - x_i)^T \sigma_i^{-1}(x'_i - x_i) \qquad (4\text{-}3)$$

Maximizing equation (4-3) is equivalent to minimizing the parameter χ^2 in equation (4-4) subject to the model constraints.

$$\chi^2 = \sum_{i=1}^{N}(x'_i - x_i)^T \sigma_i^{-1}(x'_i - x_i) \qquad (4\text{-}4)$$

Equation (4-4) is also seen as a goodness-of-fit function.

The task of finding the optimum fit to the measurement data will be to find the values of θ that minimizes the weighed sum of the squares of the deviations, χ^2 and, hence, to find the optimum model parameters that lead to the smallest sum of the squares or the *least-squares* fit. The value of χ^2depends on the following factors:

1. Uncertainties of the measurement data x_i', which are random samples from a parent population with expectation values x_i.
2. The values of uncertainties σ_i assigned to the measurement data x_i'. Incorrect assignment of σ_i leads to incorrect values of χ^2.
3. The selection of model, which provides analytical functions for x_i as approximations to "true" values.
4. The model parameters θ, which are to be found during the solution searching process.

The least-squares function shown in equation (4-4) will not be valid if the assumption of no correlations between measurements is not true or if the probability density function selected to represent the parent population of the measurement data is not the Gaussian distribution. Although different types of probability density functions lead to different forms of likelihood functions, most of them can be further simplified to convenient forms for solving. For the case where correlated measurements exist, a direct maximum likelihood method is required.

4.2. Model Based Data Reconciliation

When the measured data are reconciled to be thermodynamically consistent based on the physical based model, e.g., heat and mass balances, it is categorized as model based data reconciliation. Model based data reconciliation always results in thermodynamically consistent data for any thermodynamic system. The system model imposes constraints on the optimizer during the reconciliation process where an objective function defined based on the maximum likelihood principle is being minimized. The physical based model can be either heat-and-mass balance equations or the performance simulator, which can provide off-design performance simulations, e.g., the commercial heat balance solver such as GateCycle™.

When heat-and-mass balance equations are utilized, the measured data are reconciled for the system in a specific condition and degradation status. The unmeasured system parameters are estimated during the reconciliation process as well. There are usually no common model parameters, i.e., model parameters that represent certain degradation status and remain constant regardless of changes in operation conditions, being involved in this type of reconciliation problem. However, the reconciled data can be later used to infer model parameters in the performance simulation model.

When the performance simulator is utilized, model based data reconciliation becomes a process of simultaneous data reconciliation and model calibration, in which the model parameters are "tuned" to represent the current system status, e.g., the performance multipliers. Most of the model parameters are common factors used to calibrate the model so as to predict the off-design performance at varied operation conditions. At the end of reconciliation process, the measured data are reconciled by the simulated data from the performance simulator while the model parameters are inferred through the reconciliation process as well. The uncertainties of estimates can be reduced if more data sets are introduced into the process.

4.2.1. Data Reconciliation by Closing Heat and Mass Balance

The heat and mass balance of a thermodynamic system is a universal principle for validating the measurement data. A set of thermodynamically consistent data results in residual-free heat and mass balance equations. Substituting the measured data into balance equations usually causes residuals on the right hand sides (RHS) of equations due to measurement errors. Model based data reconciliation is, therefore, a process of rectifying the data to "close" the heat and mass balance, i.e., residual-free on the RHS. An example of the heat and mass balance equations for a mixer is given as follows:

$$\begin{aligned} &Mass\,balance: && m_1 + m_2 - m_3 = 0 \\ &Energy\,balance: && m_1 h_1(P_1, T_1) + m_2 h_2(P_2, T_2) - m_3 h_3(P_3, T_3) = 0 \end{aligned} \tag{4-5}$$

Due to measurement errors, substituting the measurement data into equation (4-5) causes non-zero residuals on the RHS of equation (4-5).

A more general form of the energy and mass balance for any thermodynamic system can be expressed as:

$$AX = 0 \tag{4-6}$$

where $\boldsymbol{A}$ is a $m \times n$ matrix representing the heat and mass balance of a thermodynamic system, and $\boldsymbol{X}$ is a column vector of a set of thermodynamically consistent data. More generally, $\boldsymbol{A}$ can represent any model constraint that describes the system. When replacing the thermodynamically consistent data with the measurement data (represented by a column vector $\boldsymbol{X}'$), the measurement errors cause residuals on the RHS of equation (4-6):

$$AX' = \varepsilon \tag{4-7}$$

where $\boldsymbol{\varepsilon}$ is a column vector of residuals from corresponding model constraints.

Each measured data in the heat and mass balance equations contributes its error to the total balance error. The total heat and mass balance error can be estimated by using the error propagation principle, through which the balance error is evaluated based on the

measurement uncertainties and on model sensitivities to input variables. The error propagation principle is given as follows:

$$u_{\varepsilon_j} = \sqrt{\sum_{i=1}^{n}\left(\frac{\partial \varepsilon_j}{\partial x_i} u_{x_i}\right)^2} \tag{4-8}$$

The heat and mass balance error ε_j is obtained by substituting the measured data into the model constrains:

$$\varepsilon_j = f_j(x_i) \tag{4-9}$$

where x_i is the measurement, f_j is the jth heat and mass balance equation, and ε_j represents the balance error in the jth balance equation.

A more rigorous expression for the error propagation principle that takes the correlations between the constraint residuals into account is given as:

$$E = A^T V A \tag{4-10}$$

where $\boldsymbol{V}$ is the variance-covariance matrix of the measurement data, constructed based on instrumental uncertainties; $\boldsymbol{E}$ is an n×n variance-covariance matrix for the correlated constraint residuals, and it can be expressed as:

$$E = \begin{bmatrix} \mathrm{cov}(\varepsilon_1,\varepsilon_2) & . & . & . & \mathrm{cov}(\varepsilon_1,\varepsilon_n) \\ . & . & & & . \\ . & & . & & . \\ . & & & . & . \\ \mathrm{cov}(\varepsilon_n,\varepsilon_1) & . & . & . & \mathrm{cov}(\varepsilon_n,\varepsilon_n) \end{bmatrix} \tag{4-11}$$

where $\mathrm{cov}(\varepsilon_i, \varepsilon_j)$ represents the covariance between the ith and jth constraint residuals defined by:

$$\mathrm{cov}(\varepsilon_i,\varepsilon_j) = \frac{\sum_{k=1}^{m} (\varepsilon_i)_k (\varepsilon_j)_k}{m-1} \tag{4-12}$$

By applying the maximum likelihood principle and imposing the model constraints such as energy and mass balances the data reconciliation problem can be formulated as a

nonlinear constrained optimization problem where the nonlinearity arises mainly from model constraints:

$$\min_{x_i} \sum_{i=1}^{N} (x'_i - x_i)^T \sigma_i^{-1} (x'_i - x_i)$$
$$s.t. AX = 0 \tag{4-13}$$

The solution to the data reconciliation problem is the set of mean values, x_i, that satisfy the model constraints and minimize the least squares objective function, i.e., maximize the likelihood of observing the measurement data x_i. Equation (4-13) shows that the weight factor for each measurement is inversely proportional to the standard deviation of its error. Since a larger value of standard deviation implies the measurement is less accurate, it gives a relatively smaller weight to the objective function, and, thus, gives larger weights to more accurate measurements. There is an advantage of using the least squares objective function shown in equation (4-13) because of its dimensionless feature since the standard deviation of a measurement error has the same unit as the measurement.

Equation (4-13) can be solved by an iterative scheme based on the *Lagrangian* and *Kuhn-Tucker* conditions [61]. The *Lagragian* is defined as:

$$\zeta(X, \lambda) = \sum_{i=1}^{N} (x'_i - x_i)^T \sigma_i^{-1} (x'_i - x_i) + \sum_{j=1}^{M} \lambda_j (AX)_j \tag{4-14}$$

The *Kuhn-Tucker* necessary conditions for $\boldsymbol{X}^*$ to define the optimum are:

$$AX^* = 0$$

and (4-15)

$$\nabla_{x_i} \sum_{i=1}^{N} (x'_i - x_i^*)^T \sigma_i^{-1} (x'_i - x_i^*) + \sum_{j=1}^{M} \lambda_j^* \nabla_{x_i} (AX)_j$$

Based on the *Lagrangian* and *Kuhn-Tucker* conditions, the reconciled values x_i can be obtained through an iterative scheme given by:

$$X^* = X' - \sigma A^T (A\sigma A^T)^{-1} A\, X' = [I - \sigma A^T (A\sigma A^T) A]\, X' = BX' \tag{4-16}$$

Equation (4-16) shows the reconciled data are obtained through linear transformations of the measured data, and, therefore, are subject to estimate uncertainties caused by the measurement errors. The reconciled data represent the expected mean values of the parent populations, given by:

$$E[X^*] = BE[X'] = BX = X \tag{4-17}$$

The corresponding covariance matrix is then calculated by the following equation:

$$\mathrm{Cov}(X) = B\sigma B^T \tag{4-18}$$

4.2.2. Serial Constrain Linearization with Explicit Model Constraints

The model constrains can be rearranged to explicit forms where some variables become dependent and are functions of the rest of the variables. For instance, the implicit energy and mass balance equations shown in equation (4-5) can be rearranged to explicit forms as shown below:

$$\begin{aligned} &Mass\,balance: && m_3 = m_1 + m_2 \\ &Energy\,balance: && h_3(P_3, T_3) = \frac{m_1 h_1(P_1, T_1) + m_2 h_2(P_2, T_2)}{m_3} \end{aligned} \tag{4-19}$$

In the explicit forms of energy and mass balance equations the mass and enthalpy of the mixed flow become functions of the other variables. A more general expression is given as follows:

$$Y = f(X, \theta) \tag{4-20a}$$

$$Z = g(X, \theta) \tag{4-20b}$$

Y and Z represent two of the variables that become dependent after rearrangement. If n duplicated measurements are available, Y and Z become column vectors with n elements. X represents an $n \times k$ matrix for the rest variables seen as independent. The objective function to be minimized then can be rewritten in terms of the dependent and independent variables. By assuming the off-diagonal elements in the variance-covariance matrix of

measurement uncertainties are all zeros, the least squares objective function can be rewritten as:

$$S = (X^{'} - X)^T \sigma_x (X^{'} - X) + (Y^{'} - Y)^T \sigma_y (Y^{'} - Y) + (Z^{'} - Z)^T \sigma_z (Z^{'} - Z) \quad (4\text{-}21)$$

By substituting equation (4-20a) in to (4-20b), the least squares objective function becomes a function of X and θ. The necessary condition of finding the optimum solution requires:

$$\begin{aligned} \frac{\partial S}{\partial X} &= 0 \\ \frac{\partial S}{\partial Y} &= 0 \end{aligned} \quad (4\text{-}22)$$

Since equation (4-20a) and (4-20b) are usually nonlinear, one can use first-order Taylor's series expansions for linearization. The linearized model constraints can be expressed in explicit forms:

$$Y^{r+1} = f(X, \theta) \approx f^r + f_x (X^{'} - X) + f_\theta (\theta - \theta^r) \quad (4\text{-}23)$$

and

$$Z^{r+1} = g(X, \theta) \approx g^r + g_x (X^{'} - X) + g_\theta (\theta - \theta^r) \quad (4\text{-}24)$$

The function f^n and g^n represent the function values of Y and Z at the previous iteration r. f_x and g_x are sparse $n \times nk$ Jacobian matrices of the two explicit model constraints with respect to the independent variables. Similarly, f_θ and g_θ are sparse $n \times l$ Jacobian matrices with respect to the model parameters. The linearized constraint equations can be substituted into Equation (4-21) and become:

$$\begin{aligned} S = {} & (X^{'} - X)^T \sigma_x (X^{'} - X) + (Y^{'} - f^r - f_x (X^{'} - X) - f_\theta (\theta - \theta^r))^T \sigma_y (Y^{'} - f^r - f_x (X^{'} - X) - f_\theta (\theta - \theta^r)) \\ & + (Z^{'} - g^r - g_x (X^{'} - X) - g_\theta (\theta - \theta^r))^T \sigma_z (Z^{'} - g^r - g_x (X^{'} - X) - g_\theta (\theta - \theta^r)) \end{aligned} \quad (4\text{-}25)$$

When the necessary conditions (4-22) for the minimum S are applied, it becomes:

$$\begin{aligned} & \sigma_x (X^{'} - X^{r+1}) + f_x^T \sigma_y (Y^{'} - f^r - f_x (X^{'} - X^{r+1}) - f_\theta (\theta^{r+1} - \theta^r)) \\ & \quad + g_x^T \sigma_z (Z^{'} - g^r - g_x (X^{'} - X^{r+1}) - g_\theta (\theta^{r+1} - \theta^r)) = 0 \end{aligned} \quad (4\text{-}26)$$

and

$$f_\theta^T \sigma_y (Y^{'} - f^r - f_x (X^{'} - X^{r+1}) - f_\theta (\theta^{r+1} - \theta^r))$$

$$+ \; g_\theta^T \sigma_z (Z' - g^r - g_x (X' - X^{r+1}) - g_\theta (\theta^{r+1} - \theta^r)) = 0 \tag{4-27}$$

In these $nk + l$ linear equations, one first solves for $(X' - X^{r+1})$ in Equation (4-26) and substitutes the expression into equation (4-27), by which the solution for $(\theta^{r+1} - \theta^r)$ can be obtained. By solving equations (4-26) and (4-27), the solutions for X^{r+1} and θ^{r+1} can be summarized as follows:

$$\Delta \theta = \theta^{r+1} - \theta^r = - [T - R^T D^{-1} R]^{-1} [U - R^T D^{-1} Q] \tag{4-28}$$

$$\Delta X = X^{r+1} - X^r = -D^{-1} [Q + R \Delta \theta] \tag{4-29}$$

where

$$D = \sigma_x + f_x^T \sigma_y f_x + g_x^T \sigma_z g_x \tag{4-30a}$$

$$R = f_x^T \sigma_y f_\theta + g_x^T \sigma_z g_\theta \tag{4-30b}$$

$$T = f_\theta^T \sigma_y f_\theta + g_\theta^T \sigma_z g_\theta \tag{4-30c}$$

$$U = f_\theta^T \sigma_y \Delta Y' + g_\theta^T \sigma_z \Delta Z' \tag{4-30d}$$

$$Q = \sigma_x \Delta X' + f_x^T \sigma_y \Delta Y' + g_x^T \sigma_z \Delta Z' \tag{4-30e}$$

where

$$\Delta X' = X' - X^r \tag{4-31a}$$

$$\Delta Y' = Y' - Y^r \tag{4-31b}$$

$$\Delta Z' = Z' - Z^r \tag{4-31c}$$

Equation (4-28) and (4-29) are the basis for the constraint linearization algorithm used to find the optimum solutions of X and θ that maximize the likelihood of measurement observations. The Jacobian derivatives of f_x, f_θ, g_x, and g_θ are evaluated at every iteration and substituted into equations (4-28) and (4-29) to obtain the adjustments ΔX and $\Delta \theta$, which are then added to previous X and θ for the next iteration updates. The need for the iterative scheme is due to the nonlinearity in the model constraints, e.g., equations of energy conservations. Since the Jacobian derivatives change with the solutions at each iteration, which are updated iteratively during the data reconciliation process, the iteration continues until the adjustments to the solutions are within the specified

tolerances. When data reconciliation is applied to a linear model such as mass balances, the iterative process is not required because of the constant Jacobian derivatives.

The convergence property of this scheme is similar to the Newton method where a good initial guess of the true values for the estimates are required. When a good starting point is used, it converges rapidly. On the other hand, a poor initial guess can cause very slow convergence or even divergence. With a good initial guess, this method poses no serious problems except for the manipulation of a considerably large matrix especially when multiple data sets are applied. This cumbersome task can be facilitated by the Gaussian-Jordan elimination or any symmetric matrix inversion procedure. Good initial estimates for model parameters are more difficult determined compared to measurement data. Most of the time the task relies on previous experience and judgment. To insure convergence at any initial estimate, a step-limit for a given direction of correction, i.e., the gradient, can be applied. The procedure is set to choose the directions of ΔX and $\Delta \theta$ that decrease the value of linearized least squares objective function. The magnitudes of the corrections, ΔX and $\Delta \theta$, are decreased until the new value of least squares is less than the previous one. If it appears that the direction of correction is perpendicular to the valley, the magnitude of the correction is further decreased.

4.2.3. Data Reconciliation Using Performance Simulator

When a thermodynamic system is represented by energy and mass balance equations, the system modeling is under the *heat balance mode*, whereby the system performance in different operation conditions cannot be obtained until the measurement data are given. If, however, system modeling is carried out by the performance simulator, sized based on given configuration and surface areas, one can obtain off-design performance at any operation condition, i.e., performance at non-design operation conditions. To provide off-design performance analyses, it is necessary to calculate the off-design performance for each system component based on its layout and geometry. In

addition, an outer loop subroutine that enforces the energy and mass balances among system components is required.

When running the off-design performance simulation, energy and mass balances are enforced by the solver at the outer loop. Therefore, the system performance only depends on model parameters such as operation conditions and performance scaling factors (or performance multipliers). The performance scaling factors are used to calibrate the model to fit the measurement data and capture system current degradation status. By running the off-design performance simulation, one can generate any data set not only satisfying energy and mass balances but also reflecting the degradation status at the given operation condition.

In the off-design mode under any specific operational condition and degradation status the simulated data satisfy energy and mass balances and, therefore, become a candidate of the data reconciliation solution. The simulated data set can be expressed as follows:

$$y_j = f(\theta_i) \tag{4-32}$$

where y_j and θ_i represent the model simulated data and the model parameters, respectively. The function f can be seen as a *black box* that carries out the off-design performance simulation. The final solution is determined by the maximum likelihood principle. From this the optimization problem can be formulated:

$$\chi^2 = \sum_{j=1}^{N} (y'_j - y_j)^T \sigma_i^{-1} (y'_j - y_j) \tag{4-33}$$

where y'_j and y_j represent the measurement data and the corresponding simulated data. Substituting equation (4-32) into (4-33) and applying the maximum likelihood principle, one can formulate the optimization problem for data reconciliation as follows:

$$\min_{\theta_i} \sum_{j=1}^{N} (y'_j - f(\theta_i))^T \sigma_j^{-1} (y'_j - f(\theta_i)) \tag{4-34}$$

Unless it is required to set constraints to the model-simulated data $f(\theta_i)$, the optimization problem in (4-34) is actually an unconstrained nonlinear optimization problem, which can be solved by any nonlinear programming (NLP) solver.

According to the least squares method, the optimum values of the parameters θ_i are obtained by minimizing χ^2 simultaneously with respect to each parameter:

$$\frac{\partial x^2}{\partial \theta_i} = \frac{\partial}{\partial \theta_i} \sum \left\{ \frac{1}{\sigma_j^2} [y'_j - y_j(\theta_i)] \right\} = -2 \sum \left\{ \frac{1}{\sigma_j^2} [y'_j - y_j(\theta_i)] \frac{\partial y_j(\theta_i)}{\partial \theta_i} \right\} = 0 \quad (4\text{-}35)$$

By taking partial derivatives of χ^2 with respect to each of the n parameters θ_i, one can yield n coupled equations with n known parameters θ_i. If these equations are nonlinear with respect to parameters θ_i, it is required to treat χ^2 as a function of the n parameters, which can be described by a hyper-surface in an n-dimensional space.

Simultaneous data reconciliation and model calibration is similar to the nonlinear fitting problem and sometimes seems to be more of an art than a science due to the fact that by nature it is an approximation process. The speed of convergence for this process depends on the method chosen to find the solution, which includes the starting point (initial guess), and the step size utilized to update the solution per iteration. Any of the methods used to find the optimum solution of a nonlinear problem requires the starting values for the initial calculation of the model values and of the chi-square function. For the pure search methods, the step sizes and initial values are both required. On the other hand, if the model is linear, neither starting values nor step sizes are needed because the partial derivatives are constant for each iteration.

The existence of multiple solutions or of a local minimum is another issue for nonlinear data reconciliation and parameter estimation. For an arbitrary function there may have to be more than one local minimum for the chi square function within reasonable ranges of parameters. A poor initial starting point may drive the solver to pick the solution of a local minimum rather than of the absolute minimum that is sought. It is therefore useful to explore the design space of the model parameters and determine

reasonable ranges for the parameters where a better starting point can be located. A very simple and convenient way is to make several plots of the model predicted values versus real data. By visual inspection one can tune the model and have an idea of where the starting point should be. But for the case where the number of model parameters is large and the model responses are highly correlated, it becomes more difficult to determine the starting point by just using a visual inspection and manually tuning the model.

A more systematic way for data reconciliation is to create a map of the chi-square, χ^2, with respect to the model parameters. The mapping procedure can be carried out with equally divided permissible ranges for parameters where the chi-square is evaluated at the vertices of each hypercube. The mapping procedure yields a coarse map of the behavior of chi-square as a function of the model parameters θ_i. One can then determine the starting point by looking at the vertex where the value of chi-square is the smallest among others. A fined grid can be further used to get a better resolution. This procedure is only practical for the model with two or three parameters. It becomes more tedious and cumbersome when the dimension of the problem rises. To solve the model with large dimensionality, a Monte Carlo technique can be utilized. The values of the model parameters are generated randomly from the corresponding mother populations with the presumed uniform distributions and reasonable ranges. After hundred to thousand trials, the trial values of model parameters that lead to the lowest chi-square value can be selected as a starting point. If the computation expense is not a problem for the nonlinear data reconciliation and parameter estimation, one can carry out the search by moving from one local minimum to another until the absolute minimum is found. This requires several runs of nonlinear data reconciliation and parameter estimation at different starting point. In general, for the high dimensionality problem, the Monte Carlo is the most convenient way to search the starting point.

When multiple local minimums exist, a poor starting point may drive the solutions to a local minimum and may also lead to physically unreasonable solutions. If

the starting point that has been carefully selected still causes unreasonable solutions, proper bounds needs to be imposed to the model parameters to ensure the solutions are within reasonable ranges after data reconciliation. Once the bounds are imposed, care must be taken that the final solution of any parameter is not one of the bounds artificially added. If some of the final solutions hit the bounds after data reconciliation, the cause should be investigated and the bounds released.

The step size of solution searching also has a crucial impact on the convergence. Usually, a smaller step size slows down the speed of convergence but it results in better solutions close to the absolute minimum. On the other hand, a larger step size makes a faster convergence with the penalty of overshooting the minimum and the need for readjustment. The choice of step sizes should depend on the parameters and the sensitivity of the chi square χ^2 to the parameters. For instance, the parameter to which the chi square χ^2 is less sensitive should be assigned to a larger step size and vice versa.

Once the starting point and step sizes of the model parameters are decided carefully, one should expect the search for solutions is headed in the right direction. The convergence criteria should be defined so that the procedure is terminated properly. The convergence condition can be defined as ε % change in χ^2 per degree of freedom (dof) ($\Delta\chi^2$/dof). The choice of ε ranges from 0.1~0.001, depending on the hypersurface of χ^2 with respect to the model parameters. If the starting point is not selected carefully and leads to the local minimum located in a very flat valley in the parameter space, one should choose different starting values and rerun the process again. To carry out a nonlinear data reconciliation and parameter estimation properly, therefore, relies on the choice of the search method, i.e., the optimization algorithm, a good starting point, proper step sizes of searching, and the cut-off criteria, all of which are related to the behavior of the objective function with respect to the model parameters and, therefore, should be decided accordingly.

There are different types of physical based models being utilized in the model based data reconciliation. These models are either linear or nonlinear functions of the model parameters depending on how the thermodynamic system is described. For the heat-balance-type models, the energy equations are the major source of nonlinearity, and very few common factors need to be determined during the reconciliation process. Because the heat-balance-type models are not highly nonlinear due to the properties of mass and energy balances, the method of serial constraint linearization is a good candidate for solving this kind of reconciliation problem. In the heat-balance-type data reconciliation problem, the expected means of the measurement data are the major independent variables to be solved. Therefore, the measurement data are good starting point candidates. In addition, there is no need to specify the step size for updating the solution since it has been determined automatically by the matrix manipulation in the constraint linearization scheme.

If a performance simulator is introduced as a physical model into the data reconciliation problem, the behavior of the chi square objective function becomes highly nonlinear because the chi square objective function is now embedded with the explicit model functions, $y_j(\theta_i)$, which themselves are also nonlinear. Since the problem is transformed into the nonlinear unconstrained type, instead of using serial constraint linearization technique, one can utilize a similar successive linearization technique for the hyper-surface of the chi square objective function or for the model functions, and search for the optimum solution in an iterative way. The successive linearization scheme requires to approximate analytical forms for the chi square objective function χ^2 or the model functions $y_j(\theta_i)$. Although the approximation to the chi square function or the model functions will introduce the errors to the estimated model parameters one can, however, approach the true minimum of the χ^2 function with increasing accuracy by means of successive iterations. The main advantage of this approach is that the number of function evaluation for the chi square objective function is fewer when compared to the

grid search or the gradient-based method. The advantage is, however, penalized by the need for good starting point without which the process may diverge or lead to local minimums, and by the fact that the computations at each point become more complicated due to the matrix manipulation.

Techniques that directly search the chi-square hyper-surface to map the variation of chi-square with respect to the model parameters such as the non-gradient-based and gradient-based techniques are also available. The non-gradient-based method such as grid search needs a large amount of function evaluations of the chi-square function, χ^2. Thus, this approach is only suitable for the problem with 2~3 model parameters and for a problem with a physical model that does not need considerable computation time. On the other hand, the gradient-based method needs a nonlinear programming algorithm, i.e., the optimizer, by which the search direction is determined based on the derivative of chi-square with respect to the model parameters.

4.2.4. Gradient Method

The search for minimum chi-square can be carried out with the gradient search method in which the solutions of each iteration are updated based on the gradient of chi-square. The gradient, $\nabla\chi^2$, is a vector constructed by the space of function parameters θ_i where each vector element is equal to the rate of change of χ^2 along each axis:

$$\nabla\chi^2 = \sum_{i=1}^{n} \frac{\partial\chi^2}{\partial\theta_i}\hat{\theta}_i \tag{4-36}$$

where $\hat{\theta}_i$ is the unit vector in the direction of the θ_i coordinate. Therefore, the gradient $\nabla\chi^2$ is toward the direction where the function χ^2increases most rapidly. If the gradient $\nabla\chi^2$ is evaluated numerically in the following way:

$$\left(\nabla\chi^2\right)_i = \frac{\partial\chi^2}{\partial\theta_i} \cong \frac{\chi^2(\theta_i + \Delta\theta_i) - \chi^2(\theta_i)}{\Delta\theta_i} \tag{4-37}$$

then one can define a dimensionless gradient $\boldsymbol{\eta}$ with an unit magnitude:

$$\eta_i = \frac{\partial \chi^2 / \partial \hat{\theta}_i}{\sqrt{\sum_{i=1}^{n} \left(\partial \chi^2 / \partial \hat{\theta}_i \right)^2}} \tag{4-38}$$

where

$$\hat{\theta}_i = \frac{\theta_i}{\Delta \theta_i} \tag{4-39}$$

If the gradient search method follows the steepest descent way, the solution per iteration is then updated by:

$$\delta \theta_i = -\eta_i \Delta \theta_i \tag{4-40}$$

The iterative process of solution updates continues until the increments of parameters $\delta \theta_i$ are within the specified tolerance. The main disadvantage of the steepest descent method is the difficulty of approaching the minimum when it is close to a solution due to the tendency of overshooting the true minimum. The other disadvantage is the inefficiency in the search when the evaluation of gradient is using a small step size. One can modify the steepest descent method by searching along one direction of the original gradient in small steps, and calculating the value of chi-square until its value begins to rise again. Then the gradient is recalculated, and the search continues in the new direction. When the search continues to a point expected to get close enough to the true minimum, a parabolic approximation to the chi-squares can be utilized to improve the location of the minimum.

The efficiency of the gradient search method deteriorates dramatically when the iterative solutions are close to the true solutions due to the fact that the difference between the function values are very small over a small step size. One can switch to the expansion method when the search is approaching the minimum.

4.2.5. Expansion Methods

In the expansion methods, the chi-square or the model function $y_j(\theta_i)$ is approximated by a Taylor's expansion series. The solutions are obtained through a successive linearization technique where the accuracy of the approximation to the true minimum is improved with each successive iteration.

Parabolic Expansion of χ^2

The chi square objective function χ^2 can be expanded to second order with respect to the model parameters about the true minimum χ_0^2:

$$\chi^2 \cong \chi_0^2 + \sum_{i=1}^{n}\left\{\frac{\partial \chi_0^2}{\partial \theta_i}\delta\theta_i\right\} + \frac{1}{2}\sum_{k=1}^{n}\sum_{i=1}^{n}\left\{\frac{\partial^2 \chi_0^2}{\partial \theta_i \partial \theta_k}\delta\theta_i \delta\theta_k\right\} \tag{4-41}$$

This is equivalent to approximating the hyper-surface of χ^2 by a parabolic surface at the true minimum. Here $\delta\theta_i \equiv \theta_i - \theta_i^*$ and the χ_0^2 is given by:

$$\chi_0^2 = \sum\left\{\frac{1}{\sigma_j^2}[y_j - y_j(\theta_i^*)]^2\right\} \tag{4-42}$$

where values of θ_i^* are the expected solutions to the model parameters leading to the true minimum of chi-square. Similar to the serial constraint linearization technique, the necessary condition for minimizing χ^2 is given by:

$$\frac{\partial \chi^2}{\partial \delta\theta_i} = \frac{\partial \chi^2}{\partial \theta_i} \cong \frac{\partial \chi_0^2}{\partial \theta_i} + \sum_{i=1}^{n}\left\{\frac{\partial \chi_0^2}{\partial \theta_i \partial \theta_k}\delta\theta_i\right\} = 0 \tag{4-43}$$

which represents a set of *n* linear equations as functions of $\delta\theta_i$, and can be written as:

$$\beta_i - \sum_{k=1}^{n}(\delta\theta_k \alpha_{ki}) = 0 \tag{4-44}$$

where

$$\beta_i \equiv -\frac{\partial \chi_0^2}{\partial \theta_i} \text{ and } \alpha_{ki} = \frac{\partial^2 \chi_0^2}{\partial \theta_i \partial \theta_k} \tag{4-45}$$

These *n* linear equations can be written in a matrix form given by:

$$\boldsymbol{\beta}=\boldsymbol{\alpha}\boldsymbol{\delta\theta} \tag{4-46}$$

Here $\boldsymbol{\beta}$ is a column vector representing the gradient of the least squares objective function with respect to the model parameter θ_i; $\boldsymbol{\delta\theta}$ is also a column vector, which represents the corrections to the expected solutions for next iteration; $\boldsymbol{\alpha}$ is an n×n symmetric matrix representing the Hessian of the χ^2 hyper-surface.

The optimum solutions for θ_i, can be obtained by the inverse of the Hessian matrix $\boldsymbol{\alpha}$:

$$\boldsymbol{\delta\theta} = \boldsymbol{\alpha}^{-1}\boldsymbol{\beta} \tag{4-47}$$

This is an iterative process, in which the updates to the solutions from previous iterations are calculated by equation (4-47) for each iteration. The process continues until the artificially assigned cutoff criteria is reached, i.e., $\boldsymbol{\delta\theta} < \boldsymbol{\varepsilon}$. Due to the fact that the expansion method requires the parabolic approximation to chi-square about the expected true minimum, the accuracy of approximation deteriorates as the solutions at a specific iteration are far from the true solutions. If the starting point is far away from the true solution, this could cause a convergence problem or lead the solution to a local minimum. In the extreme case where the starting point is so away from the true solution, the Hessian matrix $\boldsymbol{\alpha}$ may become negative and lead the solution toward the direction of maximizing the least squares objective function. To avoid this divergent situation, one should artificially force the diagonal elements of the Hessian matrix $\boldsymbol{\alpha}$ to be the positive values from the previous iteration when they turn negative. By doing so, the sign of the corrections $\boldsymbol{\delta\theta}$ will be correct even thought the magnitudes are not valid.

Expansion of the Explicit Model Function

Instead of expanding the chi square objective function χ^2 with Taylor's series, one can alternatively apply the Taylor's expansion on the model functions $y_j(\theta_i)$ and use the successive linearization technique described in previous section for the chi square expansion to find the minimum value for chi-square and the corresponding optimum solutions for θ_i.

When the model functions are expanded with a Taylor's series to the first order with respect to the parameter increments $\delta\theta_i \equiv \theta_i - \theta_i^*$, the expansions are given by:

$$y_j(\theta_i) \cong y_j(\theta_i^*) + \sum_{i=1}^{n}\left\{\frac{\partial y_j(\theta_i^*)}{\partial \theta_i}\delta\theta_i\right\} \tag{4-48}$$

where $y_j(\theta_i^*)$ represent the function values evaluated at the solutions from the previous iteration *r*; similarly, $\partial y_j(\theta_i^*)/\partial\theta_i$ are the derivatives of model functions at the solutions of the previous iteration. Taylor's 1st order expansion leads to the linearized model functions by which one can apply the maximum likelihood principle to formulate the chi square objective function. By substituting the linearized model functions $y_j(\theta_i)$ into the least squares objective function one can obtain:

$$\chi^2 = \sum\frac{1}{\sigma_j^2}\left\{y_j(\theta_i) - y_j(\theta_i^*) - \sum_{i=1}^{n}\left[\frac{\partial y_j(\theta_i^*)}{\partial\theta_i}\delta\theta_i\right]\right\}^2 \tag{4-49}$$

The minimum can then be obtained by setting the derivatives of chi-square with respect to $\delta\theta_i$ to zeros, i.e., which is the necessary condition for the minimum:

$$\frac{\partial\chi^2}{\partial\delta\theta_i} = \frac{\partial\chi^2}{\partial\theta_i} = -2\sum\left(\frac{1}{\sigma_j^2}\left\{y_j(\theta_i) - y_j(\theta_i^*) - \sum_{i=1}^{n}\left[\frac{\partial y_j(\theta_i^*)}{\partial\theta_i}\delta\theta_i\right]\right\}\frac{\partial y_j(\theta_i^*)}{\partial\theta_i}\right) \tag{4-50}$$

This leads to a set of *n* linear equations to be solved simultaneously, and the matrix form can be utilized and is given by:

$$\boldsymbol{\beta}=\boldsymbol{\alpha}\boldsymbol{\delta\theta} \tag{4-51}$$

where β_i is given by Equation (4-45) and α_{ik} is given as bellows:

$$\alpha_{ik} \cong \sum\frac{1}{\sigma_j^2}\frac{\partial y_j(\theta_i^*)}{\partial\theta_i}\frac{\partial y_j(\theta_i^*)}{\partial\theta_k} \tag{4-52}$$

Since the Jacobian is evaluated about the solutions from previous iteration, its accuracy is improved through an iterative process. The iterative process continues until the specified convergence criterion is reached, i.e., the parameter increments $\delta\theta_i$ are within the

specified tolerance. Similar to the chi square expansion, a good starting point has a crucial impact on the convergence. A poor initial guess can cause a convergence to a local minimum or even a convergence failure. Analytically, the result from the chi square expansion and that from the model function expansions are identical. This is especially true when the model functions have the analytical derivatives available. If the analytical forms of the model functions are not available, the derivative terms $\boldsymbol{\beta}$ and $\boldsymbol{\alpha}$ need to be calculated numerically using a finite difference method, which leads to numerical errors and, thus, deviations between the two methods.

One can further expand the model functions with Taylor's series to a second order with respect to the parameter increments $\delta\theta_i$:

$$y_j(\theta_i) \cong y_j(\theta_i^*) + \sum_{i=1}^{n} \frac{\partial y_j(\theta_i^*)}{\partial \theta_i} \delta\theta_i + \frac{1}{2} \sum_{i=1}^{n} \sum_{k=1}^{n} \frac{\partial^2 y_j(\theta_i^*)}{\partial \theta_i \partial \theta_k} \delta\theta_i \delta\theta_k \tag{4-53}$$

By substituting the expanded model functions into the least squares objective function χ^2 and applying the necessary condition for minimizing χ^2, i.e., setting 0 to the derivatives, one can obtain n equations to be solved simultaneously using the same matrix equations as equation (4-51) with $\boldsymbol{\beta}$ and $\boldsymbol{\alpha}$ shown bellow:

$$\beta_i = \sum \left(\frac{1}{\sigma_j^2} \left(y_j(\theta_i) - y_j(\theta_i^*) \right) \frac{\partial y_j(\theta_i^*)}{\partial \theta_i} \right) = -\frac{1}{2} \frac{\partial \chi_0^2}{\partial \theta_i} \tag{4-54a}$$

$$\alpha_{ik} \equiv \sum \frac{1}{\sigma_j^2} \left[\frac{\partial y_j(\theta_i^*)}{\partial \theta_i} \frac{\partial y_j(\theta_i^*)}{\partial \theta_k} - \left(y_j(\theta_i) - y_j(\theta_i^*) \right) \frac{\partial^2 y_j(\theta_i^*)}{\partial \theta_i \partial \theta_k} \right] = \frac{1}{2} \frac{\partial \chi_0^2}{\partial \theta_i \partial \theta_k} \tag{4-54b}$$

Equation (4-54) shows that the resulting $\boldsymbol{\beta}$ and $\boldsymbol{\alpha}$ are equivalent to those obtained from the chi square expansion. Therefore, the chi square expansion method is identical to the method of model function expansion to the second order.

Comparing these two expansion methods, one can realize that the chi-square expansion to the first order is analytically identical to the model function expansion to the second order. If the derivatives are taken rigorously in the finite differences, i.e., the selections of the intervals $\Delta\theta_i$ are tailored for the two methods such that the propagations

of numerical errors are identical. These two methods will also have identical numerical results. Therefore, the Hessian matrix $\boldsymbol{\alpha}$ obtained from equation (4-52) of the first order expansions for the model functions is actually an approximation to equation (4-54), which is obtained based on the second order expansions and is identical to the chi square expansion to the first order. In finite difference methods, it is known that evaluations of second-order derivatives need more function calls than the first order derivatives, but they result in a more accurate numerical evaluation for the Hessian matrix. The more accurate estimation of the Hessian matrix means less iterations to reach a solution. But it is more convenient to use the first order expansion to approximate the model functions since the calculations of second order derivatives can be avoided. It is preferred to use the first order expansion especially when the function evaluation takes significant time. In most cases, the need for more iterations to reach the minimum in the first order expansion method is suppressed by the saving in the number of function calls. In the case when the analytical forms of the model functions and the corresponding derivatives are available, one should always select the chi square expansion to the first order or the model function expansions to the second order since the numerical evaluations of the derivatives are not necessary.

In summary, when the analytical derivatives for the model functions are not available, the method of model function expansions provides options of first order expansions and second order expansions to the user. One can make the decision to use these methods depending on the computation budget. On the other hand, to use the chi square expansion method, the second order derivatives for the model functions are always needed, which requires more function calls in the numerical evaluation of the finite differences. The following expressions show the forward finite differences for the first order and second order derivatives of a function f with respect to the function parameters θ_i.

$$\frac{\partial f}{\partial \theta_i} \cong \frac{f(\theta_i + \Delta\theta_i, \theta_k) - f(\theta_i, \theta_k)}{\Delta\theta_i}$$

$$\frac{\partial^2 f}{\partial^2 \theta_i} \cong 4\left[\frac{f(\theta_i, \theta_k) + f(\theta_i + \Delta\theta_i, \theta_k) - 2f(\theta_i + \Delta\theta_i/2, \theta_k)}{(\Delta\theta_i)^2}\right]$$

$$\frac{\partial^2 f}{\partial\theta_i \partial\theta_j} \cong 4\left[\frac{f(\theta_i, \theta_k) + f(\theta_i + \Delta\theta_i, \theta_k + \Delta\theta_k) - f(\theta_i + \Delta\theta_i, \theta_k) - f(\theta_i, \theta_k + \Delta\theta_k)}{\Delta\theta_i \Delta\theta_k}\right] \quad (4\text{-}55)$$

4.3. Levenberg-Marquardt Optimization

Model based data reconciliation is an optimization process where the maximum likelihood principle is utilized to formulate the objective function while the physical constraints are imposed by the system model. When the performance simulator is used, the nonlinear constrained process is transformed into a nonlinear unconstrained optimization process. Although nonlinear constraints are eliminated, the nonlinearity caused by model constraints is, however, built into the least squares objective function, which is constructed based on the Gaussian distributions assumed for the measurement uncertainties.

The data reconciliation problem can be solved using different optimization methods. As explained in previous sections, the major disadvantage inherent in the analytical methods of either the chi square expansion or the model function expansion is the difficulty of making a good parabolic approximation to the objective function when the starting point is far away from the true solution. When the starting point is nearby, the expansion method converges rapidly. On the other hand, due to the sensitivity of this method to the starting point, if the search is from a point far from the true solution, the method can either converge to a local minimum or fail to converge because of the unreliable parabolic approximation. In the extreme case, the diagonal elements of the Hessian matrix become negative and lead to an opposite search direction. Even though one can force the Hessian matrix to be positive during the optimization process, the poor

approximation of the chi square objective function still causes the difficulty of convergence. In contrast, the gradient search method has better performance in approaching the solution from far away, but it becomes very inefficient when the true solution is nearby. This is due to the change of the objective function value becomes very small when getting very close to the solution.

The Levenberg-Marquardt (LM) algorithm [62~66] is a nonlinear optimization technique most suitable for solving the type of objective function expressed as the sum of squares of a nonlinear function. The LM algorithm can be thought of as a combination of steepest descent and Gauss-Newton expansion methods. It significantly outperforms gradient descent and conjugate gradient methods in a wide range of problems as well. LM is a pseudo-second order method that uses the sum of outer products of the function gradients to estimate the Hessian matrix. Because of its superior performance in solving the least-square type function, the LM algorithm is utilized to solve the nonlinear model based data reconciliation problem in this study.

The Levenberg Marquardt algorithm combines the two methods of analytical expansion and gradient search, which makes it work efficiently in the path toward the valley of the objective function. It is just like the gradient search, and it converges rapidly like the expansion method when the true solution is nearby. It also can be shown that the search direction of the steepest descent method is nearly perpendicular to the search direction of analytical expansion, and that the optimum search direction is somewhere between these two vectors. Another advantage of combining these two methods is that a second order expansion is not required in the first part of search (away from the true solution) because the accuracy of the approximation to the chi square χ^2 by the first order expansion is good enough to guide the search toward the true solution. When approaching the true solution, even the first order expansion gives a very good approximation to the objective function since the true minimum is nearby.

Recall that in the steepest descent method, the parameter increments are updated as:

$$\boldsymbol{\delta\theta} = \mu\boldsymbol{\beta} \tag{4-56}$$

where μ is the magnitude of the update from the current solution to the next solution, determined by the one-dimensional line search in the direction of $\boldsymbol{\beta}$. When using the Gaussian-Newton expansion, the solutions of $\delta\theta_i$ are given by:

$$\boldsymbol{\delta\theta} = \boldsymbol{\alpha}^{-1}\boldsymbol{\beta} \tag{4-57}$$

The technique invented by Levenberg involves "blending" between the steepest descent and Gaussian-Newton expansion. The search starts as the steepest descent until the true minimum is approached, and it is then switched to the quadric rule. How close the minimum is close can be estimated by monitoring the change of the error. In particular, Levenberg's algorithm is formalized as follows: let λ be a blending factor which determines the mix between the steepest descent and the Gaussian-Newton expansion. The update rule is:

$$\boldsymbol{\delta\theta} = \left(\boldsymbol{\alpha} + \lambda\boldsymbol{I}\right)^{-1}\boldsymbol{\beta} \tag{4-58}$$

where I is the identity matrix. As λ gets small, the algorithm approaches the quadratic approximation update rule. If λ is large, the algorithm approaches:

$$\boldsymbol{\delta\theta} = \frac{1}{\lambda}\boldsymbol{\beta} \tag{4-59}$$

which is the steepest descent. The algorithm makes the adjustment to λ according to whether the chi-square is increasing or decreasing:

1. Compute $\boldsymbol{\theta}$ and $\chi^2(\boldsymbol{\theta} + \boldsymbol{\delta\theta})$ with respect to the chosen λ.
2. If $\chi^2(\boldsymbol{\theta} + \boldsymbol{\delta\theta}) > \chi^2(\boldsymbol{\theta})$, increase λ by a factor 10 or some such significant factor, and repeat step 1.

3. If $\chi^2(\boldsymbol{\theta}+\delta\boldsymbol{\theta}) < \chi^2(\boldsymbol{\theta})$, decrease λ by a factor 10 or some such significant factor, update the solutions by $\boldsymbol{\theta}' = \boldsymbol{\theta} + \delta\boldsymbol{\theta}$ for the next iteration, and return to step 1 with the updated solutions.

The intuition is that if the chi-square is increasing, the quadratic approximation is not working well, indicating that the minimum is not nearby. Therefore, one should increase λ in order to blend more towards to the steepest descent mode. On the other hand, if the chi-square is decreasing, the quadratic approximation is working well, and one can expect that the true minimum is approached. So λ is decreased to bank more on the Gaussian-Newton expansion.

Marquardt improved this method with an incorporation of estimated local curvature information, resulting in the Levenberg-Marquardt method. The modification to Levenberg algorithm was based on the insight that when λ is large and the search is closer to the steepest descent mode, one can still get some benefit from the estimated Hessian matrix. It was suggested by Marquardt that one should move further in the directions in which the gradient is smaller in order to get around the classic. As a result, it was suggested to replace the identity matrix I with the diagonal of the Hessian in Marquardt algorithm:

$$\delta\boldsymbol{\theta} = \left(\boldsymbol{\alpha} + \lambda diag[\boldsymbol{\alpha}]\right)^{-1}\boldsymbol{\beta} \tag{4-60}$$

The LM algorithm is executed by increasing the diagonal terms of the Hessian matrix $\boldsymbol{\alpha}$ by 1 + λ per iteration, which controls the interpolation between two extreme search methods of steepest descent and Gaussian-Newton expansion. The parameter increments are, therefore, updated in the following way:

$$\boldsymbol{\beta} = \delta\boldsymbol{\theta}\boldsymbol{\alpha}' \tag{4-61}$$

where

$$\alpha'_{jk} = \begin{cases} \alpha_{jk}(1+\lambda) & for\ j = k \\ \alpha_{jk} & for\ j \neq k \end{cases} \tag{4-62}$$

When λ is small, the algorithm works like the Gaussian-Newton expansion. As λ increases, the diagonal terms in the Hessian matrix become more dominant and drive the search to behave more like the steepest descent. When λ is large, due to the dominant diagonal terms in the Hessian, the matrix equation can be broken down into n separate equations:

$$\beta_i \cong \lambda \delta\theta_i \alpha_{ii} \tag{4-63}$$

As a result, the parameter increments $\delta\theta_i$ can be obtained without the need for the matrix manipulation. In general, the solution to the parameter increments $\delta\theta_i$ are given by the matrix inversion given as follows

$$\delta\theta_i = \sum_{k=1}^{n} \beta_k \tau_{ik} \tag{4-64}$$

where

$$\tau_{ik} = \boldsymbol{\alpha}^{-1}{}_{ik} \qquad \textit{when } \lambda \textit{ is small}$$

$$\tau_{ik} \cong \begin{cases} 0 & \textit{for } i \neq k \\ 1/\alpha_{ii} & \textit{for } i = k \end{cases} \qquad \textit{when } \lambda \textit{ is large} \tag{4-65}$$

It should be mentioned that in the LM algorithm, the elements in the Hessian matrix, α, are approximated by averaging the outer products of the first order derivative:

$$\alpha_{ij} = \sum_{k=1}^{m} \frac{\partial^2 y_k}{\partial x_i \partial x_j} \approx \sum_{k=1}^{m} \frac{\partial y_k}{\partial x_i} \frac{\partial y_k}{\partial x_j} \tag{4-66}$$

The approximation becomes exact when the model functions are linear. When the search starts from the initial point far away from the true solution, the poor approximation of the Hessian does not have a significant impact since the steepest descent method dominants. When the search is approaching the true solution, the approximation is good and improves as the solution is approached. The flow chart of the Levenberg-Marquardt algorithm is given in Fig. 4-1.

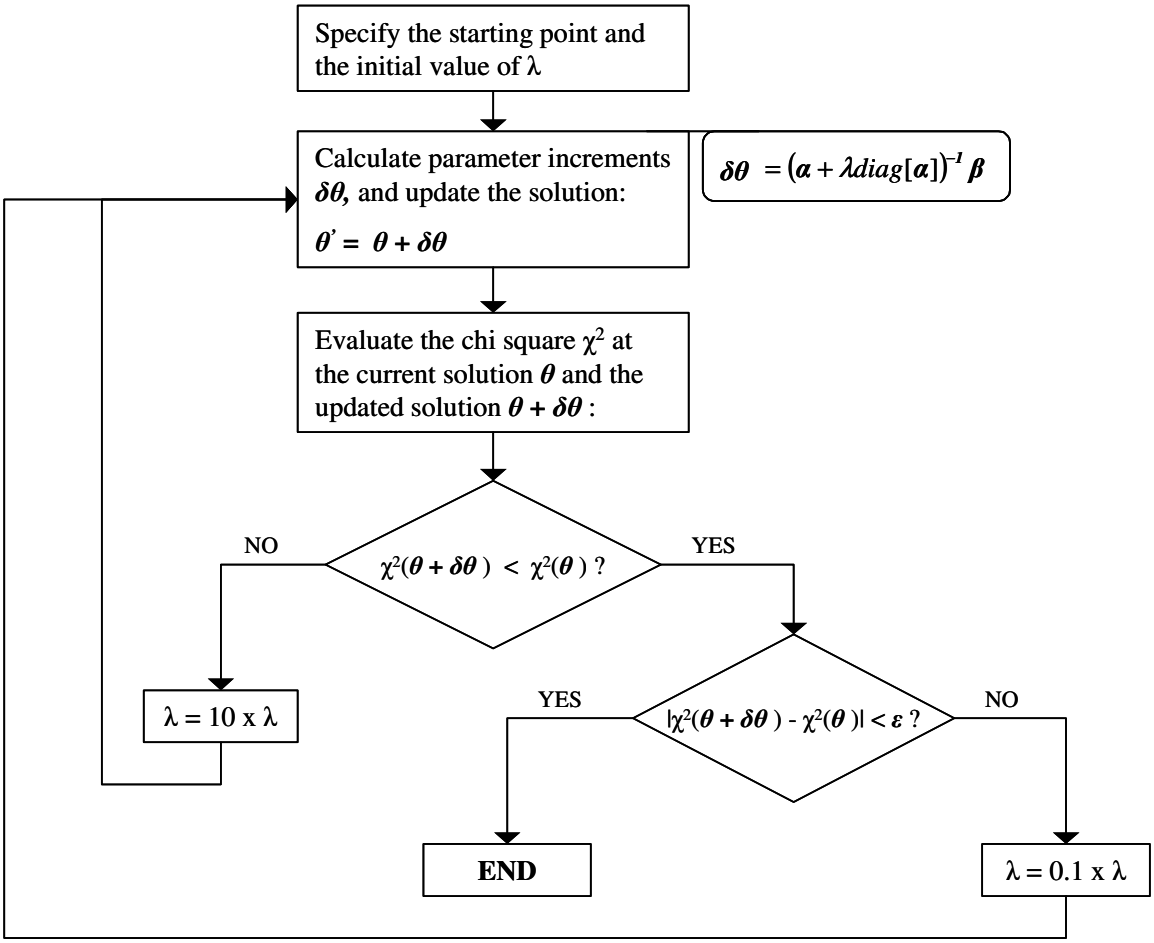

Figure 4-1: Levenberg-Marquardt algorithm

4.4. Error Analysis

In model based data reconciliation, the reconciled data and estimated model parameters are subject to uncertainties incurred by errors of the measured data utilized in the reconciliation process. Error analyses for the reconciled data and estimated model parameters determine the confidence level of using these reconciled data and estimated parameters in performance simulations. For the reconciliation process based on closed heat and mass balance, the reconciled data can be later used for model calibration, in which the reconciled data with better qualities, i.e., less uncertainties, are used as the target values in data matching. In this case, the error analysis can determine the confidence level of the calibrated model. On the other hand, when a performance simulator is used in data reconciliation, it becomes a process of simultaneous data reconciliation and model calibration. Since the estimated model parameters are used for performance predictions, the confidence being placed in the performance predictions depends on the confidence of using the estimated model parameters. An error analysis for estimated model parameters is, therefore, needed to provide the reliability of performance simulations.

4.4.1. Absolute Variances

During data reconciliation, not the absolute values of the variances but the relative relations among the variances are used due to the nature of maximum likelihood estimation. The relative values of the variances of the observed data are expressed by the weights given by:

$$w_j = \frac{1/\sigma_j^2}{(1/N)\sum(1/\sigma_j^2)} \tag{4-67}$$

where σ_j^2 represents the uncertainty of the measured data y_j; and N is the total number of data points. Determination of the model parameter θ_i does not require the knowledge

about the absolute value of σ_j^2. Instead, it is the weighting factor defined in equation (4-67) that determines the estimate of θ_i.

The least squares method is based on the hypothesis that the optimum model of describing a set of measured data or the best estimate for the set of true values, around which the measured data are observed, is the one that minimizes the weighted sum of the squares of the deviation of the measured data y_j'. These measured data are from the fitting model function $y_j(\theta_i)$ or from the estimated true values y_j. The variance of the fit s^2, an estimate of the variance of measured data, can be used to characterize the goodness of fit:

$$s^2 = \frac{1}{N-m} \frac{\sum (1/\sigma_j^2)[y_j' - y_j]}{(1/N)\sum (1/\sigma_j^2)} \tag{4-68}$$

or

$$s^2 = \frac{1}{N-m} \frac{\sum (1/\sigma_j^2)[y_j' - y_j(\theta_i)]}{(1/N)\sum (1/\sigma_j^2)} \tag{4-69}$$

where the parameter $\nu = N - m$ represents the degree of freedom, and m is the number of the parameters utilized in data reconciliation.

There is a direct relation between the variance of fit s^2 and the chi squares χ^2, which is given by:

$$\chi^2 = (N-m)\frac{s^2}{\langle \sigma_j^2 \rangle} = \nu \frac{s^2}{\langle \sigma_j^2 \rangle} \tag{4-70}$$

where $\langle \sigma_j^2 \rangle$ is the weighted average of the individual variances defined as:

$$\langle \sigma_j^2 \rangle = \frac{(1/N)\sum [(1/\sigma_j^2)\sigma_j^2]}{(1/N)\sum (1/\sigma_j^2)} \tag{4-71}$$

The parameter $\langle \sigma_j^2 \rangle$ represents the parent variance of the measurement data, i.e., the spread of the measurement data about the parent population. This spread is characterized by the uncertainties of the measurement instruments. The estimated variance of the fit s^2

is characterized by both the spread of the measurement data and the accuracy of the fit. Equation (4-71) shows that the chi-square, by definition, is the ratio of the estimated variance to the parent variance multiplied by the degree of freedom, which, therefore, is a good measure of the goodness of fit. The reduced chi-square is defined as:

$$\chi_v^2 = \frac{\chi^2}{v} = \frac{s^2}{\left\langle \sigma_j^2 \right\rangle} \tag{4-72}$$

Then one can evaluate the goodness of fit with in a more convenient way.

If the model with the optimum set of parameters θ_i can best describe the measured data, the estimated variance should agree well with the parent variance, indicating that the reduced chi square χ^2 should be approximately unit, i.e., $\chi_v^2 \approx 1$. If, on the other hand, the best estimate for the set of true values or the optimum model is not proper, the deviations will be large and will make the reduced chi square greater than 1.

For data reconciliation using the heat balance equations, a value of reduced chi-square much greater than 1 indicates the existence of gross errors since the energy and mass balances equations are universal, and it is less likely the model is incorrect. If, however, there are some parameters to be estimated in the heat and mass balance equations such as the leakage model or the heat utilization factor, a large value of reduced chi square could indicate that there are hidden parameters that are not included in the data reconciliation process.

For the process of simultaneous data reconciliation and model calibration, i.e., data reconciliation using a performance simulator, a large value of reduced chi-square indicates the possibility of the existence of both gross errors and an inappropriate model. When both of theses situations occur at the same time, one cannot make proper estimates of the model parameters and reconcile the data because these two factors are confounding with each other. One should always make sure the model being used as the fitting model is proper, meaning that if there are hidden parameters, they should either be included in

the data reconciliation process or be treated as constant parameters that describe the model properly.

The value of the estimated variance of fit s^2 itself is also a useful parameter of differentiating and selecting two fitting models. For instance, if two different models are used to fit the same data set, two different estimated variances of fit, s_1^2 and s_2^2, will most likely be obtained. If a smaller value of s^2 is obtained for the first model, i.e., $s_1^2 < s_2^2$, one can conclude that the first model provides a better representation of the data. Before making that conclusion, one should determine the significance of the difference between the two models by hypothesis testing. Hypothesis testing is based on calculating the ratio:

$$F = \frac{s_1^2}{s_2^2} \tag{4-73}$$

This ratio is expected to have the $\boldsymbol{F}$ distribution, provided that the errors due to the lack of fit are normally distributed [67]. One can specify the significance level α and compare the calculated ratio with the tabulated $\boldsymbol{F}_{\alpha/2}(v1, v2)$, where $v1$and $v2$ are the degrees of freedom for the two models. If the calculated F is greater than $\boldsymbol{F}_{\alpha/2}(v1, v2)$, the null hypothesis will be rejected, and it is concluded that these two models make a significant statistical difference.

4.4.2. Estimate Errors

In the process of data reconciliation and parameter estimation, the measurement errors are propagated and cause errors in the reconciled data and estimated parameters. By using the error propagation principle, one can evaluate estimate errors and obtain the confidence level of using these reconciled data and estimated parameters.

One of the methods used in error propagation principle is the Monte Carlo simulation - an easy technique for implementation, but it needs significant computation time. For instance, to utilize the Monte Carlo method, the data reconciliation process is required to be executed each time when a set of measurement data is randomly selected

from their known parent populations. With these data, distributions of the reconciled data and of the estimated parameters can be constructed. For a highly nonlinear system, a single run of data reconciliation and parameter estimation can take significant time, and, therefore, the use of a Monte Carlo simulation to evaluate the estimation errors is not practical since it requires at least hundreds of runs for data reconciliation.

The more practical way of evaluating the estimation errors is to estimate the variance-covariance matrix of the reconciled data and of the model parameters. The variance-covariance matrix describes the dispersions of the estimated parameters and their correlations. Therefore, it can be used to represent the multivariate space for the estimates. The diagonal elements of the variance-covariance matrix are the variances of the corresponding parameters or reconciled data. The square roots of these variances are estimates of the standard deviations of the estimated parameters, which are also a measure of the uncertainties in the estimated parameters. The off-diagonal elements of the variance–covariance matrix represent the correlations between the estimated parameters or reconciled data. If two parameters are completely independent with each other, the corresponding covariance is zero. As there is a strong correlation between two parameters, their covariance value approaches ±1.

Variance-Covariance Matrix:

System Model with Implicit Model Constraints

For the data reconciliation using implicit model constraints such as heat and mass balance equations, the variance-covariance matrix $\sum$ of the reconciled data is given by Equation (4-18) in section 4.3.1:

$$\sum = B\sigma B^T \tag{4-74}$$

where B is given by :

$$B = [I - \sigma A^T (A\sigma A^T) A] \tag{4-75}$$

In this type of data reconciliation, the model constraints can be expressed by $\boldsymbol{AX} = \mathbf{0}$, where $\boldsymbol{A}$ represent the constraint matrix and $\boldsymbol{X}$ contains the measurements to be reconciled.

This variance-covariance matrix of the reconciled data has non-zero values in the off-diagonal terms, which indicates that the estimation errors of the reconciled data are correlated due to the data reconciliation process. This matrix is actually obtained through a linear transformation of the original measurement error matrix, which is usually a diagonal matrix, indicating no correlations between measurement errors. Therefore, the uncorrelated measurement errors are propagated through the data reconciliation mechanism, which causes correlated estimate errors for the reconciled data. Although the estimation errors for the reconciled data are correlated, the standard deviations of the reconciled data, i.e., the diagonal terms, are smaller than that from the measurement error matrix. The reduced uncertainties of the reconciled data are beneficial because one can use the reconciled data for model data matching with a higher confidence.

System Model with Explicit Model Constraints

For the data reconciliation and model calibration problem that embeds the explicit model constraints into the objective function, the variance-covariance matrix can be obtained from the Jacobians evaluated at the optimum solutions of the parameters and reconciled data. By assuming the optimum solutions for model parameters and reconciled data are obtained through the optimization process such that the chi square χ^2 is minimized, one can approximate the model functions by the Taylor's expansion to first order:

$$y_j = f_j(\boldsymbol{x}, \boldsymbol{\theta}) = f_j(\boldsymbol{x}^*, \boldsymbol{\theta}^*) + F_\theta(\boldsymbol{x}^*, \boldsymbol{\theta}^*)(\boldsymbol{\theta} - \boldsymbol{\theta}^*) + F_x(\boldsymbol{x}^*, \boldsymbol{\theta}^*)(\boldsymbol{x} - \boldsymbol{x}^*) \qquad (4\text{-}76)$$

where $\boldsymbol{x}$ is a column vector of the model input variables that have correspondent measurements and are to be reconciled; $\boldsymbol{\theta}$ is a column vector of the model parameters to be estimated; F_θ and F_x are the Jacobians of the model parameters and the model input

measurement variables separately. Applying the method of the Lagrange multiplier, one can obtain:

$$\begin{aligned} -\boldsymbol{\sigma}^{-1}(\boldsymbol{x}' - \boldsymbol{x}^*) + F_x^T \hat{\boldsymbol{\phi}} = 0 \\ F_\theta^T \hat{\boldsymbol{\phi}} = 0 \\ F_\theta(\boldsymbol{\theta}^* - \boldsymbol{\theta}) + F_x(\boldsymbol{x}^* - \boldsymbol{x}) = 0 \end{aligned} \tag{4-77}$$

where $\hat{\boldsymbol{\phi}}$ is the Lagrange multiplier at the final solutions of the reconciled data $\boldsymbol{x}^*$ and the model parameters $\boldsymbol{\theta}^*$. Using matrix manipulation, one can obtain:

$$\boldsymbol{\theta}^* - \boldsymbol{\theta} = \left[F_\theta^T \left(F_x \boldsymbol{\sigma} F_x^T\right)^{-1} F_\theta\right]^{-1} F_\theta^T \left(F_x \boldsymbol{\sigma} F_x^T\right)^{-1} F_x(\boldsymbol{x}' - \boldsymbol{x}) \tag{4-78}$$

or

$$\Delta\boldsymbol{\theta} = \left\{\left[F_\theta^T \left(F_x \boldsymbol{\sigma} F_x^T\right)^{-1} F_\theta\right]^{-1} F_\theta^T \left(F_x \boldsymbol{\sigma} F_x^T\right)^{-1} F_x\right\}\Delta\boldsymbol{x} \tag{4-79}$$

Equation (4-79) shows that the estimation errors are actually the linear transformations of the measurement errors. As a result, the variance-covariance matrix $\sum$ of the estimation errors for the model parameters $\boldsymbol{\theta}$ is given by:

$$\sum = E\left\{\left(\boldsymbol{\theta}^* - \boldsymbol{\theta_0}\right)\left(\boldsymbol{\theta}^* - \boldsymbol{\theta_0}\right)^T\right\} = s^2\left[F_\theta^T \left(F_x \boldsymbol{\sigma} F_x^T\right)^{-1} F_\theta\right]^{-1} \tag{4-80}$$

In the data reconciliation and parameter estimation process that utilizes either the serial linearization technique or the nonlinear programming technique, the Jacobians F_θ, F_x and the variance of fit s^2 are evaluated at each iteration. The estimation errors are evaluated at the final iteration where the maximum likelihood estimates are obtained.

For the similar type of data reconciliation using the performance simulator, the model constraints are also explicit, and can be substituted into the objective function. By using the gradient-expansion method, such as the Levenberg Marquardt algorithm, the variance-covariance matrix of the estimated parameters is simply the inverse of the Hessian matrix $\boldsymbol{\alpha}$ evaluated at the final solutions:

$$\sum = \boldsymbol{\alpha}^{-1} \tag{4-81}$$

Once the variance-covariance matrix of the model parameters is obtained, it can be used to calculate the uncertainty of any property that is a function of the estimated parameters. If $\boldsymbol{H}(\boldsymbol{\theta})$ is a property function of $\boldsymbol{\theta}$, the uncertainty of this property σ_h^2 is given by:

$$\sigma_h^2 = h_\theta^T \sum h_\theta \tag{4-82}$$

This relation provides a convenient means of estimating the uncertainties of predictions made by the fitted model.

4.5. Strategy for Model Based Data Reconciliation and Model Calibration

Model based data reconciliation requires a proper model serving as the physical constraints in minimizing the least squares objective function. This model is defined based on the maximum likelihood principle, and it is used to justify the reconciled data and, therefore, must be selected correctly. Without a correct model, the reconciliation process will be contaminated, i.e., the presence of gross errors is confounded with the use of the incorrect model. Thus, building or selecting the right model to use is the crucial step that has a direct impact on whether the reconciliation can be carried out properly or not.

A proper selection of a model, however, relies on the system definition, by which one should achieve measurement redundancy to perform data reconciliation. In the case where the available measurements are not enough to reach redundancy, one should redefine the system boundaries or obtain more measurement data. The selection of the model type, – a model based on conservation equations or a model that can provide performance predictions, also depends on the measurement redundancy, and the computation budget, i.e., software availability and time consumption, as well. The strategy of model based data reconciliation is discussed in the following sections.

4.5.1. System Boundary

Defining the system and system boundary plays a crucial role in the data reconciliation process, especially for the type of data reconciliation utilizing the heat and mass balance equations, which depend on the system boundary definition. The system boundary determines the types of energy flows crossing the boundary and, therefore, the types of variables to be reconciled and estimated. A proper system definition strongly depends on the availability and redundancy of the measurement data. If the available measurement data do not give redundancy for the defined subsystem, one should keep expanding the system boundary to cover more subsystems until the measurement redundancy is available. For instance, if the measurements of the compressor exhaust conditions for a gas turbine are not available or the availability is not enough to reach the redundancy, one should expand the system boundary from around the compressor to include downstream subsystems like the combustor and/or the turbine such that the redundancy is achieved. By expanding the system boundary, the energy flows that are originally crossing the boundary become the internal flows inside the expanded system boundary. Expanding the system boundary usually simplifies the data reconciliation process since the number of variables is reduced. It, however, also decreases the degrees of freedom by which one can determine the subsystem parameters such as the performance correction factors that account the degradation effects. For the example of a gas turbine, if flow conditions at the compressor exhaust are not available such that one needs to expand the system boundary to include the whole gas turbine, the degree of freedom from the compressor will disappear as the system boundary is expanded downstream. In this situation one can no longer determine the component efficiency of the compressor itself due to losing that degree of freedom. Instead, only one degree of freedom is left as the system boundary covers the whole gas turbine. That degree of freedom is the overall gas turbine efficiency.

If the measurement availability is good enough such that redundancy is always achieved regardless of the way system boundaries are defined, the definition of system boundary depends on the interactions among the subsystems. When multiple system boundaries are required for a complex thermodynamic system, one should define the boundaries for the subsystems in such a way that the interactions between subsystems are minimized. For the example of a combined cycle system, the energy flow is fed down stream to the heat recovery steam generator (HRSG) from the gas turbine while there is usually no energy flows fed back from the HRSG to the gas turbine, except for the case where the steam injection to the gas turbine combustor is applied. One should define a subsystem boundary for the gas turbine, and another subsystem boundary for the HRSG.

If, on the other hand, one decomposes the system into multiple sections in such a way that the decomposed subsystem interchanges the energy flows with each other, an extra iteration process, i.e., a convergence driver, will be required to eliminate the discrepancies of the reconciled variables across the boundary where the subsystems interact with each other. For the example of a HRSG, due to its cross-counter-flow configuration, the gas exhaust flow condition from the upstream section affects the steam/water flow condition from the downstream section and vice versa. If one defines the subsystems based on the pressure levels, i.e., decomposing the HRSG into multiple sections by drum pressures, and formulates heat and mass balance equations for each of the sections accordingly, one not only has to carry out data reconciliation separately for each of the subsystems, but also needs a convergence driver at a higher level iterating among these subsystems to eliminate the discrepancies of the reconciled variables across the boundaries. This usually means more computation time and extra preparation efforts. This is because additional convergence across the boundaries are required if more interactive subsystems are defined in the data reconciliation process that relies on closing the heat and mass balance.

When a performance simulator provided by commercial software is utilized in the data reconciliation problem, e.g., GateCycle ™, extra efforts of ensuring the convergence across the boundaries can be waived since the built-in solver has already taken care of the iteration among subsystems.

4.5.2. System Model and Optimization Method

In the model based data reconciliation process, the "model" serves as the physical constraints that have to be satisfied during the optimization process of maximizing the likelihood function, i.e., minimizing the chi squares χ^2. Therefore, the right model is critical in a model based data reconciliation since it provides the way of justifying the measurements. An incorrect model will invalidate the reconciliation process such that the healthy measurements are misidentified with biases or the estimated model parameters are out of reasonable bounds. It is suggested that one should carefully build or select the model based on a thorough understanding of the system configuration, and use the healthy data to justify the model before engaging it with the data reconciliation scheme.

The type of model used in data reconciliation also has a direct impact on the selection of optimization algorithm. Two major types of models are usually utilized in model based data reconciliation for the thermodynamic system:

<u>Heat & Mass Balance Type:</u>

In this type of model based data reconciliation, one utilizes the universal physical principles such as energy and mass conservation principles to justify and correct the measurement data, among which only the energy flows crossing the boundaries are taken into account. While formulating the optimization problem, the measurements are the main variables to be solved during the reconciliation process. There are infinite sets of solutions, each of which represents a specific system status satisfying the conservation

equations. However, only a global solution near the measurement data gives the minimum least squares.

There are three major optimization schemes used to carry out the data reconciliation process with the conservation equations as model constraints:

- *Solve the nonlinear constrained problem directly:*

In this scheme, the nonlinear conservation equations serve as the constraints while the linear least squares objective function is solved by the nonlinear programming techniques (NLP) such as the sequential quadratic programming (SQP) technique, in which the one-dimensional line search is performed in the hyper-surface of the 2nd-order approximated objective function with 1st-order expanded model constraints. This method does not require any preparation for the problem formulation, but it does need a good NLP solver. Solving a nonlinear constrained problem usually needs more convergence time, and it faces more difficulty in achieving a global minimum. The optimization problem of this method can be expressed as follows:

$$\min_{y_j,\theta_i} \sum_{j=1}^{m} \left(\frac{y'_j - y_j}{\sigma_j} \right)^2$$
$$s.t.\ f(y_j, \theta_i) = 0 \tag{4-83}$$

where y_j and θ_j are the reconciled data and estimated parameters to be solved; y'_j and σ_j represent the measurement data and the correspondent measurement uncertainties.

- *Use the serial constraint linearization technique:*

In this method, instead of using the NLP technique, an iterative scheme using the Lagrange multiplier with linearized model constraints is used. For more explanation, please refer to section 7.3.2. By using the Lagrange multiplier and 1st-order expansions for the model constraints, a set of linear equations can be solved analytically for each iteration. The iterative process stops when the convergence criterion is achieved. To ensure a solution for the global minimum, a good initial guess for the solution is crucial.

When starting from an initial point far from the true solution, this algorithm has a difficulty of reaching convergence, or falls into a local minimum. But, since it is an iterative process, an NLP solver is not required, and one can use a single EXCEL spreadsheet to carry out the data reconciliation process. This scheme has the same optimization formulation as the previous scheme, i.e., a linear objective function with nonlinear model constraints. The main difference is from the optimization algorithm.

- *Transform the constrained problem into the unconstrained problem and solve it using the gradient-expansion method:*

In this method, one can transform the implicit model constraints, i.e., heat and mass conservation equations, into the explicit forms that can be substituted into the least squares, by which the nonlinear model constraints are eliminated due to the integration. As a result, the original nonlinear constrained optimization process becomes an unconstrained optimization one. A gradient-expansion scheme such as LM can be used to carry out the reconciliation process. The implicit model constraints can be expressed as follows:

$$f_i(x_i, y_j, \theta_k) = 0$$
$$\text{for } i = 1 \sim m;\ j = 1 \sim n;\ k = 1 \sim s \tag{4-84}$$

where m is the number of constraint equations, n is the number of the measurement data becoming independent, and s is the number of the parameters being estimated. In each of the implicit functions, one of the measurement data x_i can be selected as a dependent variable, and then represented as a function g_i of the rest measurement data y_j and the model parameters θ_k given by:

$$x_i = g_i(y_j, \theta_k)$$
$$\text{for } i = 1 \sim m;\ j = 1 \sim n;\ k = 1 \sim s \tag{4-85}$$

The least squares objective function is given by:

$$\chi^2 = \sum_{j=1}^{n}\left(\frac{y'_j - y_j}{\sigma_{y_j}}\right)^2 + \sum_{i=1}^{m}\left(\frac{x'_i - x_i}{\sigma_{x_i}}\right)^2 \tag{4-86}$$

This function can be integrated with the transformed explicit functions of x_i. Substituting Equation (4-85) into the least squares objective function (), one can obtain:

$$\chi^2 = \sum_{j=1}^{n}\left(\frac{y'_j - y_j}{\sigma_{y_j}}\right)^2 + \sum_{i=1}^{m}\left(\frac{x'_i - g_i(y_j,\theta_k)}{\sigma_{x_i}}\right)^2 \tag{4-87}$$

As a result, the nonlinear constrained problem becomes an unconstrained problem with the least squares objective function becoming nonlinear. The optimization problem is now given by:

$$\min_{y_j,\theta_k}\left\{\sum_{j=1}^{m}\left(\frac{y'_j - y_j}{\sigma_j}\right)^2 + \sum_{i=1}^{m}\left(\frac{x'_i - g_i(y_j,\theta_k)}{\sigma_{x_i}}\right)^2\right\} \tag{4-88}$$

The nonlinear unconstrained optimization problem can be solved efficiently by using the Levenberg Marquardt method, which blends the steepest descent method with the Gaussian-Newton method based upon how far the true solution is away from the starting point.

Performance Simulation Type:

When the thermodynamic system is defined and expressed by the conservation laws, such as heat and mass balance equations, the system status, characterized by operating conditions and degradation status, is manifested by the measurement data of system performance and energy flow conditions, i.e., flow, pressure, temperature, etc. By carrying out data reconciliation for the measurements, one can reduce the uncertainties of the estimated system status. In the heat and mass balance type of model, since the sizes and capabilities of system components inside the system boundary are not required but the energy flows crossing the boundaries, the system status is not available until the measurement data of a specific operation condition and degradation level are obtained.

This is because this type of model cannot be utilized to predict system performance. Once the measurement data are obtained, the system status can be estimated by analyzing the raw measurements or the reconciled data. The analysis must be carried out with high fidelity model that can predict the system performance based on the degradation status and capability of the system.

If, on the other hand, the system is defined and characterized by a high fidelity model that has the capability of predicting system performance based on its size and configuration, one can generate the simulated data and predict system performance by running the model at any specified system status. When the system model has the capability of good performance predictions, the conservation laws are also ensured and implemented by the internal convergence driver for the simulated data representing energy flows crossing the system boundary. Therefore, for any given system status, one can always obtain data that satisfies the energy and mass conservations when the system model is in the prediction mode.

Since the simulated data satisfy the physical constraints at any given system status, one can use the maximum likelihood principle to estimate the system status through a nonlinear unconstrained optimization process. Usually, the performance simulator is available from the commercial heat balance solver, from which the simulated data are in explicit forms given by:

$$y_j = f_j(a_i, \theta_k)$$
$$\text{for } i = 1 \sim n;\ j = 1 \sim m;\ k = 1 \sim s \tag{4-89}$$

where a_i are the model inputs associated with the operation condition, and θ_k are the common model parameters simulating the system degradation such as performance multipliers. For a given set of a_i and θ_k, one can obtain the simulated data y_j that satisfy all the physical constraints characterized by the system. As a result, by introducing the performance simulator as the system model, one can accomplish data reconciliation and

model calibration simultaneously since the goal is to find the optimum set of a_i and θ_k that lead to the reconciled data y_j,. This optimum maximizes the likelihood of observing the measurements $y_j^{'}$. The least squares objective function is given by:

$$\chi^2 = \sum_{j=1}^{m} \left(\frac{y'_j - y_j}{\sigma_{y_j}} \right)^2$$

$$\text{where} \quad y_j = f_j(a_i, \theta_k) \tag{4-90}$$

$$\text{for } i = 1 \sim n;\ j = 1 \sim m;\ k = 1 \sim s$$

The optimization problem for simultaneous data reconciliation and model calibration is then given by:

$$\min_{a_i, \theta_k} \sum_{j=1}^{m} \left(\frac{y'_j - f_j(a_i, \theta_k)}{\sigma_j} \right)^2 \tag{4-91}$$

where $y_j^{'}$ represent the measurement data.

The values of $f_j(a_i, \theta_k)$ are obtained from running the performance simulation at the specific set of a_i and θ_k. For the high fidelity performance simulator, the model execution could take significant computation time and make the data reconciliation process very time consuming. Introducing the surrogate model, such as the response surface equation (RSE) methodology, can facilitate the execution of simultaneous data reconciliation and parameter estimation.

4.5.3. Response Surface Methodology

Response Surface Methodology (RSM) [68~70] includes a number of statistical techniques for creating an empirical relation between an output variable, i.e., response, and the levels of a number of input variables. RSM is aimed to provide a fast-executed model with the analytical polynomial form that spans the entire design space within

limited ranges for a complex system response in which no analytical solution exists. A typical second-degree response surface equation is given by:

$$R = b_0 + \sum_{i=1}^{n} b_i x_i + \sum_{i=1}^{n} \sum_{j=1}^{n} b_{ij} x_i x_j \tag{4-92}$$

where b_0 is the intercept term, while b_i, and b_{ij} are the coefficients for the linear terms and the product terms that include the pure quadratic parts b_{ii} and the cross-product parts b_{ij}. These coefficients are obtained through the regression process, which itself is also a least squares type optimization process. The most common method for obtaining the regression coefficients is through the design of experiments (DOE), which provides an efficient way of determining the necessary combinations of factor levels such that one can carry out the minimum number of system model executions to get the maximum regression information. When the model execution time is long, the DOE methodology can save the computation time significantly. The x_i variables are the values for each of the input variables that span the design space and affect the response R directly.

The RSE provides a simple polynomial equation that is analytical and has the major advantage of fast execution in the modeling and simulation environment where a large amount of function calls is required. It can be used in lieu of more sophisticated, time-consuming models to evaluate the system response at values for any combination of input variables. The use of an RSE is valid only within the specified ranges of the design variables for which the design of experiments and regression are performed. To make the RSE valid in wider ranges of the values for the design variables, the DOE and the regression process need to be carried out again with wider ranges of the design variables. For a highly nonlinear system model, the accuracy of RSE deteriorates as the ranges of design variables are increased. Therefore, one should properly determine the ranges of design variables and perform necessary statistical tests to ensure that the goodness of fit for the RSE is acceptable so that the RSE is statistically representative to the real model.

In solving the problem of simultaneous data reconciliation and model calibration, a large number of function calls for the system model is required during the least squares χ^2 minimization. The use of an RSE can save significant computation time in two aspects:

- *Fast execution:*

  It takes only 10^{-2}~10^{-1} seconds to execute the polynomial-form RSE while 10^{0}~10^{3} seconds of function evaluation is usually required for typical commercial packages of performance simulators, depending on how sophisticated the function for the off-design performance calculation is built into the simulation.

- *Analytical evaluation:*

  The other advantage of using an RSE in model-based data reconciliation is the polynomial form of the RSE itself, by which the analytical formulations for the function evaluation, first-order ($\partial/\partial x_i$) and second-order ($\partial^2/\partial x_i \partial x_j$) function derivatives, are available. With the analytical formulations, the calculations of the Jacobian and Hessian matrices in the gradient-expansion search algorithm can be carried out without finite difference techniques, which need at least two function calls at the specific set of input variables.

When the properties of energy flows in the thermodynamic system are calculated by the off-design performance simulator and expressed in the forms of Equation (4-92), one can apply RSM to obtain the corresponding response surface equations as functions of a_i and θ_k:

$$y_j = f_j(a_i, \theta_k) = f_j(\boldsymbol{\Phi}) = b_{0j} + \sum_{s=1}^{N} b_{sj}\phi_s + \sum_{s=1}^{N}\sum_{t=1}^{N} b_{stj}\phi_s\phi_t \qquad (4\text{-}93)$$

where $\boldsymbol{\Phi}$ is a vector combining the system operation factors a_i and status factors θ_k.; N is the number of combined model parameters. Substituting Equation (4-93) into Equation (4-90), one can obtain the chi-squares objective function expressed as:

$$\chi^2 = \sum_{j=1}^{m} \left[\frac{y'_j - \left(b_{0j} + \sum_{s=1}^{N} b_{sj}\phi_s + \sum_{s=1}^{N}\sum_{t=1}^{N} b_{stj}\phi_s\phi_t \right)}{\sigma_{y_j}} \right]^2 \tag{4-94}$$

Using the Levenberg Marquardt algorithm, the evaluations of Jacobian and Hessian can be carried out analytically given by:

$$\beta_s \equiv -\frac{\partial \chi^2}{\partial \phi_s} = 2\sum_{j=1}^{m} \left[\frac{y'_j - \left(b_{0j} + \sum_{s=1}^{N} b_{sj}\phi_s + \sum_{s=1}^{N}\sum_{t=1}^{N} b_{stj}\phi_s\phi_t \right)}{\sigma_{y_j}} \right] \left[\frac{-\left(b_{sj} + 2b_{ssj}\phi_s\right)}{\sigma_{y_j}} \right] \tag{4-95}$$

$$\alpha_{st} \cong \sum \frac{1}{\sigma_j^2} \frac{\partial y_j(\Phi)}{\partial \phi_s} \frac{\partial y_j(\Phi)}{\partial \phi_t} = \sum_{j=1}^{m} \frac{1}{\sigma_j^2} \left[\frac{-\left(b_{sj} + 2b_{ssj}\phi_s\right)}{\sigma_{y_j}} \right] \left[\frac{-\left(b_{tj} + 2b_{ttj}\phi_t\right)}{\sigma_{y_j}} \right] \tag{4-96}$$

where *s* and *t* represent the index of the combined model parameters $\boldsymbol{\Phi}$. Since both Jacobin and Hessian matrices can be calculated directly by substituting the current solution of $\boldsymbol{\Phi}$, multiple function evaluations, required by the numerical methods such as finite difference, are not needed, and, therefore, the computation time will be reduced significantly.

4.5.4. Strategy for Model Based Data Reconciliation

A strategy for model based data reconciliation is summarized as follows:

1. *Adapt the system boundaries based on the measurement redundancy:*

The system boundaries should be tailored such that the energy flows crossing the boundaries have corresponding measurements that can be used to determine one another. For the heat and mass balance type data reconciliation, this means the available measurements for the energy flow across the boundaries must be more than what are required to "close" the heat and mass balancing over the defined system boundaries or "control volume". For the type of data reconciliation using off-design

performance simulation, the adaptive boundaries can be transformed into the concept of "degree of freedom". The degree of freedom is defined as:

d.o.f. = number of dependent variables – number of independent variables

To be able to perform data reconciliation, the degree of freedom must be greater than or equal to 1. Only, then can one use the least squares objective function for data reconciliation. If the degree of freedom is equal to 0, the maximum likelihood principle is meaningless since there is a unique solution for the model to have a perfect match to the measurement data. If the degree of freedom is less than 0, i.e., the number of independent variables is greater than the number of dependent variables. Then there are infinite sets of solutions that can make the model to exactly match the measurement data.

2. *Select the model type based on the computation budget and project scope:*

Usually, the model that provides the off-design performance simulation is only available in a commercial software package. Therefore, the selection of model type is sometimes limited by software availability. The major advantage of using the off-design performance simulator is its capability of performance prediction over any user-defined system status and operation condition by which one can carry out data reconciliation and model calibration simultaneously. If the project scope includes the estimation of system status, such as degradation, and if the performance simulation type model is available, it is suggested to perform simultaneous data reconciliation and model calibration. On the other hand, in the case when the commercial heat balance solver is not available, one should build the heat and mass balance equations on the defined system boundaries to perform data reconciliation. Since the status of the system cannot be known until the corresponding measurement data are obtained, this type of data reconciliation usually does not have the capability of determining system status, which can be simulated by system common parameters such as performance correction factors. One can, however, get the benefit from using the heat

balance type data reconciliation by saving significant computation time since the conservation laws do not require the extra functionality of the performance calculations based on the system sizing information.

3. Solve nonlinear unconstrained least squares minimization:

When an off-design performance simulator is utilized, the data reconciliation problem is automatically solved in the form of an unconstrained optimization. If the model that uses heat and mass balance equations is used, one should transform the implicit equations into explicit forms such that they can be substituted into a least squares objective function such that the least squares minimization becomes unconstrained.

CHAPTER 5

GROSS ERROR DETECTION

Gross errors are referred to as systematic errors that caused serious failures in closing system balances, e.g., mass and energy conservation. The occurrence of gross errors leads to difficulties in model calibration and data reconciliation due to the smearing effect. The reconciliation technique based on the assumption of normally distributed random errors needs to be adjusted by gross error treatments such that the smearing effect can be suppressed. Because the probability of gross error occurrences is relatively small, one can always start with a standard maximum likelihood technique without any gross error treatment. Once data reconciliation has been performed and the test statistics indicate the occurrence of gross errors, a special treatment or algorithm needs to be engaged to detect gross errors and to neutralize their effects in model calibration and data reconciliation. Figure 5-1 shows a generic process map of model calibration and data reconciliation for a thermodynamic system.

Two types of gross errors may exist. One results from the measurement error caused by non-random effects such as sensor miss-calibration, instrument malfunctioning, sensor corrosions, etc. Unlike the random error, this type of gross error has a constant magnitude and sign as the measurement is taken repeatedly within a certain period of time. When the gross error is caused by sensor miss-calibration, it often happens suddenly and maintains the same magnitude and sign. On the other hand, if the gross error is caused by sensor corrosion or wear, its magnitude changes gradually, but the rate of change is usually slow such that one can still identify it by some detecting techniques on a short-time basis. The other type of gross error is caused by a system leak, which could be a material leak such as the leak of the process flow across the pipe, or

energy leak such as heat loss of the heat exchanger. Both types of gross errors lead to large-scale system unbalances. Each type has a different gross error model, i.e., location and magnitude. However, they both can be detected by a single gross error detection (GED) scheme.

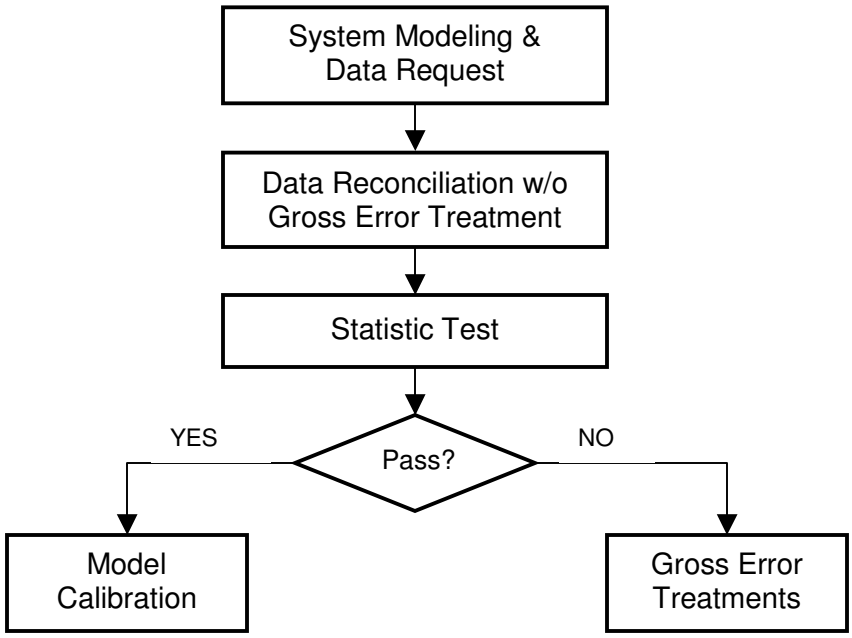

Figure 5-1: Process map for model calibration and data reconciliation

Statistical techniques such as multivariate data analysis and hypothesis testing can be used to detect gross errors, i.e., identify the location and estimate the magnitude. One can use multivariate data analysis to prescreen serious biases, which are manifested by evident outliers in multivariate system responses. Hypothesis testing then can be utilized to refine the detection process. In this research work, a hybrid scheme incorporating both techniques is suggested to perform model calibration and data reconciliation for a complex system. The goal is to use GED techniques to neutralize the smearing effects caused by gross errors in simultaneous data reconciliation and model calibration. During the GED process the location and magnitude of gross errors can be identified as well.

5.1. Smearing Effects Caused by Gross Errors

In the case where the measurements do not contain gross errors, data reconciliation does reduce the errors caused by random effects. Utilizing the maximum likelihood principle, the measurements are corrected by the optimizer (or solver) to minimize the least square objective function. The process is, however, based on the assumption that the errors are caused by random effects and, therefore, they are expected to spread within the ±3σ range of the normally distributed measurement errors. The least squares objective function is then constructed by the Gaussian type maximum likelihood functions defined by the unknown means and the covariance matrix of the measurement errors. The causes of gross error are not random effects but instead the fault of the instruments or leaks from the system, which make the signs and magnitudes of gross errors constant. Because of the nature of gross errors, the assumptions that the signs and magnitudes of errors are random and within the ±3σ ranges of Normal distributions cannot be held valid for the gross errors. Figure 5-2 shows the major difference between random and gross error.

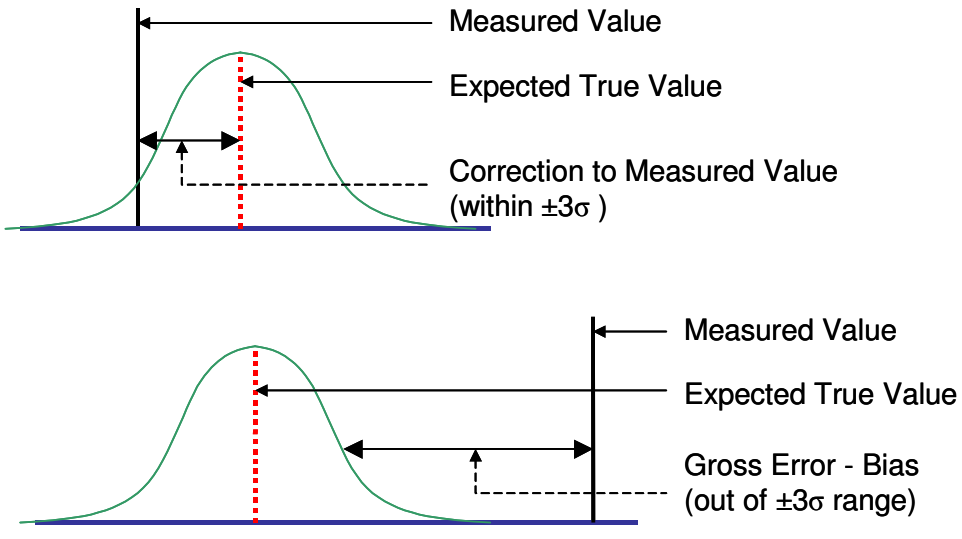

Figure 5-2: Difference between random error and gross error

In Fig. 5-2 it is shown that the measurement correction is within ±3σ of the measurement uncertainty when the measurement is subject only to a random error. On the other hand, if the measurement is biased due to the gross error, the magnitude of correction is outside the range of ±3σ.

The smearing effect, also known as "contamination effect", occurs when the least squares objective function is used in data reconciliation while gross errors exist in measurements. When it happens, the reconciliation process drives the solutions toward the measurements with gross errors; while, on the other hand, the corrections to "healthy" measurements are beyond the scope of measurement uncertainties, i.e., over-corrections. The smearing effect is mainly caused by the sensitivity of the objective function to a small deviation from the measured value. It depends on the model sensitivity and measurement uncertainties, both of which have direct impacts on the behavior of the objective function. For instance, when the smearing effect happens, after data reconciliation the corrections to those measurements with gross errors are within ±3σ ranges while the corrections to those healthy measurements are outside the scope of random errors.

The scenarios of smearing effects can be different depending on the variance-covariance matrix of the measurements and the error patterns of the system constraint equations, which are determined by the system model itself. This is especially true for a nonlinear system where the sensitivities of the error patterns to the model inputs, which are also measurements to be reconciled, are different. As a result the sensitivities of the nonlinear model can drive the optimizer in different directions. It could be that after the reconciliation process the corrections show that no gross errors exist but all the measurement corrections are beyond a 2σ range. This suggests that the gross error effects are compensated by all the other healthy measurements. Or it could be a situation that some healthy measurements are over-corrected such that gross errors are miss-identified.

Consider a model-based gas turbine data reconciliation and parameter estimation process. The process is to find out the optimal solution for component performance factors and for the turbine inlet temperatures (firing temperatures) at different operation conditions to minimize the least squares objective function. This is a process in which only random errors are assumed to exist. The details of the solving of this problem can be found in Chapter 4. The reconciliation process is carried out for three different situations: 1) only random errors occur, 2) one gross error with a moderate magnitude (4σ) is artificially imposed to the measured value of turbine exhaust temperature, and 3) one large gross error (13σ) is imposed to the measured turbine exhaust temperature. Figure 5-3 shows the comparisons among these three cases. In the first case there is no gross error, and, thus, all the measurement corrections are within the ±3σ ranges. In the second case where a moderate magnitude of gross error is applied, the smearing effect causes the over-corrections to the measured fuel flow and compressor airflow, and the correction to the measured turbine exhaust temp is within ±3σ, which contradicts the fact that there is a 4σ bias on it. In addition, all measurement corrections in this case are within ±3σ, and, thus, one is misled us to believe there is no gross error. In the third case where a large magnitude of bias is imposed, the smearing effect causes the over-correction of over ±3σ to the fuel flow. This leads to the wrong conclusion that there is a gross error in the measured fuel flow. The second case shows that the smearing effect can lead to the conclusion that no gross errors has happened, while the third case demonstrates that the smearing effect misleads us to believe there is a gross error in the measured fuel flow, whereas in reality there is not. Table 5-1 summarizes the measurement corrections for the three different cases.

Table 5-1: Measurement corrections in three test cases

Measurement Correction (per Standard Deviation)	Generator Output	Fuel Flow	Compressor Discharge Pressure	Compressor Discharge Temperature	Compressor Airflow	Exhaust Temperature
No Gross Error	0.36	0.85	0.62	1.31	0.58	0.10
A Moderate Gross Error	0.09	**3.00**	0.49	0.18	**2.15**	**2.01**
A Large Gross Error	1.40	**3.55**	1.79	0.15	**3.06**	**3.96**

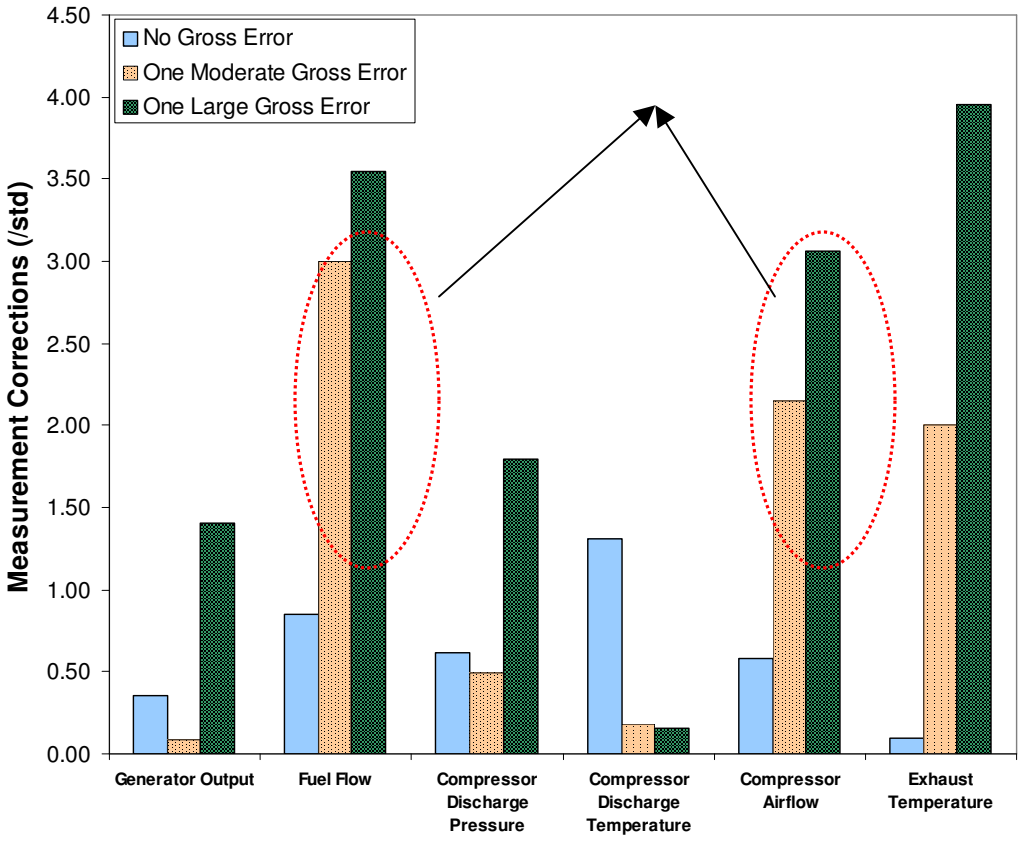

Figure 5-3: Smearing effects for gas turbine data reconciliation

5.2. Strategy for Gross Error Detection and Data Reconciliation

Due to the smearing effect, the occurrence of gross errors invalidates the result of data reconciliation that is based on least squares minimization. The cause of gross errors is nonrandom, and, therefore, the assumption that measurement errors are normally distributed around the means, i.e., the expected true values, is not valid for the case where gross errors exist. Due to the fact that gross errors have constant magnitudes and signs, they can be isolated from the total measurement errors. Therefore, the measured data can be decomposed into three major parts: expected true value, random error, and gross error.

$$\textit{Measured value} = \textit{Expected true value} + \textit{Random error} + \textit{Gross error}$$

If we have the prior knowledge about the locations, signs, and magnitudes of gross errors and remove them from those biased measurements before carrying out data reconciliation, the smearing effect can be eliminated. Most of the time, however, the prior knowledge about the gross errors is not available, and, therefore, it is necessary to incorporate a GED algorithm into the least squares type data reconciliation scheme. Another option is using different types of likelihood functions that are robust to the occurrence of gross errors so as to suppress the smearing effects during data reconciliation.

A strategy of gross error detection (GED) can be analyzed based on the method used to tackle three major problems: detection, identification, and multiple gross error identification. For gross error “detection”, the presence of single or multiple gross errors can be detected (the detection problem). For gross error “identification”, the types and locations of gross errors are to be identified (the identification problem). For multiple gross error identification, the presence of multiple gross errors as well as their locations and magnitudes are determined simultaneously.

There are two major GED techniques that can mitigate the smearing effects. One is to detect, identify, and remove the gross errors from the raw measurements prior to the

reconciliation process such that only random errors are left and the least squares objective function can be utilized. The second is to replace the least squares function with another Gaussian type likelihood function that is robust to the occurrence of gross errors. If the likelihood function is robust, i.e., insensitive to the occurrence of gross errors, the smearing effect can be suppressed. The first technique usually needs an iterative scheme, which could combine methods like multivariate data analysis and hypothesis testing. The second technique only needs one-time execution to detect all gross errors. However, the second technique requires an extra effort of tuning the likelihood function to have proper "cut-off" criteria.

The technique that utilizes hypothesis testing or multivariate data analysis relies on the model constrains and the variance-covariance matrix of the system model. The principle behind this GED technique is based on the outlier detection from correlated samples. It starts with the assumption that if random errors are the only sources of the measurement errors, the residuals of model constraints should be normally distributed with zero means and the standard deviations given by the variance-covariance matrix of the model. This is especially true for the equation-based data reconciliation problem. When gross errors occur, the residuals of model constraints violate the pattern of the variance-covariance matrix, which is formed based on the assumption that only random errors exist. By normalizing these errors, one can use the statistical test to identify the outliers. The normalized error (divided by standard deviations) follows a standard normal distribution with a zero mean and a standard deviation of one. The normalized random errors should fall inside a (1-α) confidence interval at a chosen level of significance α. Those errors falling outside the (1-α) confidence interval are identified as outliers (i.e. gross errors).

The other type of GED technique utilizes Gaussian-like distribution functions, also known as maximum likelihood estimators, or *M*-estimators. This type of probabilistic distribution functions usually has heavy tails, which give less weight on the

measurements with gross errors, so as to neutralize the smearing effects during data reconciliation. Due to the robustness of the objective function, the occurrence of gross errors does not contaminate the reconciliation of healthy measurements. The performance of the *M*-estimator also depends on tuning parameters, which determine the shape and cutting point of the likelihood function. It is suggested that the choice of these tuning parameters should best fit the specific problem, which requires an extra step of tuning the *M*-estimator, to give the best GED performance.

The technique that utilizes hypothesis testing or multivariate data analysis must be carried out with model constraints, which provide a counter check against the measurements. When the hypothesis testing is used as the GED technique, all possible gross error models are hypothesized and tested against a threshold value. To determine whether the hypothesis of a specific gross error model is a null hypothesis, i.e., no gross error, or an alternative hypothesis, i.e., gross errors occur, the reconciliation process based on least squares must be carried out with the presumed gross error model imposed. When the robust maximum likelihood function is used, there is no difference between data reconciliation and gross error detection since the reconciliation process is insensitive to gross errors such that at the end of data reconciliation the gross errors have already been isolated as well. In both GED techniques, data reconciliation and gross error detection must be carried out hand-in-hand because both techniques exploit the same information from the measurements and model constraints.

In summary, GED techniques can be categorized into two major types, hypothesis testing and robust estimation. In the technique of hypothesis testing, hypotheses are tested for all possible gross error models or in an iterative way, by which gross error models are eliminated stepwise. Because the gross error effects are already taken into account when imposing hypothesized gross error models to the measurements, the least squares objective function is still utilized. Figure 5-4 shows the structure of this type of GED strategy. On the other hand, in the robust estimator type of technique, no gross error

models are needed. Instead, robustness is built into the optimization process through the use of heavily tailed Gaussian type likelihood functions, which suppress the smearing effects during data reconciliation. Figure 5-5 shows the structure of this type of GED strategy. The technique of multivariate data analysis can be categorized as a subtype of hypothesis testing methodology since it also relies on comparing the error patterns based on the variance-covariance matrix to the measurement errors for outlier detection. It can be utilized as a prescreen process to detect serious gross errors before applying any of the GED techniques mentioned above.

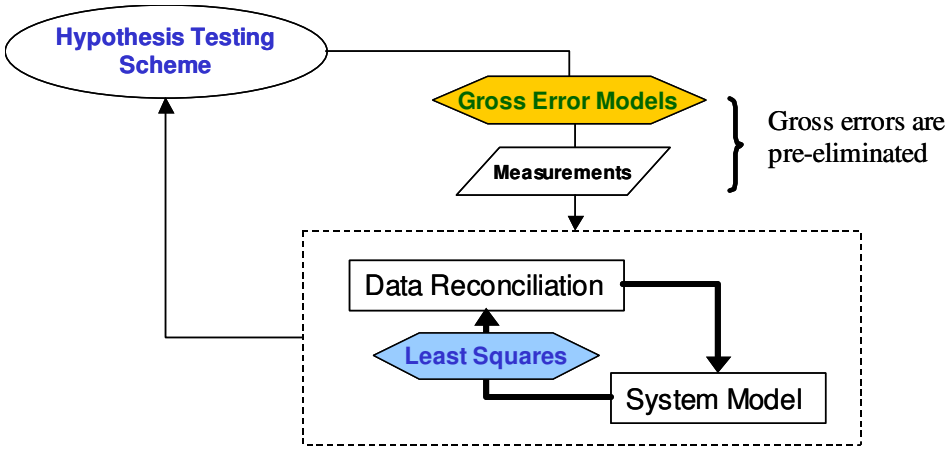

Figure 5-4: Process map for hypotheses testing based gross error strategy

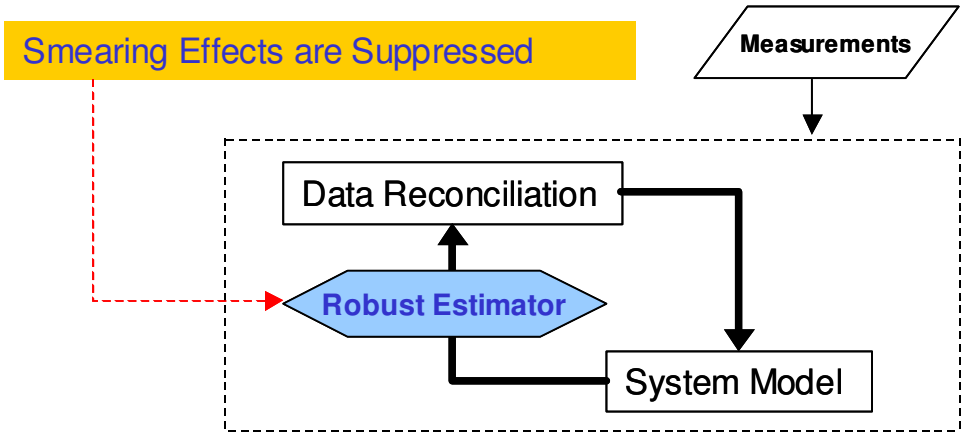

Figure 5-5: Process map of robust estimator based gross error strategy

5.3. Gross Error Prescreening

The occurrence of gross errors causes smearing effects in model-based data reconciliation and model calibration. The GED technique based on hypothesis testing needs an iterative scheme to eliminate improper gross error models. The process time for the iterative scheme can be reduced if one pre-eliminates those serious gross errors prior to the hypothesis-testing based GED technique. This can be accomplished by finding the outliers in a group of correlated data. If the data can be grouped in a two-dimensional way such that the correlation between two sets of datum can be evaluated, the identification of gross errors will become easier. Especially in the case of strong correlations among sampled data points, those data points which violate the correlation patterns can be easily identified and seen as outliers.

Multivariate Data Analysis (MDA) is referred to as a statistical method used to analyze multivariate data that are mutually correlated. When the data sets are stored in database tables containing rows and columns, MDA can process the information in a meaningful fashion. MDA provides a clear picture of how the model responses are correlated. Therefore, it can be utilized to identify the correlations between responses and reveal the dominant pattern in multivariate data sets, which can be compared against the measurement data to identify outliers. In the model-based data reconciliation problem the model parameters are unknown and to be estimated. By assigning proper bounds to the model parameters and carrying out the random sampling technique like Monte Carlo simulation, the correlations of model responses, which are functions of the model parameters, can be revealed.

Principal component Analysis (PCA) is one of the MDA technique used to analyze multi-dimensional data sets and identify outliers. PCA uses linear transformation on multivariate data sets to reduce the dimensions of system variations, by which the outliers can be identified more easily for problems with large dimensions. In this study,

PCA was utilized along with the model multivariate plots to detect serious gross errors. The advantage of using MDA is that the least squares type optimization process is not required and, thus, the smearing effects can be avoided.

5.3.1. Multivariate Data Analysis

Multivariate data analysis (MDA) utilizes a similar concept as hypothesis testing to identify gross errors. In both methods gross errors are identified through the recognition of outliers in expected mother populations, in which random errors are assumed to be the only source of errors. Hypothesis testing is usually combined with least squares optimization where the optimum model parameters are obtained. The residuals, i.e., the errors caused by measured data, are then compared to the expected error distributions to determine whether the null hypothesis, i.e., gross errors don't exist, or the alternative hypothesis, i.e., gross errors exist, is rejected. The process is usually an iterative process, in which different hypotheses of gross error models are imposed to the measurements at each run of data reconciliation and the statistic test is followed. The process terminates when the alternative hypothesis is rejected. Since the expected gross error model has been imposed during hypothesis testing, the smearing effect is eliminated.

Similar to hypothesis testing, in multivariate data analysis the measurements are compared against the expected mother populations, which are formed from the possible model responses. The gross errors are identified when significant deviations from the mother populations occur, i.e., the outliers. The major difference between MDA and hypothesis testing is that MDA can be carried out without least squares optimization, i.e., data reconciliation. Instead, a random sampling process such as Monte Carlo Simulation is required. Since data reconciliation is not required in MDA, the gross error identification process will not be biased due to smearing effects. The MDA method is, however, only for identifying the locations of serious gross errors, i.e., biases with large

magnitudes, because the least squares optimization scheme (data reconciliation) is not carried out. To reconcile the measurements and estimate the model parameters, the least squares minimization scheme is still needed after screening out serious gross errors. The MDA method can serve as a prescreening process for serious gross errors. Hypothesis testing combined with the least squares minimization scheme is then carried out with the prior knowledge of serious gross errors.

In this study MDA is demonstrated by using the multivariate plots for the model responses and the measured data. The multivariate plots show the measured data against patterns of possible model responses, which are usually normally distributed based on the ranges and distributions of model parameters imposed in the beginning. Because the data is compared to the mother populations in a multi-dimensional way, the visual recognition of outliers is not only based on the ranges, i.e., within the ranges or out of ranges of mother populations, but is also based on the violation of correlation patterns. If the model responses show significant correlations, the outliers will still be identified even though the data is within the range in each dimension of model response.

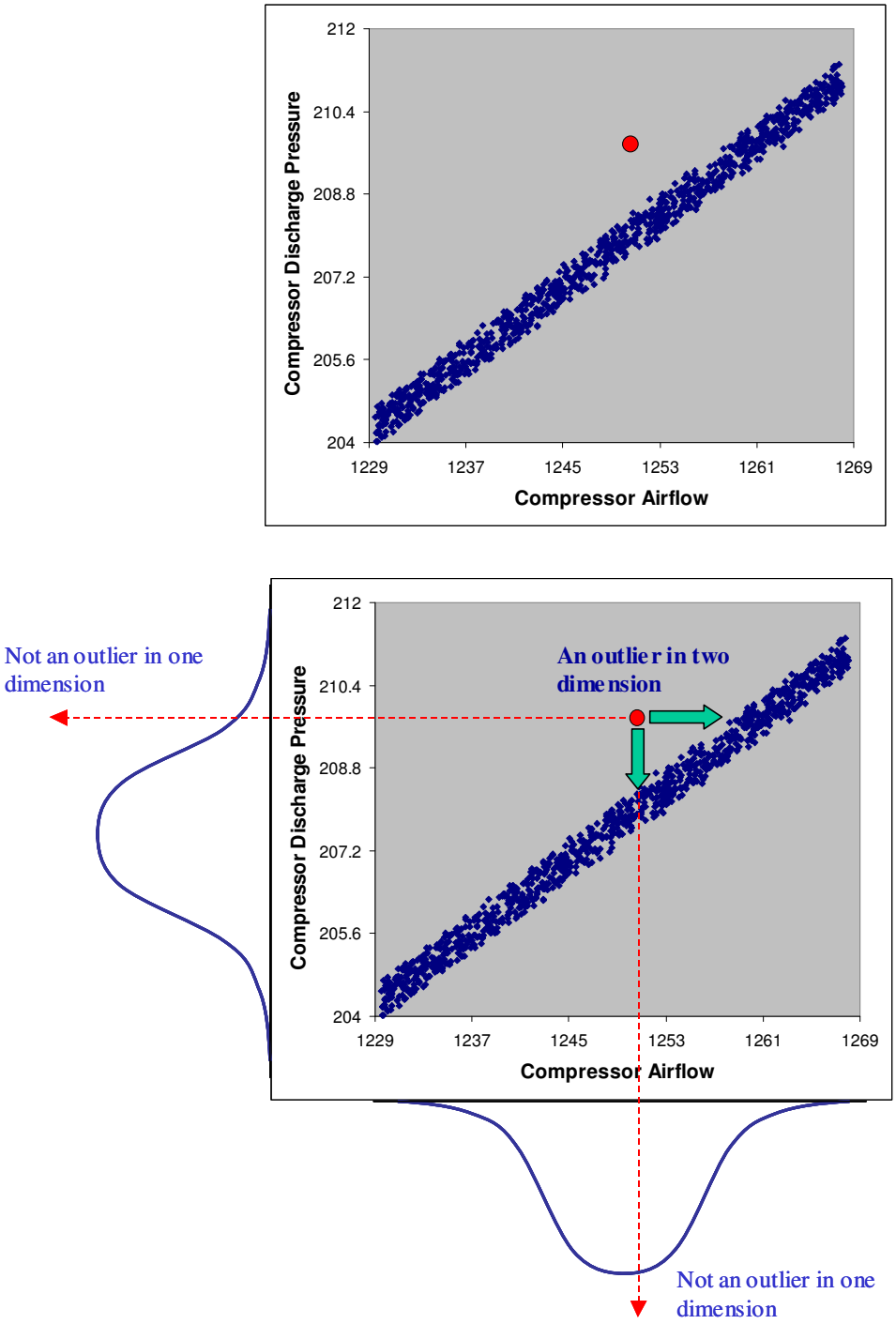

Figure 5-6: Outlier detection using multivariate data analysis

In Fig. 5-6, a bivariate plot of the gas turbine compressor airflow and compressor discharge pressure is shown. The group of data points marked by blue colors represents the possible outcomes of model predicted compressor airflow and compressor discharge pressure. The simulated data points are generated from a randomly sampling technique such as Monte Carlo Simulation and, therefore, represent the mother populations of specific model responses, i.e., compressor airflow and pressure. The red point represents a set of measured data for the compressor airflow and pressure. In Fig. 5-6 it is apparent that when the measurements are compared against their correspondent mother population in a one-dimensional way, they both are ruled out as outliers. When the measured data is compared against their mother populations in a bivariate way, i.e., two-dimensional, the data is identified as an outlier because it is outsides the cloud of correlated data points. Fig 5-7 shows the measured data point that is not considered as an outlier in the bivariate plot since it is within the cloud of data points.

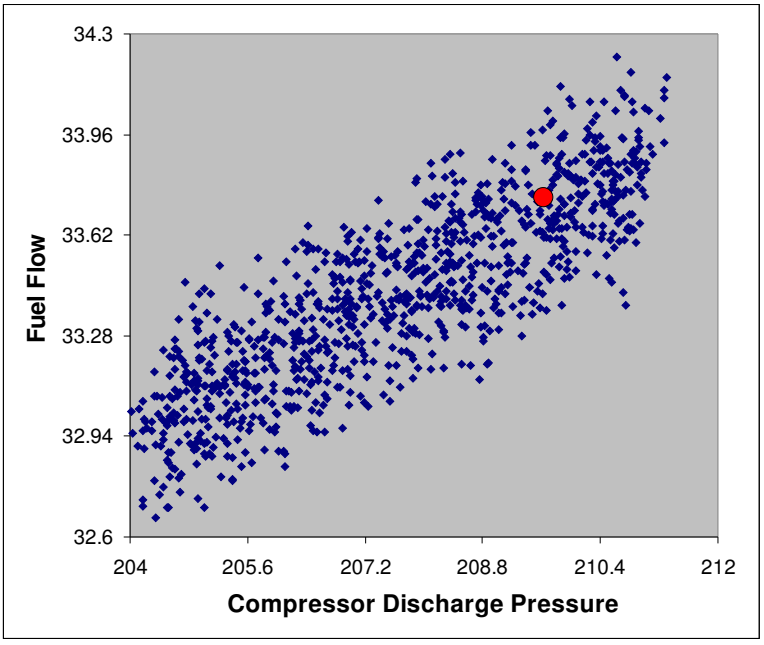

Figure 5-7: Data ruled out as an outlier

Monte Carlo Simulation

Monte Carlo Simulation is a way of evaluating multiple integrals that depends on random sampling from probability density distributions, rather than regular grid-based sampling techniques. Monte Carlo provides a way of simulating experiments and creating models of experimental data. With Monte Carlo simulation, the statistical significance of data can be tested with relatively simple calculations that require neither a deep theoretical understanding of statistical analysis nor sophisticated programming techniques. Because the Monte Carlo method requires the generation of large number of individual events, the simulation time can be expensive if the required model running time is long. To reduce the simulation time, a surrogate model such as response surface equation (RSE) can be utilized. Either the real model or the surrogate model should be expressed in an explicit form such that the model responses are functions of the model parameters:

$$\boldsymbol{Y = F(X)} \tag{5-1}$$

where both $\boldsymbol{Y}$ and $\boldsymbol{F}$ are column vectors of multiple model responses while $\boldsymbol{X}$ represents the row vector of model parameters:

$$\begin{bmatrix} y_1 \\ y_2 \\ y_3 \\ \vdots \\ y_m \end{bmatrix} = \begin{bmatrix} f_1(x_1, x_2, x_3 \cdots x_n) \\ f_2(x_1, x_2, x_3 \cdots x_n) \\ f_3(x_1, x_2, x_3 \cdots x_n) \\ \vdots \\ f_m(x_1, x_2, x_3 \cdots x_n) \end{bmatrix} \tag{5-2}$$

To generate the random deviates of model parameters from specific probability distributions, either the *transformation method* or the *rejection method* is utilized. The *transformation method* is the most useful method for obtaining random deviates drawn from particular distributions. The steps of *transformation method* is described as follows:

1. Decide proper ranges on x's. The ranges of model parameters can be determined based on prior knowledge about the current model status. For a physical-based

model, the ranges should also be reasonable so the model will neither crash nor generate non-reasonable results.

2. Decide probability functions for model parameters x's. If prior knowledge is available, Gaussian distributions are usually assigned. Without prior knowledge, uniform distributions are reasonable options.
3. Normalize the probability function. If it is necessary to impose limits on the range of model parameters x's, then the function must be renormalized to assure that the integral is unity over the newly defined range. The normalization integral should be calculated by the same analytical integration or numerical integration routine.
4. To pick a random sample *x* from the specified probability function from Step 3, a random number *r* is first generated from an uniform distribution shown as:

$$p(r)=\begin{cases}1 & for\ 0\le r<1\\ 0 & otherwise\end{cases} \tag{5-3}$$

Then find a normalization function that describes the relation between *r* and *x* such as $x = g(r)$.

5. Use the transformation integral to transform the variable *r* drawn randomly the uniform distribution into a variable *x* drawn randomly from the specific distribution *P(x)*

$$\int_{r=0}^{r} r\,dr=\int_{x=-\infty}^{x} P(x)\,dx \tag{5-4}$$

which also gives the result

$$r=\int_{x=-\infty}^{x} P(x)\,dx \tag{5-5}$$

The sampled x can then be obtained from $x = g(r)$ and fed to the model equation ***Y=F(X)*** to generate one event of model response.

Step 4 and 5 are repeated until the specified number of Monte Carlo runs is reached.

The above Monte Carlo method will generate the model responses with variances that are caused by the variations of model parameters, *x*'s, which are randomly sampled in Monte

Carlo Simulation. Each simulated event represents a set of model responses, i.e., model-calculated values, corresponding to a specific set of model parameters, and, thus, represents the expected value of measured data. To simulate the effects of measurement uncertainties, the simulated data can be imposed by the measurement uncertainty, which is called "Data Smearing". Data smearing can be carried out with simply adding the uncertainty term to the simulated data. If a particular model response, y_i, has uncertainties, σ_i, and Gaussian uncertainties are assumed, then the smeared value of y_i can be obtained:

$$y_i' = y_i + \sigma_i r_i \tag{5-6}$$

where r_i is a random variable drawn from the standard Gaussian distribution with mean 0 and standard deviation 1. The calculation is equivalent to drawing the random variable, y_i', directly from a Gaussian distribution with mean, y_i, and standard deviation, σ_i.

Multivariate Data Visualization

Monte Carlo Simulation combined with data smearing is the technique of generating simulated data from the model. The simulated data represents the mother population of model responses and can be utilized to identify the outliers when compared against the measured data.

After Monte Carlo Simulation, data sets with multiple model responses are generated. Multivariate data analysis is used to deal with data sets that have more than one response for each observational unit, i.e., the Monte Carlo simulated event. The data sets can be summarized via data matrices with m rows and p columns, where the rows represent the observations, i.e., the number of Monte Carlo runs, and the columns represent the model responses. The major multivariate methods can be categorized as those that have prior knowledge about the structure, for example, dividing the cases into groups, and those that seek to discover the structure from the evidence of the data matrix alone, also called data mining. In pattern recognition terminology the distinction is

between supervised and unsupervised methods [71]. The emphasis of this study is on unsupervised methods, in which no priori knowledge of the structure of data is assumed.

A simple way to examine multivariate data is via a pairs plot or scatter plot matrix. A scatter plot matrix is a set of two-dimensional projections of a high dimensional point cloud. This is a simple, but powerful, technique for describing relationships among response variables with correlations. An example of a scatter plot matrix of response variables $y_1, y_2, \ldots, y_n$ is shown in Fig. 5-8, which shows a matrix of all the pair wise scatter plots between $y_1, y_2, \ldots, y_n$. Each plot within the scatter plot matrix shows the correlation between two response variables. In Fig. 5-8, the data cloud (black marked data points) represents the simulated response variables and the red marked data point represents the measured data. The multivariate visualization by a scatter plot matrix makes outlier identification relatively easy, especially when strong correlations exist between response variables.

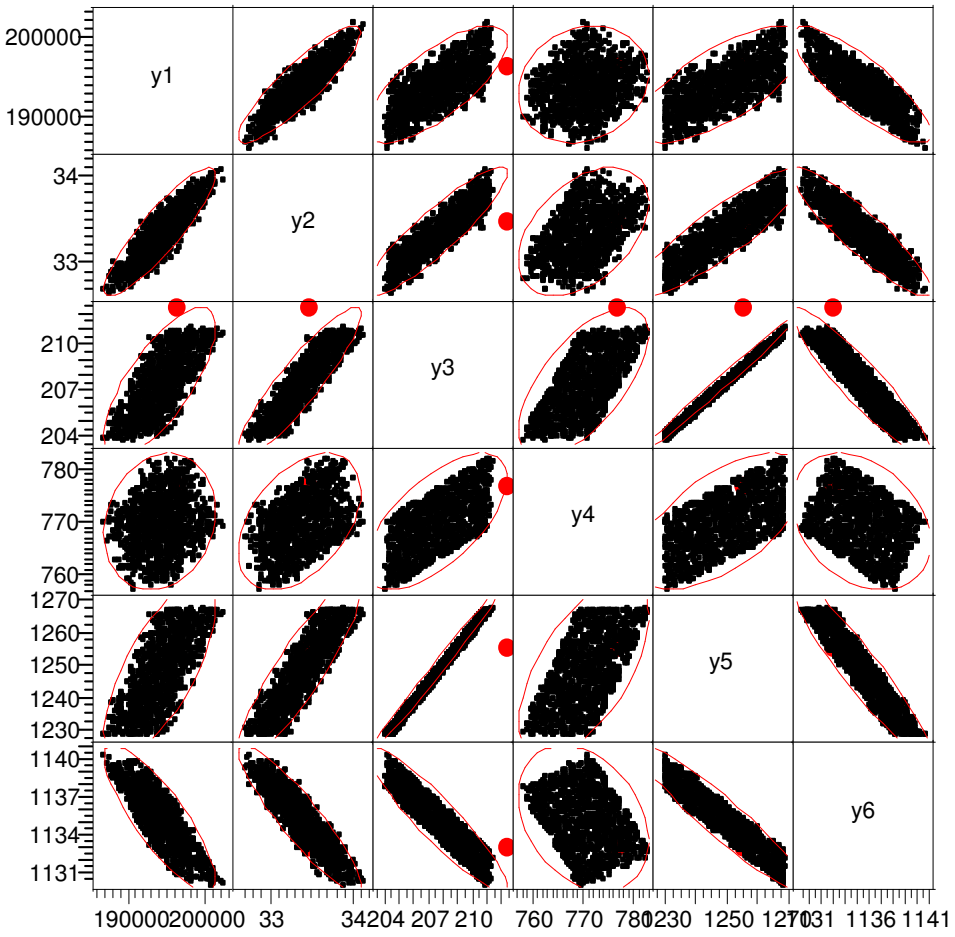

Figure 5-8: Scatter plot matrix

A scatter plotter matrix can be characterized via a covariance matrix where each element represents the covariance of a pair of response variables. The covariance of a pair of response variables y_i, y_j is defined as:

$$cov(y_i, y_j) = \frac{\sum_{k=1}^{m} (y_i - \overline{y_i})_k (y_j - \overline{y_j})_k}{m-1} \tag{5-7}$$

where y_i represents the *ith* response variable, m represents the number of simulated data sets, and $\overline{y_i}$ is the mean of mother population from y_i. The covariance matrix of response variables can then be defined as:

$$\begin{bmatrix} cov(y_1, y_2) & . & . & . & cov(y_1, y_n) \\ . & . & & & . \\ . & & . & & . \\ . & & & . & . \\ cov(y_n, y_1) & . & . & . & cov(y_n, y_n) \end{bmatrix} \tag{5-8}$$

Any measured response variable that has a significant bias can make its data point out of the data cloud in the scatter plot, and be seen as an outlier. Because the data points are shown in a two-dimensional way such that not only the ranges but also the pattern of the data cloud can be utilized to identified the outliers. As mentioned earlier, a measured response variable could be ruled out as an outlier when against the simulated data sets that are displayed in a one-dimensional way. The inner structure of the model determines how the response variables react to the variations of model parameters, i.e., sensitivity, which causes the spread of the data cloud, and how they interact with each other, i.e., correlation, which leads to the correlation pattern of data cloud.

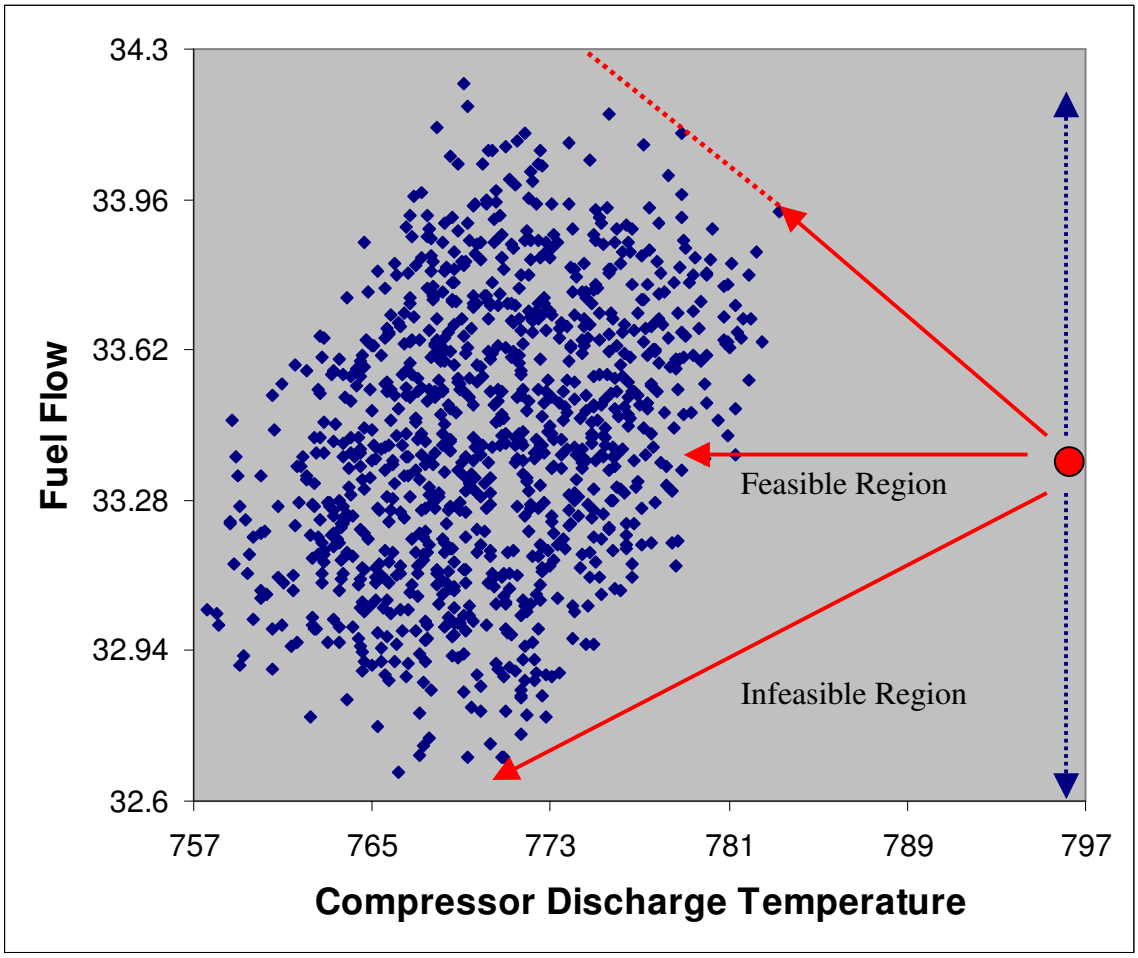

(a)

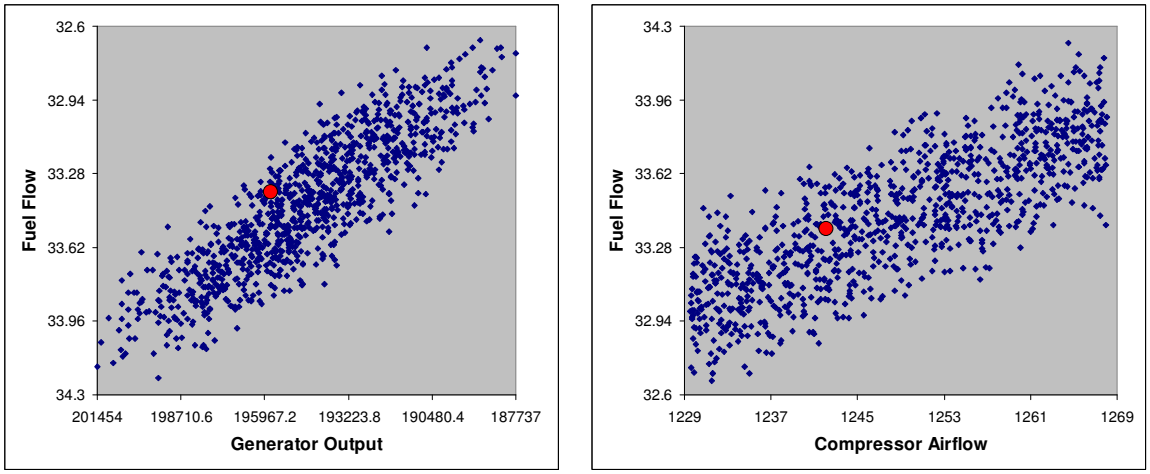

(b)

Figure 5-9: Scatter plots for fuel flow

Fig. 5-9 shows three scatter plots from a scatter plot matrix constructed based on Monte Carlo Simulation on a gas turbine model with six response variables. In Fig 5-9(a) the scatter plot of two response variables, fuel flow and compressor discharge temperature, shows that the measured data point (the red marked point) is outside the data cloud and is identified as an outlier. By compensating the two response variables with biases, the data point can be moved toward the data cloud, which represents the mother population of these two response variables. The compensated data set can be expressed as:

$$\begin{pmatrix} y_i' \\ y_j' \end{pmatrix} = \begin{pmatrix} y_i \\ y_j \end{pmatrix} + \begin{pmatrix} b_i e_i \\ b_j e_j \end{pmatrix} \tag{5-9}$$

where y_i' is the compensated value, y_i is the original measured value, b_i is the compensated bias, and e_i is the unit vector parallel to the axis of response variable, y_i. From Fig 5-9(a), if the measured data (fuel flow and compressor discharge temperature) is compensated in the feasible directions, the data point can be moved toward the data cloud. It is apparent that there must be a bias compensation to the compressor discharge temperature in order to maintain the feasible direction, indicating that there is a gross error in the measured compressor discharge temperature, but not necessary for the fuel flow measurement because the data point can be moved to the data cloud without the fuel bias compensation. In order to determine if there exists a gross error in the fuel flow measurement, other scatter plots with axes of fuel flow need to be checked. Fig. 5-9(b) shows two scatter plots, both of which have the fuel flow as one of the two response variables. In the two scatter plots shown in Fig 5-9(b), the data points are inside the data cloud, which suggests the possibility of having a gross error in the fuel flow measurement is very low and can be ruled out. From this example it is obvious that to identify gross errors in measurements, the information obtained from one scatter plot is not enough, instead, the whole scatter plot matrix needs to be studied.

The multivariate data visualization technique such as the scatter plot matrix provides an easy way to identify the outliers by intuitional visualization. Not all gross errors can be detected via this technique, and the performance of this multivariate technique depends on the error ranges applied to the model parameters and the correlation patterns of the model responses. Prior knowledge of the thermal model can help to set proper ranges on the assumed parameters. The prior knowledge can be the operations hours of the thermal machine such that a degradation curve can be utilized to estimate the changes of the model parameters due to degradation effects. The other way that helps to assign proper ranges for model parameters is to carry out data reduction for the system model and estimate and uncertainty of the estimated parameters through sensitivity study. It is assumed that the uncertainties of the estimated parameters would not be affected in the presence of gross errors. This assumption, however, would not be valid if the model is highly nonlinear, and the gradient of the model function changes significantly as biases occurs in the model inputs during data reduction. Smaller error ranges lead to narrower model responses, and the probability of type I error increases. Significant correlation patterns are also very helpful in detecting the outliers. This correlation pattern is important because the observations can be within the acceptable sigma levels for each response but are still outliers because they are out of bounds when we investigate the bivariate distributions (joint distribution). These types of outliers are identified because the correlation patterns are violated.

5.3.2. Principal component Analysis

A multivariate visualization technique such as the scatter plot matrix can miss interesting structures in the multivariate model responses when three or more model parameters are involved. In addition, as the multivariate dimensions increase with the number of model responses, it becomes more difficult to break down the source of gross errors causing outliers. The needs for handling a problem with a large number of

response variables can be satisfied by the MDA technique that explores the data in a way of less coordinate-dependent. The scatter plot matrix is a visualization technique that relies on intuitional visual recognition, by which the quantified information is not provided. Therefore, a MDA technique that provides quantified information about the breakdown of errors is also needed.

Principal Component Analysis (PCA)[72] is a well-established technique that is able to reduce dimensionality in multivariate data analyses. It has been widely applied in many areas including data compression, image processing, gross error detection, visualization, exploratory data analysis, pattern recognition, and time series prediction. A complete discussion of PCA can be found in textbooks [73], [74]. Three important features that make PCA a powerful tool and being popular in wide areas of applications: First, it is an optimal (in terms of mean squared error) linear scheme that transforms mutually related vectors into orthogonal vectors, which can be reconstructed by lower dimensional bases with minimal loss of information. Second, the model parameters can be computed directly from the data, e.g., by diagonalizing the covariance matrix of the sampled data. Third, compression and decompression are easy operations to perform given the model parameters – they require only matrix multiplication. The first feature is the most important one in GED for the capability of breaking down the source of biases among high dimensional response variables.

One of the major properties of PCA is its capability of breaking down the contribution of errors, and this makes PCA an effective tool in identifying serious gross errors from multi-dimensional data sets. PCA is also an efficient way of identifying patterns in data sets and expressing the data in the way as to highlight their similarities and differences. It transforms a group of correlated data sets into a new group of uncorrelated data sets, which are also known as principal components. Each principal component (PC) is a linear transformation of original data sets and is orthogonal to one another. The coefficients of each linear combination are obtained from the eigenvectors of the variance-covariance

matrix formed by simulated data points. If model-based data reconciliation and model calibration is considered, the variance-covariance matrix represents patterns of model variations, caused by variations of model parameters. The principal component with the highest score then constructs the axis that describes the largest portion of model variation.

Consider a system model that has m response variables, each of which is a function of model parameters and has its correspondent measurement. The system model can be expressed as:

$$\begin{bmatrix} y_1 \\ y_2 \\ y_3 \\ \vdots \\ y_m \end{bmatrix} = \begin{bmatrix} f_1(\alpha_1,\alpha_2,\alpha_3\cdots\alpha_n) \\ f_2(\alpha_1,\alpha_2,\alpha_3\cdots\alpha_n) \\ f_3(\alpha_1,\alpha_2,\alpha_3\cdots\alpha_n) \\ \vdots \\ f_m(\alpha_1,\alpha_2,\alpha_3\cdots\alpha_n) \end{bmatrix} \tag{5-10}$$

where y_m represents a response variable as a function, f_m, of model parameters $\alpha_{1\sim n}$. The task is to identify serious gross errors in measurements $[\hat{y}_1\ \hat{y}_2\ \hat{y}_3\cdots\ \hat{y}_m]^T$ before carrying out hypothesis testing and data reconciliation.

The basic concept of utilizing PCA to identify gross errors is using principal components as dimensional bases to describe the variations of response variables in an uncorrelated way. This requires the knowledge about the variance structure of response variables, i.e., the covariance matrix. For a nonlinear system with high dimensional responses, it is difficult to obtain an analytical form for its covariance matrix. Instead, the Monte Carlo simulation is utilized to approximate the propagation of parameter variations to response variations, by which the system covariance matrix can be constructed. The variations of model parameters lead to status variations, and the measurement uncertainties also contribute to the variations of system responses at a specific system status. Therefore, to simulate the deviates of response variables both Monte Carlo simulation and the data smearing technique are required. Figure 5-10 depicts the process.

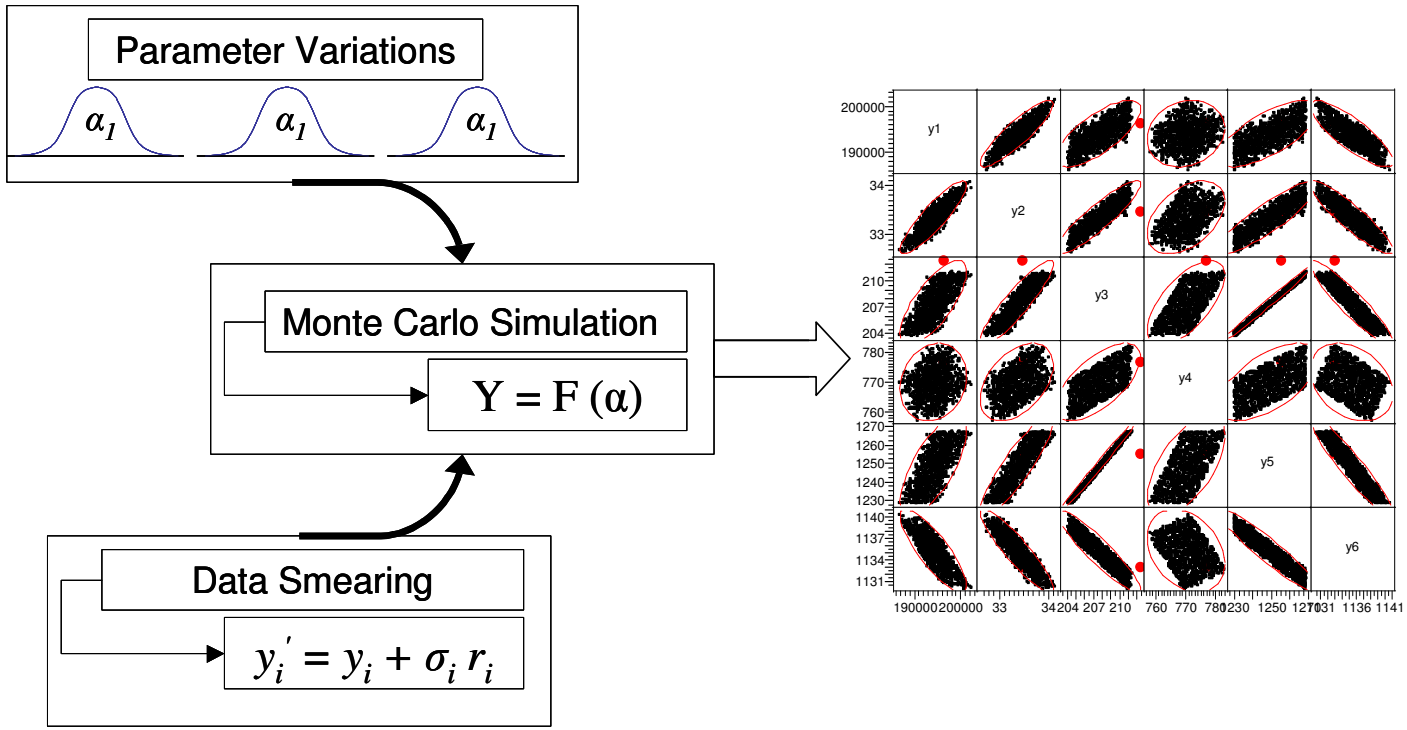

Figure 5-10: Data smearing in a Monte Carlo process

Once the deviates of system responses are obtained from Monte Carlo simulation and data smearing, the data sets can be expressed by a $\ell \times m$ matrix where ℓ is the number of data sets and m represents the number of response variables. The simulated response variables are then centralized by the their mean values:

$$\hat{y} = y - y^{*} \qquad or \qquad \hat{y}_{ij} = y_{ij} - y_{ij}^{*} \tag{5-11}$$

The matrix form can also be shown as follows:

$$\begin{pmatrix} \hat{y}_{11} & \hat{y}_{12} & \cdots & \hat{y}_{1m} \\ \hat{y}_{21} & \hat{y}_{22} & \cdots & \hat{y}_{2m} \\ \vdots & \vdots & \vdots & \vdots \\ \hat{y}_{\ell 1} & \hat{y}_{\ell 2} & \cdots & \hat{y}_{\ell m} \end{pmatrix} = \begin{pmatrix} y_{11} & y_{12} & \cdots & y_{1m} \\ y_{21} & y_{22} & \cdots & y_{2m} \\ \vdots & \vdots & \vdots & \vdots \\ y_{\ell 1} & y_{\ell 2} & \cdots & y_{\ell m} \end{pmatrix} - \begin{pmatrix} y_{11}^{*} & y_{12}^{*} & \cdots & y_{1m}^{*} \\ y_{21}^{*} & y_{22}^{*} & \cdots & y_{2m}^{*} \\ \vdots & \vdots & \cdots & \vdots \\ y_{\ell 1}^{*} & y_{\ell 2}^{*} & \cdots & y_{\ell m}^{*} \end{pmatrix} \tag{5-12}$$

Where y_{ij}, y_{ij}^{*}, and $\hat{y}_{ij}$ represent simulated, mean, and centered response values separately. The covariance of two response variables can be calculated as following:

$$cov(\hat{y}_i, \hat{y}_j) = \frac{\sum_{k=1}^{\ell} \hat{y}_{ki}\, \hat{y}_{kj}}{\ell - 1} \tag{5-13}$$

The covariance matrix of the centered response variables, *He*, is then obtained as follows:

$$H_e = \begin{bmatrix} cov(\hat{y}_1, \hat{y}_2) & . & . & . & cov(\hat{y}_1, \hat{y}_m) \\ . & . & & cov(\hat{y}_i, \hat{y}_j) & . \\ . & . & & & . \\ . & & & . & . \\ cov(\hat{y}_m, \hat{y}_1) & . & . & . & cov(\hat{y}_m, \hat{y}_m) \end{bmatrix} \tag{5-14}$$

The covariance matrix of response variables is very important to PCA because it represents the ranges and correlation patterns of response variables, and, therefore, has a direct impact on the outlier identification.

Once the covariance matrix of system response variables, $\boldsymbol{H_e}$, is obtained, its eigenvectors and eigenvalues can also be calculated. The obtained m eigenvectors, $\boldsymbol{p_1}$,

…$\boldsymbol{p_m}$, are then normalized by their length (i.e. $\| \boldsymbol{p_i} \| = 1$) and stored as column vectors in the $m \times m$ matrix, $\boldsymbol{P_e}$, in such a way that their corresponding eigenvalues, $\lambda_{1, \ldots} \lambda_{m,}$ follow:

$$\lambda_1 \geq \lambda_2 \ldots \geq \lambda_m \tag{5-15}$$

Where $\boldsymbol{P_e} = [\, \boldsymbol{p_1} \mid \boldsymbol{p_2} \mid \ldots \mid \boldsymbol{p_m} \,]$, and has two important properties:

- The columns of $\boldsymbol{P_e}$ are linearly independent (by construction), and, therefore, there exists $\boldsymbol{P_e}^{-1}$
- Because $\boldsymbol{P_e}$ is formed by column vectors of orthogonal eigenvectors, it follows that $\boldsymbol{H_e}\, \boldsymbol{P_e} = \boldsymbol{P_e}\, \boldsymbol{\Lambda_e}$, where $\boldsymbol{\Lambda_e}$ is a diagonal matrix consisting of the eigenvalues of $\boldsymbol{H_e}$, λ_i, $i = 1, \ldots, m$, on its diagonal.

$$\Lambda_e = \begin{bmatrix} \lambda_1 & 0 & \cdots & 0 \\ 0 & \lambda_2 & & \vdots \\ \vdots & & \ddots & 0 \\ 0 & \cdots & 0 & \lambda_m \end{bmatrix} \tag{5-16}$$

- Since $\boldsymbol{H_e}$ is symmetric, its normalized eigenvectors are orthogonal to each other, and follow:

$$\boldsymbol{P_e}^{\mathrm{T}}\, \boldsymbol{P_e} = \boldsymbol{P_e}\, \boldsymbol{P_e}^{\mathrm{T}} = \boldsymbol{I} \rightarrow \boldsymbol{P_e}^{-1} = \boldsymbol{P_e}^{\mathrm{T}} \tag{5-17}$$

When the measured data set is brought in and centered by the mean of corresponding simulated response variables, it can be expressed as follows:

$$\hat{y}' = y' - y^* \tag{5-18}$$

Now the principal components can be obtained by a linear combination of the centered measured data set, $\hat{y}'$:

$$y_e = W_e^T\, \hat{y}' \tag{5-19}$$

Vector, $\boldsymbol{y_e}$, is composed of principal components, and the values of its elements are the PCA scores. The linear combination coefficients given in $\boldsymbol{W_e}$ form the eigenvectors of $\boldsymbol{H_e}$, which satisfy:

$$W_e = P_e \Lambda_e^{-1/2} \tag{5-20}$$

If there is no biases in the measurements, the centered data set should follow $\hat{y}' \sim (\boldsymbol{0}, \boldsymbol{H_e})$, and it can be proved that $\boldsymbol{y_e} \sim (\boldsymbol{0}, \boldsymbol{I})$. Therefore, the original set of correlated response variables, $\hat{y}'$, is transformed into a new set of uncorrelated principal component, $\boldsymbol{y_e}$. The principal components are then listed in a descending order ranked by the magnitudes of corresponding eigenvalues:

$$[y_{e1}, y_{e2}, \ldots, y_{em}]$$

with

$$\lambda_1 \geq \lambda_2 \ldots \geq \lambda_m. \tag{5-21}$$

When all the principal components are retained, i.e., $y_e \in R^m$, the response variable can be reconstructed without losing any information. The reconstruction can be carried out through the following expression:

$$y' = y^* + P_e \Lambda_e^{1/2} y_e \tag{5-22}$$

If fewer principal components than *m* are retained, the reconstruction is subjected to certain loss of information. To fully recover the original response variables, the error term should be added. The reconstruction with fewer principal components is shown as:

$$y' = y^* + P_e \Lambda_e^{1/2} y_e + \left(y' - \tilde{y}\right) \tag{5-23}$$

with

$$\tilde{y} = y^* + P_e \Lambda_e^{1/2} y_e \tag{5-24}$$

Equation (5-24) is referred to as the principal component model for y'. When all principal components are retained, y' can be fully reconstructed from its principal

component model $\tilde{y}$, i.e., $y' = \tilde{y}$. Equation (5-23) also indicates that the measured response variables, y', can be decomposed into the contributions from their expected values, y^*, principal component, $\boldsymbol{y_e}$, and the residuals of the principal component model, $y' - \tilde{y}$. Since the principal components, $\boldsymbol{y_e}$, represent the linear combinations of the centered data, $\hat{y}$, and follow $\boldsymbol{y_e \sim N(0, I)}$, hypothesis testing can be applied to $\boldsymbol{y_e}$ directly.

From Equation (5-20) and the fact that $\boldsymbol{y_e \sim N(0, I)}$, i.e.,

$$y_{e,i} = \left(W_e^T \hat{y}\right)_i \sim N(0,1), \qquad i = 1,\ldots,k_e \tag{5-25}$$

, each principal component, $\boldsymbol{y_{e,i}}$, can be tested against a tabulated threshold value of a standardized normal distribution. Equation (5-25) also shows that the *i*th principal component is equal to the product of the *i*th eigenvector from $\boldsymbol{W_e}$ and the centered response variables, $\hat{y}$. Since each principal component is obtained from the linear combination of the original centered response variables, it can be decomposed into the contributions of each centered response variable. The decomposition can be expressed as:

$$g_j = \left(w_{e,i}\right)_j \hat{y}_j \qquad j = 1,\ldots,m \tag{5-26}$$

where $\boldsymbol{g_j}$ is the contribution from the *j*th response variable, $\hat{y}_j$, and $w_{e,i}$ represents the *i*th eigenvector in $\boldsymbol{W_e}$. A vector $\boldsymbol{g' = (g_1', \ldots, g_m')}^T$, where $\boldsymbol{g_j'}$ is the absolute value of $\boldsymbol{g_j}$, i.e., the magnitude of the contribution, can be defined such that the contribution of each response variable to the principal component can be studied. In general, the contribution of each response variable is different than one another, but the overall contribution is dominated by the first few elements. These major contributors to the suspect principal component that is above the threshold value indicate suspicious gross errors in the measured response variables.

It should be mentioned that the retained principal components that have large values and significant contributions to the chi-square statistic are not the ultimate indicators of gross

errors. It is the residuals that have large contributions to the suspect principal components that need to be investigated and suspected as gross errors.

The principal component analysis can be summarized as follows:

1. Obtain the covariance matrix of system response variables. The covariance matrix represents the ranges and correlations of response variables, which set the spreads and patterns for the system mother populations. The covariance matrix can be obtained by an analytical way if the system model is linear or by a numerical method such as Monte Carlo simulation. When utilizing the Monte Carlo method, the simulated data can be formulated based on Equations (5-13) and (5-14) to construct the covariance matrix.
2. Compute the eigenvalues and corresponding eigenvectors of the covariance matrix. The eigenvectors are stored in the descending order with respect to the magnitudes of corresponding eigenvalues. The eigenvector with the highest score, i.e., with the largest eigenvalue, represents the primary axis that captures the largest part of system variation. The first few principle axes (i.e. eigenvectors) can be used to describe the system variation with minimum information loss.
3. Introduce the measured data centered by the means of response variables, and use the normalized principal component, $\boldsymbol{W_e}$ (see Equation (5-20)), to transform the residuals to the principal components, each of which is a linearization of original system response variables. It can be decided whether or not to retain all the principal components since the first few describe most of the deviations of the measured data from its mother population. Since it is not the intention to compress the data, but to identify the gross errors, it is reasonable to remain all principal components.
4. Each principal component is a linear transformation of original response variables. It is NOT the principal component flagged as an outlier. Instead, it is the contribution of each response variable to the inflated principal component

being identified as a gross error. Each principal component follows $\boldsymbol{y_e} \sim (\boldsymbol{0}, \boldsymbol{I})$, and can be tested against a tabulated threshold value based on the desired confidence level. For example the threshold value for 95% confidence level is 1.96.

Figure 5-11 shows the bar charts of principal components (on the top) and the corresponding contributions from response variables (on the bottom). Each principal component is compared against the threshold value, e.g., ±1.96 for ***N(0, I)*** at a 95% confidence level. A further investigation on the response variable that contributes to the most is carried out for the inflated principal components.

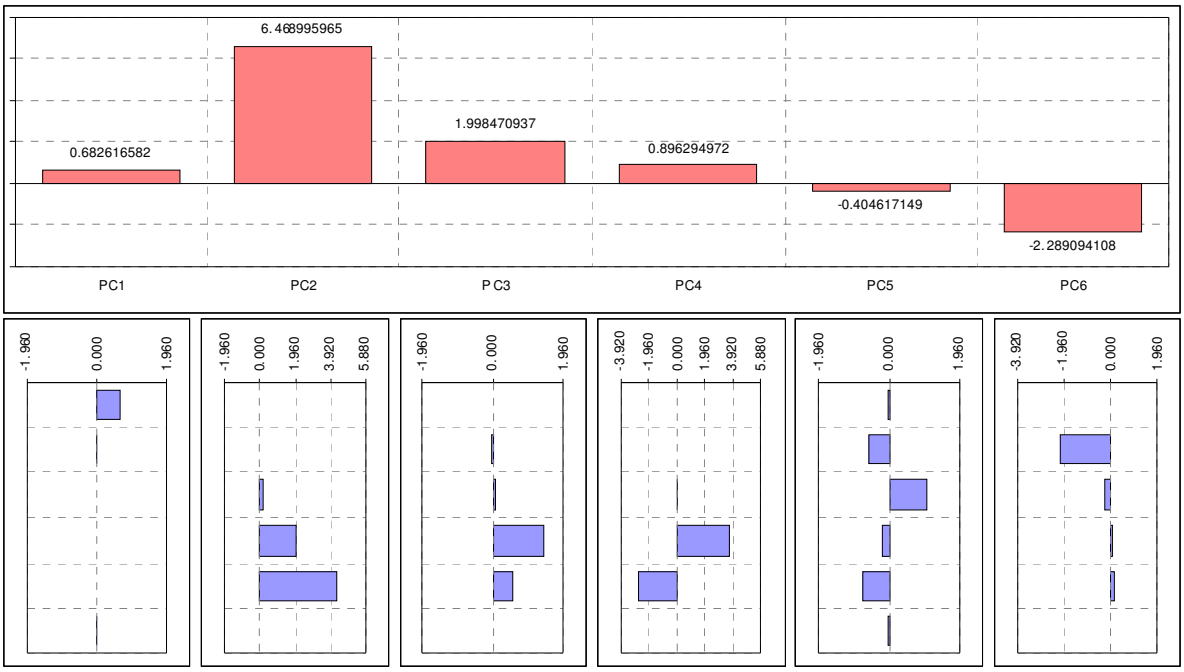

Figure 5-11: Bar charts for principal components analysis

Visualization of Principal component Analysis

It is difficult to visualize the hyper-surface of multidimensional correlated responses with more than three dimensions. In the principal component analysis, variations of the response variables are combined linearly and transformed into principal components. The principal components are in the descending order ranked based on the magnitudes of corresponding eigenvalues. The first few principal components capture the majority of overall response variations. Therefore, the variations of system responses can be summarized by the first few principal components with minimum loss of information, and the dimensionality of multivariate attributes can be reduced.

In order to visualize the variations of correlated responses in a three-dimensional way, the first three principal components are retained and used to construct the bases of hyper surface. If there are gross errors in measured data, the outlier can be visualized by rotating the axes of three retained principal components. Figure 5-12 (a) shows a three-dimensional spin plot for a system model with six responses, which is constructed by three of the original response variables. It shows strong correlations among the selected three variables. This plot cannot capture most of the system variations unless all six of system responses are used as hyper-surface bases. Figure 5-12 (b) shows, on the other hand, the three-dimensional spin plot constructed by the first three principal components as bases. According to the eigenvalues of the system covariance matrix, the first three principal components describe 99% of the system variations. Therefore, this 3-D spin plot can capture almost all the system variations. Also, there is no apparent pattern shown in fig 5-12(b). This is because the correlated system response variables are combined linearly and transformed into un-correlated principal components.

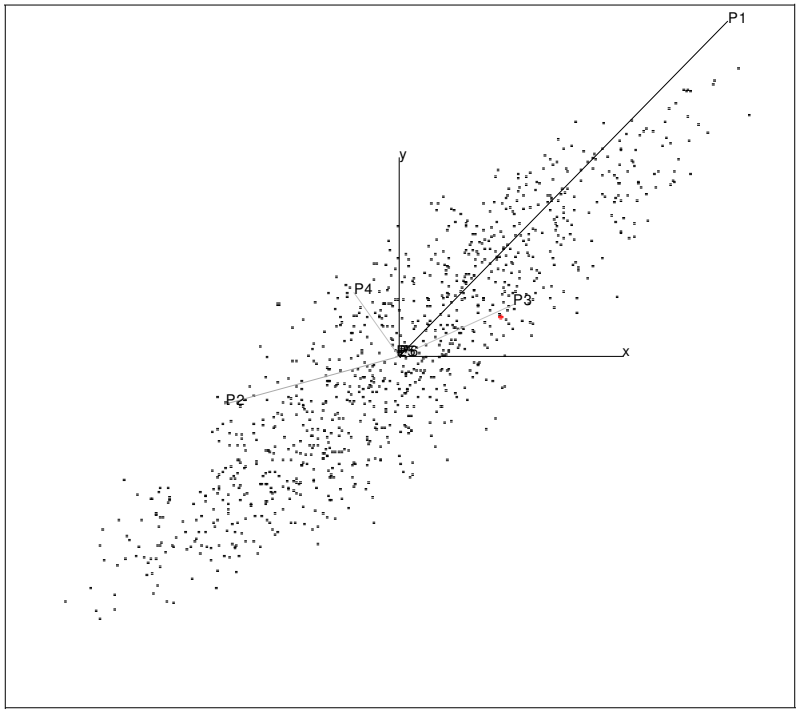

Figure 5-12(a): 3-D spin plot for original system response, y_1, y_2, y_3

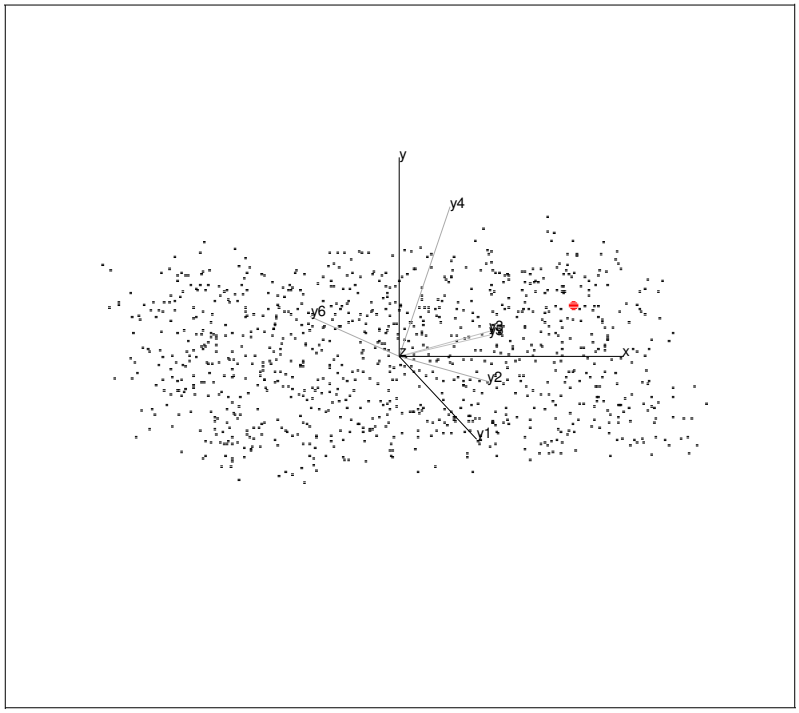

Figure 5-12(b): 3-D spin plot for principal components, p_1, p_2, p_3

5.4. Robust Estimator for Gross Error Detection

Smearing effects are inevitable when gross errors occur in the measurements and the least squares type objective function is used. To eliminate the smearing effects, a screening process of removing possible gross errors before data reconciliation is necessary. In the previous section, the multivariate data analysis (MDA) is one of the prescreening processes that can be utilized to identify possible gross errors. The two-step process, i.e., removing gross error in prior and reconciling data next, is sometimes not favorable, especially in the situation of online monitoring where a fast run of data reconciliation is required.

The option other than the two-step process is to utilize the robust estimator. The robust estimator is referred to as a statistical estimator that is "insensitive to small departures from the idealized assumptions for which the estimator is optimized" [75, 76]. The "small departures" can have two different interpretations, both of which are important: either means small departures for all data points, or means large departures for a small group of data points from the majority population. It is the latter interpretation that leads to the notion of outliers, which is usually the most stressful issue in statistical procedures. Because the robust estimator is insensitive to outliers, the smearing effects can be suppressed to a certain point during data reconciliation, and the two-step procedure of data reconciliation where the least squares estimator is used can be simplified to a one-step optimization process.

Various types of robust estimators have been developed. Among the categories, the maximum likelihood estimators, or *M*-estimators, are the most relevant class of the type of problem such as data reconciliation and parameter estimation. The concept of robust estimators can be shown in Fig 5-13.

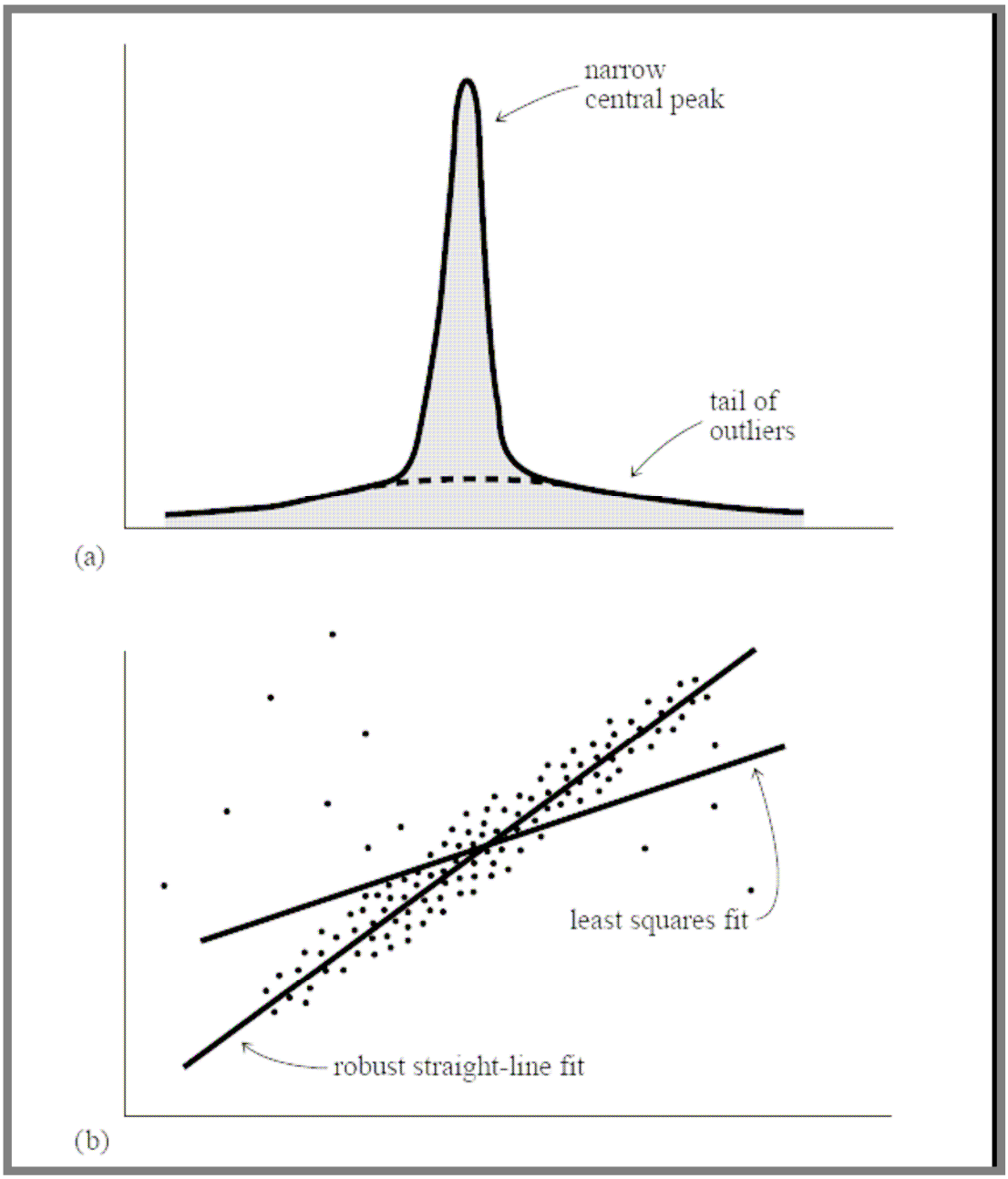

Figure 5-13: Example of using robust *M*-estimator in straight-line fitting

5.4.1. Introduction to Robust Maximum Likelihood Estimator

Simultaneous data reconciliation and model calibration is based on the maximum likelihood principle where the measured data are reconciled so as to maximize the likelihood function. The likelihood function, i.e., the objective function in the optimization process, is constructed by probability density functions representing measurement uncertainties. When the likelihood function is formed by Gaussian functions, it can be simplified to a weighted least squares function, the most used likelihood estimator. The least squares function is a type of maximum likelihood estimator which is sensitive to the occurrence of gross errors and, therefore, causes smearing effects during data reconciliation. The concept of the robust maximum likelihood estimation is to build robustness into the likelihood function such that the smearing effects can be mitigated. This can be done through constructing a likelihood function with hybrid distribution functions, which can handle both random and gross errors. These types of estimators are referred to as robust maximum likelihood estimators or robust *M*-estimators.

A robust *M*-estimator can be constructed by combining multiple Gaussian-like functions so as to become largely distribution independent and, thus, produce unbiased results in presence of data deviated from an assumed ideal distribution, i.e., Gaussian distribution, due to its insensitivity to large residuals. The robustness of an estimator can be defined as follows:

Let $f(x)$ be the true distribution for $(x_1, x_2, x_3, \ldots x_n)$, T is the estimator of parameter p, and $a(x)$ is an approximated model for distribution $f(x)$. The unbiased estimate of parameter p is $T[f(x)]$ with a distribution $\Gamma(p, f)$, and the approximation of the estimate is $T[a(x)]$ with a distribution $\Gamma(p, a)$. The estimator is robust if and only if

$$\forall \varepsilon, \exists \delta : d(f, a) < \varepsilon \Rightarrow d[\Gamma(\hat{p}, f), \Gamma(\tilde{p}, a)] < \delta$$

where d is a distance function. Under the condition of robustness, a finite difference between the true and the approximated probability distribution function leads to a bounded estimated parameter, p. If the residual, ε, of the estimation process is obtained from the probability distribution, $f(\varepsilon)$, and $T[f(\varepsilon)]$ is an unbiased estimator of parameter, p, the influence function of an estimator, which represents the effect of observations on the estimated parameter, can be defined as:

$$IF = \psi(\varepsilon_0) = \lim_{t \to 0} \left(\frac{T[(1-t)f + t\delta(\varepsilon - \varepsilon_0)] - T[f]}{t} \right) \tag{5-27}$$

The influence function of a robust estimator is bounded based on the definition of robustness.

If $l(x_i|p)$ is the likelihood function of an observation, x_i, with the parameter, p, which determines the probability density function of the observation, the likelihood function for N observations with measurement errors can be denoted as:

$$L = \prod_{i=1}^{N} l(x_i \mid p) \tag{5-28}$$

The M-estimator is then formulated by taking the negative logarithm of the likelihood function:

$$\rho^M = \sum_{i=1}^{N} \rho_i = -\log(L) = -\sum_{i=1}^{N} \log\, l(x_i \mid p) \tag{5-29}$$

The M-estimators have different forms, depending on how the associated likelihood functions are constructed.

5.4.2. Different Types of M-estimators

To build robustness into the estimator, one of the options is taking into account contributions from both random errors and gross errors during data reconciliation. This can be accomplished by using the likelihood function that combines two Gaussian distributions, one has heavy tails with a larger standard deviation and the other has a normal standard deviation set by the measurement uncertainty. The hybrid distribution

function that combines two Gaussian functions is referred to as the Contaminated Gaussian function. The major advantage of using a hybrid distribution function is its insensitivity to the occurrence of gross errors due to the heavy tailed section whereby the smearing effects can be mitigated.

The probability density function of a Gaussian distribution is given by:

$$f = \frac{1}{\sigma\sqrt{2\pi}} e^{(-0.5\varepsilon^2/\sigma^{-2})} \tag{5-30}$$

Where ε is the measurement error and σ is the standard deviation. A linear combination of two Gaussian distributions can be formed as:

$$f = \frac{1}{\sigma\sqrt{2\pi}} \left[(1-p) e^{(-0.5\varepsilon^2/\sigma^{-2})} + \frac{p}{b} e^{(-0.5\varepsilon^2/\sigma^{-2})} \right] \tag{5-31}$$

where p is the probability of gross error occurrence, and b is the ratio of standard deviations from a gross error and a random error. Applying the maximum likelihood principle, the *M*-estimator associated with the Contaminated Gaussian distribution for an observation is given by:

$$\psi = \ln \frac{1}{f} = -\ln \left[(1-p) e^{(-0.5\varepsilon^2/\sigma^{-2})} + \frac{p}{b} e^{(-0.5\varepsilon^2/\sigma^{-2})} \right] + \ln\sigma + \ln\sqrt{2\pi} \tag{5-32}$$

For N measurements, the likelihood function becomes:

$$\phi = \sum_{i=1}^{N} \psi_i = -\sum_{i=1}^{N} \ln \left[(1-p) e^{(-0.5\varepsilon^2/\sigma^{-2})} + \frac{p}{b} e^{(-0.5\varepsilon^2/\sigma^{-2})} \right] + \sum_{i=1}^{n} \ln\sigma \tag{5-33}$$

which is subject to model constraints. At the end of data reconciliation, the deviations between measured and reconciled data can be tested against the combined Gaussian distributions. The measured data have gross errors if the residuals are greater than the scopes of random errors. After data reconciliation, the combined Gaussian distribution can be used as a rational basis for gross error detection. If the deviation ε_μ satisfies the inequality, i.e., the probability of ε_μ to be an outlier against the probability of ε_μ to be within the range of random error:

$$(1-p)e^{(-0.5\varepsilon^2/\sigma^{-2})} < \frac{p}{b}e^{(-0.5\varepsilon^2/\sigma^{-2})} \tag{5-34}$$

then ε_μ is identified as a gross error.

Comparing the objective function formed by Contaminated Gaussian functions to the least squares objective function, it can be found that the maximum likelihood function has a general form:

$$\min \sum_i \rho\left(\frac{y_i - x_i}{\sigma_i}\right) \tag{5-35}$$

where ρ represents any reasonable monotone function of the standardized error, $\varepsilon_i = (y_i - x_i) / \sigma_i$. The generalized *M*-estimators are referred to as the type of likelihood functions that can suppress the smearing effects caused by gross errors during data reconciliation. These maximum likelihood objective functions can be used without assuming the underlying measurement error probabilities.

Besides the Contaminated Gaussian function, Cauchy and Logistic functions can also be used to formulate robust *M*-estimators. In addition, Fair function, "Lorentzian" function, and Hampel's redescending *M*-estimator are three other robust generalized maximum likelihood functions that can be employed in the data reconciliation process. Fair function is formulated by a combination of ordinary-least squares for small deviations, i.e., random errors, and least-absolute residual (LAR) for large deviations, i.e., gross errors [77]. "Lorentzian" function was introduced by Johnston and Kramer [78], while Hampel's redescending *M*-estimator was introduced by Hampel [79]. The redescending estimator has the capability of being tuned to best fit the data under investigation by optimizing its tuning constants. The ρ functions, i.e., *M*-estimators, described above are listed in table 5-2.

Table 5-2: Different types of *M*-estimators

***M*-estimator**	**Distribution Function**	**Parameters**
Least Squares	$\frac{1}{2}\varepsilon_i^2$	N/A
Contaminated Gaussian	$\ln\left[(1-p_{CN})\exp(-\frac{\varepsilon_i^2}{2}) + \frac{p_{CN}}{b_{CN}}\exp(-\frac{\varepsilon_i^2}{2b_{CN}^2})\right]$	p_{CN}, b_{CN}
Cauchy	$c_c^2 \ln\left(1+\frac{\varepsilon i^2}{c_c^2}\right)$	c_C
Logistic	$2\ln\left(1+\exp\left(\frac{\varepsilon_i}{c_{Lo}}\right)\right)-\left(\frac{\varepsilon_i}{c_{Lo}}\right)$	c_{Lo}
Lorentzian	$-\frac{1}{1+\left(\varepsilon_i^2/2c_L^2\right)}$	c_L
Fair	$2c_F^2\left[\frac{\lvert\varepsilon_i\rvert}{c_F}-\ln\left(1+\frac{\lvert\varepsilon_i\rvert}{c_F}\right)\right]$	c_F
Hampel's Redescending M-estimator	$\frac{1}{2}\varepsilon_i^2, \quad 0\le\lvert\varepsilon_i\rvert\le a_H$ $a_H\lvert\varepsilon_i\rvert-\frac{1}{2}a_H^2, \quad a_H\le\lvert\varepsilon_i\rvert\le b_H$ $a_H b_H-\frac{1}{2}a_H^2+(c_H-b_H)\frac{1}{2}a_H^2\left[1-\left(\frac{c_H-\lvert\varepsilon_i\rvert}{c_H-b_H}\right)^2\right] \quad b_H\le\lvert\varepsilon_i\rvert\le c_H$ $a_H b_H-\frac{1}{2}a_H^2+(c_H-b_H)\frac{1}{2}a_H^2 \quad c_H\le\lvert\varepsilon_i\rvert$	a_H b_H c_H

5.4.3. Tunings for Robust M-estimators

As mentioned in Chapter 4, data reconciliation is a process of estimating the mean of a sample from a univariate distribution such as the Gaussian distribution. If one changes the weighted least squares objective function with a robust *M*-estimator, the estimation of sample mean is subject to less smearing effects caused by gross errors. The efficiency of a robust *M*-estimator can be defined as the inverse of the variance of the final estimated means under the ideal model distribution, i.e., the Gaussian distribution. If a rejection rule is applied, the efficiency of a robust *M*-estimator is recalculated based on the ideal model distribution after the identified gross errors are removed from the sample. When comparing the performances of robust *M*-estimators, it is crucial to tune these estimators to have the same efficiency. The tuning process is carried out for the tuning parameters of robust *M*-estimators. Tuning constants for some robust *M*-estimators such as Fair and Cauchy are given based on their asymptotic efficiencies. For instance, the Fair function has one tuning constant c_F, which can be set based on its asymptotic efficiency and allows the user to adjust the insensitivity to the outliers. Because the asymptotic variances only give rough estimations to the actual variances, to simulate the actual variances of the sample, the Monte Carlo simulation can be carried out to calculate the finite sample variances and consecutively relative efficiencies.

For Hampel's redescending *M*-estimator, the constant a_H has a direct impact on the degree of contamination in the data. It can be obtained from b_H, c_H, based on the suggested relation: $c_H \geq a_H + b_H$. The relations among b_H, a_H, and c_H depends on how wide the redescending area is desired. Setting $b_H = c_H$ will make the estimator unable to differentiate rounding and grouping errors. If the sample is drawn from a Gaussian distribution, it is desired to have very few data points lying outside [$-b_H$, b_H], and, thus, having a large value of b_H is more reasonable. If, on the other hand, the sample is drawn from a heavy-tailed distribution, it is suggested to have a small b_H. The decisions of these parameters need some data preprocessing, which may require significant efforts. A tuning

strategy suggested by Biegler [80] is based on minimizing the AIC, Akiake information criterion, which is also dependent on the slope of the redescending region of the ρ function.

Model-based data reconciliation and gross error detection can be seen as a model discrimination and parameter estimation problem, in which the model parameters are being "tuned" to fit the data subject to random and gross errors. Here the model represents both physical model and sample distribution model, i.e., the estimator. The model parameters are, therefore, referred to as the independent variables in the physical-based model, e.g., gas turbine heat balance model, and the tuning constants of the maximum likelihood estimators. Due to the fact that the maximum likelihood function is asymptotically efficient under certain conditions and that the maximum likelihood function is sensitive to deviations of the model parameters from their true values, it can be used to differentiate models when more than one model can be fitted to the data under consideration. The Akiake information criterion (AIC) is an estimate of the Kullback-Leibler mean information for the deviation between the true model and the model under consideration. It can be expressed as follows:

AIC = -2 * log (maximum likelihood) + 2 * (number of model parameters) (5-36a)

or

$$AIC = 2\sum_{i=1}^{N} - \log(\ell(\varepsilon(i, p), i, p)) + 2 \times (number\ of\ \ p) \tag{5-36b}$$

where ε is the standardized measurement error, which is obtained after data reconciliation, l represents the likelihood function, and p represents the model parameters. Here the number of model parameters includes the number of gross errors due to the fact that during data reconciliation the corrections to measurements with gross errors are driven by the reconciliation of the measurements with random errors. This is especially true when robust M-estimators are utilized whereby the contaminate effects are suppressed during data reconciliation.

Since the AIC is a good model differentiator, one can tune the *M*-estimator by minimizing the AIC, in which the tuning constants of maximum likelihood functions are optimized. In the beginning, a wide range of tuning constants is assigned to the estimator, resulting in different estimator models. Data reconciliation is then carried out over these estimators with a wide range of tuning constants, by which the upper and lower bounds of the minimum AIC can be determined. Once the minimum of the resulting AIC is bounded, a one-dimensional line search can be applied to obtain the optimal solution for the tuning constants.

In the example of Hampel's redescending *M*-estimator where there are three model parameters to be tuned, the tuning process with AIC is actually a multidimensional search. Due to the fact that the influences of a_H and b_H on the objective function are relatively small compared to c_H, one can simplify the optimization problem to a one-dimensional line search by performing *golden section search* for the parameter c_H. For each iteration, the other two parameters are set by the following relationships:

$$b_H = \frac{c_H}{2} \quad \text{and} \quad a_H = \frac{c_H - b_H}{2} \tag{5-37}$$

Once the optimal solution for c_H is located, the Hampel's redescending *M*-estimator can be tuned to best fit the measured data under consideration.

5.4.4. Cut-off Criteria

The cut-off point has a direct impact on the power of gross error detection. For instance, if the cut-off point has a smaller value, the power of detecting gross errors increases, while the probability of Type I error, i.e., false detection, also rises. When the probability distribution function for the measurement errors is available, the hypothesis testing works well in identifying the occurrence of gross errors. The rejection of the gross errors can be carried out by setting the desired confidence level, α. A measurement with a probability less than (α×100)% of the cumulative probability can be identified as having

a gross error, i.e., the measured value with an error larger than the cut-off point is identified as an outlier with an uncertainty of α. When using the robust M-estimator, since the smearing effects are mitigated, gross errors can be detected by comparing the standardized error against the ideal distribution function, i.e., the Gaussian function.

The rejection criteria based on the hypothesis testing could cause misleading if the prior assumption of the probability distribution function for measurement errors is not correct. In addition, without prior knowledge about the underlying distribution function, the decision on cut-off criteria could be subjective. Alternative options for defining the rejection criteria have been suggested. One of them is based on the 1st derivative of the influence function. For example, the rejection criteria proposed by Farris and Law [81] for the Contaminated Gaussian distribution function is defined by the cut-off point value, xc, that gives:

$$\max\left\{P((y_i \in \mathbf{G}) \cap (y_i > x_c)) - P((y_i \notin \mathbf{G}) \cap (y_i > x_c))\right\} \tag{5-38}$$

where y_i represents the measurement data, and **G** represents the space of gross errors. The cut-off point decided based on this method is on the descending section of the influence function for Contaminated Gaussian and Hampel's redescending estimators. Within the descending region of the influence function, the point at the maximum, minimum, or inflection can be selected as the cut-off point. For instance, the cut-off point for Hampel's redescending function can be set to be c_H since it represents the inflecting point of the influence function.

For those *M*-estimators lack of descending part like Fair function and Logistic functions, the cut-off points can be obtained either from the redescending functions as long as these functions are tuned to have the same efficiencies, or by the exploratory data analysis (EDA) such as boxplot. In order to construct boxplots, data are sorted and their fourth spreads are calculated as follows:

$$d_F = F_U - 3/2 d_F \tag{5-39}$$

where F_U and F_L represent the upper and lower fourths accordingly. A measurement y_i is identified as a gross error if $y_i \leq F_U - 3/2d_F$ or $y_i \geq F_U + 3/2d_F$.

Alternative rejection criteria can be obtained based on the robust median and median deviation, which has a code name X84. The rule rejects any measurement with residual larger than 5.2 median deviations away from the median of the residuals. This rule can serve as a universe criterion for all robust *M*-estimators.

5.4.5. Example

An example of applying robust *M*-estimators to data reconciliation for a thermodynamic system is demonstrated as follows. The thermo system demonstrated here is a three-pressure-reheat heat recovery steam generator, or HRSG, containing a series of heat exchangers at three pressure levels that are controlled by pressurized drums, shown in Fig. 5-14. The HRSG transfers the heat from the gas turbine exhaust to the feed water, by which steams are generated. The performance of the HRSG depends on the gas turbine exhaust conditions, i.e., gas flow rate and gas temperature, drum pressures, and degradation status of each heat exchanger. There are two ways of reconciling the measurements of HRSG – reconciling the data over the model in prediction mode, or reconciling the data in a heat balance mode. In the first option, the measurements on steam/water side are functions of gas turbine exhaust conditions, heat exchanger performance factors, and the drum pressures, which are determined by the steam turbine throttle pressure. Each measurement has its corresponding function of the above variables. In the second option, which is to be demonstrated in this example, mass and energy balances are employed. Instead of solving the implicit forms of these balance equations, these equations are rearranged to be explicit such that one variable is on the right hand side of the balance equation and the rest of variables on the left hand side. The choice of dependent variables can be made based on the error propagation rule, i.e., rearrange the implicit equations in such a way that propagation of uncertainties from the

independent variables to the dependent variable is minimized. This can be determined through a random sampling technique such as Monte Carlo simulation or the sensitivity analysis for each variable. The variable that has least uncertainty caused by the rest variables will be selected as the dependent variable. The rearranged heat balance equation has the following form:

$$y_j = f_j(x_i) \tag{5-40}$$

, where y and x represent dependent and independent variables correspondently; i is the number of independent variables, and j is the number of heat balance equations.

In this example, the Contaminated Gaussian function is used as a robust M-estimator to reconcile the measurements of HRSG. The reconciliation problem can be expressed as followed:

$$\min_{x_i}\left\{\sum_{j=1}^{m}\ln\left[(1-p_{CN})\exp\left(-\frac{\left(y_j^{'}-f(x_i)\right)^2}{2}\right)+\frac{p_{CN}}{b_{CN}}\exp\left(-\frac{\left(y_j^{'}-f(x_i)\right)^2}{2b_{CN}^2}\right)\right]\right.$$

$$\left.+\sum_{i=1}^{n}\ln\left[(1-p_{CN})\exp\left(-\frac{\left(x_i^{'}-x_i\right)^2}{2}\right)+\frac{p_{CN}}{b_{CN}}\exp\left(-\frac{\left(x_i^{'}-x_i\right)^2}{2b_{CN}^2}\right)\right]\right\} \tag{5-41}$$

$$s.t. L_i \le x_i \le U_i$$

where $y^{'}$ and $x^{'}$ represent the measured dependent and independent variables; L_i and U_i are the lower and upper bounds of the independent variable, x_i. Since the rearranged heat balance equations are in explicit forms such that during data reconciliation the optimizer is varying the independent variables, x_i, to minimize the objective function constructed by Contaminated Gaussian functions containing terms of both measured dependent and independent variables.

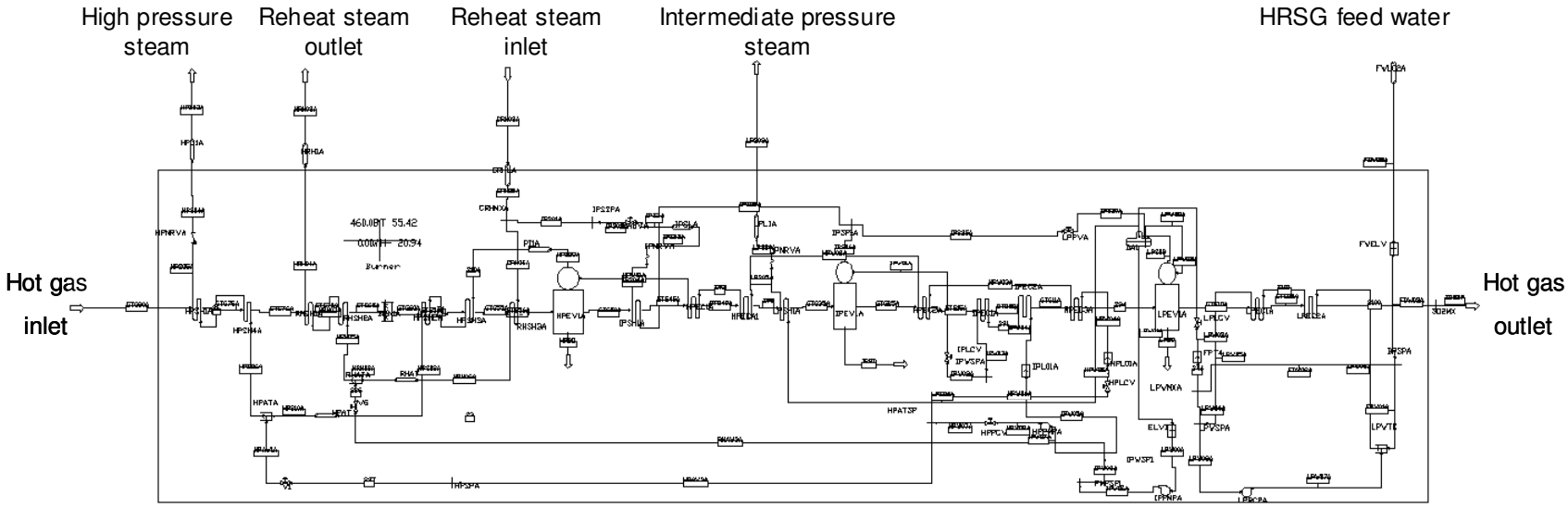

Figure 5-14: Three-pressure-reheat HRSG

Two tuning constants p_{CN} and b_{CN} determine the shape and behavior of the Contaminated Gaussian function. Figure 5-15(a) shows the impact of p_{CN} on the function shape (function value versus measurement adjustment) while b_{CN} is kept constant (b_{CN} = 10). It is shown as p_{CN} increases, the slope of the function decreases and the cut-off point is shifted to a lower value, indicating more Type I errors could be committed and the convergence speed will slow down during data reconciliation. The influence of b_{CN} on the behavior of Contaminated Gaussian function is also given in Fig. 5-15(b), which shows the main impact of b_{CN} is the shift of cut-off point. As b_{CN} increases, the cut-off point is shifted toward a larger value, indicating the probability of committing Type II errors will increase. The values of b_{CN} and p_{CN} used for this example are based on Ozyurt's guideline [40], where b_{CN} = 20 and p_{CN} = 0.435. One can, however, utilize the AIC principle to obtain the most representative tuning constants for the specific model. Figure 5-16 shows the influence functions of the Gaussian distribution and the Contaminated Gaussian distribution with b_{CN} = 20 and p_{CN} = 0.435. The corresponding *M*-estimator functions for these two distributions are given in Figure 5-17. It is shown, from these two figures, that as the measurement adjustment is within the cut-off point, the *M*-estimator of Contaminated Gaussian acts like the least squares function (the *M*-estimator of Gaussian distribution). When the measurement adjustment is beyond the cut-off point, the influence function drops dramatically around the cut-off point, and then increases with a very flat slope. Therefore, when gross errors occur, the robust *M*-estimator is less sensitive to a large measurement adjustment than the least squares, while it behaves like the least squares as the measurement adjustment is within the cut-off point, i.e., random error adjustment.

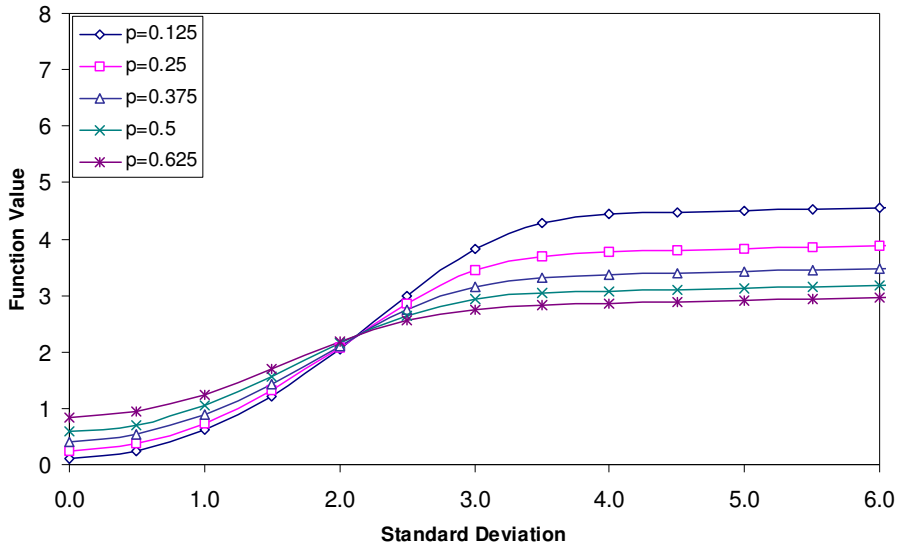

Figure 5-15(a): Effect of p_{CN} on the Contaminated Gaussian function

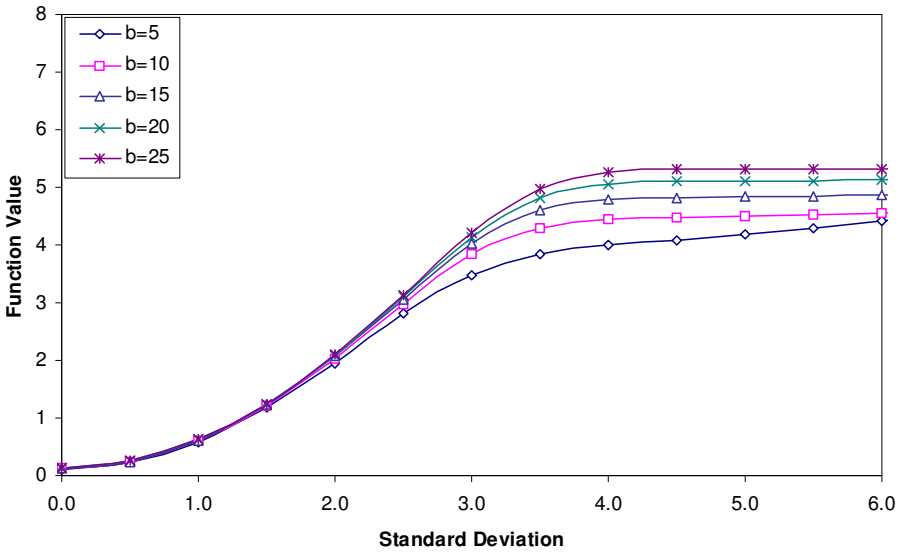

Figure 5-15(b): Effect of b_{CN} on the Contaminated Gaussian function

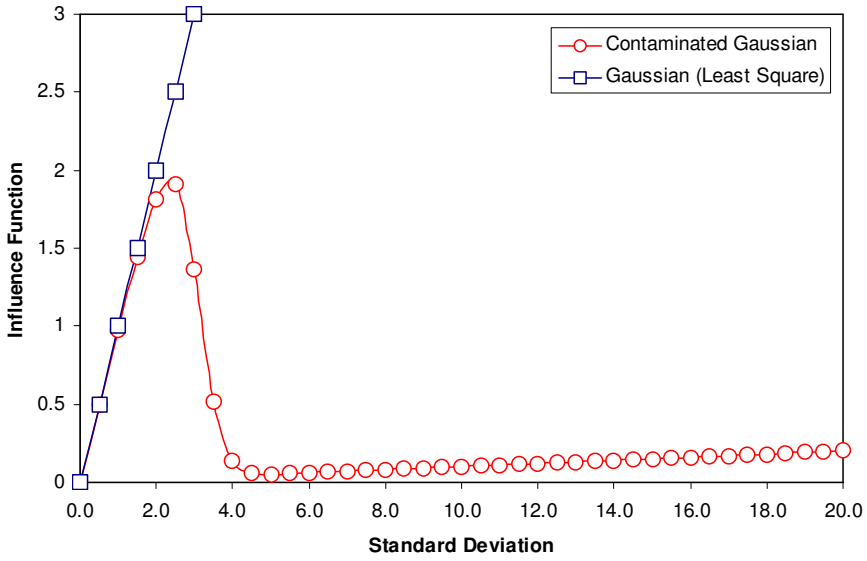

Figure 5-16: Influence functions for Gaussian and Contaminated Gaussian distributions

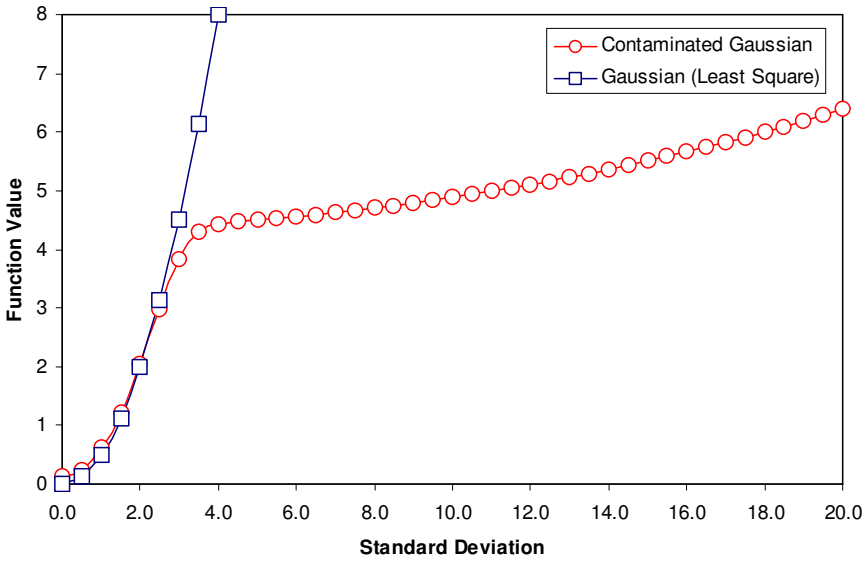

Figure 5-17: *M*-estimators for Gaussian and Contaminated Gaussian distributions

In this example for HRSG, the heat and mass balances are carried out in such a way that the high-pressure steam flow, the reheat steam flow, and the stack temperature are calculated and treated as the reconciled values once the heat & mass balance input variables are reconciled by the solver, i.e., optimized for minimizing the *M*-estimator.

Two gross errors are artificially imposed to the simulated data: 6 sigma of uncertainty on the low-pressure steam flow (LPSH steam flow) and –5 sigma of uncertainty on the high-pressure steam temperature (HPSH steam temperature), each of which has a healthy redundancy, i.e., redundant measurement subject to random error only. The HRSG data reconciliation is carried out with both the least squares objective function (Gaussian) and the robust *M*-estimator formed by the Contaminated Gaussian distribution. After running data reconciliation with the robust *M*-estimator, the function value is converted to the corresponding least squares and compared to the result obtained from data reconciliation that uses the regular least squares estimator.

Figure 5-18 shows the function values of the least squares for before running data reconciliation, after running data reconciliation with least squares estimator, and after running data reconciliation with robust *M*-estimator using Contaminated Gaussian distribution. It is shown that the least squares estimator gives a lower least squares value than the robust *M*-estimator. However, if one only looks at the summation of the least squares terms from healthy data, given in Fig. 5-19, the robust *M*-estimator gives a much lower least squares values than the regular least squares estimator. While, the least squares terms from the biased data make the majority contributions to the overall least squares function value for the robust *M*-estimator, but not for the least squares estimator.

The comparison demonstrates the robust *M*-estimator significantly mitigates the smearing effects caused by the gross errors. This is verified by looking at two groups of least squares terms – the group of healthy data and the group of biased data. When gross errors occur, the reconciliation process should make the majority adjustments to the biased data if smearing effects don't take place, which makes the least squares terms

contribute most of the overall least squares function value. The overall least squares function value does not tell the whole story, since the least squares estimator gives a lower value than the robust *M*-estimator. The decomposition of the overall least squares by the healthy data and the biased data shows there are significant smearing effects in data reconciliation with the least squares estimator but not with the robust *M*-estimator. The corrections to the measurements after data reconciliation with two estimators are given in Fig. 5-20. It shows the smearing effects occurring in the least squares data reconciliation as measurement corrections beyond the ranges of random errors are made to the two healthy data. On the other hand, in the data reconciliation with robust *M*-estimator, the corrections beyond the ranges of random errors are made to the two measurements that are simulated with gross errors.

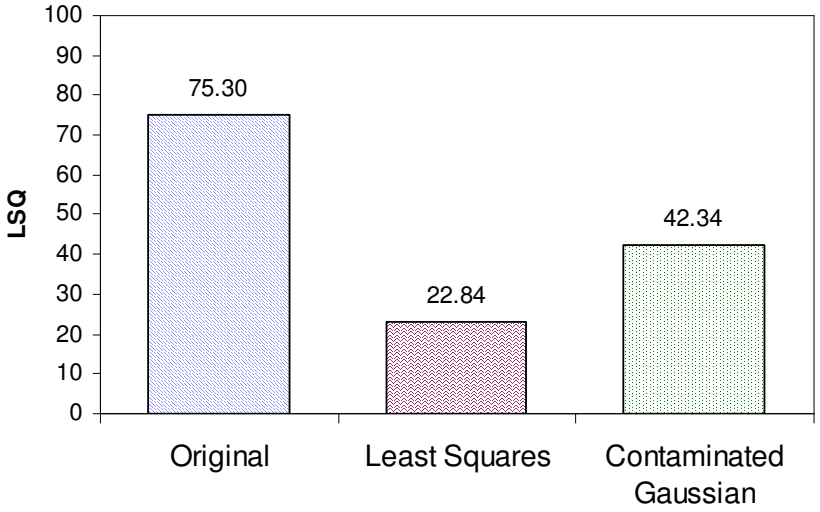

Figure 5-18: Least squares of two data reconciliation methods

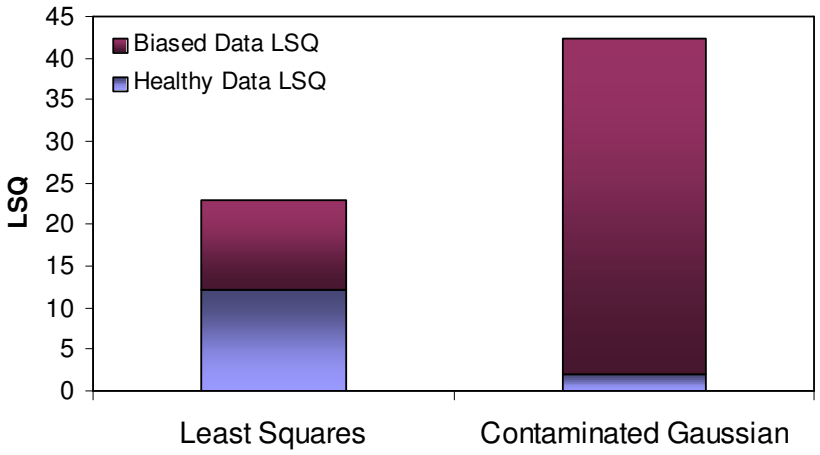

Figure 5-19: Decompositions of the overall least squares

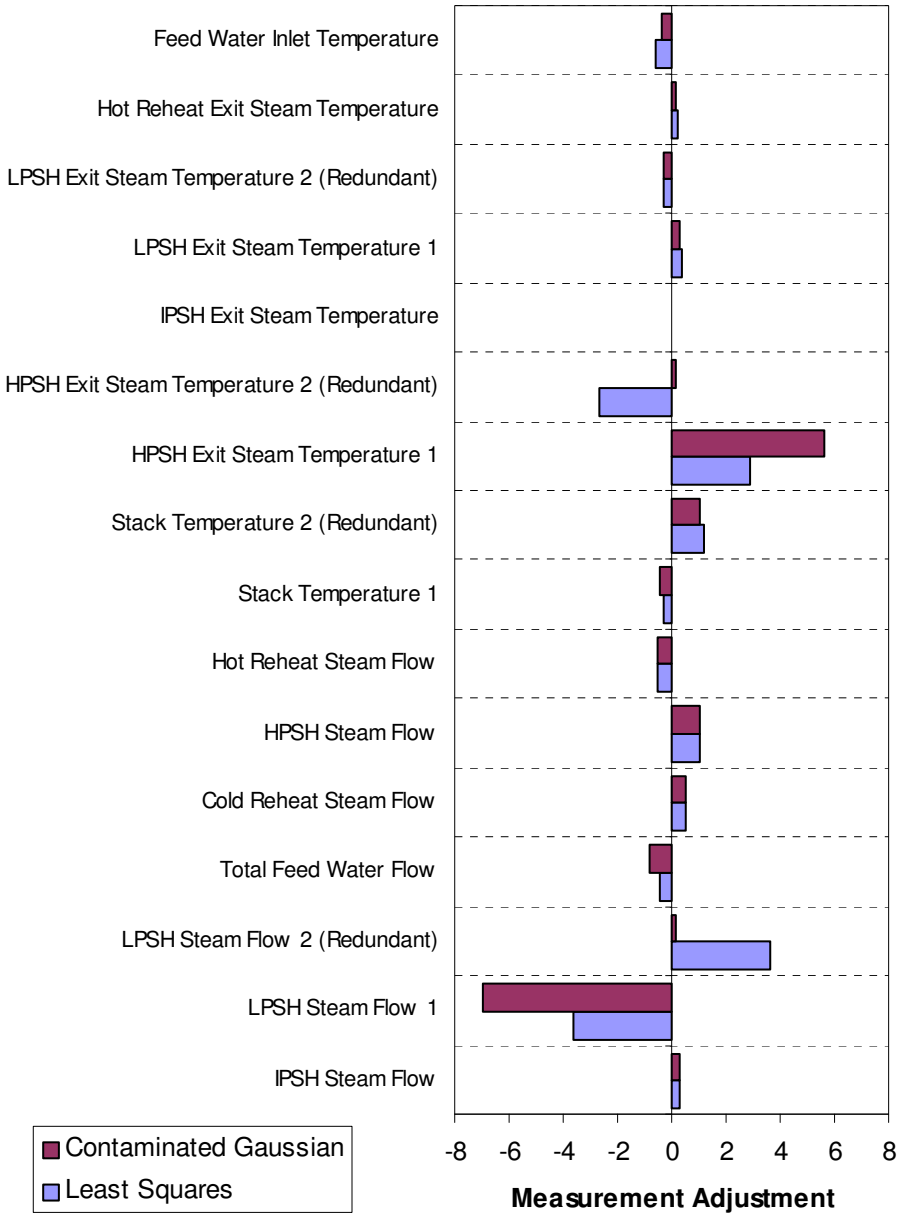

Figure 5-20: Measurement corrections for two *M*-estimators

5.5. Gross Error Detection by Hypothesis Testing

The multivariate technique such as PCA is suitable for detecting gross errors with large magnitudes. When model calibration is coupled with data reconciliation, i.e., simultaneous data reconciliation and model calibration, the PCA technique often fails to detect delicate gross errors. This happens especially when the multivariate data are not smeared with random effects or the ranges assigned to the model parameters are not representative. Therefore, it is suggested to utilize the multivariate technique as a screening process by which large biases can be filtered out in advance.

A technique that integrates the gross error detection into the data reconciliation scheme is needed. The robust *M*-estimator introduced in previous section is considered as this type of technique that performs data reconciliation and gross error detection at the same time. The performance of a robust *M*-estimator, however, is strongly affected by the type of likelihood function and the corresponding tuning constants. If significant amount of gross errors occur, the robust *M*-estimator technique becomes sensitive to the starting points and number of healthy data sets.

Hypothesis testing is the method that can be incorporated into the data reconciliation and model calibration scheme without the need for using non-Gaussian distributions, required by robust *M*-estimator techniques. When combined with a data reconciliation scheme, hypothesis testing is carried out over different gross error models, in which the locations and magnitudes of gross errors are presumed. During the test, the gross error models are plugged into the least squares objective function and the typical chi-squares type data reconciliation is performed. Each gross error model is ranked by its score, defined based on the absolute value of chi-squares, χ^2, or the ratio of chi-squares obtained after the reconciliation process. The gross error model with the highest score, i.e., lowest chi-squares value is then considered to best represent the locations and magnitudes of gross errors.

There have been many research works related to the use of hypotheses testing on the outlier detection. Rollins, et al. [82] proposed a method of fast gross error detection by efficiently selecting a small subset of hypothesis tests from large set based on the new developed test criteria. Narasimhan and Mah utilized the generalized likelihood ratio test in gross error detection for steady state [83] and dynamic [84] systems. Terry and Himmelblau [85] used the meta-model created from artificial Neural Networks to carry out data reconciliation and gross error detection. Kim [86] proposed a method of iterative hypotheses testing for gross error detection. Renganathan [87] summarized and compared several GED techniques that utilize the hypothesis testing. These research works mainly focused on pure data reconciliation for the chemical process represented by the balance equations, i.e., chemical reactions and heat-and-mass conservations. In this research work data reconciliation and model calibration are carried out simultaneously for the model that is represented by the performance simulator.

5.5.1. Hypothesis Testing

Hypothesis testing is a statistical process of making a statement about an unknown parameter associated with a probability distribution function, which represents a certain sampled data. A value of the model parameter is first hypothesized, followed by confirming or disproving the hypothesized value based on the sampled data. Two hypotheses, the null hypothesis (H_0) and alternate hypothesis (H_1), are tested against each other for their validity based on the sampled data. At the end of testing, the null hypothesis is either accepted or rejected. The steps of hypothesis testing can be summarized as:

1. Postulate the null and alternative hypothesis, i.e., problem statement
2. Collect the data in a randomly sampling way
3. Select the test statistic τ, by which the null hypothesis H_0 is assumed to hold with a known distribution

4. Determine the significance level α, by which the critical value for the test statistic τ_c can also be decided. Then one can obtain:

$$F(\tau_c) = P(\tau \leq \tau_c) = (1 - \alpha) \tag{5-42}$$

5. Calculate τ based on the sampled data. If $\tau > \tau_c$, the null hypothesis is rejected; otherwise, the null hypothesis is accepted.

The outcome of hypothesis testing is not perfect and always contains some types of errors. A test result may state that there exist gross errors while in fact there is no. In this situation, the test commits a Type I error. If, on the other hand, gross errors do exist but the test result declares there are no gross errors, a Type II error is committed. The *power* of hypothesis testing is defined as 1 – Type II error, and is strongly related to the Type I error probability. The *power* of a statistical test is increased by allowing a larger Type I error probability. The hypothesis testing can be tailored to balance the *power* and the Type I error probability. Once the distribution of the test statistics is obtained based on the assumption of the null hypothesis, the test threshold can be decided so that the probability of Type I error is less than or equal to a specified value α, which is referred as the significance level for the hypothesis testing.

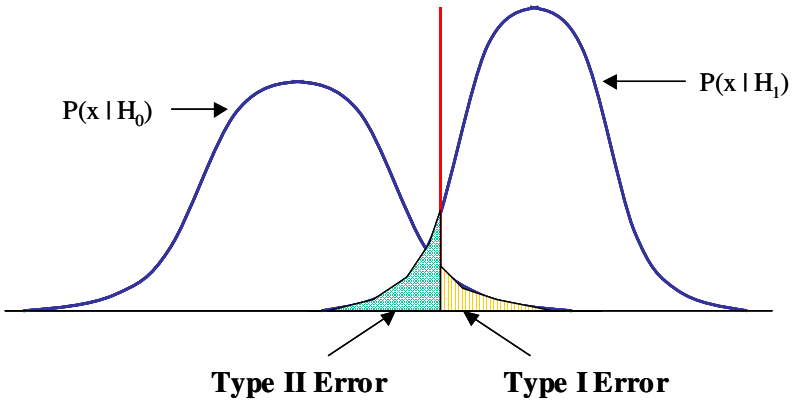

Figure 5-21: Type-I and Type-II error regions for null and alternative hypotheses

As shown in Figure 5-21, H_0 represents the null hypothesis and H_1 represents the alternative hypothesis. Consider a single observation x with the null hypothesis and the alternative hypothesis, the false alarm rate is equal to the Type I error, and the missed detection rate is equal to the Type II error.

When the hypothesis testing is applied to GED, the null hypothesis states there are no gross errors; while the alternative hypothesis assumes there are one or multiple gross errors. To reject or accept the null hypothesis, the test statistics, τ, is compared against the critical value, τ_c; both τ and τ_c are determined by the chosen testing methodology.

5.5.2. Basic Statistical Tests for Gross Error Detections

In general, the measurement errors and parameter deviates are propagated through the system model, conservation equations or performance simulator, leading to the multivariate model residuals, which can be represented by the variance-covariance matrix. When the model is given by the conservation equations and utilized in data reconciliation and gross error detection, the residual vector, $\boldsymbol{r}$, of the model constraints is the major test statistics that one can use to compare with the expected variance-covariance matrix. For example, the mass balance model is given by:

$$\boldsymbol{A}\boldsymbol{y} = \boldsymbol{0} \tag{5-43}$$

where $\boldsymbol{A}$ is the linear constraint matrix, and $\boldsymbol{y}$ is the measurement data. The model residuals, $\boldsymbol{r}$, follows a multivariate normal distribution with zero mean and variance-covariance matrix, $\boldsymbol{V}$, given by:

$$\boldsymbol{V} = \mathrm{cov}(\boldsymbol{r}) = \boldsymbol{A}\Sigma\boldsymbol{A}^{\mathrm{T}} \tag{5-44}$$

The variance-covariance matrix can be utilized to define the test statistics and the associated threshold value. In this example the null hypothesis H_0 is accepted when the residual vector, $\boldsymbol{r}$, follows a multivariate normal distribution, $\boldsymbol{r} \sim N(\boldsymbol{0}, \boldsymbol{V})$. As gross errors occur, the residual vector $\boldsymbol{r}$ becomes an outlier while against its expected variance-covariance structure.

5.5.3. Gross Error Model

A gross error model defines the locations and magnitudes of gross errors, both of which are considered to be unknowns in the data set (measurement bias) and/or in the system model constraints (leaks). The locations and magnitudes of gross errors need to be determined through GED techniques. Two types of gross errors exist: gross errors caused by measurement biases and gross errors caused by system leaks. They differ in the way of gross error modeling. When the measurement bias is the source of gross error, the gross error model is imposed to the measured data. In this case, the gross error model can be expressed as:

$$\boldsymbol{y}' = \boldsymbol{y} + \boldsymbol{\varepsilon} + \boldsymbol{b} \tag{5-46}$$

where $\boldsymbol{b}$ is the vector of gross errors; $\boldsymbol{\varepsilon}$ is the vector of random errors; $\boldsymbol{y}'$ and $\boldsymbol{y}$ represent the vector of measured data and the vector of the corresponding true values separately. In the heat & mass balance type data reconciliation problem where the system model is represented by conservation equations, the measurement errors are propagated through the constrain equations with the gross error model, and cause the residuals of model constrains:

$$\boldsymbol{A}\ (\boldsymbol{y} + \boldsymbol{\varepsilon} + \boldsymbol{b}) = \boldsymbol{r} \tag{5-47}$$

where $\boldsymbol{A}$ is the matrix of model constrains; $\boldsymbol{r}$ is a column vector of the model residuals arising from the measurement errors that include random and gross errors.

For the data reconciliation problem that utilizes the performance simulator, the gross error model can be integrated into the chi-squares function, χ^2:

$$\chi^2 = (\boldsymbol{\varepsilon} + \boldsymbol{b})\ \boldsymbol{\Sigma}^{-1}\ (\boldsymbol{\varepsilon} + \boldsymbol{b})^{\mathrm{T}} \tag{5-48}$$

where $\boldsymbol{\Sigma}$ is variance-covariance matrix for the measurement uncertainties.

If gross errors are caused by material or energy leaks, the gross error model needs to be added to the system model. In the heat & mass balance type data reconciliation problem, the gross error model for leaks is added to the system model constrain in the following way:

$$\boldsymbol{A}\,\boldsymbol{y}' - \boldsymbol{l} = \boldsymbol{r} \tag{5-49}$$

where $\boldsymbol{l}$ is the column vector indicating the locations of the leaks. It is relatively easy to construct the vector $\boldsymbol{l}$ when only the leakages of mass flows are involved. If the leak is from a process unit, then $\boldsymbol{l}$ is identical to $\boldsymbol{b}$ since only the flow constraint for this unit vector is affected. If, on the other hand, the energy balances are involved, the vector $\boldsymbol{l}$ can only be approximated by engineering judgment.

For the data reconciliation problem that utilizes the performance simulator, the gross error model for leaks is directly added to the model such as:

$$\boldsymbol{y}' = \boldsymbol{f}(\boldsymbol{a}, \boldsymbol{\theta}, \boldsymbol{l}) + \boldsymbol{\varepsilon} + \boldsymbol{b} \tag{5-50}$$

where $\boldsymbol{f}(\boldsymbol{a}, \boldsymbol{\theta}, \boldsymbol{l})$ is the system model as a function of model parameters $\boldsymbol{a}$, $\boldsymbol{\theta}$, and the gross error model $\boldsymbol{l}$ for leaks. For the mass flow leak, one can simulate it by adding a splitter for the mass flow leak and setting the flow fraction as a new variable. For the energy leak, it can be modeled by adding a heat loss across the pipe or the heat exchanger and by setting the magnitude of the heat loss as a new design variable. Figure 5-22 shows the way of adding the gross error model due to leaks to the physical-based model represented by GateCycle™.

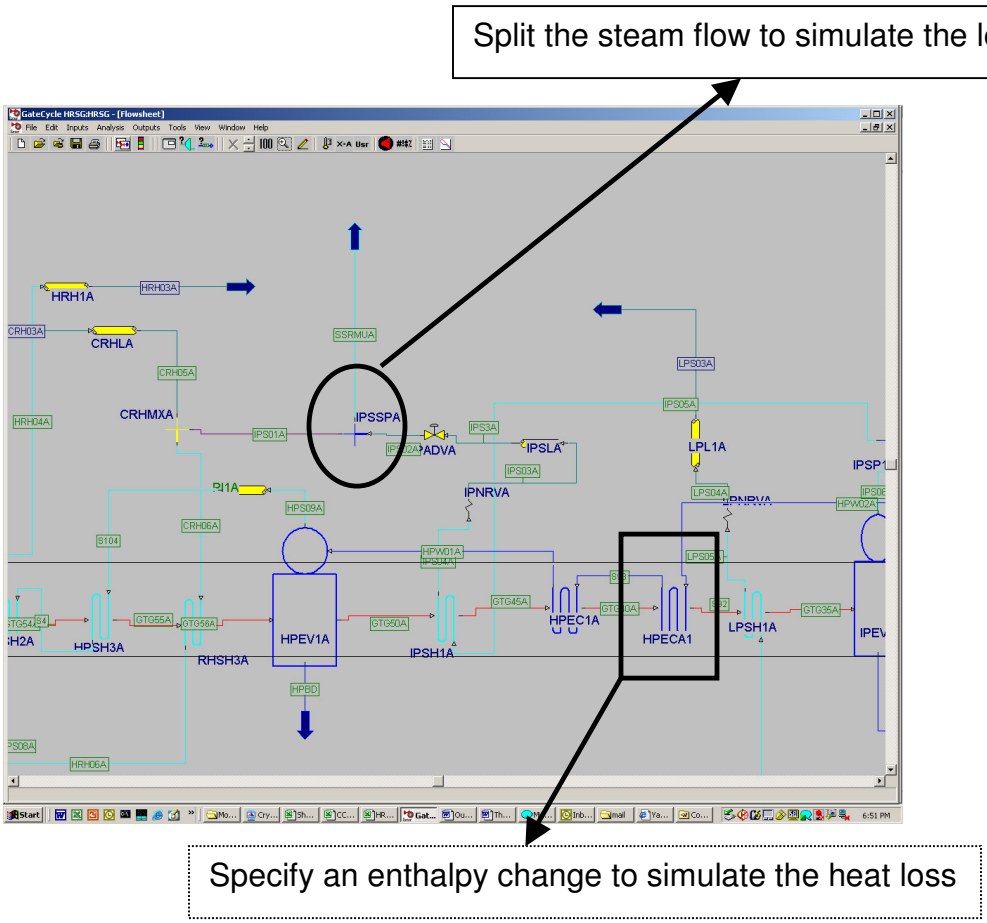

Figure 5-22: Gross error model for systems leaks

5.5.4. Hypothesis Testing on Gross Error Models

As described in the previous section, a gross error model specifies the locations and magnitudes of gross errors. To justify the gross error model, one can apply the gross error model to the system model by "compensating" the measured data and carry out data reconciliation. To "compensate" the measured data, one can simply subtract the measured values by the gross errors presumed in the gross error model:

$$\boldsymbol{y_c}' = \boldsymbol{y}' - \boldsymbol{b} \tag{5-51}$$

where $\boldsymbol{y_c}'$ represents the vector of compensated measurements. If the measurement data are compensated with the correct gross error model, the compensated data are subject to random errors only, and, therefore, smearing effects will not occur during data reconciliation. The occurrence of smearing effects can be indicated by the test statistics, which is determined based on the test methodology discussed in previous section. Thus, one can utilize the hypothesis testing to verify the gross error model. While applying the hypothesis testing to GED, the null hypothesis and alternative hypothesis can be stated as follows:

H_0: without the gross error model there is no smearing effect

$$P(\tau \le \tau_c \mid \boldsymbol{y_c}' = \boldsymbol{y}') = (1 - \alpha) \tag{5-52}$$

H_1^g: with the gross error model there is no smearing effect

$$P(\tau \le \tau_c \mid \boldsymbol{y_c}' = \boldsymbol{y}' - \boldsymbol{b}) = (1 - \alpha) \tag{5-53}$$

where τ is the test statistics obtained from the result of data reconciliation.

Before obtaining the test statistics, τ, the measurement data are compensated with the hypothesized gross error model. The magnitudes of gross errors need to be estimated and become unknown variables in the data reconciliation process, in which the optimum solutions for the reconciled data and the gross error magnitudes are to be determined by the maximum likelihood principle. Since the test statistics for the alternative hypothesis, H_1^g, is obtained from the optimum solutions of the gross error magnitudes, a test statistics

lower than the threshold value, $\tau \leq \tau_c$, indicates the hypothesized gross error model is statistically correct, and vice versa.

For the heat-and-mass balance type model, after integrating the hypothesized gross error model, the data reconciliation problem becomes:

$$\min_{b_j, y_j, \theta_i} \sum_{j=1}^{m} \left(\frac{y'_j - b\ e_j - y_j}{\sigma_j} \right)^2$$
$$s.t.\ f(y_j, \theta_i) = 0 \tag{5-54}$$

For the performance simulation type model, when applying the gross error model, the data reconciliation problem is given by:

$$\min_{b, a_i, \theta_k} \sum_{j=1}^{m} \left(\frac{y'_j - b\ e_j - f_j(a_i, \theta_k)}{\sigma_j} \right)^2 \tag{5-55}$$

where $\boldsymbol{e}$ is a vector composing "0" and "1", indicating the gross error locations. When hypothesized model presumes the location of the gross error in the jth measurement, e_j = 1, otherwise, $e_j = 0$. For example, $\boldsymbol{e}^T$ = [0 1 0 0 1] means there are gross errors in the 2nd and 5th measurements while the total number of measurements is five.

5.5.5. Serial Bias Compensation Strategy for Gross Error Detection

The locations and magnitudes of measurement biases are the main elements hypothesized in a gross error model. The index vector $\boldsymbol{e}$ can be used to represent the locations of biases: as e_j =1 there is a gross error in the jth measurement, and there is not while $e_j = 0$. Once the index vector $\boldsymbol{e}$ is specified in a gross error model, the magnitudes of biases can be determined through the data reconciliation process. If the presumption about the bias locations is not correct, the gross error model will not pass the hypothesis testing. The gross error detection by hypotheses testing can now be summarized as:

Keep modifying the presumption about the index vector ***e*** *and solving the data reconciliation problem until the presumed gross error model passes the hypothesis testing* (Fig. 5-23).

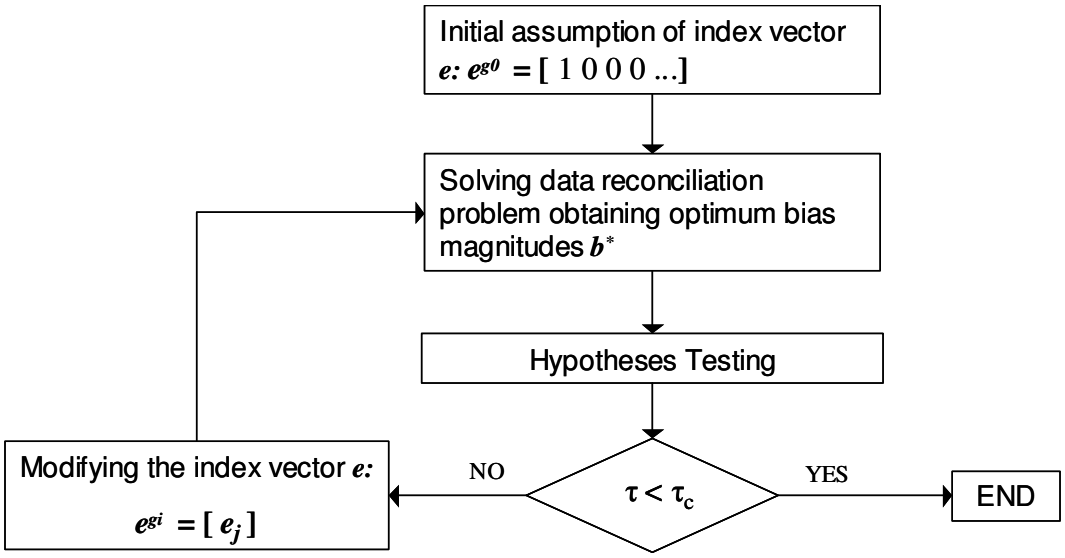

Figure 5-23: Gross error detection by hypotheses testing

In the case of one gross error, one can test all the hypotheses for their corresponding bias locations and compare the resultant test statistics τ. The gross error model with the highest score of the test statistics will be selected as the correct model. The process follows the flow chart illustrated in Figure 5-23. The index vector ***e*** can be simply updated by switching e_j from 0 to 1 and e_{j-1} from 1 to 0 for j =1 to m where m represents the total number of measurements. For example, the index vector ***e*** for the system model with four measured data is a 4 by 1 vector with e_j= 1 (bias) or 0 (no bias). Since there is only one gross error existing, only one vector element can be 1 while the rests should be 0. In the serial bias compensation scheme, the element of index vector e_j is switched from 0 to 1, each of which represents a bias model and is compared for its test statistics. The serial updating of the bias location is shown below:

$$H_1^{g1}: \boldsymbol{e}^{g1} = \begin{bmatrix} 1 \\ 0 \\ 0 \\ 0 \end{bmatrix}, \; H_1^{g2}: \boldsymbol{e}^{g2} = \begin{bmatrix} 0 \\ 1 \\ 0 \\ 0 \end{bmatrix}, \; H_1^{g3}: \boldsymbol{e}^{g3} = \begin{bmatrix} 0 \\ 0 \\ 1 \\ 0 \end{bmatrix}, \; H_1^{g4}: \boldsymbol{e}^{g4} = \begin{bmatrix} 0 \\ 0 \\ 0 \\ 1 \end{bmatrix} \tag{5-56}$$

For each hypothesized index vector, $\boldsymbol{e}^{gk}$, data reconciliation and bias estimation are performed simultaneously to obtain the test statistics, τ^{gk}, and the optimum bias magnitude, b^{gk}. After the serial testing for each hypothesis, one can compare the test statistics for each bias model and select the one that gives the highest score. The data reconciliation process carried out for the bias model that has the highest score of test statistics is free of smearing effects since the hypothesized bias location is correct and the corresponding bias magnitude has been estimated and compensated to the measured data. In this example, if the chi-square, χ^2, is chosen as the test statistics, the gross error model giving the lowest chi-squares value represents the correct model.

In the case of multiple gross errors, the serial bias compensation strategy can be used to test the hypotheses for all possible gross error models. Each gross error model is associated with presumed gross error locations and unknown magnitudes, which need to be estimated in the joint data reconciliation process, i.e., data reconciliation and gross error estimation. If the total number of measurements is r and the presumed bias number is s, then the total combinations of bias locations is given by:

$$C_s^r = \frac{r!}{s!(r-s)!} \tag{5-57}$$

Using the index vector $\boldsymbol{e}$ for the indication of bias locations can facilitate the processes of defining gross error models and hypotheses testing, especially for the case of multiple gross errors. For multiple gross errors, the index vector $\boldsymbol{e}$ has multiple elements equal to 1, i.e., $e_j = 1$, and the number of possible combinations for e_j follows equation (5-57). The hypotheses testing can then be carried out over different scenarios of gross error models. The alternative hypotheses for different scenarios can be expressed as:

$H_1^{g\,pq}$: the alternative hypothesis of the q-th gross error model in the p-th scenario

The scenarios are set based on the number of total bias, e.g., 1-bias scenario, 2-bias scenario, …p-bias scenario. In each of the scenario, all possible gross error models are hypothesized and tested. For instance, when the alternative hypothesis, $H_1^{g\,pq}$, is tested, the gross error model, g_{pq}, is given by:

$$y'_j = y_j + \varepsilon + b_j e_j^{g\,pq} \tag{5-58}$$

, by which the measurement data are compensated. Following the step of measurement compensation is the joint data reconciliation where p extra variables for bias magnitudes from the qth bias model are added to the optimization scheme.

The process of hypotheses testing for multiple gross errors can be summarized as follows:

1. Carry out data reconciliation without any presumed gross error model and test the null hypothesis, H_0. If the null hypothesis is rejected, go to step 2 where the scenarios of alternative hypotheses $H_1^{g\,pq}$ are assigned.
2. Start from the scenario of p = 1, i.e., one-bias scenario. Construct the index vectors $\boldsymbol{e}$ for all possible gross error models. Carry out joint data reconciliation for each gross error model, by which one can get the optimum solutions to the bias magnitudes for each bias model and the corresponding test statistics. Rank the gross error models by their test statistics.
3. Increase the value p by 1, i.e., $p = p + 1$, and rebuild the index vector for all possible gross error models in the current scenario where number of p gross errors occur simultaneously. Follow the similar procedure in step 2 for hypothesis testing.
4. Repeat step 3 until the value of p is equal to the total number of the model constraints.

The maximum allowable number of gross errors must be less or equal to the number of the model constraints or model functions. The joint data reconciliation problem becomes ill posed if the added variables of bias magnitudes make the total number of independent variables greater than the number of total model constraints

The major disadvantage of testing all possible gross error models for multiple gross error detection is the significant computation time, since each hypothesis test requires an exact run of joint data reconciliation, in which the number of independent variables is increased by the added variables for the bias magnitudes. If the number of the total measurement data is large and the system model is nonlinear, it becomes impractical to test all possible gross error models.

Instead of testing all scenarios with different bias numbers, one can carry out the serial bias compensation in such a way that the bias is detected one at a time. At beginning of the test, one bias is assumed, followed by the hypotheses testing carried out for all one-bias models whose locations are defined by the associated index vectors $\boldsymbol{e}$. The bias model that gives the best test statistics is picked and then proceeds to the next "round". Here the one-bias model with the highest test score does not necessary make the alternative hypothesis of one gross error accepted. If the alternative hypothesis is accepted in the first round, it is suggested that only one gross error exists and there is no need for the second round hypotheses testing. On the other hand, if the alternative hypothesis for one gross error is rejected, one proceeds to the next round.

In the second round, the detected gross error from the first round is retained for its location, while a new search for one gross error is performed. Although at this round the algorithm is still searching for one gross error other than the one that has been identified from first round, the hypotheses testing are actually carried out for all two-bias models, each of which has an index vector with a constant value of e_{j1}, determined from the first round, and a "floating" value of e_{j2}, being tested in the second round. Only the information about the bias location from the first round is retained; the bias magnitude

obtained from the first round is discarded and re-estimated along with the second bias in the second round. After the two-bias models have all been tested, they are ranked by their test statistics. The gross error model with the highest test score will be retained; if the associated alternative hypothesis is still rejected, one proceeds to the third round; otherwise, the process stops.

The process continues until the alternative hypothesis for a certain bias number is accepted. At each round of hypotheses test, only the locations of previously detected biases are assumed to be correct and retained, while the magnitudes of all biases are assumed to be unknown and estimated in the current round. This method combines the serial bias compensation strategy with a serial elimination algorithm. The steps can be summarized as follows:

1. Perform data reconciliation without any presumed bias model and test the associated null hypothesis, H_0. If the null hypothesis is rejected, go to step 2; otherwise, stop the process.
2. Start the hypotheses testing for the one-bias model, i.e., only one element in the index vector $\boldsymbol{e}$ can be 1. Perform the joint data reconciliation for each of the one-bias model and rank these hypotheses by their test statistics. Retain the bias model with the highest test score. If the test statistics rejects the alternative hypothesis H_1^{g1}, go to step 3; otherwise, stop the process.
3. Retain the non-zero element of the index vector from the previous round, e_{j_1}, and perform hypotheses testing for the two-bias models by remaining e_{j_1} and floating the other element, e_j ($j \neq j_1$), one at a time. The two-bias model with the highest test score proceeds to the next round if the associated alternative hypothesis $H_1^{g2/g1}$ is rejected.

4. Repeat Step 3 until the alternative hypothesis for a certain bias number $H_1^{g_k/g_{k-1}/\ldots/g_1}$ is accepted. The joint data reconciliation problem at the previous round of hypotheses test can be expressed as:

$$\min_{y,b_k}\left(y'-E_k^*b_k-y\right)^T\sum{}^{-1}\left(y'-E_k^*b_k-y\right) \tag{5-59}$$

while the next round of data reconciliation with the information of bias locations obtained from the previous round is given by:

$$\min_{y,b_k,b_i}\left(y'-E_k^*b_k-b_ie_i-y\right)^T\sum{}^{-1}\left(y'-E_k^*b_k-b_ie_i-y\right) \tag{5-60}$$

where b_k is a vector containing k unknown biases; E_k is a matrix containing columns of the unit vectors. The jth column vector of E_k has a value of "1" in the position corresponding to the measurement identified as biased in the jth round of hypotheses testing.

Similarly, one should be aware that the maximum allowable gross errors must be less or equal to the number of model constraints to avoid an ill posed data reconciliation problem. Figure 5-24 shows the process of serial bias compensation for GED.

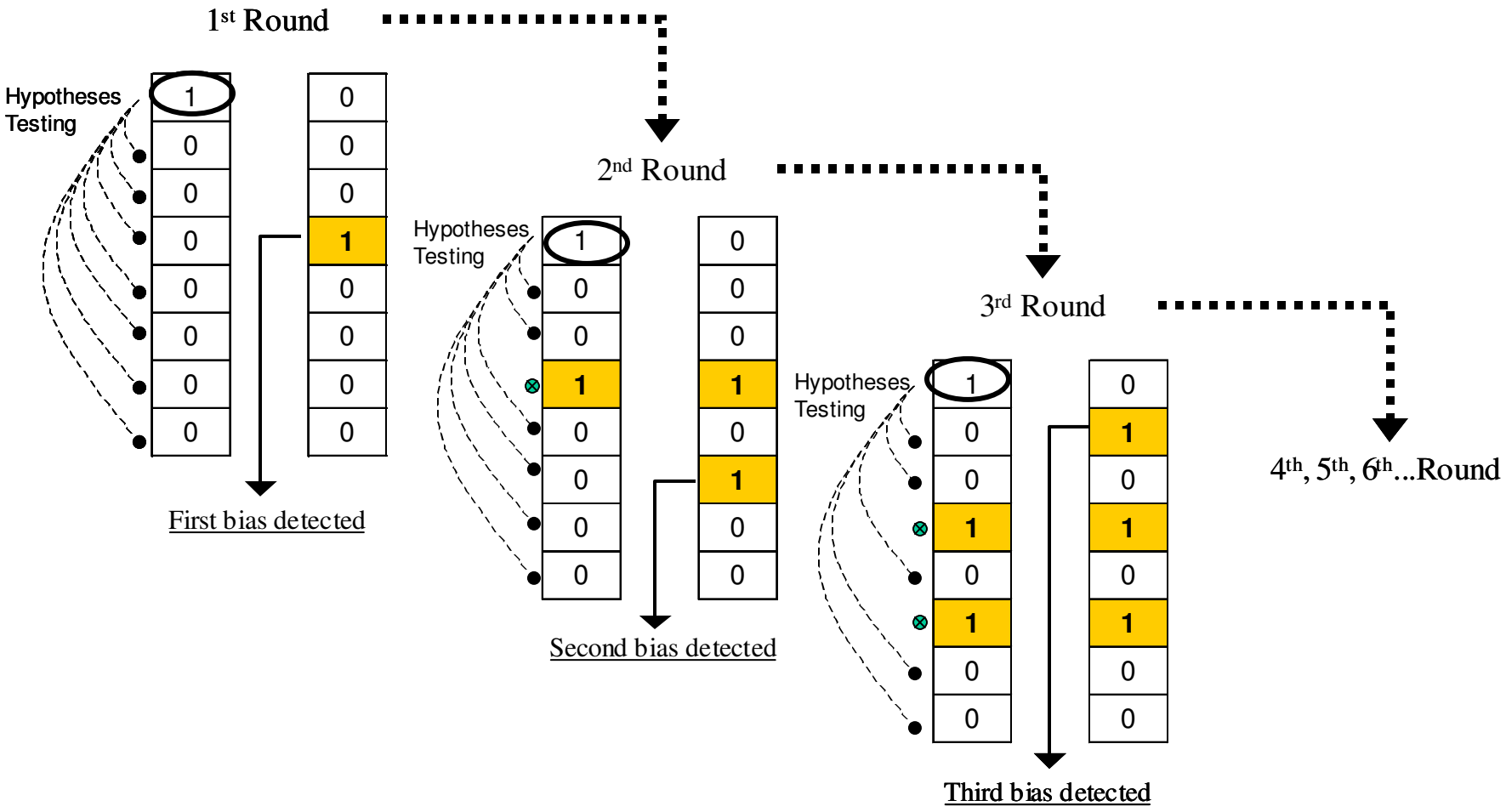

Figure 5-24: Process of serial bias compensation

5.5.6. Serial Bias Compensation Strategy for Simultaneous Data Reconciliation and Model Calibration

In model-based data reconciliation and model calibration, the presence of gross errors invalidates the reconciled results due to the smearing effects. By compensating the measured data with a correct gross error model, one can neutralize the smearing effects while carrying out the least squares type data reconciliation. In order to obtain the statistically "correct" gross error model, a gross error detection technique utilizing hypotheses testing is required. In this study, it is suggested to combine hypotheses testing with the serial bias compensation strategy for the gross error detection. As discussed in Chapter 4, the problem of simultaneous data reconciliation and model calibration is given by:

$$\min_{a_i,\theta_k} \sum_{j=1}^{m} \left(\frac{y'_j - f_j(a_i,\theta_k)}{\sigma_j} \right)^2 \tag{5-61}$$

where

$$y_j = f_j(a_i,\theta_k)$$
$$\text{for } i = 1 \sim n;\ j = 1 \sim m;\ k = 1 \sim s \tag{5-62}$$

If the model parameters, θ_k, are known in prior, it becomes a problem of simultaneous data reconciliation and gross error detection. One can apply the serial bias compensation scheme to the hypothesis testing for gross error detections.

In most applications, however, the model parameters are unknown and need to be estimated through reconciling the measured data which are subject to random and gross errors. In Chapter 4, the solutions to the problem of simultaneous data reconciliation and model calibration, in which the measurements are subject only to random errors, have been discussed. Using the same scheme as the inner loop for data reconciliation and

model calibration, one can impose the serial bias compensation method with hypotheses testing as an outer loop for gross error detection.

The process starts from the null hypothesis, H_0, in which it is assumed there is no gross error and there is no bias adjustment for the measured data. The null hypothesis and the associated test statistics are given by:

$$
\begin{aligned}
&H_0: \\
&\quad \textit{gross error model}: \qquad y'_j = y_j + \varepsilon_j = f_j(a_i, \theta_k) + \varepsilon_j \\
&\quad \textit{test statistics}: \qquad \chi^2_{H0} = \sum_{j=1}^{m} \left(\frac{y'_j - f_j(a_i, \theta_k)}{\sigma_j} \right)^2
\end{aligned}
\tag{5-63}
$$

Without the hypothesized bias model, the test statistics for the null hypothesis is obtained from carrying out simultaneous data reconciliation and model calibration:

$$
\min_{a_i, \theta_k} \sum_{j=1}^{m} \left(\frac{y'_j - f_j(a_i, \theta_k)}{\sigma_j} \right)^2 \tag{5-64}
$$

When the test statistics rejects the null hypothesis, the hypotheses test on the gross error models, carried out by the serial bias compensation scheme, is then introduced. The serial bias compensation strategy can be performed in two ways as discussed in previous section. The first option is testing all possible bias models at different scenarios of total biases number. In the scenario of p biases, the alternative hypothesis for the qth bias model is given by:

$$
\begin{aligned}
&H_1^{g\,pq}: \\
&\quad \textit{gross error model}: \qquad y'_j = y_j + \varepsilon_j + \left(\boldsymbol{E}_{pq} \boldsymbol{b}_p\right)_j = f_j(a_i, \theta_k) + \varepsilon_j + \left(\boldsymbol{E}_{pq} \boldsymbol{b}_p\right)_j \\
&\quad \textit{test statistics}: \qquad \chi^2_{H_1)_{g\,pq}} = \sum_{j=1}^{m} \left(\frac{y'_j - \left(\boldsymbol{E}_{pq} \boldsymbol{b}_p\right)_j - f_j(a_i, \theta_k)}{\sigma_j} \right)^2
\end{aligned}
\tag{5-65}
$$

where $\boldsymbol{E}_{pq}$ represents the index matrix of the qth gross error model in the scenario of p biases. All elements except for the diagonal terms in the matrix $\boldsymbol{E}_{pq}$ are zero while number of p positions in the diagonal terms are equal to 1 and the rest diagonal elements are zeros. In each scenario of p biases, there are C_p^r bias models to be tested. Each bias model is simply represented by the index matrix $\boldsymbol{E}_{pq}$ with p non-zero elements in the diagonal terms. The structure of the index matrix $\boldsymbol{E}_{pq}$ is shown in Fig. 5-25.

The test statistics for each bias hypothesis is obtained by carrying out the joint data reconciliation process given by:

$$\min_{a_i,\theta_k,b_p} \sum_{j=1}^{m} \left(\frac{y'_j - \left(\boldsymbol{E}_{pq}\boldsymbol{b}_p\right)_j - f_j(a_i,\theta_k)}{\sigma_j} \right)^2 \tag{5-66}$$

where the magnitudes of the hypothesized biases, b_p, are optimized along with the model parameters, θ_k, and measurements, a_i.

The second option is eliminating gross error models one at a time. The alternative hypothesis for the mth gross error model at the lth round is given by:

$H_1^{g_{lm}/g_{l-1}/\ldots/g_1}$:

$$\textit{gross error model}: \qquad y'_j = y_j + \varepsilon_j + \left(\boldsymbol{E}_l\boldsymbol{b}_l\right)_j = f_j(a_i,\theta_k) + \varepsilon_j + \left(\boldsymbol{E}_l\boldsymbol{b}_l\right)_j$$

$$\textit{test statistics}: \qquad \chi^2_{H_1}\Big)_{g_{lm}/g_{l-1}/\ldots/g_1} = \sum_{j=1}^{m} \left(\frac{y'_j - \left(\boldsymbol{E}_{lm}\boldsymbol{b}_l\right)_j - f_j(a_i,\theta_k)}{\sigma_j} \right)^2 \tag{5-67}$$

where $\boldsymbol{E}_{lm}$ represents the index matrix of the m-th bias model at the l-th round hypotheses testing. Unlike $\boldsymbol{E}_{pq}$, there is only one floating element in the diagonal terms of $\boldsymbol{E}_{lm}$ at each round of hypotheses testing. In the l-th round of testing, there are $(l - 1)$ non-zero elements at the fixed positions determined in the previous round, i.e., $(l - 1)$-th round. The number of all possible bias models at the l-th round is $(r - l - 1)$ where r is the number of measured data. The structure of the index matrix $\boldsymbol{E}_{lm}$ is shown in Fig. 5-26.

Similarly, the test statistics for each bias hypothesis is obtained by carrying out the joint data reconciliation process, which is the least squares type minimization problem given by:

$$\min_{a_i,\theta_k,bl} \sum_{j=1}^{m} \left(\frac{y'_j - \left(\boldsymbol{E}_{lm}\boldsymbol{b}_l\right)_j - f_j(a_i,\theta_k)}{\sigma_j} \right)^2 \tag{5-68}$$

where the magnitudes of the hypothesized biases, b_l, are optimized along with the model parameters, θ_k, and measurements, a_i.

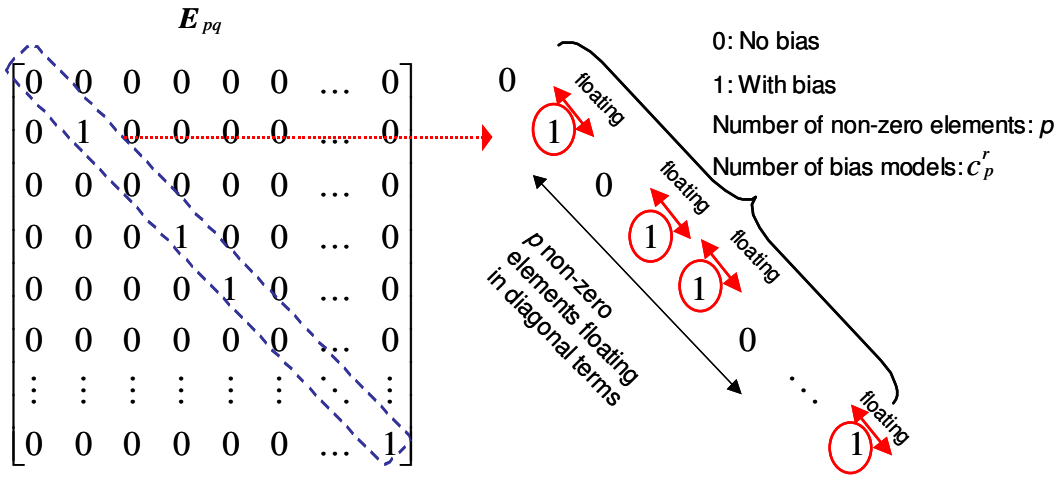

Figure 5-25: Structure of index matrix E_{pq}

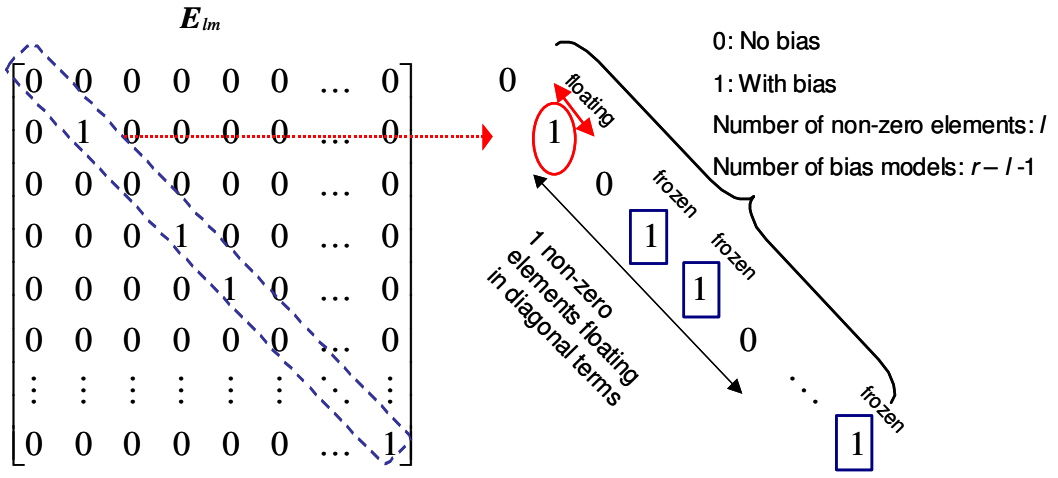

Figure 5-26: Structure of index matrix E_{lm}

5.5.7. Model Exploration for Gross Error Removal

Measurements with gross errors should be removed prior to simultaneous data reconciliation and model calibration (SDRMC) to eliminate smearing effects. Not all detected gross errors can be removed and the SDRMC can still be performed properly. The main purpose of SDRMC is to utilize the available measured data to estimate the model parameters while the measured data are also reconciled. When the measured data with gross errors are identified and removed from the reconciliation process, it could cause the loss of measurement redundancy or availability such that the model parameters cannot be estimated properly.

In a typical data reconciliation problem with linear or bilinear model constraints, the availability or redundancy of measurements can be checked by the rank of the constraint matrix. In the case of a highly nonlinear explicit model, redundancy or availability check becomes not so obvious. Model exploration is, therefore, required prior to removing all measured data that are identified with gross errors. With a careful study on the model responses with respect to model parameters, one can know if removing the data from the reconciliation process will cause the loss of redundancy and availability. When carrying out model exploration, the behavior of the model with respect to the model parameters is studied. It can be aided by using the prediction profilers and Pareto charts.

The prediction profilers demonstrate the system sensitivities to the model parameters, by which one can tell if the redundancy is still available after removing some measurements. The Pareto chart shows the contribution of each model parameter to the system response, providing the insight of the sensitivity of SDRMC. Some of the model parameters are dominant compared to others such that the removal of those measurements that have direct impacts on the dominant model parameters could cause indetermination of model parameters or increase estimate errors regardless of measurement redundancy. If removing data leads to indetermination of certain model

parameters, one may still predict the other model parameters, but assumptions must be made for those undetermined parameters. The other benefit of exploring the model prior to data reconciliation is that one can determine the maximum allowable biased data that the model can afford to lose. More importantly, model exploration provides the information required for sensor optimization, i.e., place more budget on the measurements that have dominant impacts on the determination of model parameters.

CHAPTER 6

COMBINED CYCLE DATA RECONCILIATION AND DEGRADATION STATUS ESTIMATION

The main purpose of performance monitoring is to track power plant equipment degradation over time. Once the degradation of plant equipment is known, recommendations of the plant optimal operating mode and potential equipment upgrade strategies can be provided to the plant operator to improve the reliability, efficiency and profitability of their equipment.

The degradation status of a thermo system is estimated by its current performance data, whose measurements are subject to uncertainties and possible biases. Justifying the performance data requires a representative thermodynamic model that describes the thermo system correctly. If the thermodynamic model is the heat and mass balance type, the data is reconciled first, and then populated to the thermodynamic model that serves as a performance simulator for the model calibration. The calibrated model represents the current degradation status of the thermo system, from which one can quantify the degradation by comparing the performance of the calibrated model to the design new & clean model. If the model is a performance simulation type, a simultaneous scheme for data reconciliation and parameter estimation is performed, and the model is calibrated through the data reconciliation process. The model parameters are usually the performance multipliers or correction factors that adjust the performance to reflect the degradation effect. In this type of application, data reconciliation and model calibration are combined to a process of simultaneous data reconciliation & degradation estimation.

In this research, the techniques of data reconciliation and gross error detection are applied to a combined cycle system. It is aimed to provide a probability way to assess the system

degradation by reconciling the performance data. One can get the major benefit of reducing the estimate uncertainties by performing data reconciliation as compared to conventional data reduction.

The related research works of model calibration for the aircraft gas turbine engines can be found in [88, 89, 90], in which the gross errors effects were not taken into account.

6.1. Case Study I: Gas Turbine Data Reconciliation Using Heat and Mass Balance

Without the commercial software for gas turbine performance simulation, one can carry out gas turbine data reconciliation by utilizing heat & mass balance equations. Since the flow conditions of a gas turbine exhaust have a significant impact on the performance of bottom cycle, the reconciled gas turbine exhaust flow conditions, which have less uncertainties than their measured values, can be used as the model inputs to reduce the uncertainties of bottom cycle data reconciliation. To reconcile the measurements of a gas turbine and estimate its degradation status, the gas turbine heat balance solver can be utilized or the heat balance equations can be solved directly. By solving the conservation equations in different orders, different sets of the model inputs can be chosen with flexibilities. Among these sets of model inputs one can be selected that results in the least uncertainties of the calculated values. Since the purpose of data reconciliation is to make thermodynamically consistent measurements, a set of reconciled measurements satisfies the conservation equations at each control volume and, thus, provides a closed heat balance. Because the heat balance equations for energy conservation are nonlinear, getting the solutions by a simple matrix inversion is not possible. The traditional way is to perform the data reduction by plugging the known values (measured flow parameters) into the heat balance equations and calculating the values for either the known (measured) or unknown parameters. The calculated values

are then used to rectify the measured flow parameters and to predict the parameters that can't be measured, like the firing temperature and turbine inlet temperature. The measured values used as model inputs have measurement uncertainties and these uncertainties are propagated to the calculated flow parameters. Appropriately selecting a set of measurements for the inputs could lead to less uncertainty for the calculated flow parameters.

6.1.1. Gas Turbine Heat and Mass Balance

There are many ways of defining a set of measurements for model inputs, and each of them gives a different set of calculated flow parameters, among which some unmeasured parameters may be the same, like the firing temperature. For example, the measured value of compressor airflow can be selected as one of the inputs and let the turbine exhaust temperature, which can also be measured, be calculated. Or, make the measurement of turbine exhaust temperature as one of the model inputs, and calculate the value of compressor airflow. In both cases the firing temperature is calculated due to the impossible measurement for that parameter. In the first case the turbine exhaust temperature will be reconciled by the model-calculated values, while in the second case the compressor airflow will be rectified. Ideally, the predicted values in both cases, for example, the firing temperature, should be the same. But, because of the imperfect measurements with uncertainties and biases, the predicted values from different ways of solving the heat balance equations do not match with each other. In the traditional way the method selected is that gives the least uncertainty for the predicted flow parameters. But even the method is chosen that gives the least uncertainty for the predicted values, those measured inputs are still heavily relied upon, which themselves have measurement uncertainties. In addition, by using the traditional way of data reduction only the calculated flow parameters are rectified. To reconcile all the gas turbine measurements, the input measurements have to be treated as variables and be defined as an objective

function to find the optimum set of model inputs. By doing this, all of the major measurements can be reconciled. Measurements that are taken as model inputs are obtained through the optimization, and the others are directly calculated from the model equations. Also, for those parameters that cannot be measured, like the firing temperature, turbine inlet temperature, compressor efficiency and turbine efficiency, can be estimated after data reconciliation. By calculating the values of parameters like turbine throat area, compressor efficiency and turbine efficiency, the degradation status of the gas turbine can be determined. Once the degradation status is determined with a certain confidence level, the heat balance model can be utilized to predict the gas turbine performance at different operating conditions or upgrade combinations. To solve the gas turbine heat balance, the gas turbine is divided into several control volumes, each of which has its own conservation equations.

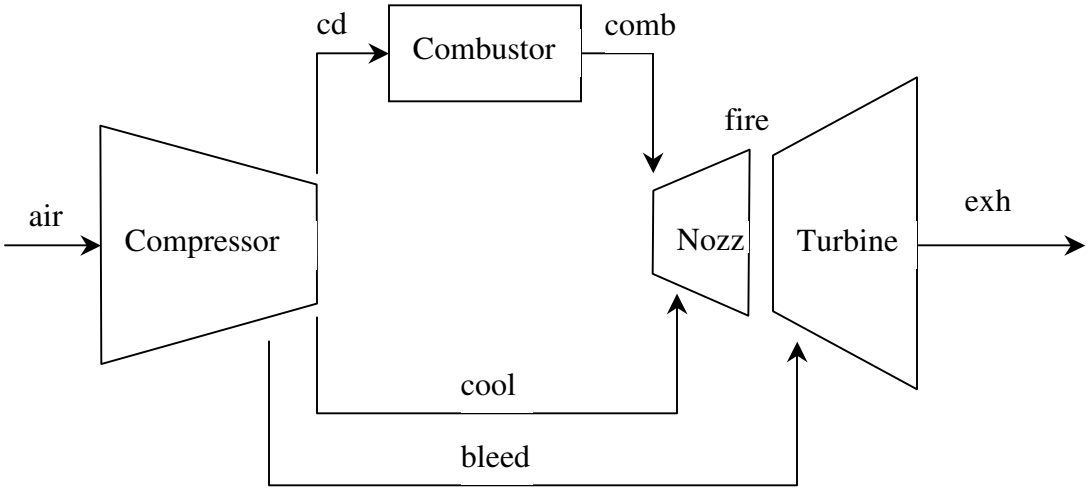

Figure 6-1: Control volumes for gas turbine heat balance analysis

Gas Turbine Heat and Mass Balance Equations

Gas turbine heat balance analysis applies mass and energy conservation equations to each of the four control volumes illustrated in Figure 6-1. An additional equation of the choked flow relationship at the first stage nozzle is needed to close the heat balance. These heat balance equations for each control volume are given below:

Compressor

Conservation of Mass:

$$w_{air} = w_{cd} + w_{cool} + w_{bleed} \tag{6.1}$$

Conservation of Energy:

$$w_{air} Cp_{air} T_{inlet} + PW_{compressor} = w_{cd} Cp_{cd} T_{cd} + w_{cool} Cp_{cool} T_{cool} + w_{bleed} Cp_{bleed} T_{bleed} \tag{6.2}$$

Combustor

Conservation of Mass:

$$w_{comb} = w_{cd} + w_{fuel} + w_{water} \tag{6.3}$$

Conservation of Energy:

$$w_{cd} Cp_{cd} (T_{cd} - T_{ref}) + w_{fuel} \eta_{comb} (LHV + Cp_{fuel} (T_{fuel} - T_{ref})) + w_{water} (H_{water} - H_{ref}) = w_{comb} Cp_{comb} (T_{comb} - T_{ref}) \tag{6.4}$$

Nozzle

Conservation of Mass:

$$w_{fire} = w_{comb} + w_{cool} \tag{6.5}$$

Conservation of Energy:

$$w_{comb} Cp_{comb} T_{comb} + w_{cool} Cp_{cool} (T_{cool} - \Delta T_{cool}) = w_{fire} Cp_{fire} T_{fire} \tag{6.6}$$

Turbine

Conservation of Mass:

$$w_{exh} = w_{fire} + w_{bleed} \tag{6.7}$$

Conservation of Energy:

$$w_{fire} Cp_{fire} T_{fire} + w_{bleed} Cp_{bleed} (T_{bleed} - \Delta T_{bleed}) = w_{exh} Cp_{exh} T_{exh} + PW_{turbine} \tag{6.8}$$

Shaft Power, Net Power and Auxiliary Power Balance:

$$\eta_{shaft} PW_{turbine} = PW_{shaft} + PW_{compressor} \tag{6.9}$$

$$PW_{net} = \eta_{generator} PW_{shaft} - PW_{aux} \tag{6.10}$$

Choked Flow Relationship at First Stage Nozzle:

$$w_{comb} = C_{noz} A_{noz} \frac{P_{comb}}{\sqrt{T_{comb}}} \tag{6.11}$$

Combustor Pressure Loss:

$$P_{comb} = (1 - \Delta P_{comb}) P_{cd} \tag{6.12}$$

Specification of Compressor Extraction:

$$\begin{aligned} w_{cool} &= \lambda_{cool} w_{air} \\ w_{bleed} &= \lambda_{bleed} w_{air} \end{aligned} \tag{6.13}$$

$$\begin{aligned} T_{cool} &= \delta_{cool} T_{cd} \\ T_{bleed} &= \delta_{bleed} T_{cd} \end{aligned} \tag{6.14}$$

Equations (6.1)~(6.14) are needed to close the gas turbine heat and mass balances, and the flow constants, like the cooling flow fractions, combustor pressure drop, and the turbine nozzle area, must be known prior to the data reduction. These design constants and fluid properties are listed in table 6-1. Once all the flow parameters, including the unknowns and those to be reconciled, are obtained from these equations, these values are utilized to estimate the degradation factors and performance parameters. These estimated parameters are listed below:

Compressor Efficiency:

$$T_{cd} - T_{inlet} = \frac{T_{inlet}}{\eta_{compressor}} \left[\left(\frac{Pcd}{Pinlet} \right)^{\frac{k_{air}-1}{k_{air}}} - 1 \right] \tag{6.15}$$

Turbine Efficiency:

$$T_{fire} - T_{exh} = \eta_{turbine} T_{fire} \left[1 - \left(\frac{Pexh}{Pcomb} \right)^{\frac{k_{gas}-1}{k_{gas}}} \right] \tag{6.16}$$

Gas Turbine Heat Rate:

$$HR = \frac{w_{fuel} LHV}{PW_{net}} \tag{6.17}$$

Turbine Inlet Temperature:

$$T_{in\ turbine} = \frac{w_{air} Cp_{cd} (T_{cd} - T_{ref}) + w_{fuel} \eta_{comb} (LHV + Cp_{fuel} (T_{fuel} - T_{ref})) + w_{water} (H_{water} - H_{ref})}{(w_{air} + w_{fuel} + w_{water}) Cp_{comb}} + T_{ref} \tag{6.18}$$

Table 6-1: Gas turbine flow constants and properties used as heat balance inputs

Gas Turbine Design Constants and Fluid Properties as Inputs to Heat Balance Equations			
Constants	**Definitions**	**Constants**	**Definitions**
λ_{cool}	1st stage nozzle cooling flow fraction	Cp_{cool}	Compressor discharging air specific heat
λ_{bleed}	Turbine cooling flow fraction	Cp_{bleed}	Compressor bleed air specific heat
δ_{cool}	Cooling air temperature fraction	Cp_{comb}	Compressor exhaust gas specific heat
δ_{bleed}	Bleeding air temperature fraction	Cp_{fire}	Gas specific heat at 1st rotor inlet
ΔT_{cool}	Cooling air temperature drop	Cp_{exh}	Exhaust gas specific heat
ΔT_{bleed}	Bleeding air temperature drop	Cp_{fuel}	Specific heat of fuel
η_{shaft}	Shaft Efficiency	LHV	Lower heating value of fuel
$\eta_{generator}$	Generator Efficiency	C_{nozzle}	Choked flow constant
η_{comb}	Combustor Efficiency	k_{air}	Ratio of specific heats for air
ΔP_{comb}	Combustor pressure loss fraction	k_{gas}	Ratio of specific heats for gas
Cp_{air}	Inlet air specific heat	T_{ref}	Reference temperature at which gas enthalpy equals zero
Cp_{cd}	Compressor cooling air specific heat	$H_{reference}$	Difference between reference enthalpies of gas and steam

6.1.2. Multiple Heat Balance Analyses

As mentioned earlier, to solve heat balance equations, the decision must be made for what measured flow parameters are to be used as inputs and what are to be calculated and reconciled. Once the decision is made based on the available measurements, the gas turbine heat balance equations are then solved in a specific order that requires the selected measurements as inputs. There are several ways of solving these conservation equations depending on how the combination of the measurement inputs is decided, and each way gives the set of calculated flow parameters with certain uncertainties. For those flow parameters that cannot be measured and must be calculated, like the firing

temperature and turbine inlet temperature, the uncertainties of the calculated values are different in each different way because the errors are propagated through different mechanisms from different sources. Theoretically, if perfect measurements occur, the calculated flow parameters and performance factors will be the same for each method, and there will be no uncertainties in these calculated values. In reality, the perfect measurements that represent true values of the flow parameters are not possible, and the uncertainties happen on the estimated values. By selecting a proper method of solving the gas turbine heat balance and performing the model-based data reconciliation, the uncertainties of the estimated gas turbine flow parameters can be reduced. In the following sections two methods of solving the gas turbine heat and mass balances are demonstrated. Their resultant uncertainties of certain calculated flow parameters are compared, and a model-based data reconciliation and degradation estimation will be performed by utilizing one of the methods that gives the least estimation uncertainties.

Method 1- Calculate the Compressor Air Flow and Combustor Efficiency

In this method the compressor air flow and combustor efficiency are to be calculated instead of being the inputs to the heat balance equations. The firing temperature and turbine inlet temperature are flow parameters that cannot be measured and must be calculated through the heat balance analysis. To make the compressor air flow and combustor efficiency the inputs, the heat balance equations are solved in the following way.

Combined with the mass conservation equation, Equation (6-2), and the equations that specify the compressor extractions (Equation (6-13) & (6-14)), the energy conservation equation of the compressor, Equation4.12, can be rewritten as:

$$w_{cd}\left[\frac{Cp_{air}T_{inlet}}{1-\lambda_{cool}-\lambda_{bleed}}-Cp_{cd}T_{cd}-\frac{\lambda_{cool}}{1-\lambda_{cool}-\lambda_{bleed}}Cp_{cool}\delta_{cool}T_{cd}-\frac{\lambda_{bleed}}{1-\lambda_{cool}-\lambda_{bleed}}Cp_{bleed}\delta_{bleed}T_{cd}\right]$$

$$+ \quad PW_{compressor} \quad = \quad 0 \tag{6.19}$$

This equation contains two unknowns: the compressor discharge flow, w_{cd}, and the power to the compressor, $PW_{compressor}$. Also, the two energy equations of the nozzle and turbine, Equation (6-6) and Equation (6-7), can be combined together along with their related mass conservation equations, Equations (6-3), (6-5) and (6-7). This forms one equation that contains three unknowns: compressor discharge flow, w_{cd}, combustor exit gas temperature, T_{comb}, and turbine power, $PW_{turbine}$.

$$(w_{cd}+w_{fuel}+w_{water})Cp_{comb}T_{comb}+\frac{\lambda_{cool}}{1-\lambda_{cool}-\lambda_{bleed}}w_{cd}Cp_{cool}(\delta_{cool}T_{cd}-\Delta T_{cool})$$

$$+ \quad \frac{\lambda_{bleed}}{1-\lambda_{cool}-\lambda_{bleed}}w_{cd}Cp_{bleed}(\delta_{bleed}T_{cd}-\Delta T_{bleed}) \tag{6.20}$$

$$= \quad \left(\frac{w_{cd}}{1-\lambda_{cool}-\lambda_{bleed}}+w_{fuel}+w_{water}\right)Cp_{exh}T_{exh}+PW_{turbine}$$

Then the shaft power balance equation, Equation (6-9), is introduced to replace the power terms with the shaft power, PW_{shaft}, in the above two equations. The shaft power, PW_{shaft}, can be related to the net power, PW_{net}, which is available from the measurement. Then, the above two equations, Equations (6-19) and (6-20), can be combined into one equation:

$$w_{cd}\left[\frac{Cp_{air}T_{inlet}}{1-\lambda_{cool}-\lambda_{bleed}}-Cp_{cd}T_{cd}-\frac{\lambda_{cool}}{1-\lambda_{cool}-\lambda_{bleed}}Cp_{cool}\delta_{cool}T_{cd}-\frac{\lambda_{bleed}}{1-\lambda_{cool}-\lambda_{bleed}}Cp_{bleed}\delta_{bleed}T_{cd}\right]$$

$$+\ \eta_{shaft}\left[\begin{array}{l}(w_{cd}+w_{fuel}+w_{water})Cp_{comb}T_{comb}+\frac{\lambda_{cool}}{1-\lambda_{cool}-\lambda_{bleed}}w_{cd}Cp_{cool}(\delta_{cool}T_{cd}-\Delta T_{cool})\\ +\ \frac{\lambda_{bleed}}{1-\lambda_{cool}-\lambda_{bleed}}w_{cd}Cp_{bleed}(\delta_{bleed}T_{cd}-\Delta T_{bleed})\\ -\ \left(\frac{w_{cd}}{1-\lambda_{cool}-\lambda_{bleed}}+w_{fuel}+w_{water}\right)Cp_{exh}T_{exh}+PW_{turbine}\end{array}\right]$$

$$-\ PW_{tshaft}\ =\ 0 \tag{6.21}$$

This combined equation contains two unknowns, the compressor discharge flow, w_{cd}, and the combustor exit gas temperature, T_{comb}. Combined with the mass conservation equation, equation (6-3), the choked flow relationship of the first stage nozzle, Equation (6-11), also contains these two unknowns:

$$w_{cd}=C_{noz}A_{noz}\frac{P_{comb}}{\sqrt{T_{comb}}}-w_{fuel}-w_{water} \tag{6.22}$$

Solving equations (6-21) and (6-22) gives the values of the compressor discharge flow, w_{cd}, and the combustor exit gas temperature, T_{comb}. Substituting these two values into the energy conservation equation of the combustor, Equation 6-3, the combustor efficiency can be obtained. Table 6-2 shows the major inputs and outputs for the procedure of solving the gas turbine conservation equations in Method 1.

Table 6-2: Major inputs and outputs for Method 1 gas turbine heat balance

Inputs (Measurements)	**Outputs** (Heat balance calculated)
Gas Turbine Net Power	Combustor Efficiency
Fuel Flow	Compressor Airflow
Fuel LHV	Tfire
Compressor Discharge Temperature	Turbine Inlet Temperature
Compressor Discharge Pressure	
Turbine Exhaust Temperature	
Stage 1 Nozzle Throat Area	

For those performance parameters and degradation factors that are not included in the conservation equations, like heat rate, compressor efficiency and turbine efficiency, their values can be obtained by plugging the calculated or measured values of the flow parameters into the definitions or extra relationships like the isentropic relationships. In Method 1, the measurements listed on the left hand side of table 6-2 are taken as inputs, and the other flow parameters (right hand side of table 6-2) including the combustor efficiency and compressor airflow are calculated. By doing this, only the measured values of the combustor efficiency and compressor airflow are reconciled due to their redundant measurements. Although the heat and mass balances are satisfied by reconciling two flow parameters, there are, however, no data reconciliations for the other measured flow parameters. In reality, the measurement uncertainties occur in every measurement and each of them should be reconciled. In order to reconcile all measured flow parameters simultaneously, these input measurements must be treated as independent variables that can be varied within the bounds of their measurements, and an object function should be formulated so the optimum set of reconciled values can be found. Method 1 provides a transfer function that closes the gas turbine mass and heat balances by any set of inputs. However, Method 1 is not the only way to close the heat and mass balances. By switching the input variables among the available measurements the heat and mass balances can be solved in a different order and a different set of output parameters is obtained.

Method 2- Calculate the Turbine Exhaust Temperature and Choked Flow Constant

As mentioned, Method 1 is not the only way to solve the mass and heat balances. By switching the inputs of available measurements, the mass and heat balances can be solved in a different way. For example, the way of solving the conservation equations can be changed such that the original output flow parameters become the inputs to the heat balance equations. In the second method of solving the conservation equations the compressor airflow, w_{cd}, and combustor efficiency, η_{comb}, become two of the inputs and the turbine exhaust temperature, T_{exh}, and the choked flow constant, C_{nozzle}, are the calculated parameters. In order to solve these equations, the energy equation of the combustor (Equation (6-4)) is used to obtain the combustor exit gas temperature, T_{comb}. By substituting this value into Eq.4.32 the turbine exhaust temperature, T_{exh}, can be solved, and this value is used to obtain the choked flow constant, C_{nozzle}, in Equation (6-22). Table 6-3 shows the major inputs and outputs for solving the gas turbine heat balance equations in Method 2.

Table 6-3: Major inputs and outputs for Method 2 gas turbine heat balance

Inputs (Measurements)	**Outputs** (Heat balance calculated)
Gas Turbine Net Power	*Turbine Exhaust Temperature*
Fuel Flow	*Choked Flow Constant*
Fuel LHV	Tfire
Compressor Airflow	Turbine Inlet Temperature
Compressor Discharge Temperature	
Compressor Discharge Pressure	
Combustor Efficiency	
Stage 1 Nozzle Throat Area	

In Method 2, because of the measurement redundancies for the turbine exhaust temperature and the choked flow constant, these two parameters can be reconciled by their calculated values. The flow parameters that are unable to be measured and need to be calculated, like the firing temperature and turbine inlet temperature, are also obtained

through solving the conservation equations. Usually, the values are not equal to those obtained in Method 1 because of the imperfect measurements of the input flow parameters. If perfect measurements, which represent the "true" values of the flow parameters, are available, the predicted flow parameters will be the same in both methods. For example, the firing temperatures are calculated in both methods and the results are given differently due to the measurements errors. In addition, because the two methods use different sets of inputs and mechanisms of calculations (solving the conservation equation in a different order), the uncertainties of the calculated firing temperatures are also different. This is because the uncertainties of the input flow parameters are propagated through different mechanisms in these two methods. Since the values of input flow parameters come from the measurements with certain uncertainties, the uncertainties of the calculated firing temperatures can be compared after using a Monte Carlo simulation illustrated in Figure 6-2. By assigning the Normal distributions, which represent the measurement uncertainties, to the input flow parameters in both methods, the Monte Carlo simulation gives the resultant distributions of the calculated firing temperatures. The results are given in Fig. 6-3 for Method 1 and Method 2. After superimposing the two distributions in one plot, the distributions of the firing temperatures resulted from the two different methods can be compared. Figure 6-3 also shows the superimposed distributions of the firing temperatures computed with the two methods.

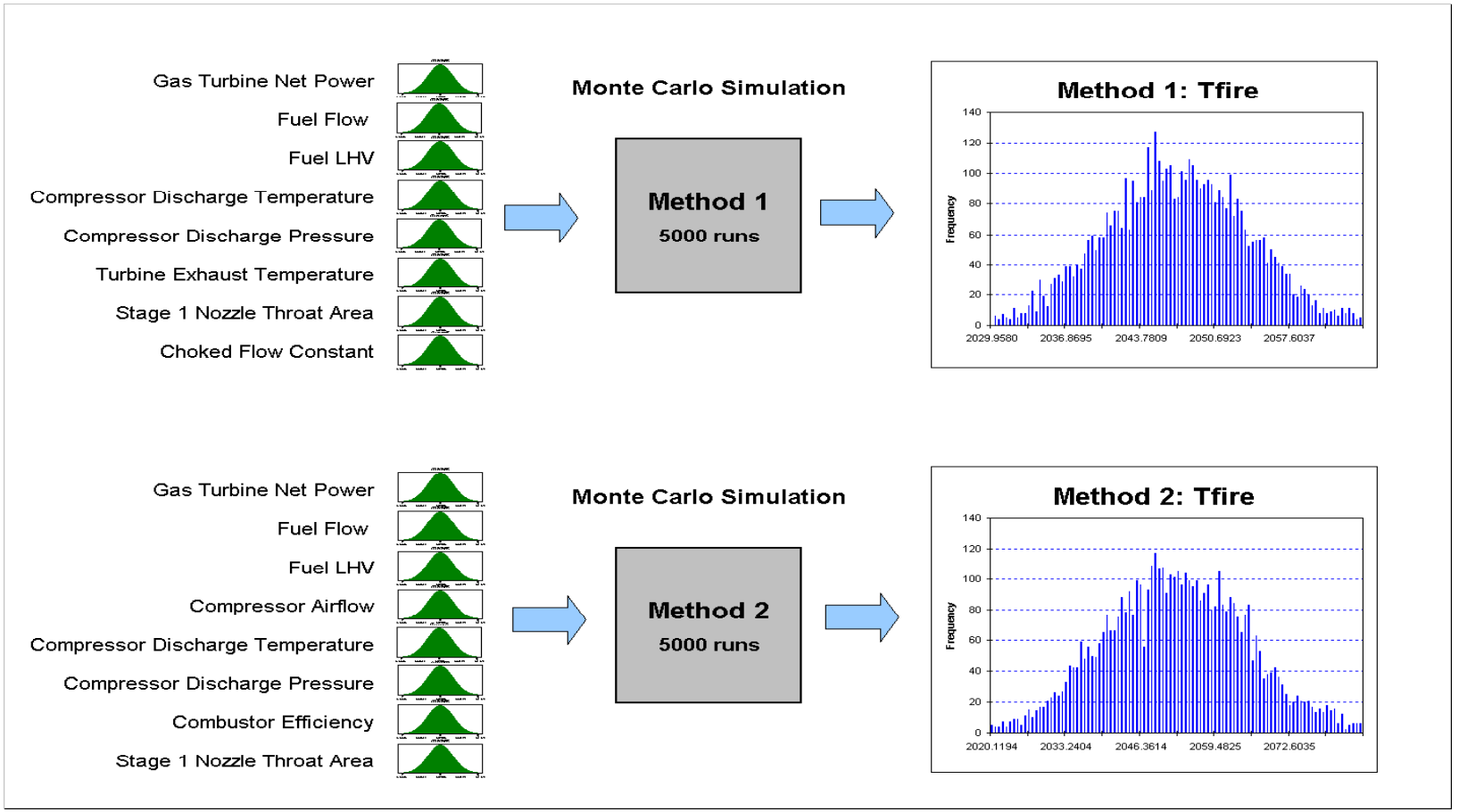

Figure 6-2: Monte Carlo simulation for determining uncertainties of firing temperatures

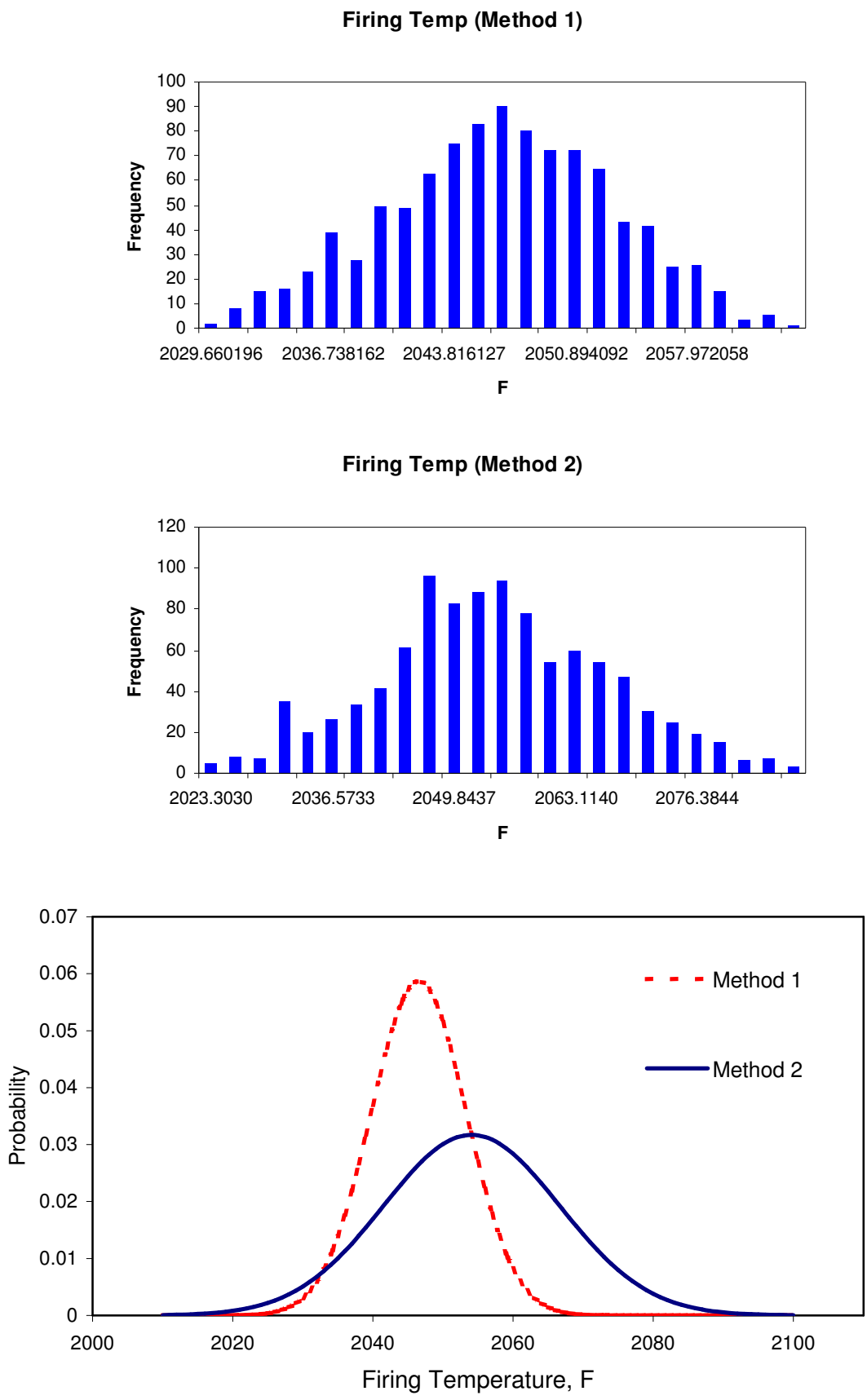

Figure 6-3: Uncertainties of the firing temperatures of two different methods

6.1.3. Deviation Penalty Function

By comparing these two obtained distributions of the firing temperatures from the Monte Carlo simulation, it was found that Method 1 gives the result with a smaller uncertainty. This is mainly because the sensitivity of the transfer function formed by Method 1 to the uncertainties of the input flow parameters is less than that formed by Method 2 and/or the set of input flow parameters in Method has less uncertainty. The determination of the firing temperature is very important since it affects the gas turbine control algorithm, which is necessary for maintaining the constant firing temperature. Thus, if a method is needed for the gas turbine data reduction and the firing temperature prediction, Method 1 is a better candidate since it predicts the firing temperature with less uncertainty.

Using Method 1 to solve the heat balance equations results in a smaller uncertainty for the calculated firing temperature than using Method 2. However, to this point this result relies on the inputs, which are themselves measurements with uncertainties, and only the calculated parameters with available measurements are reconciled. In addition, it is questionable to make reconciliations to only a few measured flow parameters while in reality all the measured flow parameters contribute to the total imbalance error. In order to reconcile all available gas turbine measurements, the transfer function formulated by Method 1 is needed to treat the input flow parameters as independent variables. The outputs of the transfer function also include parts of the measured flow parameters. The goal is to find the optimum set of the input flow parameters that either maximizes the likelihood function defined by all the measured flow parameters or minimizes the uncertainty of each reconciled flow parameter (these are two possible ways of forming the object function). On the other hand, although Method 2 results in a larger uncertainty of the calculated firing temperature, its value can be compared to that obtained in Method 1 to form a deviation penalty function, which represents the difference of the calculated firing temperatures between Method 1 and

Method 2. By adding the deviation penalty function, the goal is to find out the optimum set of model inputs that can minimize the deviation penalty function. Thus, the gas turbine data reconciliation can now be formulated as an objective of searching the optimum set of the model (transfer function formed by Method 1) inputs that not only maximizes the likelihood functions defined by the Normal distributions of the measurements but also minimizes the deviation penalty function, which represents the discrepancies of the predicted performance parameters from two methods. When the input flow parameters are assumed to be Normal distributed, maximizing the likelihood function is simplified to minimizing the least square function. The least square and deviation penalty functions can be combined to formulate the optimization problem as:

$$\min_{f_j} \sum \left[\frac{f_{i,recon} - f_{i,measured}}{\sigma_i} \right]^2 + \sum \left[\frac{F_i\left(f_1, f_2, f_3, \ldots\right)_{recon} - f_{i,measured}}{\sigma_i} \right]^2 + \sum \left(f_{i,predicted}\Big|_{Method\ 1} - f_{i,predicted}\Big|_{Method\ 2} \right)^2 \tag{6-23}$$

The first term of the object function is the least square formed by the input flow parameters, and the second term represents the least square formed by the output flow parameters. Both are measured by instruments and calculated by the transfer function. The third term is the deviation penalty function, which represents the discrepancies of the predicted performance factors between Method 1 and Method 2. By using this form of object function, two problems are taken care of simultaneously:

The reconciled flow parameters result in minimizing the least square function but cause significant discrepancies of the predicted parameters between the two methods.

The reconciled flow parameters minimize the discrepancies of predicted performance parameters but cause significant deviations from their measured values and, thus, lead to a significant least square.

The variations of the least square function and the deviation penalty function during the data reconciliation are given in Fig. 6-4. It shows that in the end of the process

when the optimum set of the inputs is reached, the deviation penalty function is almost zero, while the least square function is at a certain finite value. This implies that during the process the input measured flow parameters are reconciled in the way such that the likelihood function is maximized (a finite value of the least square function) and the deviations between Method 1 and Method 2 are minimized to almost zero. Figure 6-5 and 6-6 illustrate the variations of the calculated firing temperatures and turbine efficiencies from Method 1 and Method 2 during the data reconciliation. These show that because of the use of the deviation penalty function, the predicted flow parameters and performance factors from the two different methods match very well when the optimization is reached. By performing the data reconciliation, all the gas turbine flow measurements are rectified. Table 6-4 shows the comparisons between the original measured data and the final reconciled values, and the amounts of the rectifications for each of the flow parameters are given in Fig. 6-7. Without the use of the deviation penalty function, the discrepancies of the flow parameters between Method 1 and Method 2 are present. Figure 6-8 and 6-9 shows the predicted firing temperatures and turbine efficiencies from two methods during the data reconciliation without the use of deviation penalty function. These figures show that in the end of the optimization there are discrepancies of the predicted flow parameters between the two methods. This suggests that even though the measured data has been reconciled such that the least square function is minimized, but the reconciled values are still not the “true” values because they cause imbalances in the transfer function formed by Method 2. The “true” values should result in the balance of any transfer function formulated in a different way of closing the heat balance.

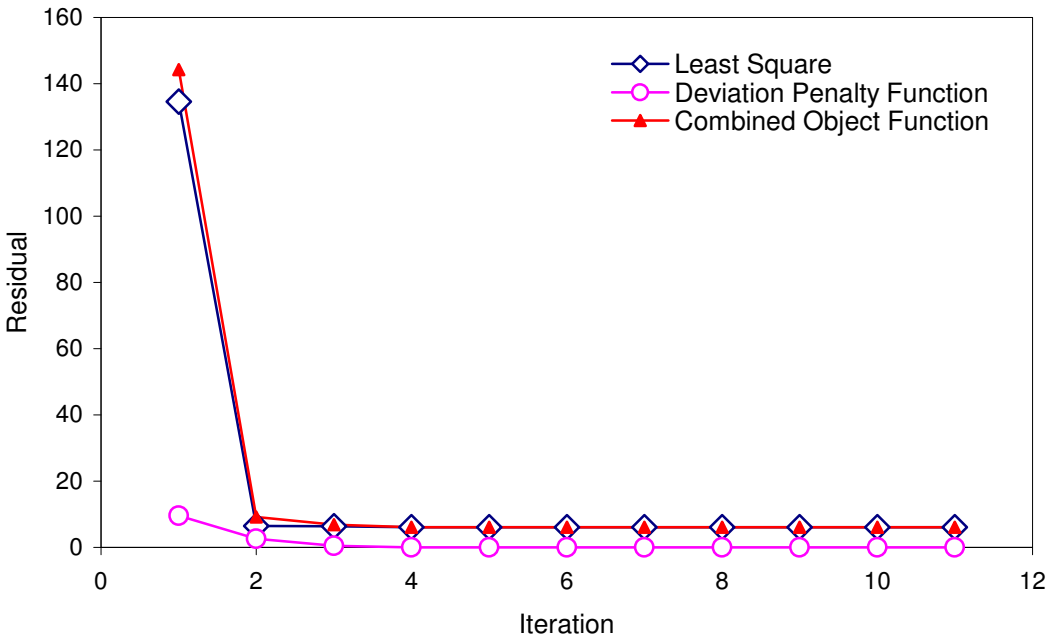

Figure 6-4: Convergence history for three objectives functions

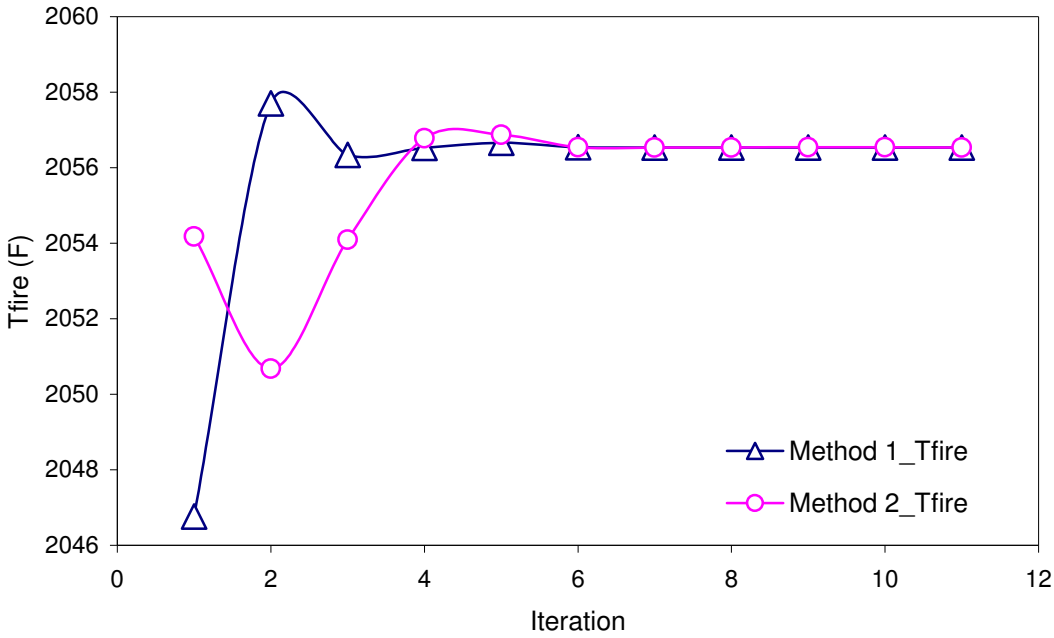

Figure 6-5: Convergence history of firing temperatures for Method 1 & 2

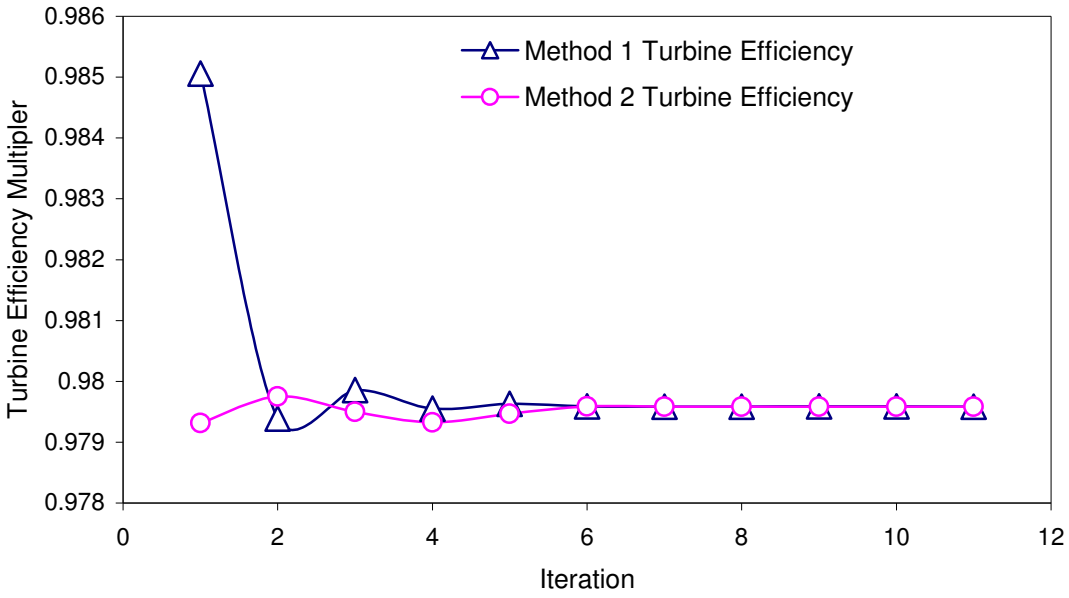

Figure 6-6: Convergence history of estimated turbine efficiencies for Method 1 & 2

Table 6-4: Comparison of measured the reconciled values

low Parameters	Reconciled	Measured	Deviation (Number of σ)	1 σ Uncertainty
Generator Output (kW)	45602.6121	45595.091	0.15861134	47.4188946
Fuel Flow (lb/sec)	6.95106751	6.96615206	-1.0827036	0.0139323
Compressor Discharge Pressure (psia)	-172.57316	-172.14598	0.9925817	-0.430365
Compressor Discharge Temperature (F)	661.862499	662.56629	-0.2307513	3.05
Compressor Airflow (lb/sec)	302.291664	303.803671	-0.4976923	3.03803671
Exhaust Temperature (F)	1044.4542	1033.66161	1.82925252	5.9

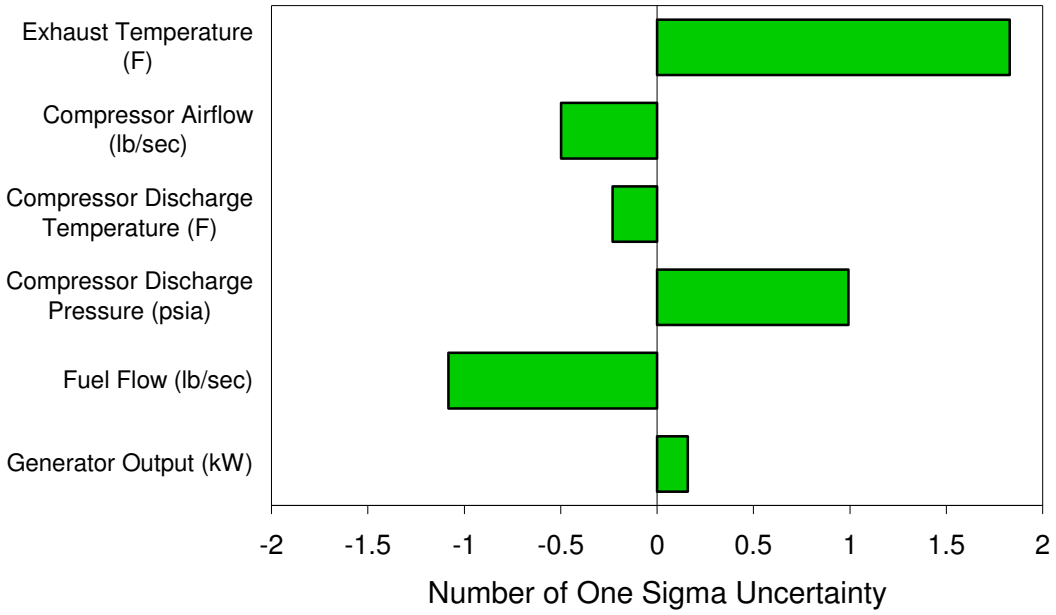

Figure 6-7: Measurement corrections for the gas turbine flow parameters

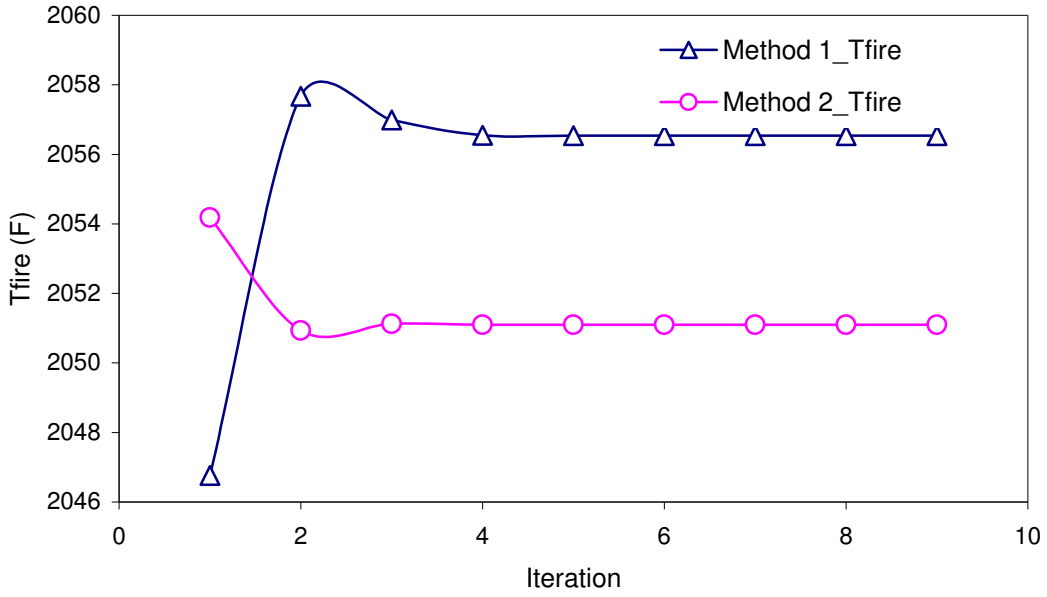

Figure 6-8: Convergence history of firing temperatures for Method 1 & 2 using least squares

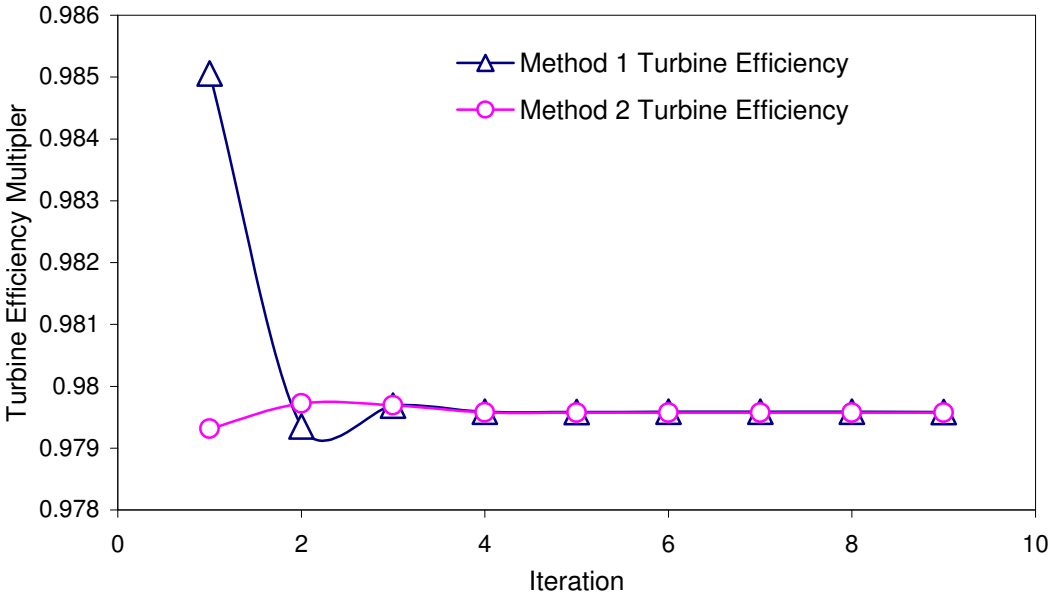

Figure 6-9: Convergence history of turbine efficiencies for Method 1 & 2 using least squares

6.1.4. Uncertainty Analysis of Reconciled Data

The uncertainties of reconciled values can be obtained by running the Monte Carlo simulation or estimated by utilizing the error propagation principle. Since the average running time of gas turbine data reconciliation is around twenty minutes, the Monte Carlo simulation, which needs a large amount of running time, is not a feasible option. However, if response surface equations (RSMs) of the reconciled parameters as functions of the input measurements are created, the Monte Carlo simulation can be used to estimate the uncertainties of the reconciliation. The principle of error propagation is another way to estimate the reconciliation uncertainties, and was used in this study.

Data reconciliation is essentially a problem of estimating the "true" values of the flow parameters, x_i^*, which not only close the gas turbine heat balance but also minimize the least square function (maximize the likelihood function) and the deviation penalty function. The reconciled flow parameters are actually functions of the input flow measurements, $x_i^* = f_i(x_1,\ x_2,\ x_3...,\ x_n)$, where $x_1,\ x_2,\ x_3...,\ x_n$ are the input flow measurements. Because the input flow measurements have uncertainties, U_i, the reconciliation process itself also has an uncertainty. Based on the principle of error propagation, the uncertainty of x_i^* can be estimated by:

$$U_i^* = \left(\frac{\partial f_i}{\partial x_i} U_i\right)^2 + \sum_{j \neq i} \left(\frac{\partial f_i}{\partial x_j} U_j\right)^2 \tag{6.24}$$

The coefficients of partial derivatives in Equation (6-24) can be obtained by using the finite differences:

$$\frac{\partial f_i}{\partial x_i} = \frac{f_i(x_1,\ x_2,...x_i + \Delta x_i...,\ x_n) - f_i(x_1,\ x_2,...x_i - \Delta x_i...,\ x_n)}{2\Delta x_i}$$

$$\frac{\partial f_i}{\partial x_j} = \frac{f_i(x_1,\ x_2,...x_j + \Delta x_j...,\ x_n) - f_i(x_1,\ x_2,...x_j - \Delta x_j...,\ x_n)}{2\Delta x_j} \tag{6.25}$$

In the above example of the gas turbine data reconciliation, the calculated coefficients of the partial derivatives and the estimated reconciliation uncertainties are given in Table 6-5. By assuming Normal distributions with the means of the reconciled values and the standard deviations of the reconciliation uncertainties for the reconciled flow parameters, their distributions can be plotted and compared to their original measurements. Figure 6-10~6-15 show the probability density functions of the measured and reconciled gas turbine flow parameters. Except for the generator output, the results show that not only the measured values are reconciled to be close to the "true" values but the uncertainties of these parameters are also reduced. In addition, from the result of the predicted firing temperature (shown in Fig. 6-16), which shows a significant reduction in the uncertainty of prediction, the significant mitigation effect of this data reconciliation process on the propagations of the errors from the measurements can be seen. This helps to reduce the uncertainty of gas turbine performance prediction and, thus, the costs due to errors in the modeling and simulation environment.

Table 6-5: Partial derivatives and estimated reconciliation uncertainties

		$\partial x_1^*/\partial x_i$	$\partial x_2^*/\partial x_i$	$\partial x_3^*/\partial x_i$	$\partial x_4^*/\partial x_i$	$\partial x_5^*/\partial x_i$	$\partial x_6^*/\partial x_i$	$\partial x_7^*/\partial x_i$	U_i	U_i^*
Generator Output	x_1	0.99842	84.27895	1.89665	0.03167	-0.09730	-0.38651	0.99842	47.42	**47.42**
Fuel Flow	x_2	0.00001	0.81304	-0.00495	-0.00016	0.00000	0.00079	0.00001	0.014	**0.013**
Compressor Discharge P	x_3	0.00022	-4.71587	0.82104	-0.00628	-0.03262	0.01833	0.00022	0.43	**0.39**
Compressor Discharge T	x_4	0.00067	-8.83278	-0.31476	0.98540	-0.04525	0.03411	0.00067	3.05	**3.02**
Compressor Airflow	x_5	-0.00053	-1.79439	-1.73109	-0.05246	0.07406	-0.05424	-0.00053	3.04	**0.86**
Exhaust Temperature	x_6	-0.00675	152.70338	3.58571	0.11628	-0.21343	0.35759	-0.00675	5.90	**3.61**
Firing Temperature	x_7	0.00514	129.91390	5.21650	0.91361	-0.32225	0.43093	0.00514	-	**4.94**

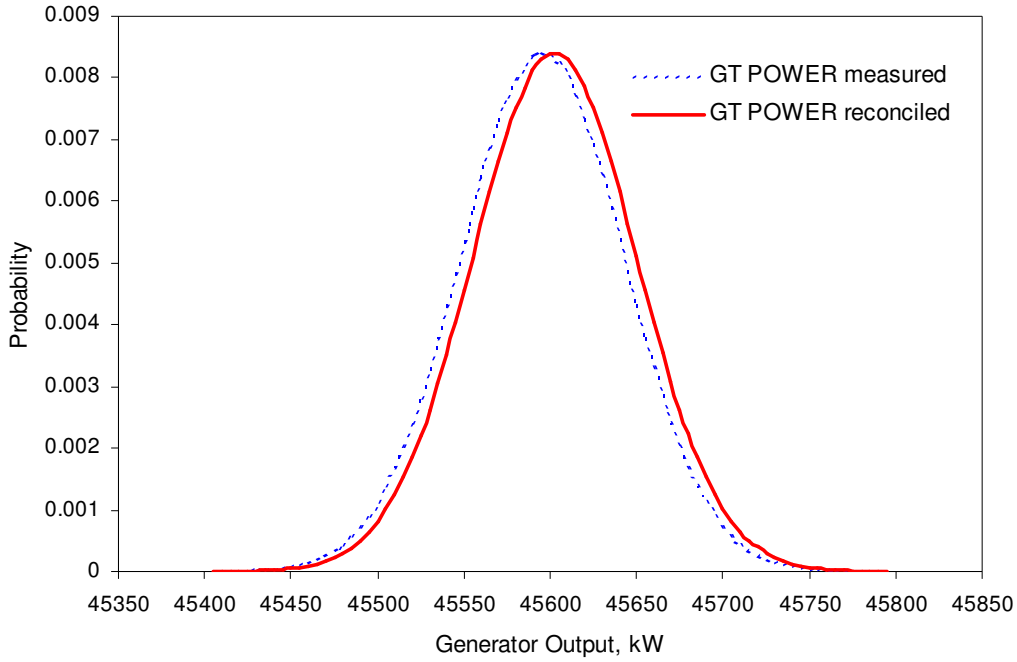

Figure 6-10: Uncertainties of measured and reconciled generator outputs

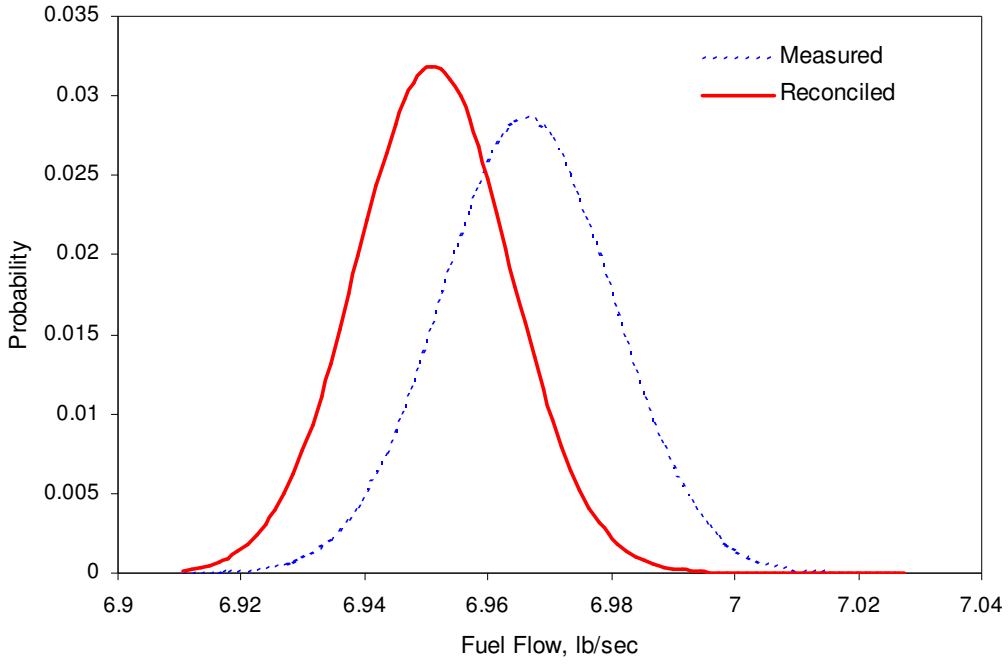

Figure 6-11: Uncertainties of measured and reconciled fuel flows

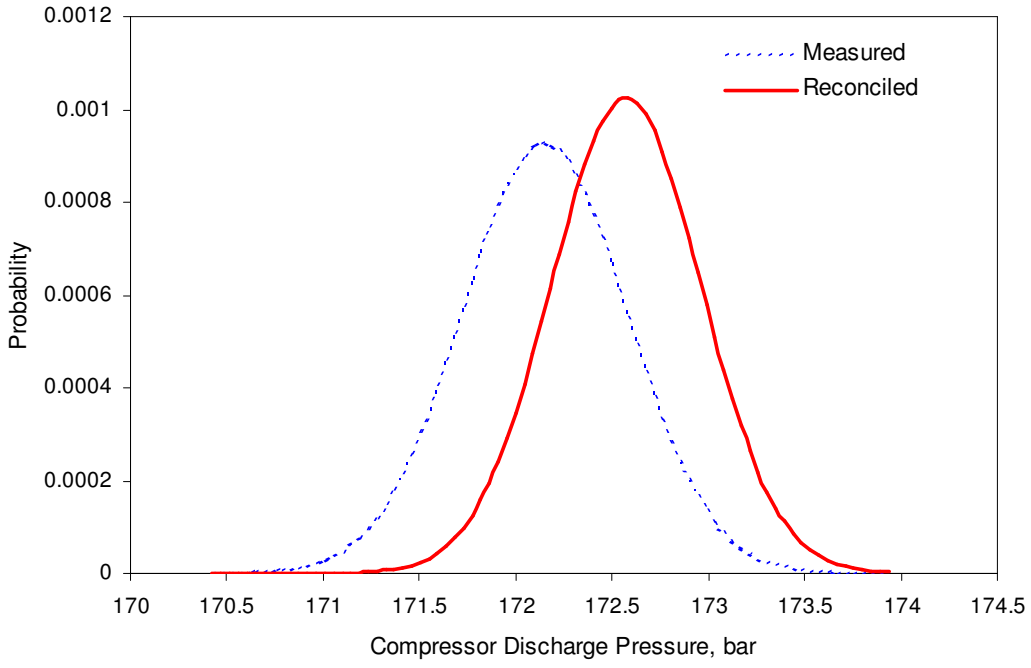

Figure 6-12: Uncertainties of measured and reconciled compressor discharge pressures

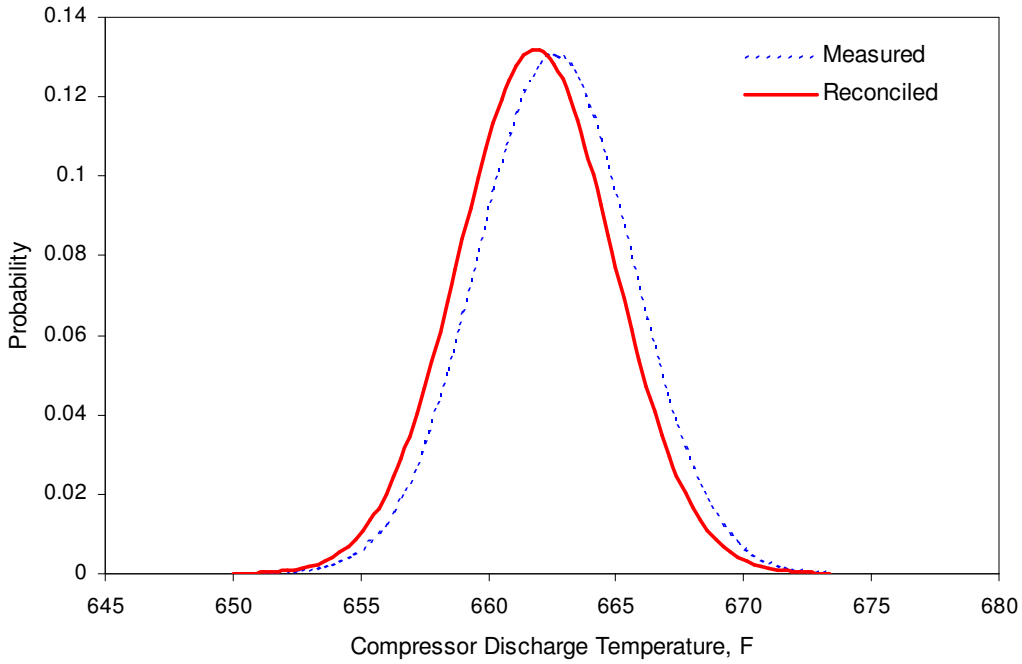

Figure 6-13: Uncertainties of measured and reconciled compressor discharge temperatures

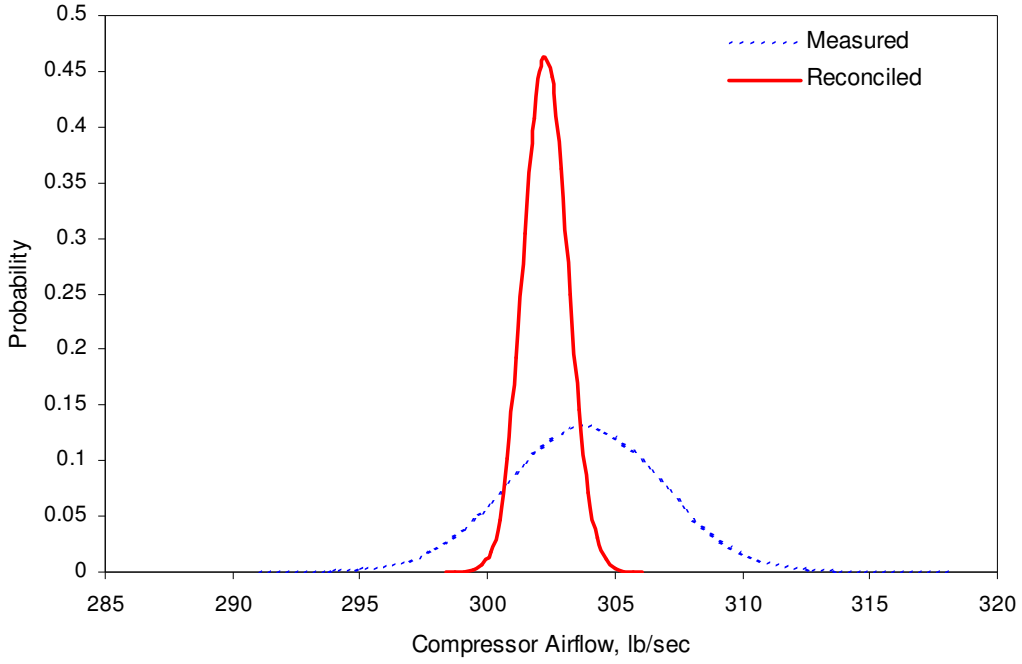

Figure 6-14: Uncertainties of measured and reconciled compressor airflows

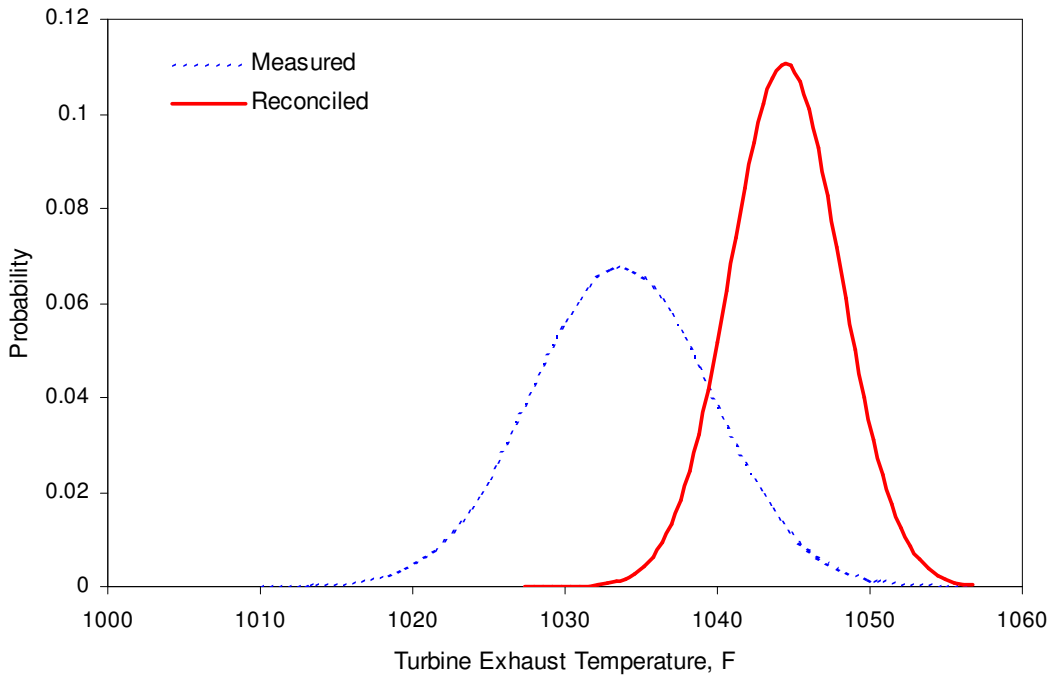

Figure 6-15: Uncertainties of measured and reconciled exhaust temperatures

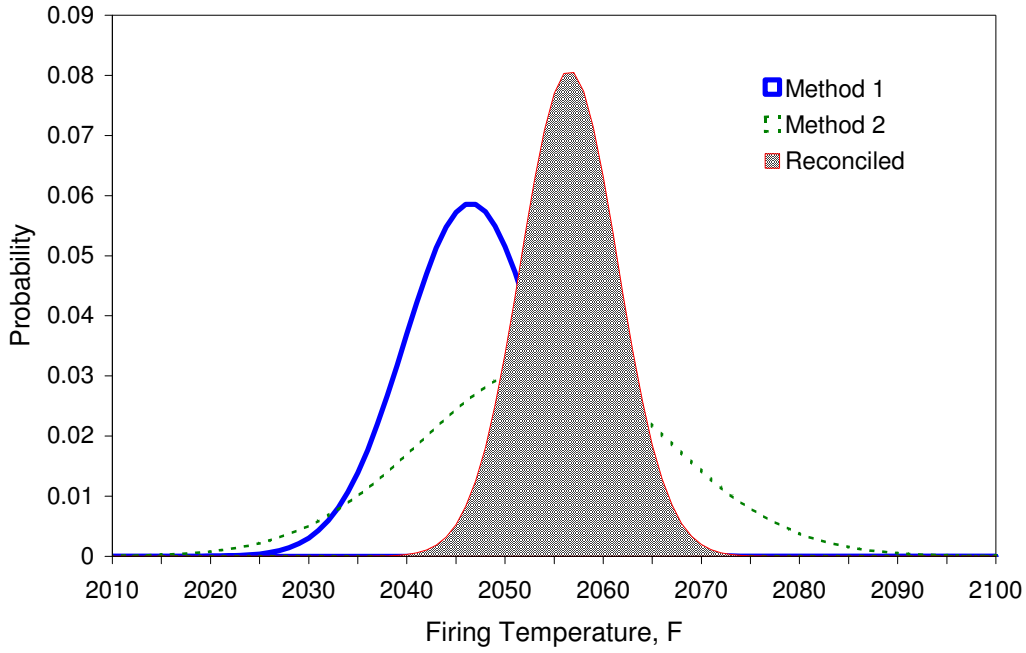

Figure 6-16: Uncertainties of firing temperatures for heat balance analyses and data reconciliation

6.2. Case Study II: Gas Turbine SDRMC Using Performance Simulator

When the performance simulation code for a gas turbine is available, one can carry out data reconciliation and degradation estimation simultaneously. In this case study, the gas turbine simulation code, GTP^{TM}, was utilized as a performance simulator – an off-design heat & mass balance solver capable of performance predictions at varied operation conditions and degradation status. In general, the gas turbine performance i.e. power and heat rate, along with the characteristic flow parameters, which are directly affected by the component efficiencies or performance correction factors, can be expressed as functions of the operation parameters and the performance factors: $\boldsymbol{y} = \boldsymbol{f}(\boldsymbol{a}, \boldsymbol{\theta})$ where $\boldsymbol{y}$ is a column vector of the outputs from the performance simulation; $\boldsymbol{f}$ represents the functions of performance simulation; $\boldsymbol{a}$ is a vector of the parameters that defines the operation conditions; $\boldsymbol{\theta}$ is the vector of the performance factors, which reflect the degradation status and are independent of the operations condition.

By assuming the measurements of ambient conditions i.e. ambient pressure, temperature, humidity, etc, and the operation parameters such as IGV angle and fuel compositions have insignificant magnitudes of uncertainties as compared to the other characteristic flow measurements, one can treat these model parameters as constant inputs. Further, if the simulations of cooling flows or secondary flows are also reliable, the gas turbine performance and the characteristic flow parameters are only functions of the performance factors, which are utilized to mimic the loss of component efficiencies due to degradation, and the firing temperature, which is controlled by the gas turbine control system. In this case study, five performance factors and the firing temperature are used as model input variables while one performance parameter and five characteristic flow parameters are to be reconciled.

Table 6-6: Independent and dependent variables in gas turbine data reconciliation

Operational Condition a	Performance Factors θ	Model Outputs y
Ambient Temperature	Compressor Efficiency (DMM)	Generator Output
Ambient Pressure	Compressor Flow (DMM)	Fuel Flow
Specific Humidity	Combustor Efficiency (DMM)	Compressor Discharge Pressure
Inlet Pressure Drop	Turbine Efficiency (DMM)	Compressor Discharge Temperature
Exit Pressure Drop	Turbine CQ (DMM)	Compressor Airflow
IGV	Firing Temperature	Exhaust Temperature

$d.o.f = 0$ (number of $\boldsymbol{y}$ – number of $\boldsymbol{\theta}$)

Table 6-7: Increase *d.o.f* by reducing number of independent variables

Operational Condition a		Performance Factors θ	Model Outputs y
Ambient Temperature		Compressor Efficiency (DMM)	Generator Output
Ambient Pressure		Compressor Flow (DMM)	Fuel Flow
Specific Humidity	⊗	Combustor Efficiency (DMM)	Compressor Discharge Pressure
Inlet Pressure Drop		Turbine Efficiency (DMM)	Compressor Discharge Temperature
Exit Pressure Drop	⊗	Turbine CQ (DMM)	Compressor Airflow
IGV		Firing Temperature	Exhaust Temperature

$d.o.f = 2$ (number of $\boldsymbol{y}$ – number of $\boldsymbol{\theta}$)

Table 6-8: Increase *d.o.f* by reducing number of independent variables

Operational Condition a *Data Sets 1, 2, 3...*	Performance Factors θ	Model Outputs y *Data Sets 1, 2, 3...*
Ambient Temperature	Compressor Efficiency (DMM)	Generator Output
Ambient Pressure	Compressor Flow (DMM)	Fuel Flow
Specific Humidity	Combustor Efficiency (DMM)	Compressor Discharge Pressure
Inlet Pressure Drop	Turbine Efficiency (DMM)	Compressor Discharge Temperature
Exit Pressure Drop	Turbine CQ (DMM)	Compressor Airflow
IGV	Firing Temperature *(Data Sets 1, 2, 3...)*	Exhaust Temperature

$d.o.f = (k+1) \times$ Imber $y -$ (Imber $\theta + k$)

Table 6-6 lists the independent and dependent variables of the gas turbine in simultaneous data reconciliation and degradation estimation. If only one data set is used, the degree of freedom is zero, indicating only the exact data match can be carried out since the number of independent variables is equal to the number of dependent variables. The definition of the degree of freedom is defined as: *number of dependent variable – number of independent variable*. In this study, due to the assumption that the variables of operation condition are treated as constants, the degree of freedom is then equal to: *number of y – number of* θ. In order to perform data reconciliation, the degree of freedom has to be at least greater or equal to 1. There are two options to increase the *d.o.f*: one is reducing the number of independent variables, and the other is increasing the number of data sets. In this case, the combustor efficiency and the turbine stage 1 nozzle are normally constant during the normal operation. Therefore, the corresponding performance factors, combustor efficiency DMM and turbine CQ DMM, can be assumed to be constant, and the degree of freedom will be increased to 2 by reducing the number of independent variables. Table 6-7 shows the increased degree of freedom by reducing the number of θ. The assumption of constant combustor efficiency and turbine stage 1 nozzle area can be biased if there are significant degradations occurring. To increase the degree of freedom, the other option is increasing the number of data sets. By introducing more data sets of different operation conditions, one can obtain the reconciled data and estimated model parameters with less uncertainty. The performance factors of the efficiency or flow multipliers are constant across the different operations i.e. there is one optimum set of DMM's for all data sets. For the firing temperature, however, since the gas turbine control system adjusts the fuel consumption, which directly affects the firing temperature, based on the operation conditions, one should add the firing temperature for a specific operation as a new variable. Therefore, when adding k extra data sets for data reconciliation, one can get the *d.o.f* equal to:

$$(k+1)\times \text{mber} \qquad y-(\text{mber} \qquad \theta+k) \tag{6.26}$$

Table 6-8 shows the increased *d.o.f* by increasing the number of data sets.

In this case study, five data sets were reconciled. In order to reduce the time of reconciliation process, five sets of response surface equations (six responses per data set) were created as surrogated models. Although the execution time for GTP itself is also fast (about 0.5 ~ 1 seconds), but in the gross error detection scheme where large amount of function calls are required, the function calls for GTP still take significant amount of time. As compared to the execution time of 0.05 ~ 0.1 seconds for the response surface equations, one gets the benefit in time saving mainly in the gross error detection scheme. The response surface equations are created via regressing the simulated data generated by 1000 GTP runs. These runs are scenarios of the model independent variables at their possible values within presumed ranges. The 1000 scenarios include the simulations based on design of experiments (DoE) and Monte Carlo simulations (table 6-9). The simulations based on Doe cover the minimum required scenarios for exploring the design space; the scenarios that are randomly generated from Monte Carlo simulations are added for two purposes: one is to get better regressions i.e. reduce the uncertainties of estimated RSE coefficients; the other is to prepare the data for the multivariate data analyses including the multivariate visualization and principal component analysis (PCA) for gross error detections. Since running the GTP simulation of all five data sets for one scenario is about 1 second, the total simulation time for 1000 scenarios is less than 20 minutes. The effort of creating the surrogated model has a tremendous pay back during the gross error detection.

Table 6-9: Gas turbine simulations for RSE regression and multivariate analysis

Runs	DMM1	DMM2	DMM3	DMM4	DMM5	Tfire 1	Tfire 2	Tfire 3	Tfire 4	Tfire 5
1	0.9876	0.9951	0.9987	0.9754	1.001	2359.799	2354.672	2358.7	2358.751	2348.353
2	1.002458	1.00233	0.992345	0.964107	1.000346	2365.055	2354.736	2354.974	2353.024	2354.684
3	1.004553	1.008358	0.981803	0.974012	1.001571	2371.784	2335.608	2336.953	2343.992	2333.085
.	.	.	.	.	.	.	.	.	.	.
.	.	.	.	.	.	.	.	.	.	.
.	.	.	.	.	.	.	.	.	.	.
998	0.977418	1.004908	0.974023	0.971911	1.000429	2367.705	2370.782	2352.077	2361.405	2330.162
999	0.992424	0.972704	1.008965	0.970107	0.998112	2344.675	2372.226	2365.235	2379.207	2369.449
1000	0.989185	1.002194	0.983744	0.984873	0.998308	2360.105	2360.38	2361.013	2349.013	2363.853

Data 1

Runs	y1	y2	y3	y4	y5	y6
1	196101	33.52	209.84	776	1261	1133
2	197929	34.24	211.62	769	1270	1144
3	204640	34.96	213.03	770	1278	1137
.	.	.	.	.	.	.
.	.	.	.	.	.	.
.	.	.	.	.	.	.
998	196476	34.67	212.64	787	1274	1139
999	187843	32.28	204.75	764	1233	1135
1000	201614	34.22	211.95	778	1270	1122

Data 2, 3, 4 

Data 5

Runs	y1	y2	y3	y4	y5	y6
1	196101	33.52	209.84	776	1261	1133
2	197929	34.24	211.62	769	1270	1144
3	204640	34.96	213.03	770	1278	1137
.	.	.	.	.	.	.
.	.	.	.	.	.	.
.	.	.	.	.	.	.
998	196476	34.67	212.64	787	1274	1139
999	187843	32.28	204.75	764	1233	1135
1000	201614	34.22	211.95	778	1270	1122

NOMENCLATURE

DMM1	Compressor Efficiency (DMM)
DMM2	Compressor Flow (DMM)
DMM3	Combustor Efficiency (DMM)
DMM4	Turbine Efficiency (DMM)
DMM5	Turbine CQ (DMM)
Tfire 1	Firing Temperature (Data 1)
Tfire 2	Firing Temperature (Data 2)
Tfire 3	Firing Temperature (Data 3)
Tfire 4	Firing Temperature (Data 4)
Tfire 5	Firing Temperature (Data 5)
y1	Generator Output
y2	Fuel Flow
y3	Compressor Discharge Pressure
y4	Compressor Discharge Temperature
y5	Compressor Airflow
y6	Exhaust Temperature

In this case study, the measurement data were artificially generated by imposing random errors on five simulated data sets obtained by running GTP at five predefined operation conditions for a specific degradation status i.e. the presumed performance factors. For the purpose of validating the methodology, one should screen out factors that are not due to the defeats of the reconciliation methodology but could lead to biased results. For example, if the measurement data are from the gas turbine that has a specific cooling system but the selected GTP model does not have the cooling flows set properly, performing data reconciliation can cause biased results such that one is misled to the conclusion that there are biases in measurements while the actual cause is the mismatch between the physical model and real system. Simulating the measurement data can eliminate the errors caused by the mismatch between the physical model and the real data i.e. the physical model selected does not represent the real system. The simulated data is drawn randomly from the inverse of normal cumulative distribution by using the random number generator.

The normal inverse function is defined in terms of the normal cdf as

$$x = F^{-1}(p \mid \mu, \sigma) = \{x : F(x \mid \mu, \sigma) = p\} \tag{6.27}$$

where

$$p = F(x \mid \mu, \sigma) = \frac{1}{\sigma\sqrt{2\pi}} \int_{-\infty}^{x} e^{\frac{-(t-\mu)^2}{2\sigma^2}} dt \tag{6.28}$$

μ and σ are the mean and standard deviation of the normal distribution; *p*, obtained by the random number generator, represents the probability of observing *x*.

Table 6-10 lists the presumed operation conditions for five data sets. The parameters listed in table 6-10 are assumed to have much smaller measurement uncertainties as compared to the measurements that are to be reconciled. In the model-based data reconciliation one can, however, include these parameters into the reconciliation process if these parameters have significant measurement uncertainties that cannot be ignored. Table 6-11 listes the "true values' of the parameters that are to be

estimated during the reconciliation process. The values given in table 6-11 are assigned artificially for the purposes of demonstrating the methodology and generating the pseudo data. In reallity, the true status is unknown and needs to be estimated by performing simultaneous data reconciliation and parameter estimation. As the operation conditions and the system degradation status are given, the theoretical values of the characteristic flow parameters and the system off-design performance can be simulated by the performance simulator, GTP. These theoretical values, listed in table 6-12, represent the "true" values of the gas turbine off-design performance. The pseudo measurement data for the gas turbine was then generated by imposing the random errors on the "true values" obtained from the performance simulation code. Table 6-13 listed the pseudo measurement data for the the gas turbine at the presumed operation conditions and degradation status. The sensitivities of the theoretical gas turbine outputs i.e. characteristic flow parameters, to the model input parameters- firing temperature and performance correction factors, are given by the prediction profiler (Fig 6-17), a tool showing the system Jacobian graphically. In Fig 6-17, it is found that all gas turbine outputs, y_i, are affected significantly by the compressor air flow DMM, which suggests that more sources of measurement uncertainties contribute to the uncertainty of its estimate. But since most of the sensitivity curves for the compressor flow DMM have large gradients, the measurement uncertainties are propagated in a less significant level

Table 6-10: Presumed gas turbine operation conditions for five data sets

Operation Conditions	Unit	Data Set 1	Data Set 2	Data Set 3	Data Set 4	Data Set 5
Ambient Temp	F	85	54	63	73	59
Ambient Pressure	psia	14.61	14.85	14.85	14.69	14.69
Specific Humidity		0.0163	0.0027	0.0031	0.0102	0.0063
Inlet Pressure Drop	in H2O	2.74	3.25	3.22	3.12	3.51
Exit Pressure Drop	in H2O	10.02	10.02	10.02	10.02	15
IGV	degree	88	88	88	88	88

Table 6-11: Presumed gas turbine performance multipliers and firing temperatures

Performance Factors	Prespecified Values
Compressor Efficiency (DMM)	0.9876
Compressor Flow (DMM)	0.9951
Combustor Efficiency (DMM)	0.9987
Turbine Efficiency (DMM)	0.9754
Turbine CQ (DMM)	1.001
Firing Temperature (Data 1)	2360
Firing Temperature (Data 2)	2355
Firing Temperature (Data 3)	2359
Firing Temperature (Data 4)	2359
Firing Temperature (Data 5)	2348

Table 6-12: Theoretical values for gas turbine system outputs

Theoretical Values for System Outputs						
System Outputs	Unit	Data Set 1	Data Set 2	Data Set 3	Data Set 4	Data Set 5
Generator Output	kW	196248	225241	218224	208013	216005
Fuel Flow	lb/sec	33.69	37.05	36.22	35.01	36.01
Compressor Discharge Pressure	psia	210.1173	227.9367	224.1672	217.0163	222.6868
Compressor Discharge Temperature	F	776	734	747	759	738
Compressor Airflow	lb/sec	1263	1379	1355	1308	1347
Exhaust Temperature	F	1133	1103	1111	1121	1106

Table 6-13: Simulated data for gas turbine system outputs

Simulated Measurements for System Outputs (Model Calculated Values + Random Errors)						
System Outputs	Unit	Data Set 1	Data Set 2	Data Set 3	Data Set 4	Data Set 5
Generator Output	kW	196044	224834	217987	208124	216766
Fuel Flow	lb/sec	33.79	37.15	36.23	34.95	35.86
Compressor Discharge Pressure	psia	210.7714	228.3135	224.0094	217.1300	221.4638
Compressor Discharge Temperature	F	777	737	745	760	734
Compressor Airflow	lb/sec	1261	1383	1354	1311	1346
Exhaust Temperature	F	1133	1105	1114	1120	1103

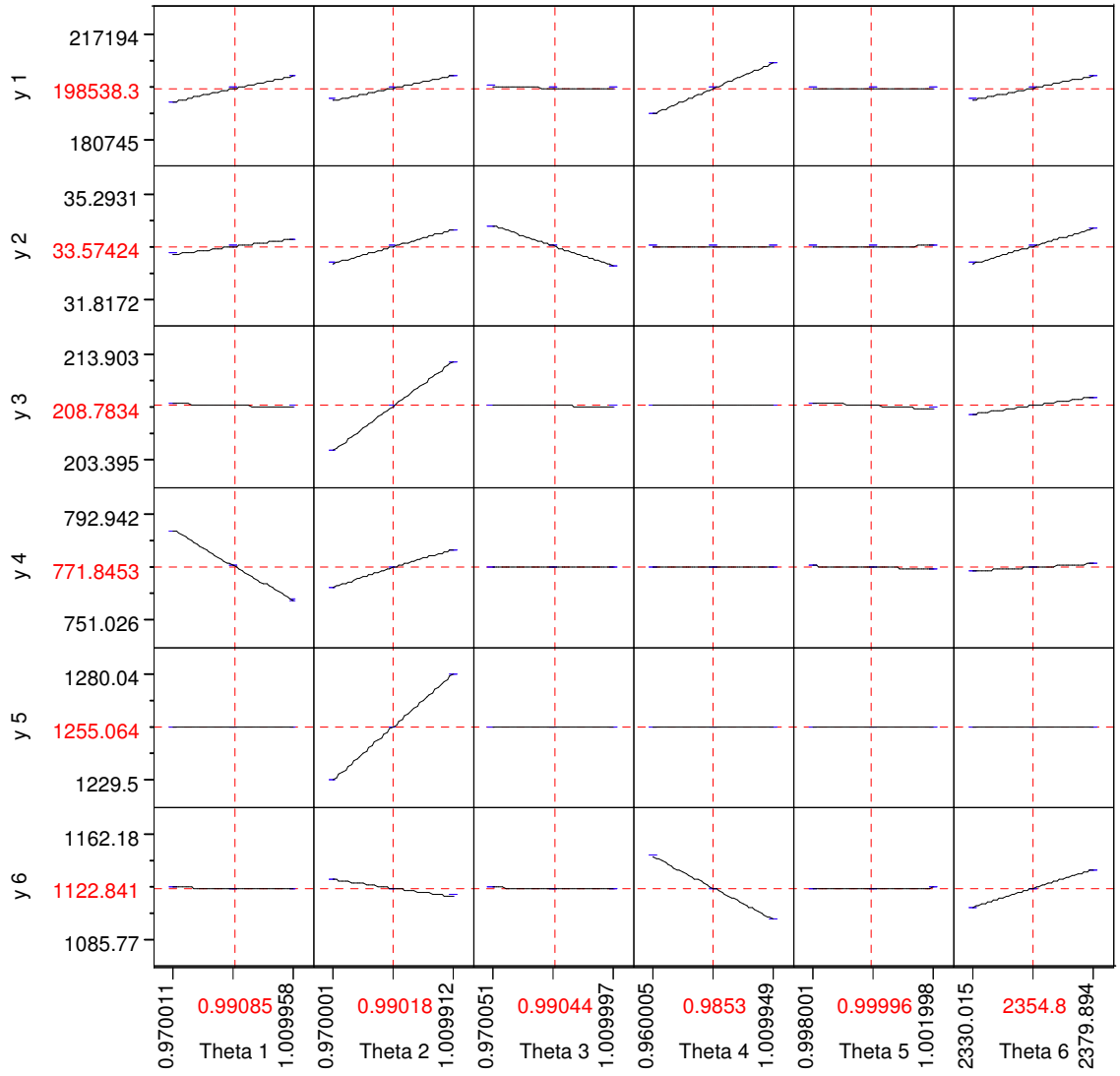

NOMENCLATURE

Theta 1	Compressor Efficiency (DMM)	**y1**	Generator Output
Theta 2	Compressor Flow (DMM)	**y2**	Fuel Flow
Theta 3	Combustor Efficiency (DMM)	**y3**	Compressor Discharge Pressure
Theta 4	Turbine Efficiency (DMM)	**y4**	Compressor Discharge Temperature
Theta 5	Turbine CQ (DMM)	**y5**	Compressor Airflow
Theta 6	Firing Temperature (Data 1)	**y6**	Exhaust Temperature

Figure 6-17: Prediction profiler for gas turbine characteristic responses – sensitive studies

On the other hand, the sensitivity curves for most gas turbine outputs versus the turbine CQ DMM show much flatter trends as compared to others, indicating larger estimate uncertainties caused by the measurement errors. This is because the changes of system responses due to the variation of the turbine CQ DMM are relatively small such that when one tend to perform status matching by varying the turbine CQ DMM to match the measured system responses, the small perturbations due to measurement uncertainties cause a significant variation in the turbine CQ DMM. The prediction profiler is a visualization tool that gives an insight of how the measurement uncertainties are propagated through the system model. The estimate uncertainties also depend on the measurements uncertainties, which are determined by the instrument accuracies. Therefore, the knowledge of system behavior against the variations of system inputs i.e. the system Jacobian, can be used to identify the key measurements that need to be reduced by the uncertainties. For instance, as shown in Fig 6-17, the variation tendencies of the compressor discharge pressure and temperature against the variation of turbine CQ DMM are flat, which indicates that small perturbations of theses two measurements require a large adjustment on the turbine CQ DMM, therefore, cause a large uncertainty to its estimate. If a small uncertainty of the estimate is required for the turbine CQ DMM, one should put more efforts on the measurement accuracies of the compressor discharge pressure and temperature.

The pair-wise multivariate visualization plot is given in Fig. 6-18, which indicates the measured data is within the ranges of degradation spaces, spanned based on the presumed ranges of system input variables, θ_i. The PCA analysis, given in Fig. 6-19, also shows there are no principal components exceeding the threshold value, 1.96 sigma for a 95% confidence level. Since the pseudo data was generated via imposing the random errors only, there are no gross errors expected in the gross error detection scheme.

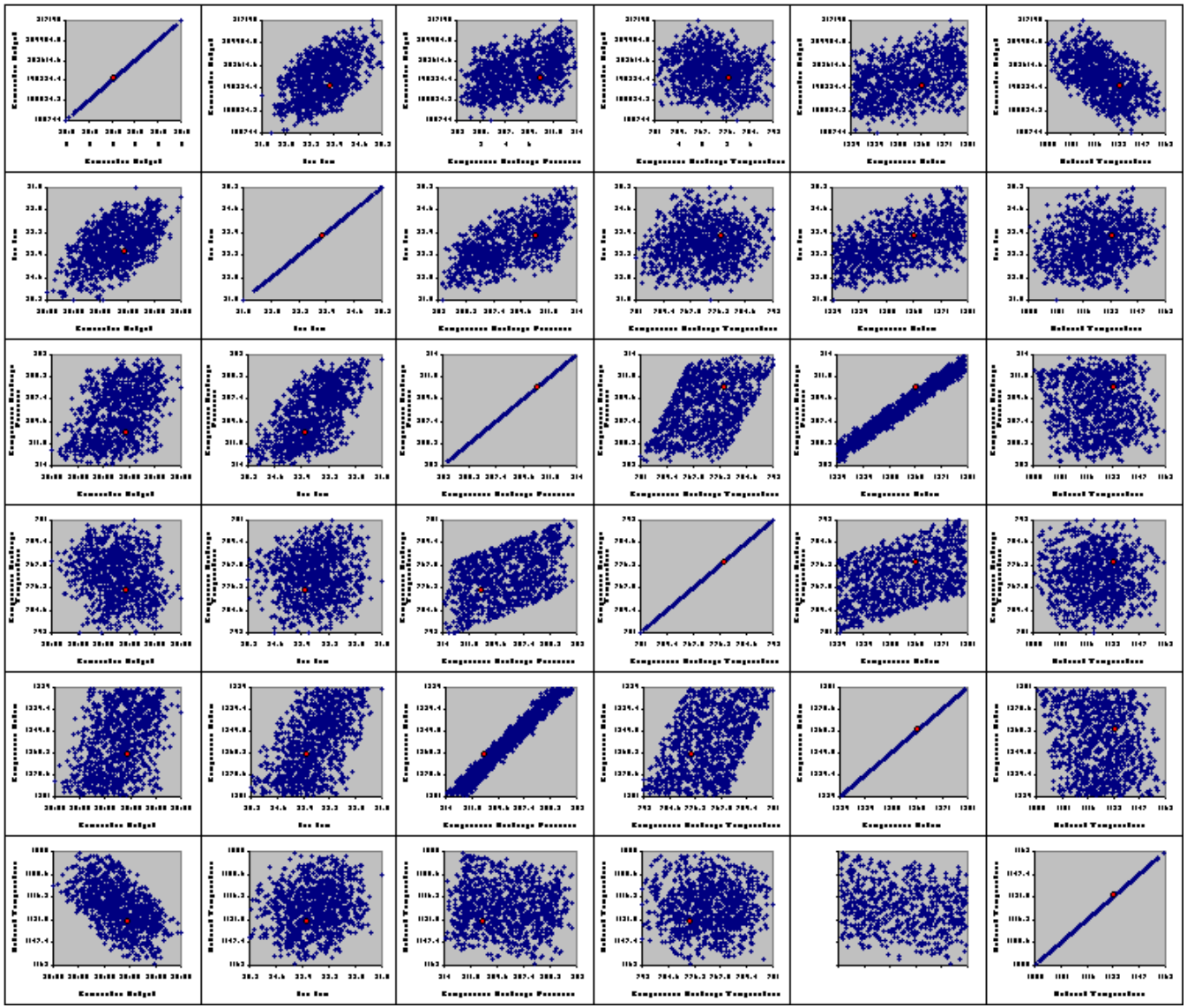

Figure 6-18: Scatter plot matrix for the case of no gross errors

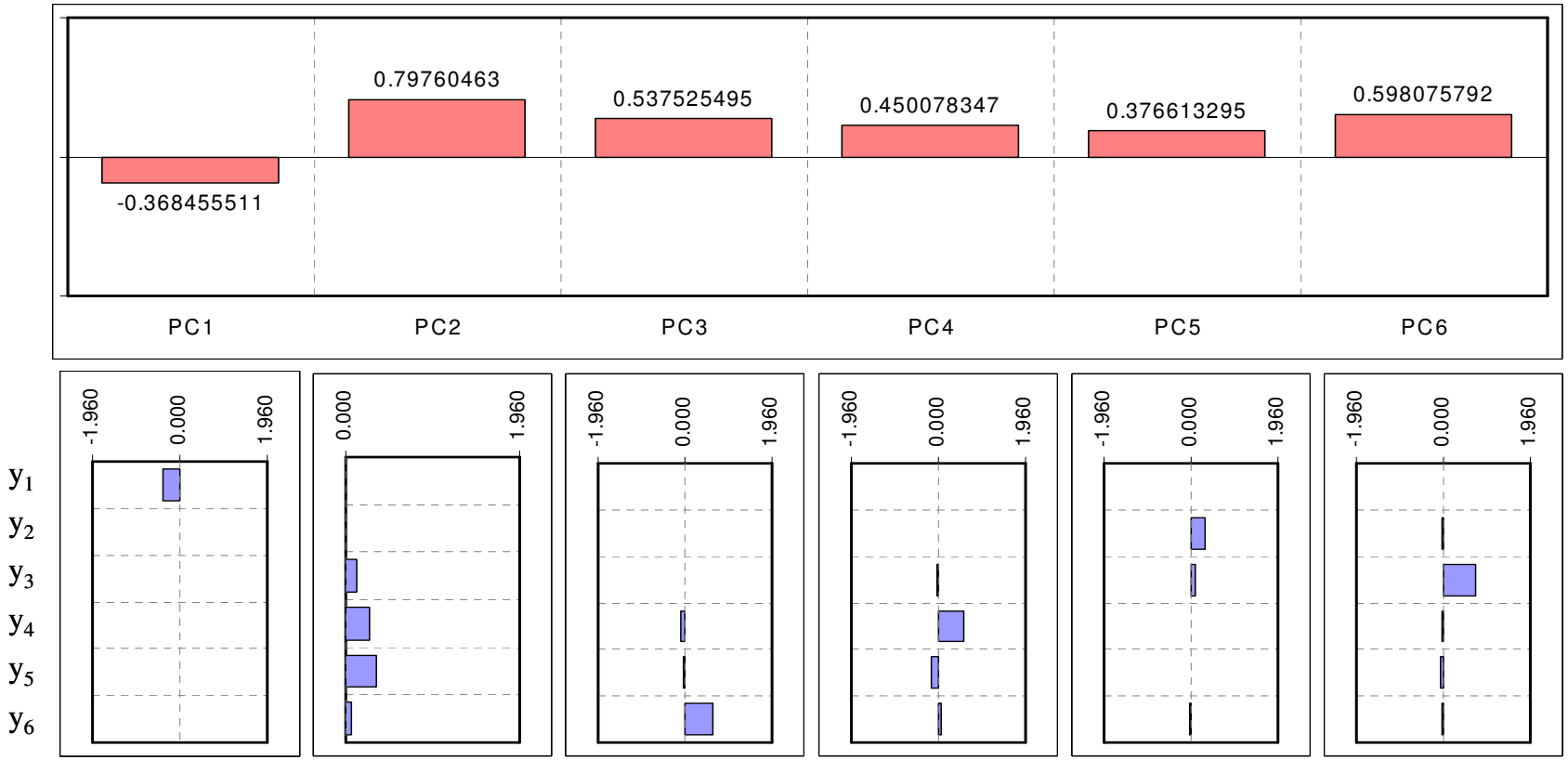

y_1 : Generator Output
y_2 : Fuel Flow
y_3 : Compressor Discharge Pressure
y_4 : Compressor Discharge Temperature
y_5 : Compressor Airflow
y_6 : Turbine Exhaust Temperature

Figure 6-19: Principal component analysis for the case of no gross errors

The model-based data reconciliation utilizing the performance simulator GTP as the gas turbine model was carried out. During the reconciliation process, the Levenberg-Marquardt algorithm served as the solver to minimize the least squares objective function by searching the optimum solutions for the model independent variables i.e. DMM's and firing temperature. The problem of minimizing the least squares objective function is given by:

$$\min_{\theta_i,\phi_k} \sum_{k=1}^{5}\sum_{j=1}^{6} (y'_{jk} - f_{jk}(\theta_i,\phi_k))^T \sigma_{jk}^{-1} (y'_{jk} - f_{jk}(\theta_i,\phi_k)) \qquad (6\text{-}29)$$

where θ_i represent the DMM's, which are independent of the operation conditions; φ_k represents the firing temperature of the kth data set; y'_{jk} represents the measured data of the jth system response in the kth data set while f_{jk} represents the explicit model function of the jth system response in the kth data set. The optimization process continues until the change of the chi-squares $\Delta\chi^2$ is less than 1×10^{-7} or the number of iteration exceeds 100. The convergence history is given in Fig 6-20.

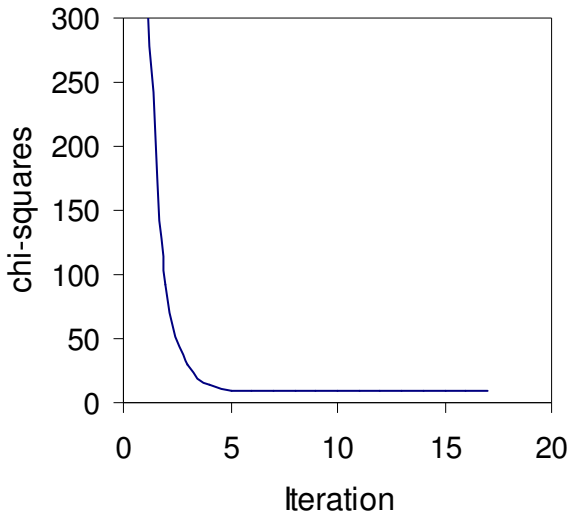

Iteration	Chi-squares
1	346.2233
2	92.7911
3	29.6465
4	13.8760
5	9.9353
6	8.9500
7	8.7037
8	8.6422
9	8.6268
10	8.6229
11	8.6220
12	8.6217
13	8.6217
14	8.6216
15	8.6216
16	8.6216
17	8.6216

Figure 6-20: Iteration history for the case of no gross errors

The iteration stopped at the 17th trial, in which $\Delta\chi^2$ is less than 1×10^{-7}. The minimized chi-squares value is 8.62. Using the Global Test, to reject the alternative hypothesis H_1, which assumes the occurrence of at least one gross error, the value of the chi-squares after reconciliation should be less than a threshold value determined by the degree of freedom given by:

$$\chi^2_{opt} \leq d.o.f \tag{6-30}$$

In this case the *d.o.f* is 20, greater than the minimized chi-squares value 8.62. Therefore, the alternative hypothesis is rejected, by which one can confirm that the reconciliation process was not contaminated by the gross error effect. If the Global Test rejects the null hypothesis H_0, in which it is assumed there is no gross error, one should proceed to the gross error detection process. The measurement uncertainties for all data sets are listed in table 6-14, based on the generic guideline of typical DCS instruments. The uncertainties listed in table 6-14 were converted to the absolute values from their original relative values e.g. percentages. Except for the temperature measurements, whose uncertainties are usually expressed as absolute values, the measurements for flow properties are displayed by the percentages of their measured values. The pseudo data of six system outputs are listed in table 6-15 and their reconciled values are given in table 6-16. The corresponding measurement corrections to the whole data sets are shown in table 6-17 and figure 6-21. It is shown that the corrections to all the measurements except for the compressor discharge pressure of data set 5 are within 2 sigmas, which are expected since the pseudo data were generated by imposing random errors only. The correction to the compressor discharge is above 1.96 sigma (2.07 sigma) because the simulated uncertainty is 1.75 sigma, close to the typical threshold value for a gross error.

Table 6-14: Measurement uncertainties for gas turbine characteristic outputs

Measurements/System Outputs	Unit	Data Set 1	Data Set 2	Data Set 3	Data Set 4	Data Set 5
Generator Output	kW	500	574	557	530	552
Fuel Flow	lb/sec	0.17	0.19	0.18	0.18	0.18
Compressor Discharge Pressure	psia	0.54	0.59	0.57	0.55	0.57
Compressor Discharge Temperature	F	3.6	3.6	3.6	3.6	3.6
Compressor Airflow	lb/sec	6.6	7.2	6.9	6.7	6.9
Exhaust Temperature	F	3.6	3.6	3.6	3.6	3.6

Table 6-15: Simulated measurements (pseudo data) for gas turbine characteristic outputs

Measurements/System Outputs	Unit	Data Set 1	Data Set 2	Data Set 3	Data Set 4	Data Set 5
Generator Output	kW	196044	224834	217987	208124	216766
Fuel Flow	lb/sec	33.79	37.15	36.23	34.95	35.86
Compressor Discharge Pressure	psia	210.77	228.31	224.01	217.13	221.46
Compressor Discharge Temperature	F	777	737	745	760	734
Compressor Airflow	lb/sec	1261	1383	1354	1311	1346
Exhaust Temperature	F	1133	1105	1114	1120	1103

Table 6-16: Reconciled data for gas turbine characteristic outputs

Measurements/System Outputs	Unit	Data Set 1	Data Set 2	Data Set 3	Data Set 4	Data Set 5
Generator Output	kW	196259	225243	218232	208012	216009
Fuel Flow	lb/sec	33.69	37.05	36.22	35.01	36.01
Compressor Discharge Pressure	psia	210.08	227.89	224.12	216.97	222.64
Compressor Discharge Temperature	F	776	734	747	759	738
Compressor Airflow	lb/sec	1263	1379	1355	1308	1348
Exhaust Temperature	F	1133	1103	1111	1121	1106

Table 6-17: Measurement corrections for gas turbine characteristic outputs

Measurements/System Outputs	Unit	Data Set 1	Data Set 2	Data Set 3	Data Set 4	Data Set 5
Generator Output	Sigma	0.43	0.71	0.44	-0.21	-1.37
Fuel Flow	Sigma	-0.55	-0.55	-0.05	0.32	0.83
Compressor Discharge Pressure	Sigma	-1.29	-0.72	0.20	-0.28	2.07
Compressor Discharge Temperature	Sigma	-0.48	-0.85	0.48	-0.48	1.35
Compressor Airflow	Sigma	0.40	-0.54	0.15	-0.34	0.31
Exhaust Temperature	Sigma	0.13	-0.56	-0.96	0.32	1.07

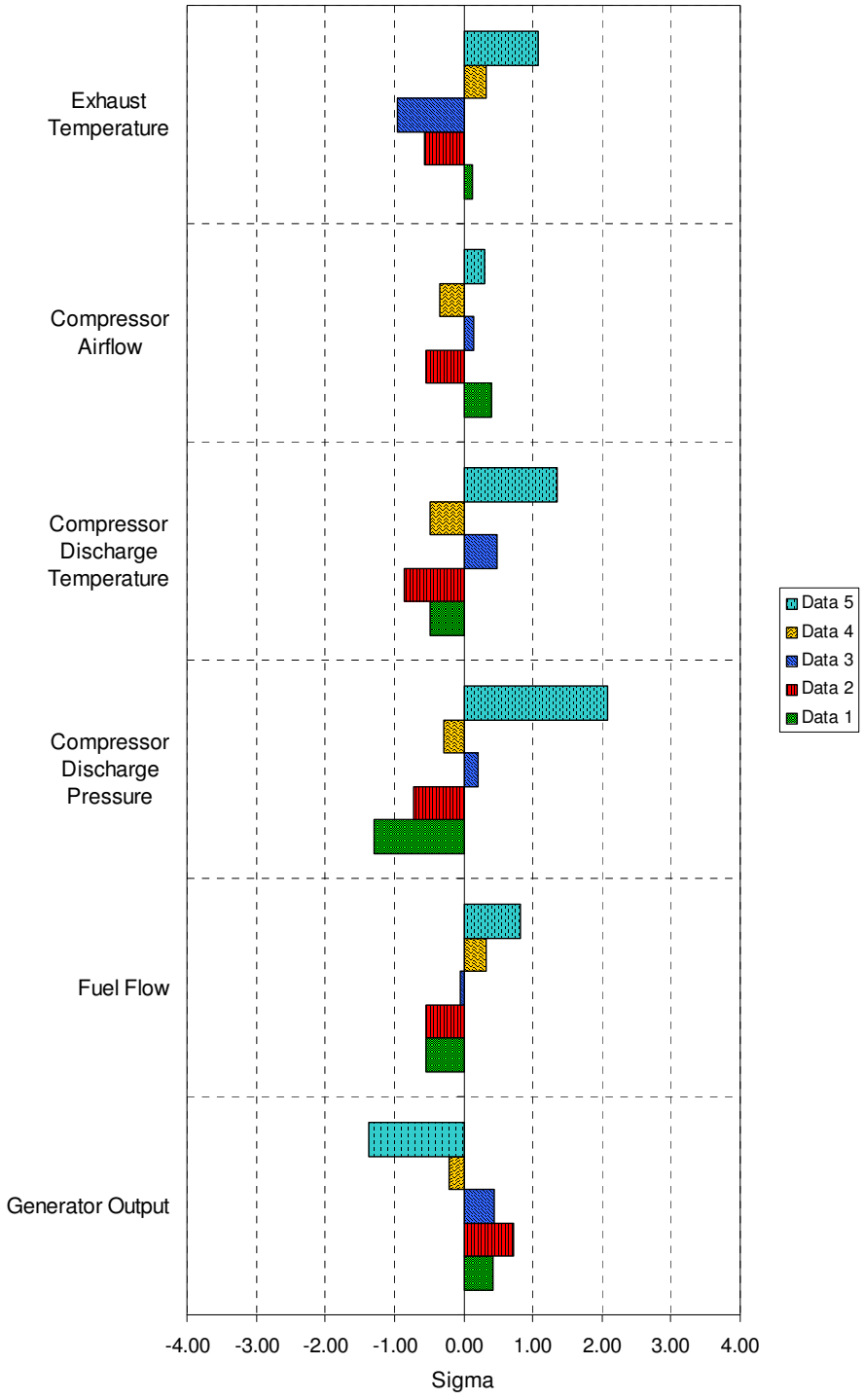

Figure 6-21: Measurement corrections for gas turbine characteristic outputs

The specified values (true values) for the performance factors, DMM's and firing temperatures, and their estimates along with the estimate uncertainties are listed in table 6-18. It is shown that the true values are within the ranges of the estimate uncertainties, which indicates the key concept of data reconciliation & parameter estimation:

> *It is not likely to obtain the exact true values for the system properties being measured and the system parameters to be estimated; by reconciling the data one can, however, obtain the estimates that are expected to be close to their true values.*

If the data is reconciled properly i.e. there is no gross error effect and the measurement redundancies are high enough, the true values would stay within the ranges of estimate uncertainties. The results obtained from simultaneous data reconciliation & parameter estimation are compared to the results from the heat & mass balance calculation of *Method 1*, in which the compressor airflow and combustor efficiency are calculated. The comparison is shown in table 6-19 and Fig. 6-22 ~ 6-24. In Fig 6-22 ~ 6-23 it is shown that the uncertainties of the estimated DMM's and firing temperatures from simultaneous data reconciliation & parameter estimation are less than those from the heat & mass balance calculations. Since the estimated performance multipliers i.e. DMM's are used to determine the current degradation status and to predict the performance of the gas turbine with new hot gas path upgrades, as the uncertainties of their estimates are reduced, the uncertainties of performance predictions will also be mitigated, by which the risk of the performance guarantees is reduced. As shown in the Fig. 6-22, the uncertainties of estimated firing temperatures are reduced as compared to the results from the heat & mass balance calculations. By reducing the uncertainties of estimated firing temperatures, one can impose less margins for the life cycle and/or safety reasons on the control system to gain more performance benefits i.e. power recapture. As shown in Fig. 6-23, simultaneous data reconciliation & parameter estimation gives a single value for each of the DMM's at different operation conditions while the heat & mass balance method leads

to inconsistent results. Since the degradation status does not change with the operation conditions, one should expect one single set of performance multipliers (DMM's) representing a certain degradation status for all data sets of different operation conditions. This suggests another benefit of simultaneous data reconciliation & parameter estimation, which is the unified results of the system parameters due to the fact the measurement errors are filtered out during the reconciliation process. In the heat & mass balance method, however, one obtains inconsistent results because of the measurement errors. A closer look at the comparison of estimated compressor efficiency DMM along with the estimate uncertainty between data reconciliation and data reduction methods is shown in Fig. 6-24.

Table 6-18: Specified (true) and estimated values of performance multipliers and firing temperatures

Performance Factors (Model Inputs)	Specified	Estimated	Uncertainty (Sigma)
Compressor Efficiency (DMM)	0.9876	0.9883	0.002463
Compressor Flow (DMM)	0.9951	0.9968	0.002294
Combustor Efficiency (DMM)	0.9987	0.9946	0.003211
Turbine Efficiency (DMM)	0.9754	0.9745	0.001513
Turbine CQ (DMM)	1.001	1.0017	0.003093
Firing Temperature (Data 1)	2360	2359	3.45
Firing Temperature (Data 2)	2355	2355	3.50
Firing Temperature (Data 3)	2359	2357	3.48
Firing Temperature (Data 4)	2359	2358	3.47
Firing Temperature (Data 5)	2348	2345	3.47

Table 6-19: Comparison of estimated performance multipliers between data reconciliation and data reduction

	Data Reconciliation		Heat & Mass Balance									
			Data Set 1		Data Set 2		Data Set 3		Data Set 4		Data Set 5	
Performance Factors	Estimates	Uncertainty	Estimates	Uncertainty	Estimates	Uncertainty	Estimates	Uncertainty	Estimates	Uncertainty	Estimates	Uncertainty
Compressor Efficiency (DMM)	0.988276	0.002463	0.987376	0.005460	0.984639	0.005536	0.990589	0.005503	0.986033	0.005485	0.992893	0.005533
Compressor Flow (DMM)	0.996788	0.002294	0.998618	0.002919	0.996452	0.002936	0.994665	0.002911	0.995890	0.002906	0.990953	0.002911
Combustor Efficiency (DMM)	0.994650	0.003211	0.992150	0.006497	0.992159	0.006480	0.995027	0.006485	0.995136	0.006490	0.993723	0.006484
Turbine Efficiency (DMM)	0.974507	0.001513	0.973701	0.003387	0.974291	0.003280	0.972575	0.003264	0.976374	0.003319	0.978288	0.003278
Turbine CQ (DMM)	1.001742	0.003093	1	0	1	0	1	0	1	0	1	0

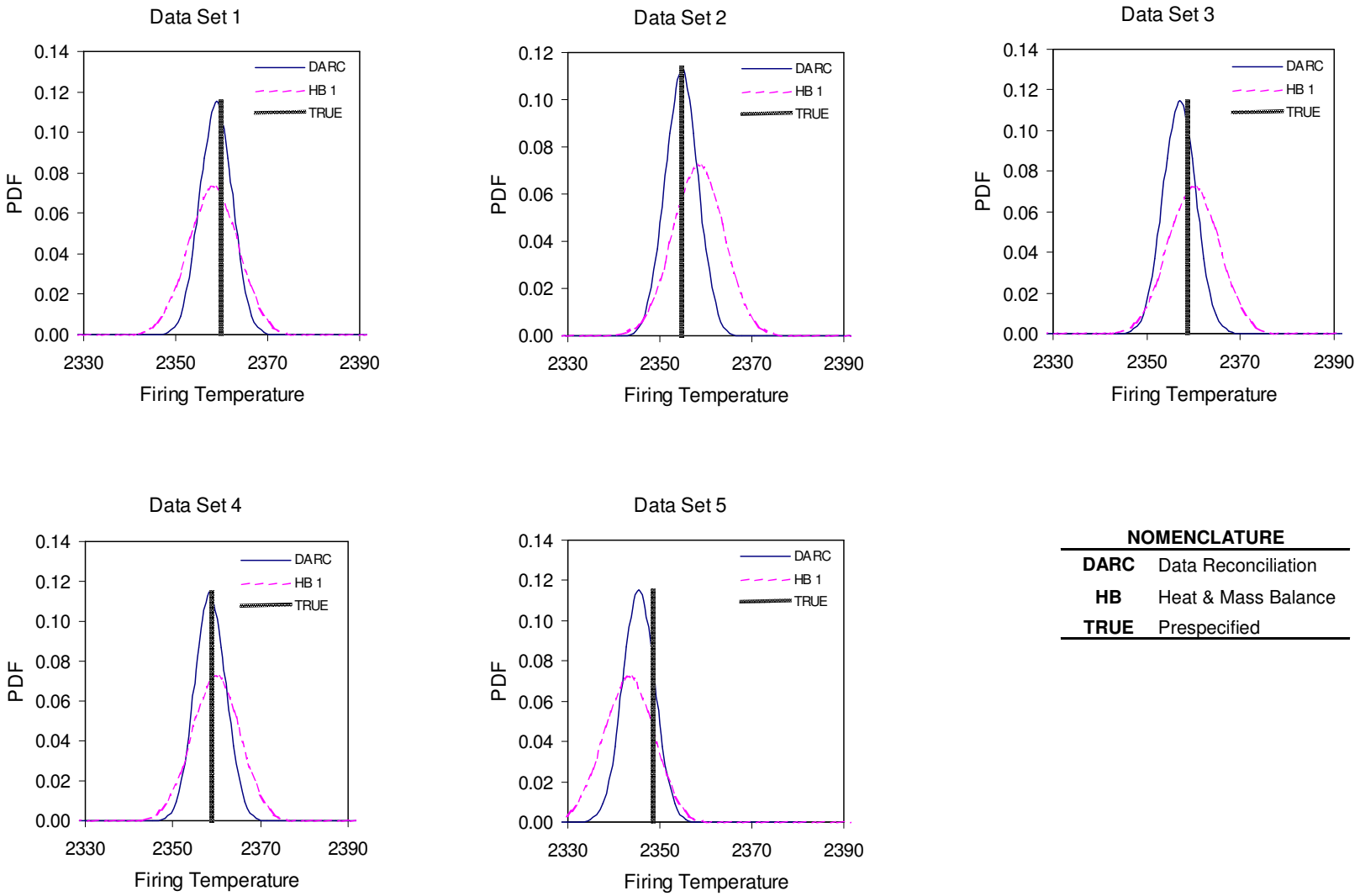

NOMENCLATURE

DARC	Data Reconciliation
HB	Heat & Mass Balance
TRUE	Prespecified

Figure 6-22: Estimated firing temperatures and estimate uncertainties from data reconciliation and data reductions

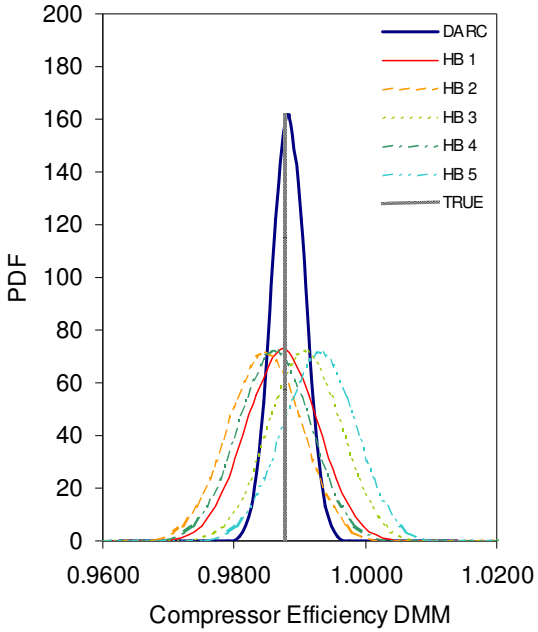

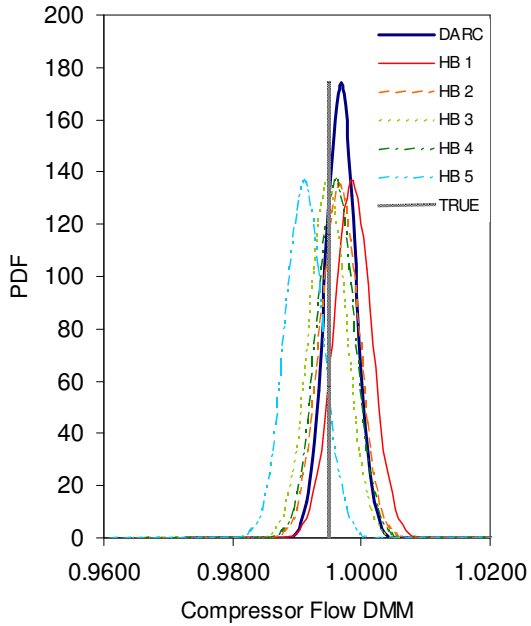

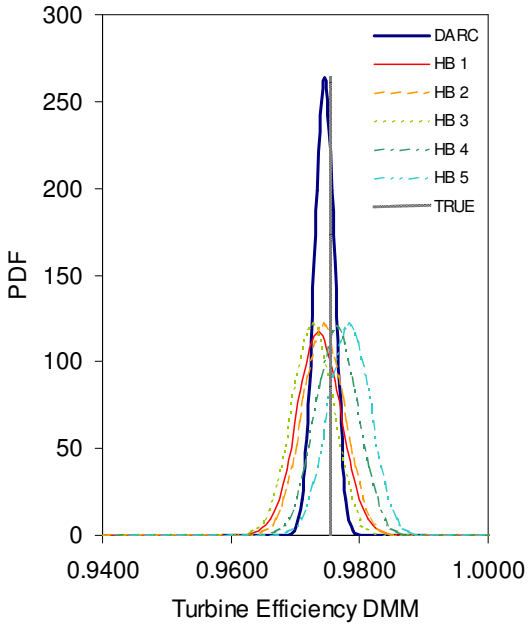

NOMENCLATURE	
DARC	Data Reconciliation
HB 1~5	Heat & Mass Balance for Data Set 1 ~5
TRUE	Prespecified

Figure 6-23: Estimated performance multipliers and estimate uncertainties from data reconciliation and data reductions

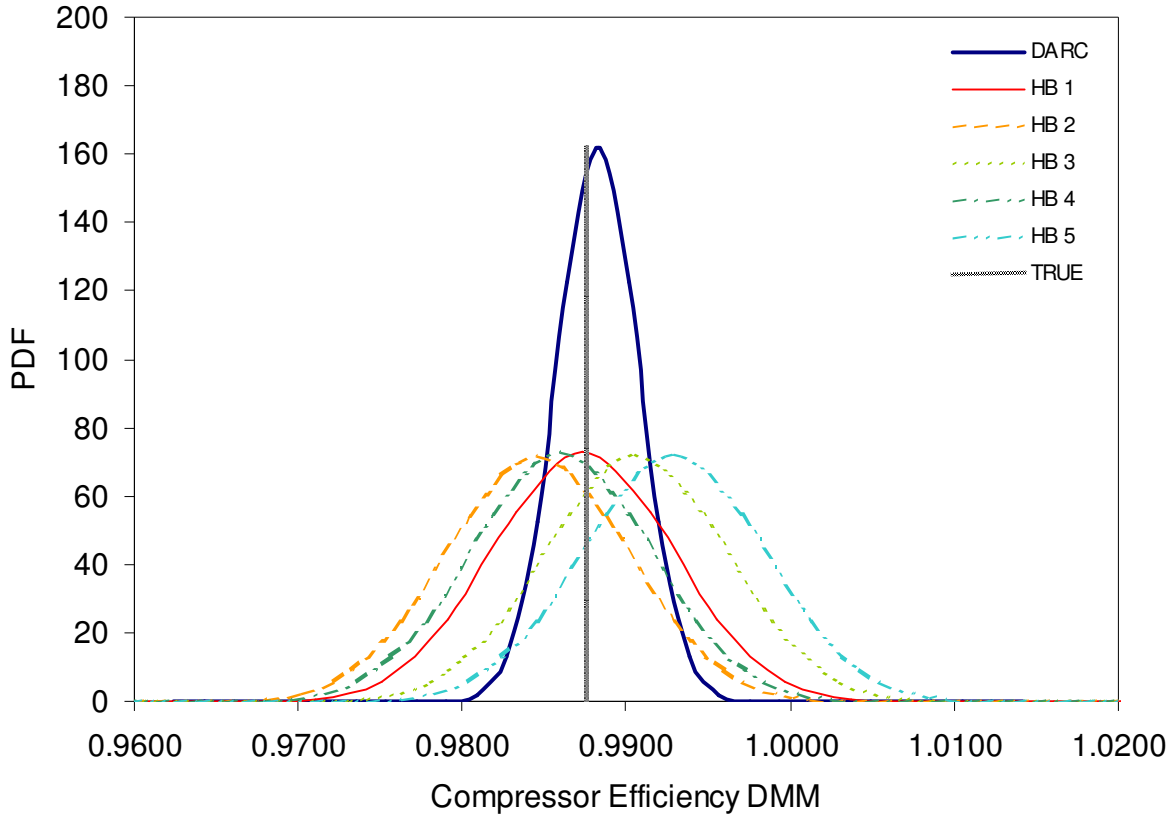

Figure 6-24: Estimated compressor efficiency DMM and estimate uncertainties from data reconciliation and data reductions

6.3. Case Study III: Gas Turbine SDRMC with GED

In the previous case study, the pseudo data were only subject to random errors. To investigate the gross error effects and test the proposed gross error detection methods, in this case study both gross errors and random errors were simulated. Since the gross errors are considered to have constant magnitudes and signs at certain locations, pre-specified biases were artificially imposed to selected measurements to simulate the pseudo data containing gross errors. The gross error detection schemes were then incorporated to simultaneous data reconciliation & degradation estimation to identify the locations of gross errors and estimate their magnitudes.

In the first testing case, a bias of 7-sigma was designated to the measurements of compressor discharge temperatures in the first two data sets while the rest data sets were bias-free. This scenario was simulated to mimic the situation when the measurements are mixed by healthy and biased data sets. The multivariate data analyses (MDA) i.e. Multivariate Data Visualization and Principal component Analysis were first carried out to detect large-scale biases (biases with magnitudes greater than 10-sigma) and differentiate the biased data sets from the healthy data sets. The scatter plot matrix used in Multivariate Data Visualization is given in Fig. 6-25, from which it is shown that the measured data points appear to be outliers in all scatter plots that contain the compressor discharge temperature as one of the axes. A closer look of the scatter plots containing the compressor discharge temperatures is given in Fig. 6-26, from which one can see that the measurement of compressor discharge temperature leads to outliers in the multivariate system responses. This is justified by the fact that the only way of moving the outliers back to the clouds must include the bias adjustment to compressor discharge temperature and the fact that the rest of scatter plots do not show outliers caused by other measurements.

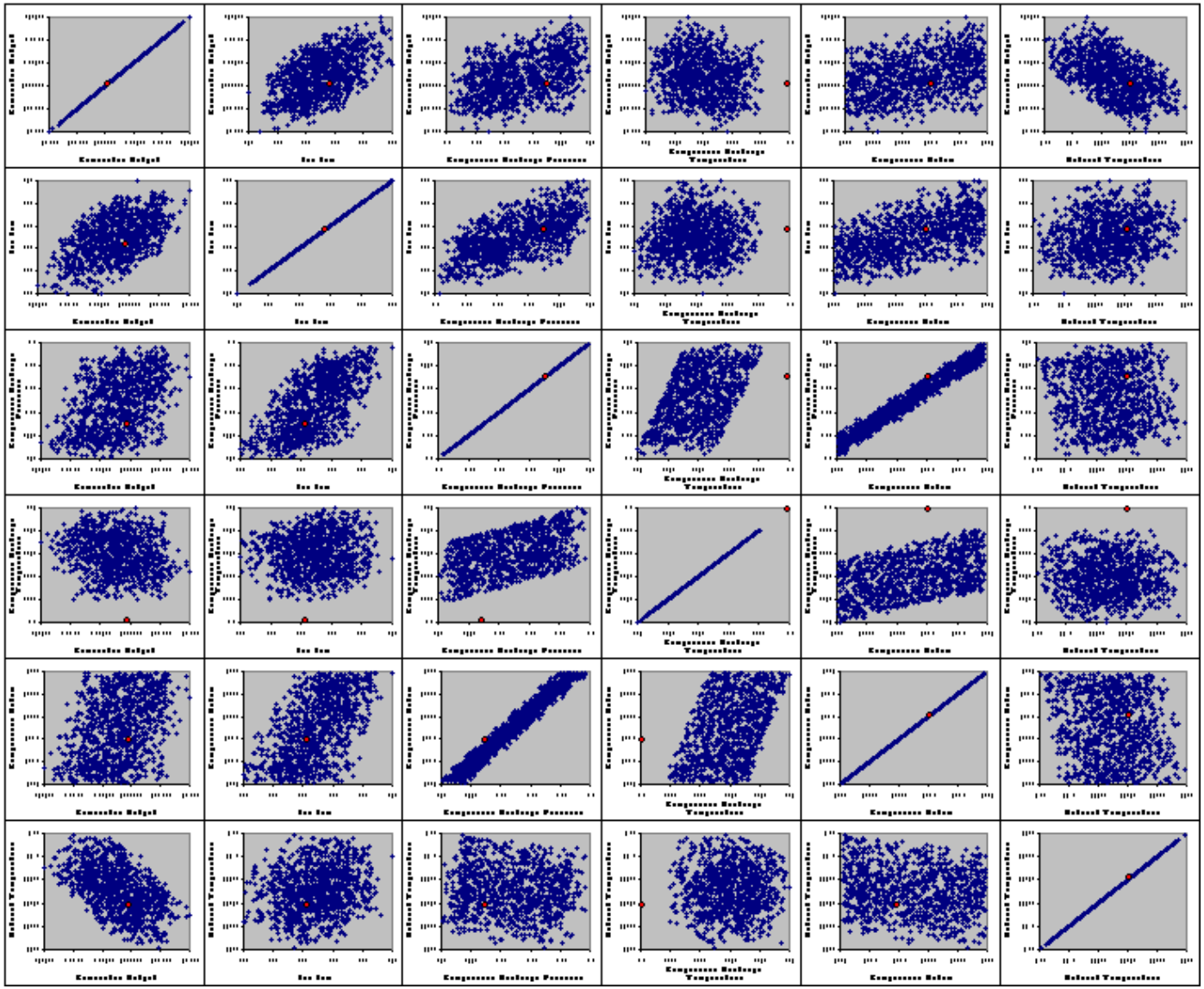

Figure 6-25: Scatter plot matrix for measurements with single gross error in compressor discharge temperature

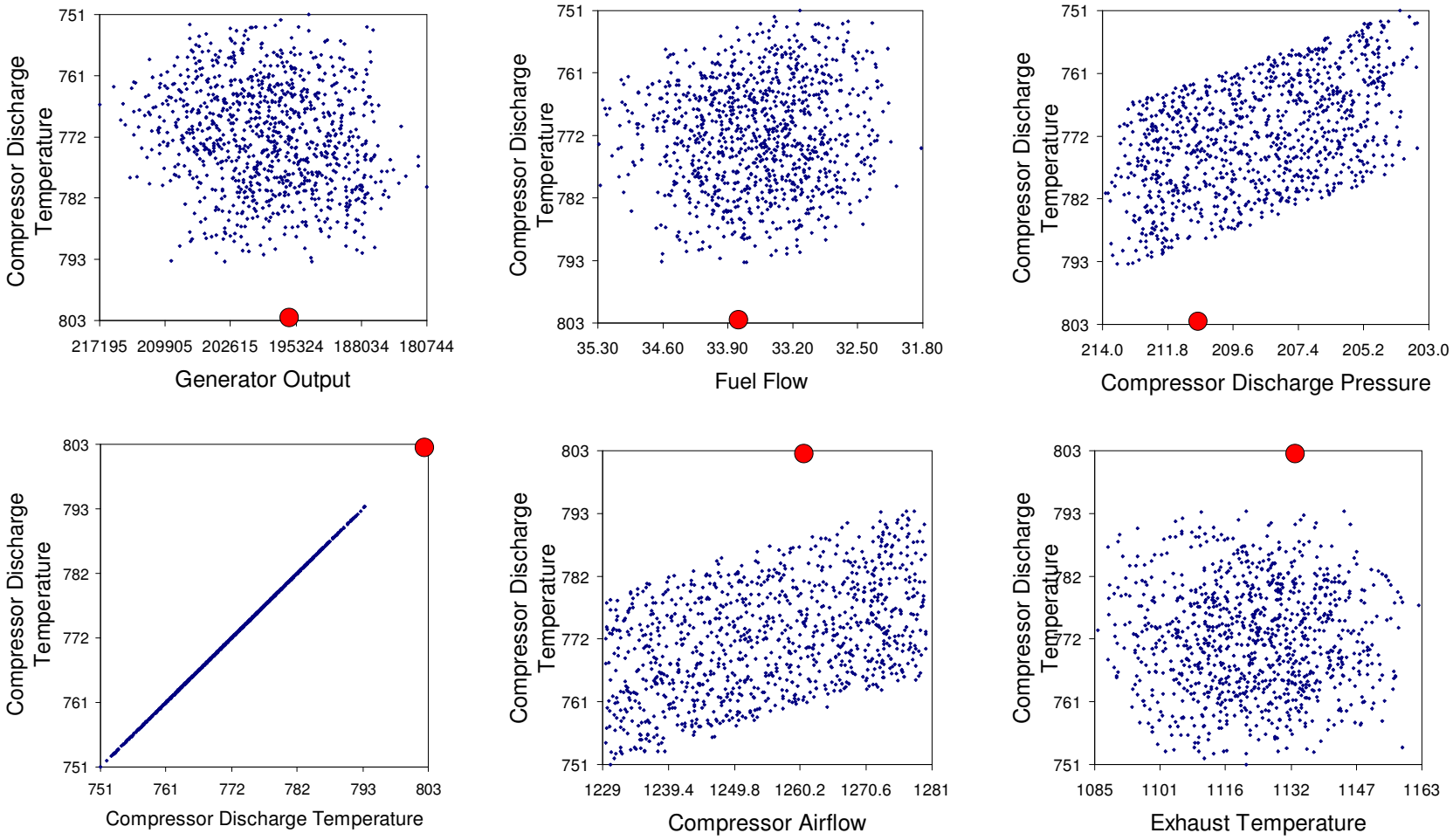

Figure 6-26: Scatter plots containing compressor discharge temperature as one of the axes (1 gross error imposed)

The principal component analysis (PCA) was performed following the multivariate data visualization. The PCA provides the quantitative description about the relative position of measured data against the expected populations of model responses. From PCA one can obtain the statistics for the measured data about its relative position to the correlated model responses in the scatter plots. These correlated data points were generated by randomly sampling the parameter space of the system model i.e. Monte Carlo simulations on the performance multipliers. Each principal component contains a linear combination of system responses and is uncorrelated to each other. In addition, these principal components are standardized such that a standardized Gaussian distribution can be used to determine the test statistics. In this case study the threshold value 1.96, representing the 95% population of the expected data sets, was used as the criteria for outlier identification. If the test statistics of a principal component is greater than this threshold value, a further investigation for each response's contribution to the overall variance of that principal component is needed. The PCA for the first testing case with one gross error simulated is shown in Fig. 6-27 ~ 6-29. Figure 6-27 shows the PCA result for the first data set. It is shown that the 2^{nd} and 4^{th} principal components have the test statistics greater than the threshold value - ~1.97 and ~ 2.97 separately. A further investigation shows both PC's have the compressor discharge temperature as the biggest contributor to the overall variances. The PCA for the second data set is given in Fig. 6-28, which also shows that both 2^{nd} and 4^{th} PC's have test statistics above the threshold value 1.96 and that the compressor discharge temperature is the major contributor to the variances of these two PC's. The PCA for the rest data sets is shown in Fig. 6-29, in which all the principal components have test statistics below the threshold values. From the PCA it can be concluded that the data of compressor discharge temperature in the first and second data sets are outliers but are within the expected ranges in the rest data sets.

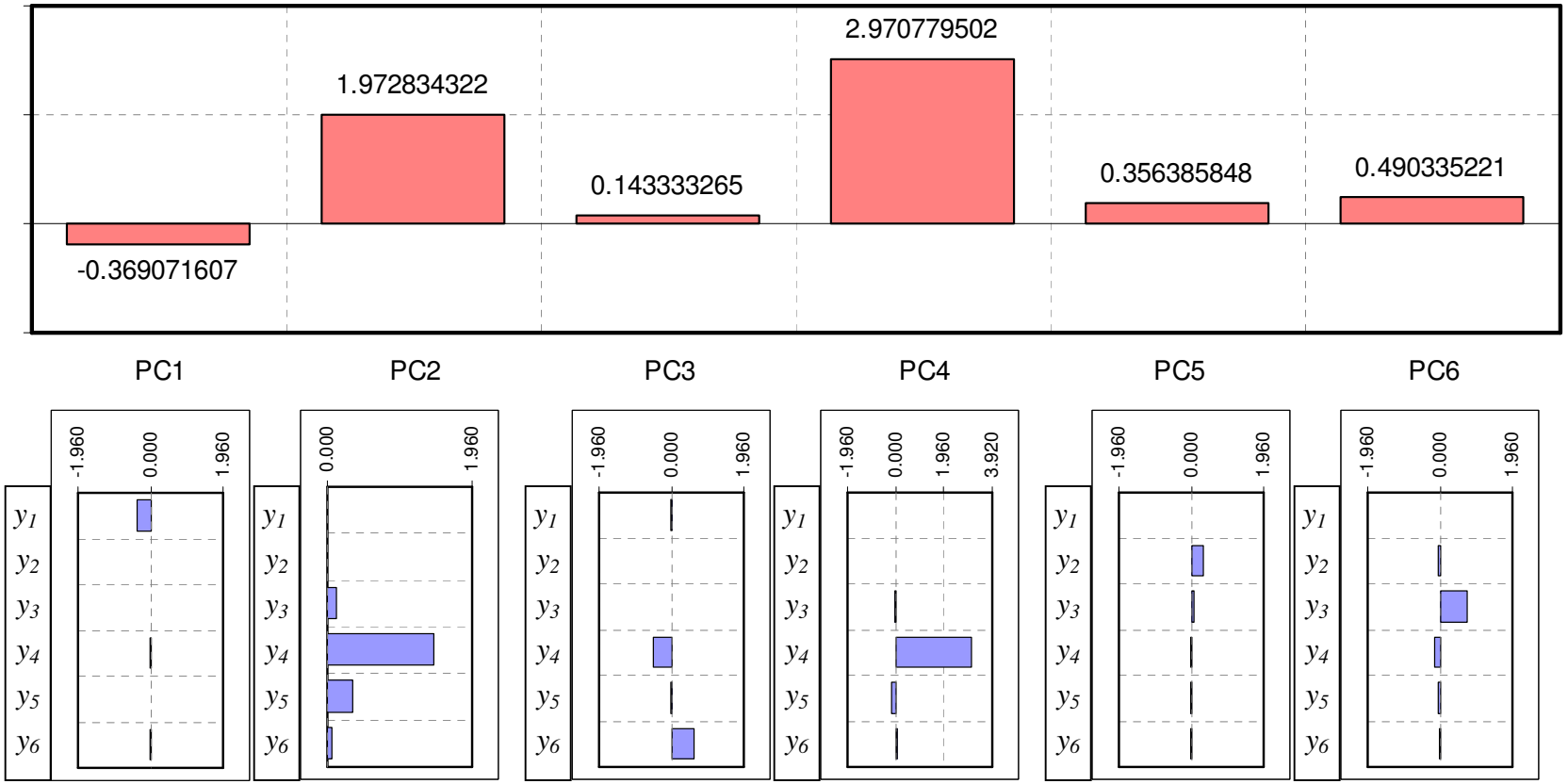

NOMENCLATURE

y_1 : Generator Output
y_2 : Fuel Flow
y_3 : Compressor Discharge Pressure
y_4 : Compressor Discharge Temperature
y_5 : Compressor Airflow
y_6 : Turbine Exhaust Temperature

Figure 6-27: PCA for the 1st data set with single gross error in compressor discharge temperature

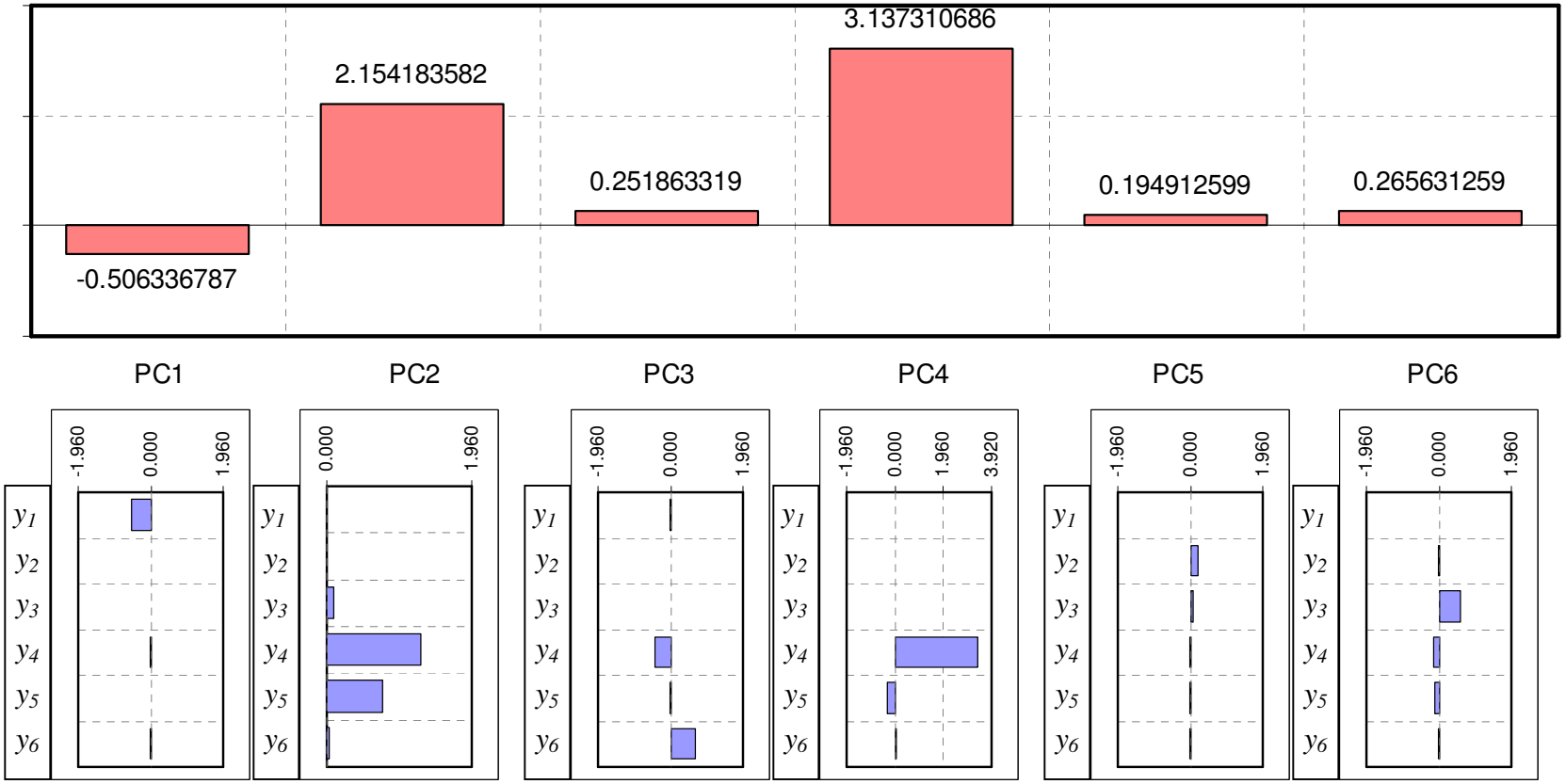

NOMENCLATURE

y_1 : Generator Output
y_2 : Fuel Flow
y_3 : Compressor Discharge Pressure
y_4 : Compressor Discharge Temperature
y_5 : Compressor Airflow
y_6 : Turbine Exhaust Temperature

Figure 6-28: PCA for the 2nd data set with single gross error in compressor discharge temperature

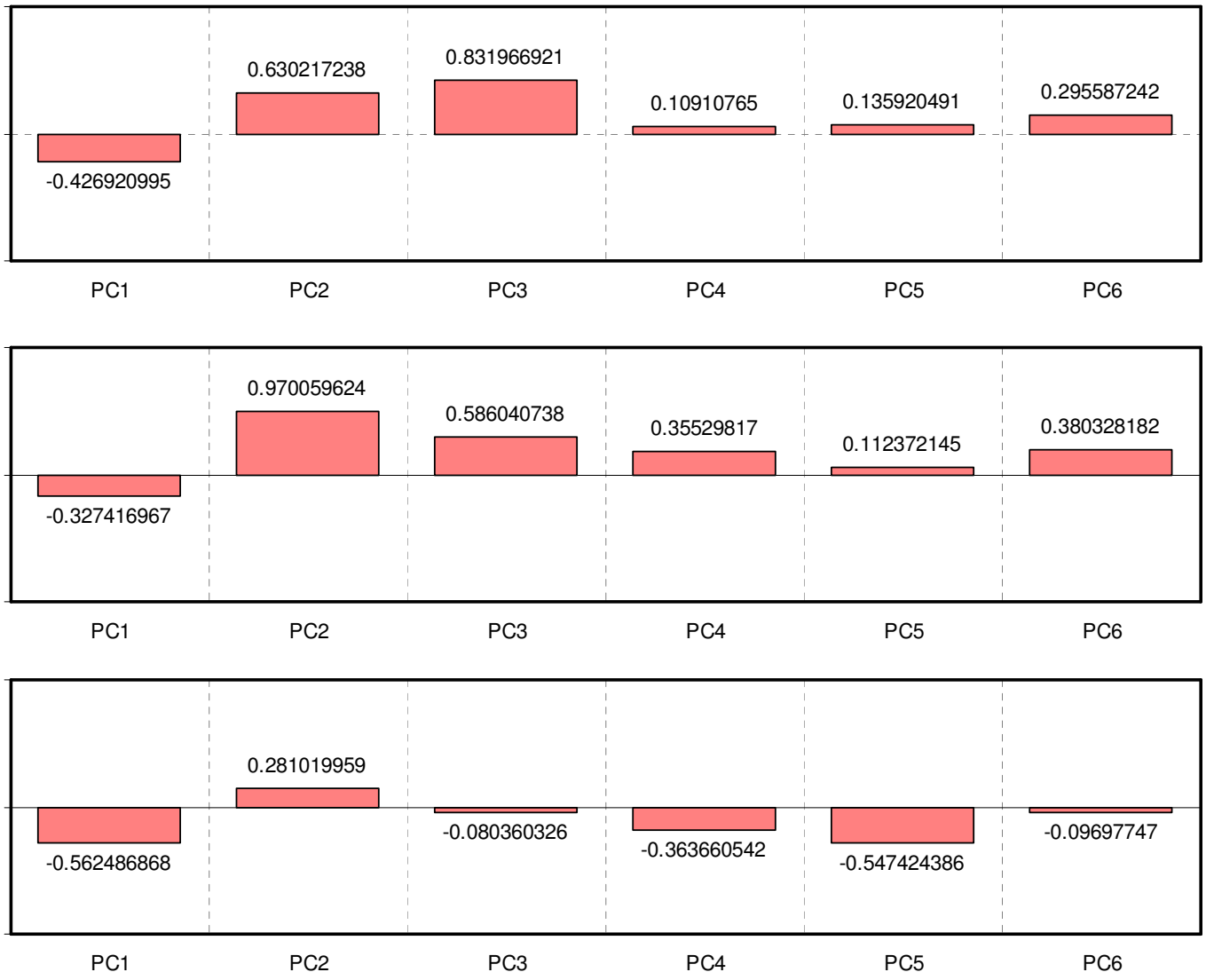

Figure 6-29: PCA for the 3rd, 4th, and 5th data sets with single gross error in compressor discharge temperature

The MDA techniques can be used to detect gross errors with large magnitudes. For subtle gross errors, the MDA techniques could lead to significant type II errors due to lacking correlations or wider ranges of system responses. The type II errors can be reduced if one uses the reconciliation techniques based on the maximum likelihood principle. The reconciliation process will be, however, smeared without eliminating the gross error effects. In this testing case, data reconciliation based on least squares minimization was first carried out without any gross error detection scheme such as the robust *M*-estimator or the serial bias compensation technique. The iteration history of data reconciliation in this testing case where one bias was designated was compared to the previous case where no biases were imposed. The results given in Fig. 6-30 shows that the minimized chi-squares in previous case study was 8.26, less than the threshold value, 20, determined based on the system *d.o.f* while in this case of one bias simulated, the minimized chi-squares had the value of 47.25, greater than the system *d.o.f*. The large chi-squares value indicates the occurrence of the gross errors but gives no information about their locations. Since the reconciliation was performed under the smearing effects, the estimated performance multipliers and the reconciled data were corrupted. The results are shown in table 6-20, which shows that the estimated DMM's for compressor efficiency and turbine efficiency are deviated from their designate values outside the scopes of estimated uncertainties. In table 6-20 it is also shown that the estimated firing temperatures for the first and second data sets are deviated from their designate values by about 2-sigma of estimate uncertainty, indicating the corrupted estimation due to smearing effects. The corrections to the measurement data are given in table 6-21 and Fig. 6-31. It is shown that the corrections to the compressor discharge temperatures in the first and second data sets are 4.64 sigma and 5.06 sigma, much less than the designated 7-sigma bias, while the corrections to the rest data sets are more than 2 sigma (3.28, 2.32, and 4.13). Since the pseudo data of compressor discharge temperature in the 3rd, 4th, and 5th data sets were not imposed by gross errors, the corrections of more than 2 sigma

indicates the smearing effects caused by the gross errors occurred in the first and second data sets.

The estimated firing temperature and performance multipliers (DMM's) from the smeared data reconciliation based on least squares minimization were compared to the results obtained from the *Method I* data reduction i.e. heat & mass balance. The comparisons of firing temperatures for all data sets and the DMM's are given in Fig. 6-32 ~ 6-33. It is shown that the expected value of estimated firing temperature from the heat balance method is more than 3-sigma away from the designate value, while the estimated value from data reconciliation is about 2-sigma although the reconciliation is corrupted with the gross error effects. Due to the gross error effects, the estimated firing temperatures from both methods are deviated significantly from the true value. The result from the smeared data reconciliation is, however, more close to the true value. Most importantly, the estimate uncertainty of firing temperature in data reconciliation is less than the estimate uncertainty in the data reduction method. It is also shown that the deviations of estimated compressor efficiency and turbine efficiency, obtained in data reconciliation, from the true values are more than 3 sigma because of the smearing effects. The data reduction method gives close estimates for the unbiased data sets but gives deviated estimates in the first and second data sets where gross errors were imposed. In Fig. 6-33 one can also see that the simultaneous data reconciliation and parameter estimation gives unified estimates of performance multipliers with less uncertainties as compared to the inconsistent estimates with larger uncertainties from the data reduction method. One gets the major benefits of obtaining unified estimates of system parameters with less uncertainty from data reconciliation, but the smearing effects can cause contaminated estimates.

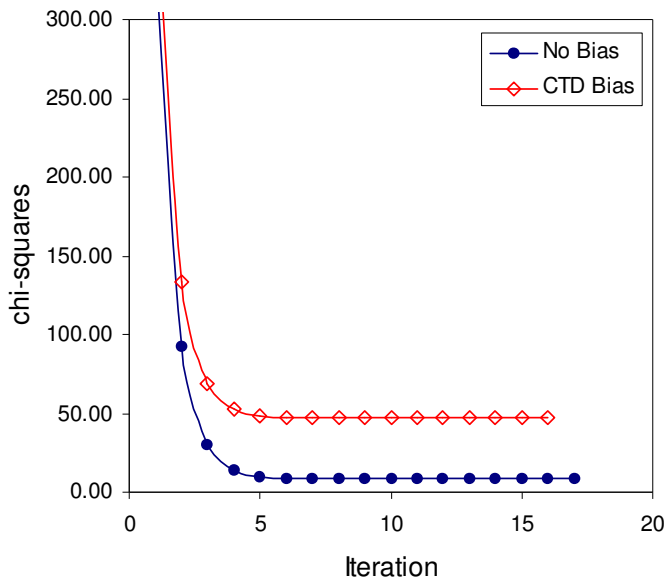

No Bias	
Iteration	Chi-squares
1	346.2233
2	92.7911
3	29.6465
4	13.8760
5	9.9353
6	8.9500
7	8.7037
8	8.6422
9	8.6268
10	8.6229
11	8.6220
12	8.6217
13	8.6217
14	8.6216
15	8.6216
16	8.6216
17	8.6216

CTD Bias GED Off	
Iteration	Chi-squares
1	392.6612
2	132.9302
3	68.6017
4	52.5863
5	48.5883
6	47.5902
7	47.3409
8	47.2787
9	47.2632
10	47.2593
11	47.2583
12	47.2581
13	47.2580
14	47.2580
15	47.2580
16	47.2580

Figure 6-30: Iteration history of data reconciliation for no bias and one bias of compressor discharge temperature imposed

Table 6-20: Estimated DMM's and firing temperatures from data reconciliation with smearing effects

Performance Factors (Model Inputs)	Specified	Estimated	Uncertainty (Sigma)
Compressor Efficiency (DMM)	0.9876	0.9735	0.002396
Compressor Flow (DMM)	0.9951	0.9968	0.002294
Combustor Efficiency (DMM)	0.9987	0.9947	0.003213
Turbine Efficiency (DMM)	0.9754	0.9801	0.001510
Turbine CQ (DMM)	1.001	1.0042	0.003103
Firing Temperature (Data 1)	2360	2367	3.45
Firing Temperature (Data 2)	2355	2362	3.50
Firing Temperature (Data 3)	2359	2364	3.47
Firing Temperature (Data 4)	2359	2366	3.47
Firing Temperature (Data 5)	2348	2352	3.46

Table 6-21: Measurement corrections by smeared data reconciliation with one gross error imposed

Measurements/System Outputs	Unit	Data Set 1	Data Set 2	Data Set 3	Data Set 4	Data Set 5
Generator Output	Sigma	0.73	1.06	0.23	-0.45	-1.58
Fuel Flow	Sigma	-5.18	-5.21	3.06	3.43	3.93
Compressor Discharge Pressure	Sigma	-1.20	-0.67	0.15	-0.32	2.02
Compressor Discharge Temperature	Sigma	**-4.63**	**-5.05**	**3.27**	**2.32**	**4.12**
Compressor Airflow	Sigma	0.44	-0.50	0.19	-0.29	0.35
Exhaust Temperature	Sigma	3.98	3.16	-3.49	-2.17	-1.45

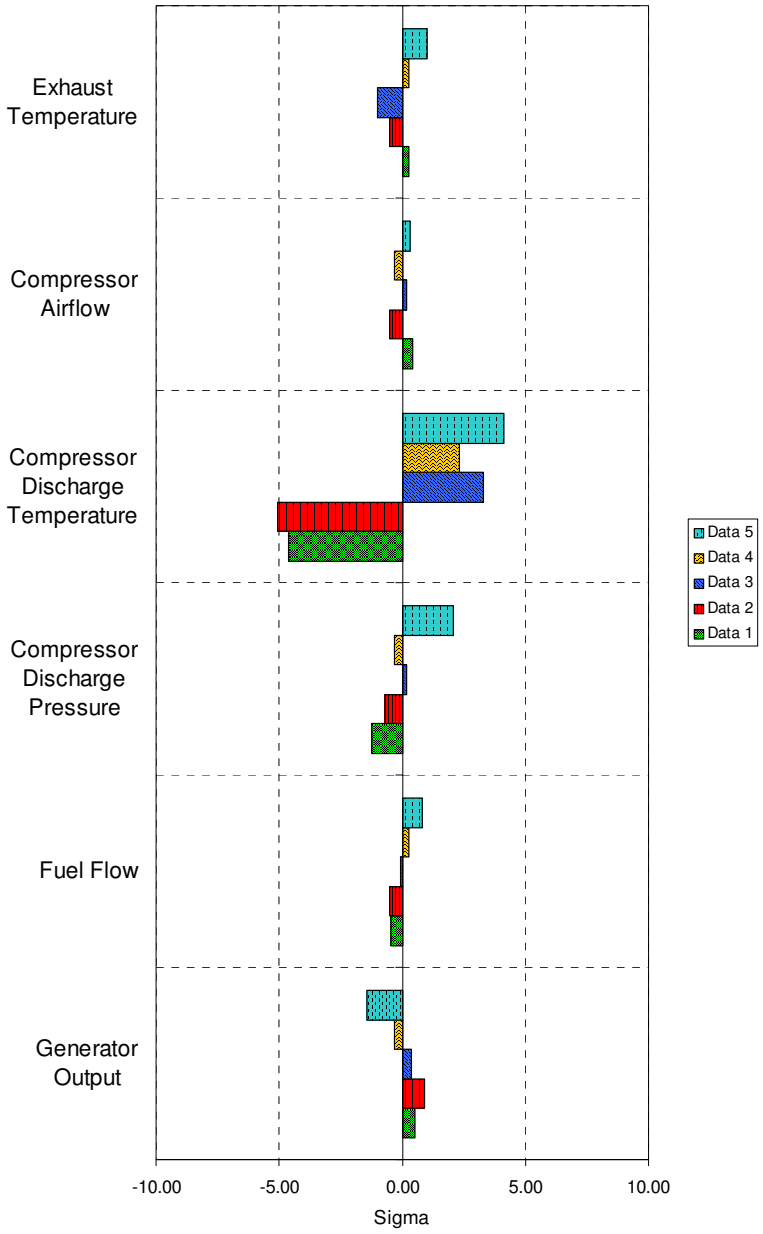

Figure 6-31: Measurement corrections by smeared data reconciliation with one gross error imposed

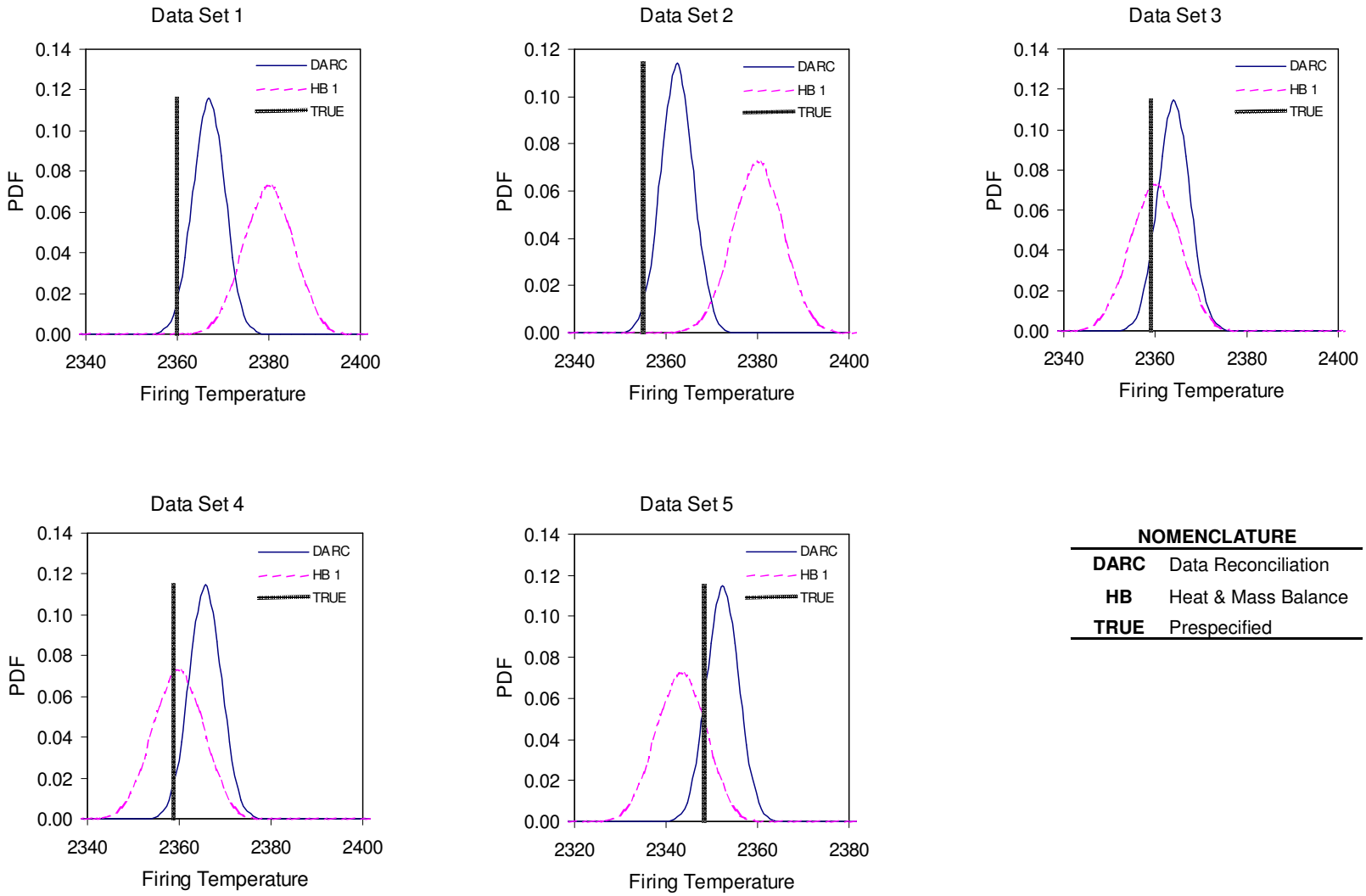

NOMENCLATURE	
DARC	Data Reconciliation
HB	Heat & Mass Balance
TRUE	Prespecified

Figure 6-32: Estimated firing temperatures and estimate uncertainties by smeared data reconciliation with one gross error

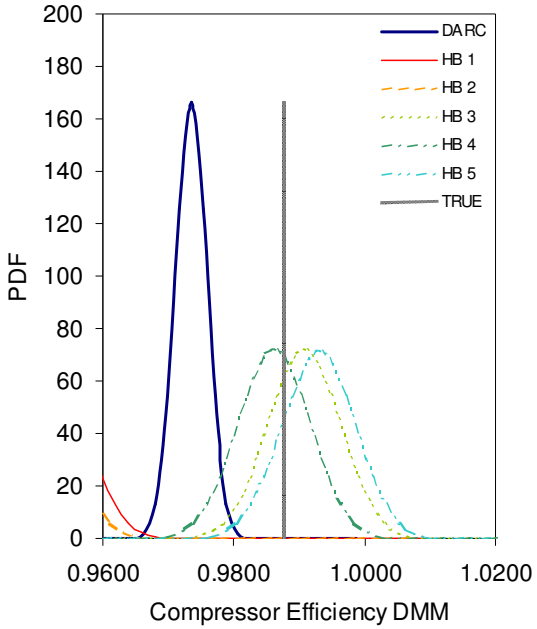

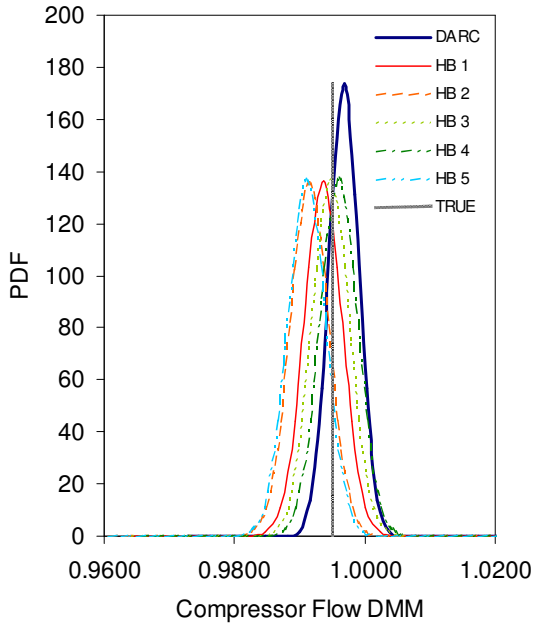

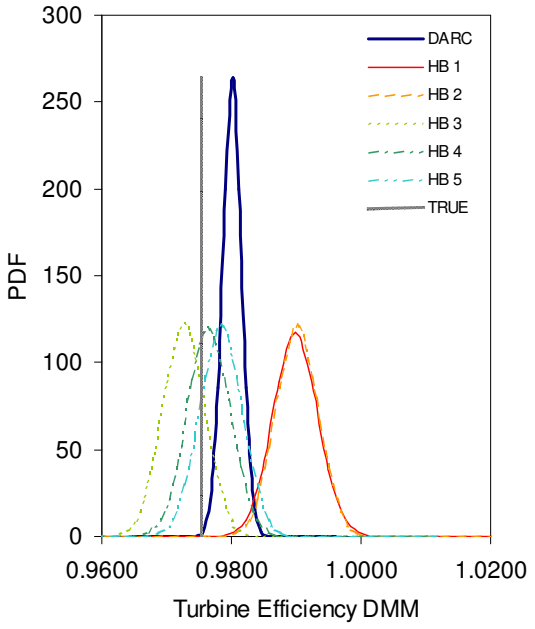

NOMENCLATURE	
DARC	Data Reconciliation
HB 1~5	Heat & Mass Balance for Data Set 1 ~5
TRUE	Prespecified

Figure 6-33: Estimated performance multipliers and estimate uncertainties by smeared data reconciliation with one gross error

The robust *M*-estimator was first applied to the maximum-likelihood-based data reconciliation as the gross error detection scheme. The *Hampel's Redescending M*-estimator was selected as the new likelihood function to replace the least squares objective function. The tuning constants $a_{H,}$ $b_{H,}$ and c_H of the *Hampel's Redescending M*-estimator were chosen based on the AIC principle discussed in Chapter 5, and are listed as follows:

$$a_H = 1.3_{,}\ b_H = 2.6_{,}\ c_H = 5.2$$

The corrections to the measurements are given in table 6-22 and Fig. 6-34. It is shown that the corrections to the compressor discharge temperature from the first and second data sets are 6.95 and 7.31, which are within1-sigma deviations from the designate bias magnitude (7-sigma), and that the corrections of it at the rest data sets are within 1-sigma, whereas these data sets are bias free. One can see that the smearing effects due to gross errors were suppressed significantly by the use of the robust *M*-estimator. The estimated firing temperatures and performance multipliers along with their estimate uncertainties are given in table and plotted in Fig. 6-35 ~ 6-36. It is shown that the estimates are shifted toward to their true values and the deviations are less than 2-sigma of the estimate uncertainties. It is also shown that the uncertainties of the estimates by simultaneous data reconciliation and parameter estimation are less than the estimate uncertainties from the heat & mass balance method. Since the influence function of the robust *M*-estimator is equal to the influence function of the least squares in the region where the corrections to the measurements are small, the estimate uncertainties by the robust *M*-estimator are almost the same as the estimate uncertainties from the least-squares-based data reconciliation. Sufficient measurement redundancies are required for the robust *M*-estimator to be performed efficiently. The serial bias compensation method performs better when the redundancies are not sufficient.

Table 6-22: Measurement corrections by using robust *M*-estimator with one gross error imposed

Measurements/System Outputs	Unit	Data Set 1	Data Set 2	Data Set 3	Data Set 4	Data Set 5
Generator Output	Sigma	0.14	0.84	0.08	-0.29	-2.34
Fuel Flow	Sigma	-0.48	-0.32	-0.03	0.46	0.59
Compressor Discharge Pressure	Sigma	-1.06	-0.41	0.41	-0.01	2.16
Compressor Discharge Temperature	Sigma	**-6.95**	**-7.31**	1.00	0.05	1.84
Compressor Airflow	Sigma	0.33	-0.61	0.07	-0.41	0.24
Exhaust Temperature	Sigma	0.05	-0.47	-1.12	0.32	0.61

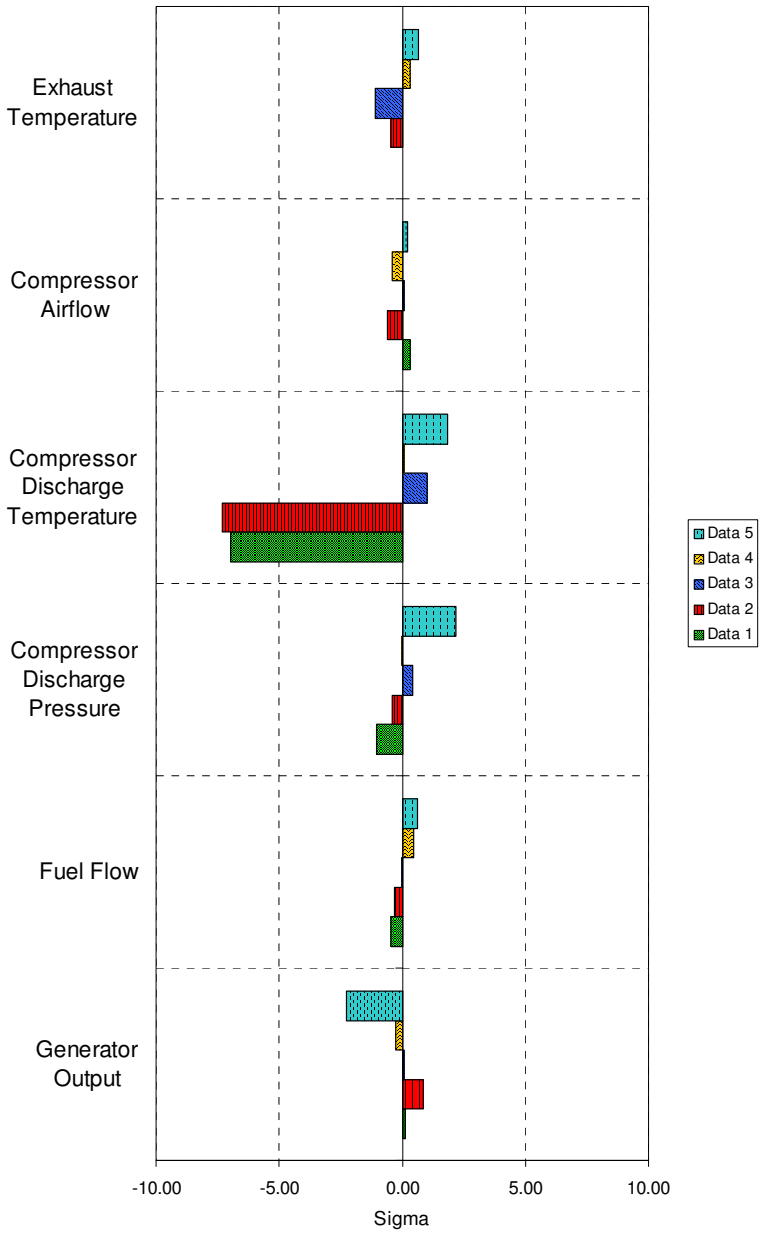

Figure 6-34: Bar chart of measurement corrections

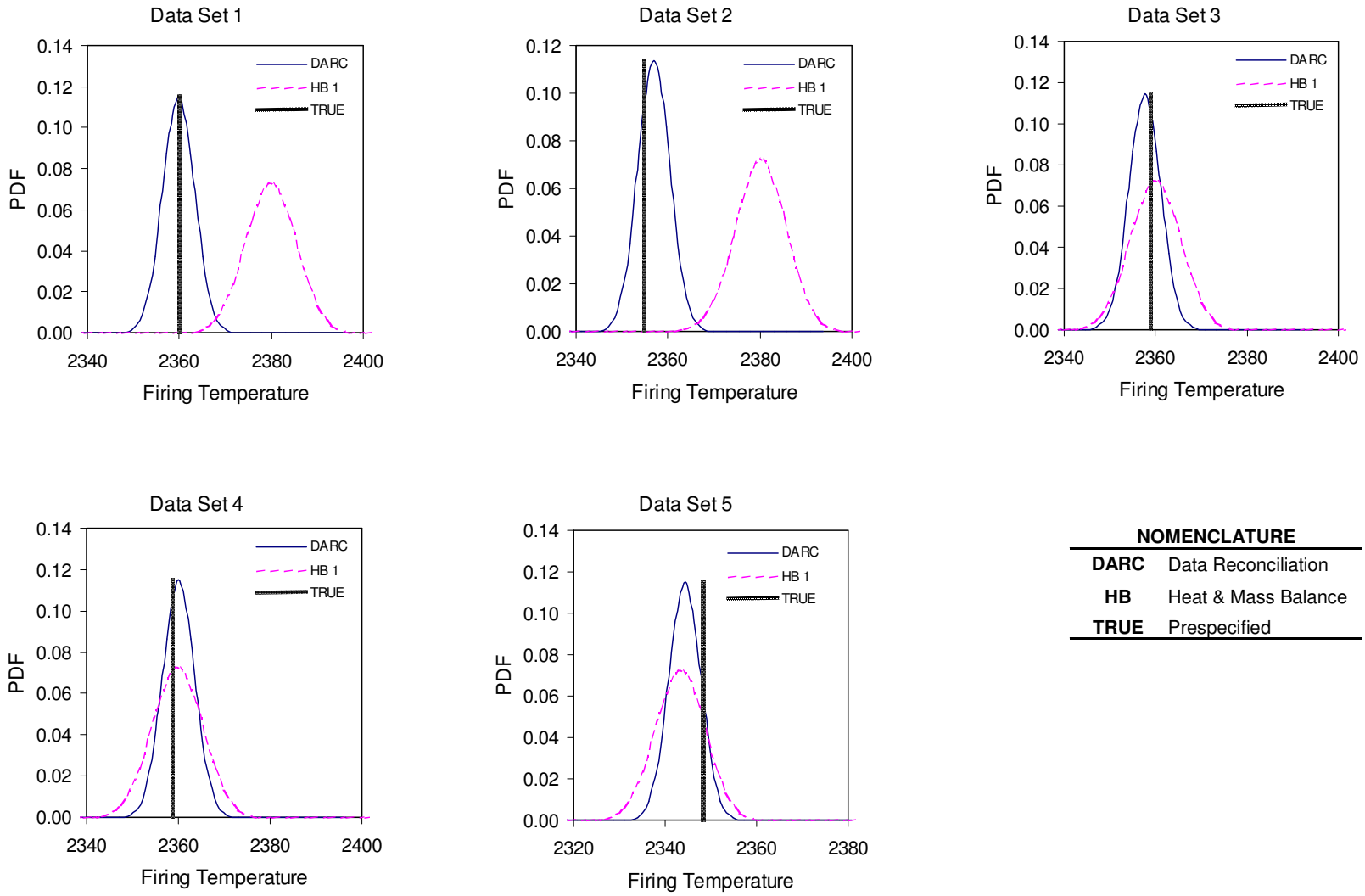

NOMENCLATURE	
DARC	Data Reconciliation
HB	Heat & Mass Balance
TRUE	Prespecified

Figure 6-35: Estimated firing temperatures and estimate uncertainties using robust *M*-estimator with one gross error imposed

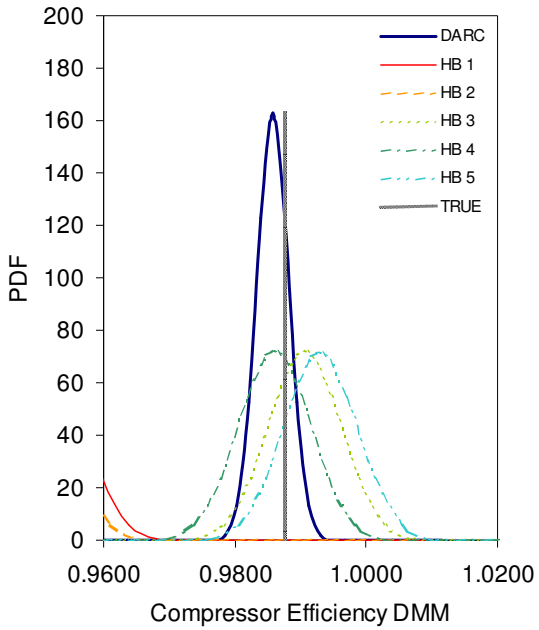

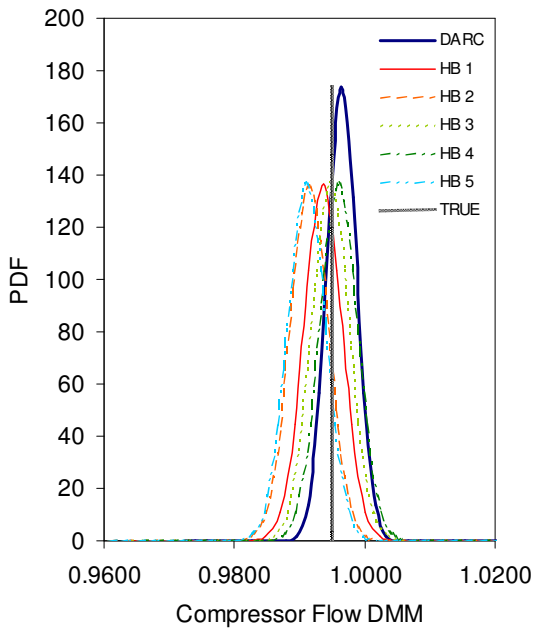

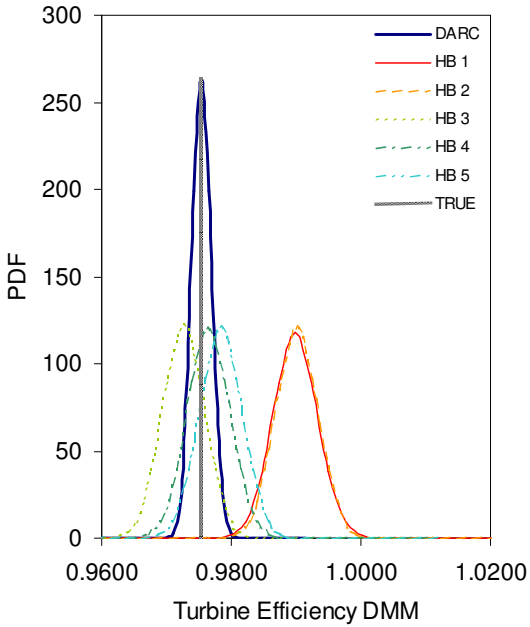

NOMENCLATURE

DARC	Data Reconciliation
HB 1~5	Heat & Mass Balance for Data Set 1 ~5
TRUE	Prespecified

Figure 6-36: Estimated performance multipliers and estimate uncertainties by using robust *M*-estimator with one gross error imposed

From the MDA and robust *M*-estimator one can locate the biased data sets and use the serial bias compensation strategy to validate the results. In this testing case, the first two data sets were known as biased based on the MDA and data reconciliation using the robust *M*-estimator. The hypotheses of gross error models were, therefore, tested on the first two data sets. Each gross error detected in previous round was added to the new gross error model in the next round where the bias magnitudes were reevaluated. The process of serial bias compensation stopped after two rounds of hypotheses testing, from which the gross error model of single bias in the measurement of compressor discharge temperature was selected due to its highest test score. Since in each hypothesis test simultaneous data reconciliation and parameter estimation is carried out to get the test statistics, the reconciled data and estimated model parameters come along with the picked gross error model with the highest test score. In this testing case, after the hypotheses testing, it was concluded that the measurement of compressor discharge temperature has the gross error. At the same time, the magnitude of the gross error was obtained; the measured data was reconciled and the performance multipliers and firing temperatures were also estimated. The corrections to the measured data are shown in table 6-23 and Fig. 6-37. It is shown that the corrections to the compressor discharge temperature of the first two data sets were 7.94 sigma and 8.30 sigma, for which their deviations from the designate bias magnitude 7-sigma are contributed by the measurement uncertainties. The estimated performance multipliers and firing temperatures along with the estimate uncertainties are given in Fig. 6-38 ~ 6-39, from which one can see the true values are within the estimate uncertainties. It is also shown that one gets the benefits of reducing the estimate uncertainties from data reconciliation. The serial bias compensation strategy also confirms the results obtained from the robust estimation.

Table 6-23: Measurement corrections by using serial bias compensation with one gross error

Measurements/System Outputs	Unit	Data Set 1	Data Set 2	Data Set 3	Data Set 4	Data Set 5
Generator Output	Sigma	0.41	0.68	0.45	-0.20	-1.36
Fuel Flow	Sigma	-0.56	-0.56	-0.04	0.32	0.83
Compressor Discharge Pressure	Sigma	-1.29	-0.72	0.20	-0.28	2.08
Compressor Discharge Temperature	Sigma	**-7.94**	**-8.30**	0.03	-0.93	0.91
Compressor Airflow	Sigma	0.40	-0.54	0.15	-0.34	0.31
Exhaust Temperature	Sigma	0.11	-0.57	-0.95	0.33	1.08

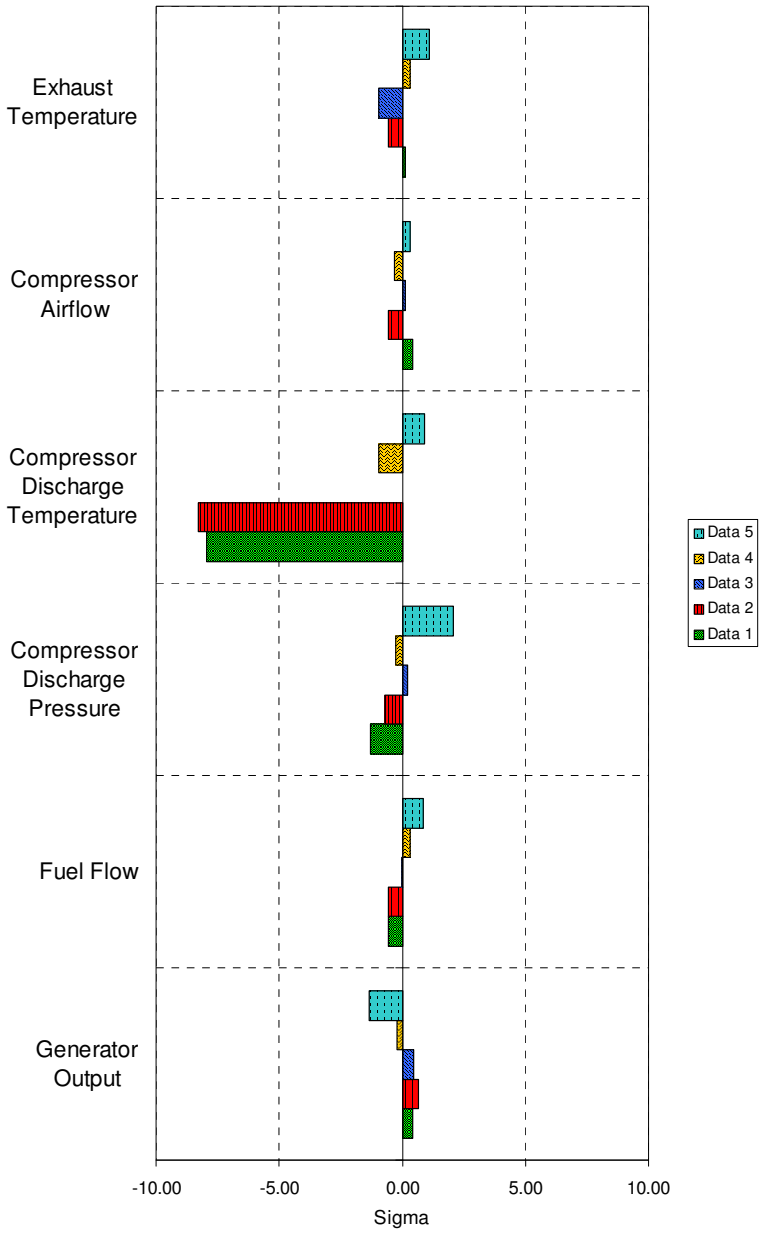

Figure 6-37: Bar chart of measurement corrections using serial bias compensation with one gross error imposed

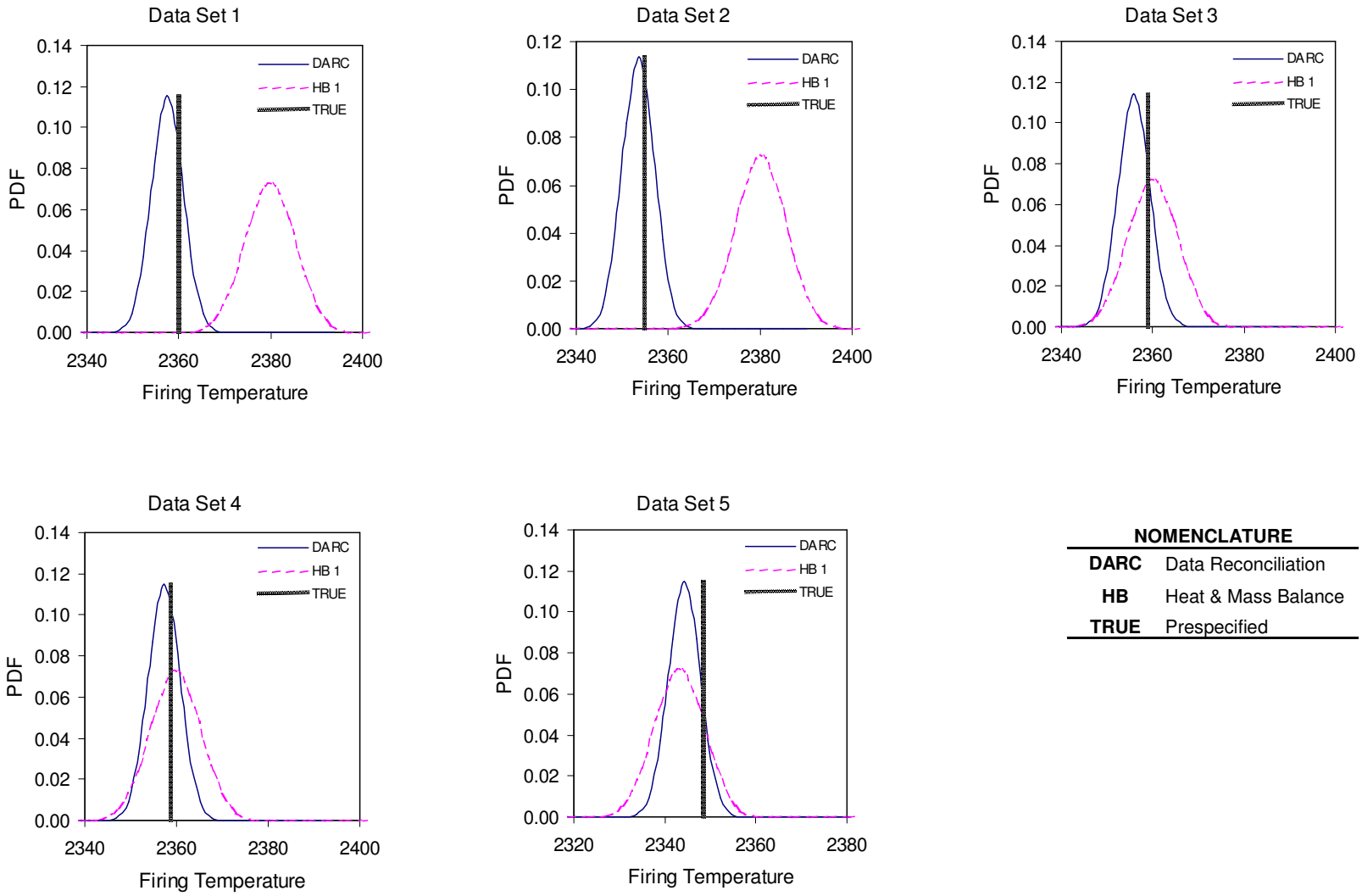

NOMENCLATURE	
DARC	Data Reconciliation
HB	Heat & Mass Balance
TRUE	Prespecified

Figure 6-38: Estimated firing temperatures and estimate uncertainties by using serial bias compensation with one gross error imposed

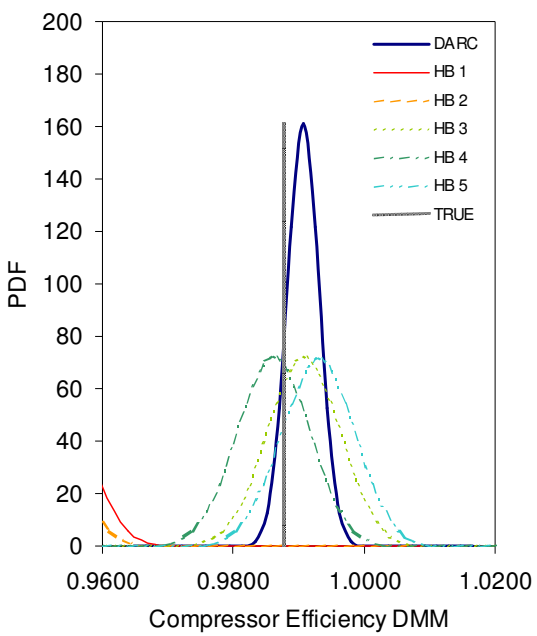

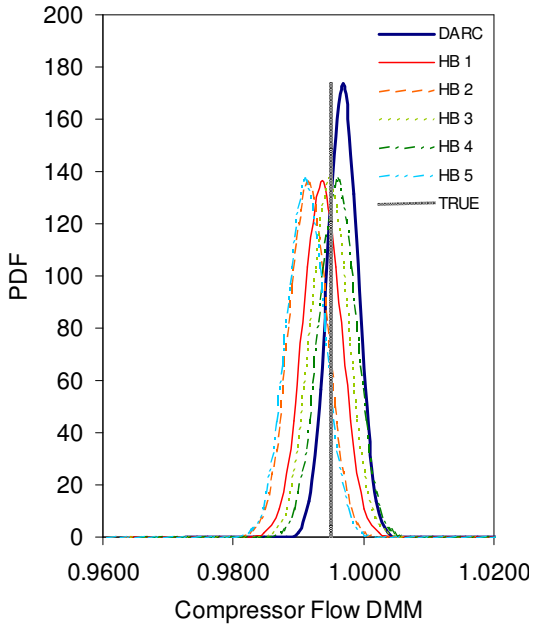

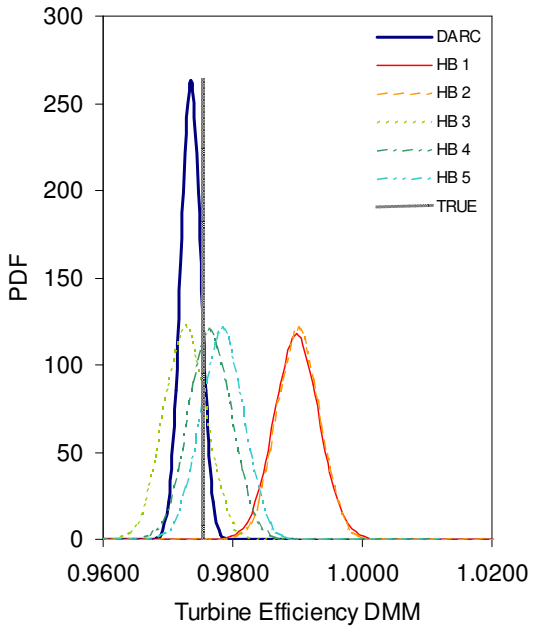

NOMENCLATURE

DARC	Data Reconciliation
HB 1~5	Heat & Mass Balance for Data Set 1 ~5
TRUE	Prespecified

Figure 6-39: Estimated performance multipliers and estimate uncertainties by using serial bias compensation with one gross error imposed

In the second testing case, multiple biases were imposed to measurements of fuel flow, compressor discharge temperature, and turbine exhaust temperature, for the first two data sets with presumed magnitudes of 8, 7, and –6 sigma while the rest data sets were subject to random errors and bias-free. Like the first testing case, the MDA techniques i.e. Multivariate Data Visualization and Principal component Analysis were first carried out for detecting serious biases and differentiating biased data sets from healthy data sets. In Multivariate Data Visualization, the scatter plot matrix presents measured data points as outliers in all pair wise scatter plots that have fuel flow and compressor discharge temperature as one of the axes. The scatter plots that contain fuel flow, compressor discharge temperature, and turbine exhaust temperature as one of a pair responses is given in Fig. 6-40 ~ 6-42. Theses scatter plots show the fuel flow and the compressor discharge temperature are outliers as compared to the mother populations simulated by the Monte Carlo simulation while the turbine exhaust temperature does not present itself as an outlier.

The principal component analyses were performed following the multivariate data visualization. The PCA for all data sets in the second testing case where three gross errors were imposed are shown in Fig. 6-43~ 6-45. Figure 6-43 shows the PCA result for the first data set. It is shown that the 4^{th} and 5^{th} principal components have the test statistics greater than the threshold value - ~2.82 and ~ 2.51. A further investigation shows the 4^{th} PC has the compressor discharge temperature as the biggest contributor while in the 5^{th} PC the fuel flow causes the biggest variance. The PCA for the second data set is given in Fig. 6-44, which shows the 2^{nd},4^{th}, and 5^{th} PC's have test statistics above the threshold value 1.96. Both 2^{nd} and 4^{th} PC's have the compressor discharge temperature as the biggest contributor to the variances of these two PC's while in the 5^{th} PC the fuel flow is the major contributor. The PCA for the rest data sets is shown in Fig. 6-45 where all the principal components have the test statistics below the threshold values and are, therefore, considered as bias free.

Both MDA techniques failed to identify the turbine exhaust temperature as an outlier. The reasons of causing detection failure are mainly because of the wide range of turbine exhaust temperature and lack of correlations between turbine exhaust temperature and other responses. The MDA techniques rely on the simulation of mother populations for system responses, which is significantly affected by the ranges chosen for the model parameters- performance multipliers and firing temperatures in this case. To improve the detecting rate, simultaneous data reconciliation and parameter estimation with a gross error detection scheme is needed. In the second testing case with multiple gross errors, the robust M-estimator and serial bias compensation method were also carried out to improve the detection rate, and, most importantly, to estimate model parameters and reconcile the data. In the gross error detection scheme, the locations and magnitudes of gross errors can also be detected.

Like the first testing case, data reconciliation based on the least squares minimization without any gross error detection scheme was carried out first in the second testing case. The minimized chi-squares had the value of 113.3, greater than the value for one gross error in the first testing case (47.25) and the system *d.o.f* 20, which is expected because more gross errors were imposed. The chi-squares value greater than the threshold value determined by *d.o.f* indicates the occurrence of the gross errors but gives no information about their locations and magnitudes. Since the reconciliation was performed under the smearing effects, the estimated performance multipliers and the reconciled data are corrupted. The corrections to the measurement data are given in table 6-24 and Fig. 6-46. It is shown that the corrections to the three biased measurements – fuel flow, compressor discharge temperatures, and turbine exhaust temperature in the first and second data sets are much less than the designate bias magnitudes, while the corrections to the rest data sets show the occurrence of biases, whereas no biases were applied. The estimated firing temperature and performance multipliers (DMM's) along with their uncertainties obtained from the smeared data reconciliation were compared to the results

obtained from the Method I data reduction i.e. heat & mass balance. The comparisons are given in Fig. 6-49 ~ 6-50, which shows that except for the firing temperature the true values of compressor efficiency and turbine efficiency are presented as outliers against their estimated values with uncertainties due to the smearing effects. The data reduction method gave results close to the designate values in bias-free data sets while leading to corrupted estimates for the first and second data sets where gross errors were imposed.

The *Hampel's Redescending M*-estimator was then utilized to replace the least squares and served as the gross error detection scheme. The tuning constants a_H, b_H, and c_H were the same as those used in the first testing case i.e. $a_H = 1.3$, $b_H = 2.6$, $c_H = 5.2$. The corrections to the measurements are given in table 6-25and Fig. 6-47, which show the bias corrections only occur to the designate biased measurements in the first and second data sets, indicating the smearing effects are eliminated during the reconciliation. The estimated firing temperatures and performance multipliers along with their estimate uncertainties are given in Fig. 6-51 ~ 6-52. It is shown that the true values were captured by the estimated values within the estimate uncertainties. It is also shown that the uncertainties of the estimates by simultaneous data reconciliation and parameter estimation are less than the estimate uncertainties from the heat & mass balance method.

The serial bias compensation method was also performed for the second testing case where multiple gross errors were simulated. From the MDA and robust estimation technique one can locate the biased data sets and apply gross error models accordingly. In this testing case, the first two data sets were known as biased from the MDA and robust estimation technique. The hypotheses of gross error models were then tested on the first two data sets. The process of serial bias compensation stopped after four rounds of hypotheses testing, from which the gross error model of three biases in the measurement of fuel flow, compressor discharge temperature, and turbine exhaust temperature was selected based on its highest testing score. It was, therefore, concluded that the measurement of fuel flow, compressor discharge temperature, and turbine exhaust

temperature have gross errors. Coming along with the determination of the gross error model are the calculated bias magnitudes, reconciled data, and estimated performance multipliers and firing temperatures. The corrections to the measured data are shown in table 6-26 and Fig. 6-48, which show that the bias corrections only occur to the designate biased measurements in the first and second data sets. The estimated firing temperatures and performance multipliers along with their estimate uncertainties are given in Fig. 6-53 ~ 6-54. It is shown that the true values were also captured by the estimated values within the estimate uncertainties. The estimate uncertainties from the data reduction method are also presented in the same plot, showing that the uncertainties of the estimates by simultaneous data reconciliation and parameter estimation are less than the estimate uncertainties from the heat & mass balance method. This proves again data reconciliation results in less estimate uncertainties than the heat & mass balance based data reduction method.

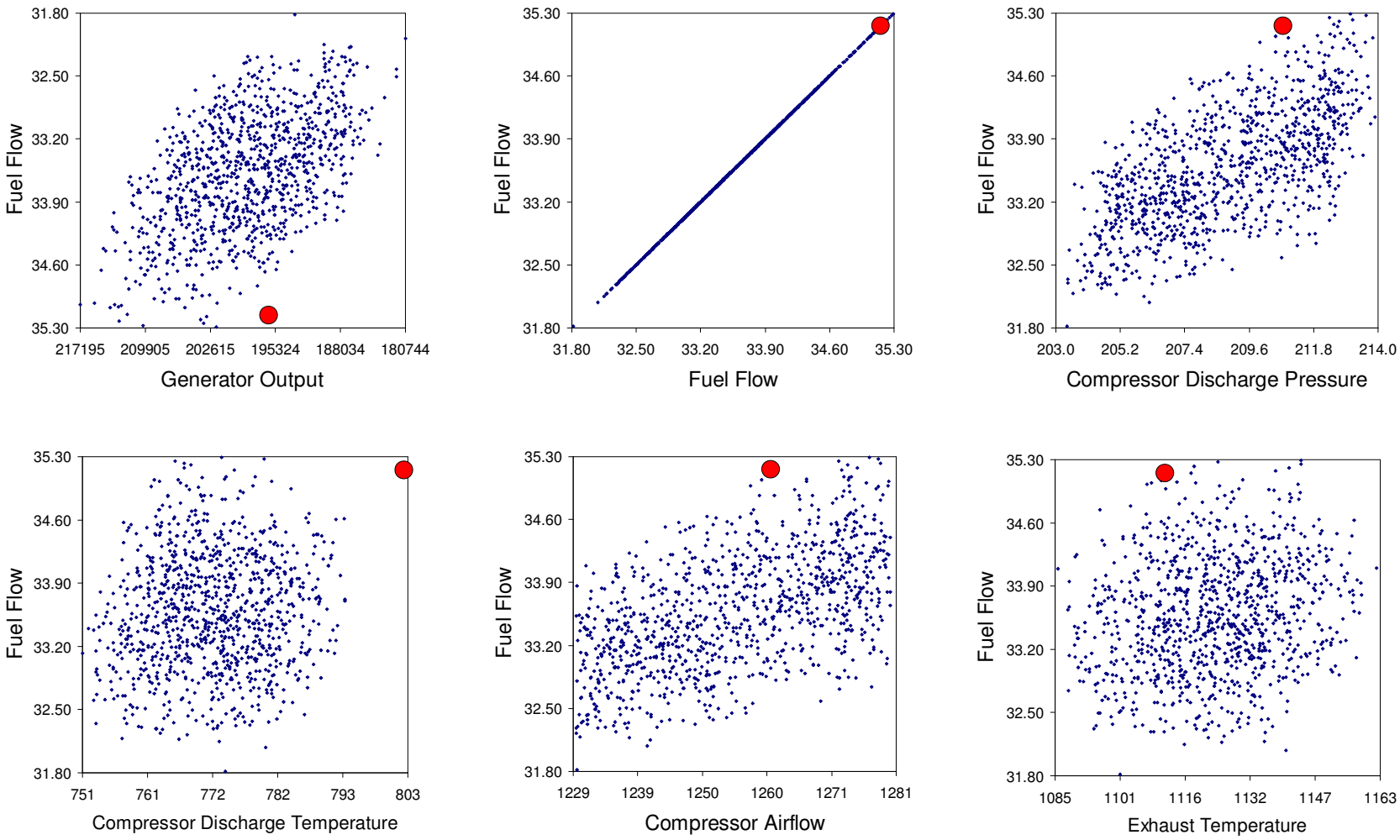

Figure 6-40: Scatter plots containing fuel flow as one of the axes (3 gross errors imposed)

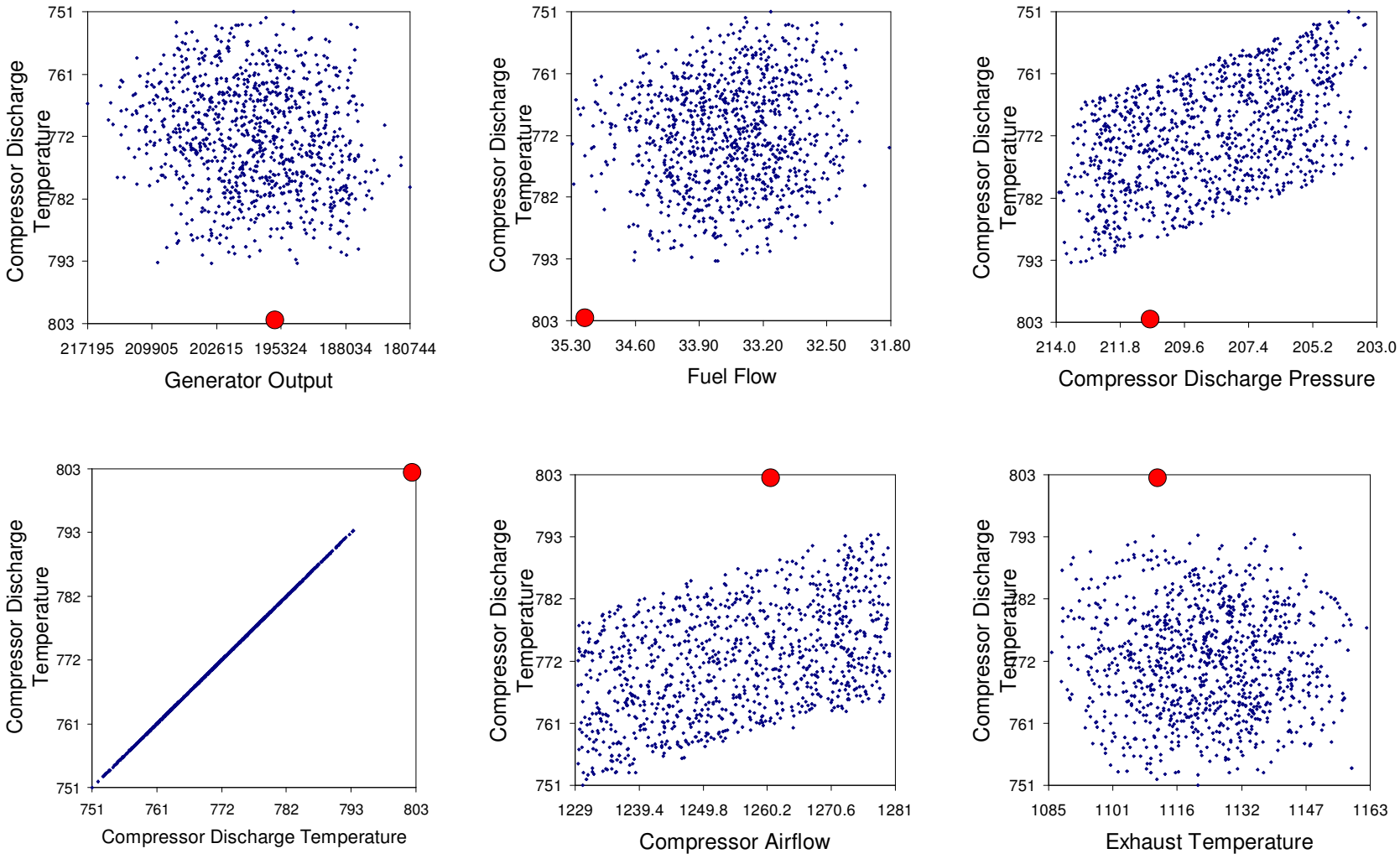

Figure 6-41: Scatter plots containing compressor discharge temperature as one of the axes (3 gross errors imposed)

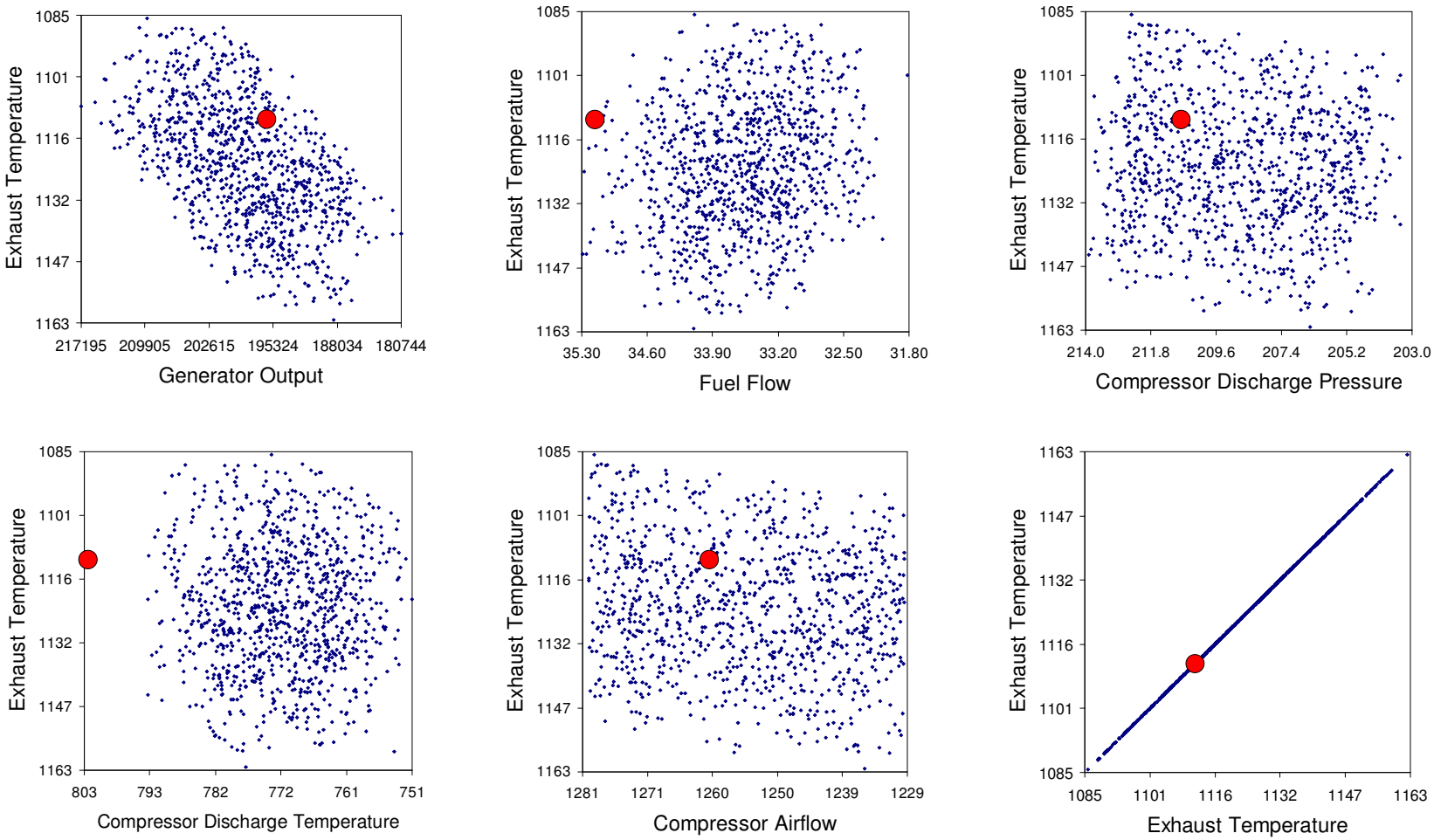

Figure 6-42: Scatter plots containing exhaust temperature as one of the axes (3 gross errors imposed)

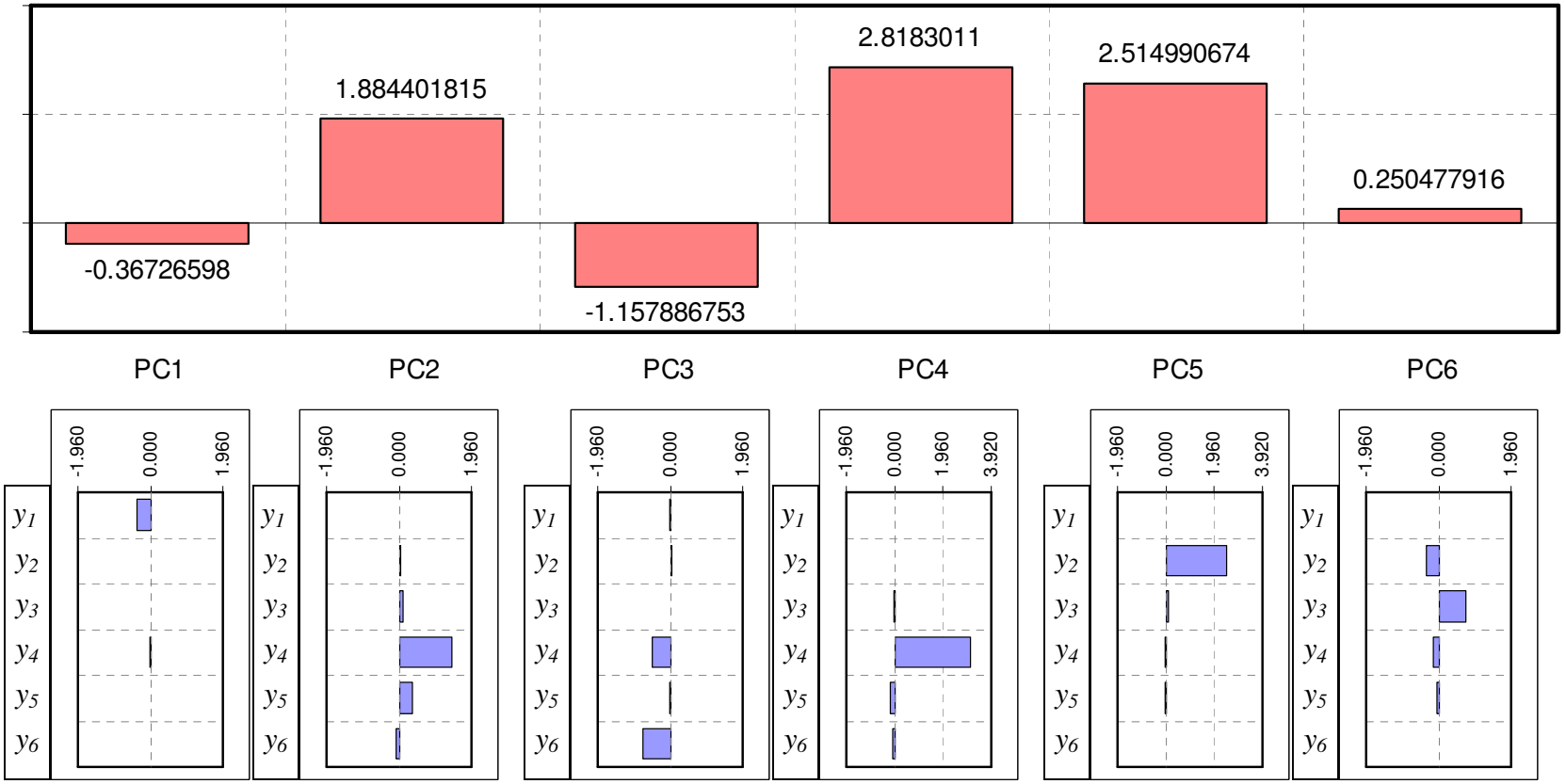

NOMENCLATURE

y_1 : Generator Output
y_2 : Fuel Flow
y_3 : Compressor Discharge Pressure
y_4 : Compressor Discharge Temperature
y_5 : Compressor Airflow
y_6 : Turbine Exhaust Temperature

Figure 6-43: Principal component analysis for the 1st data set with three gross errors imposed

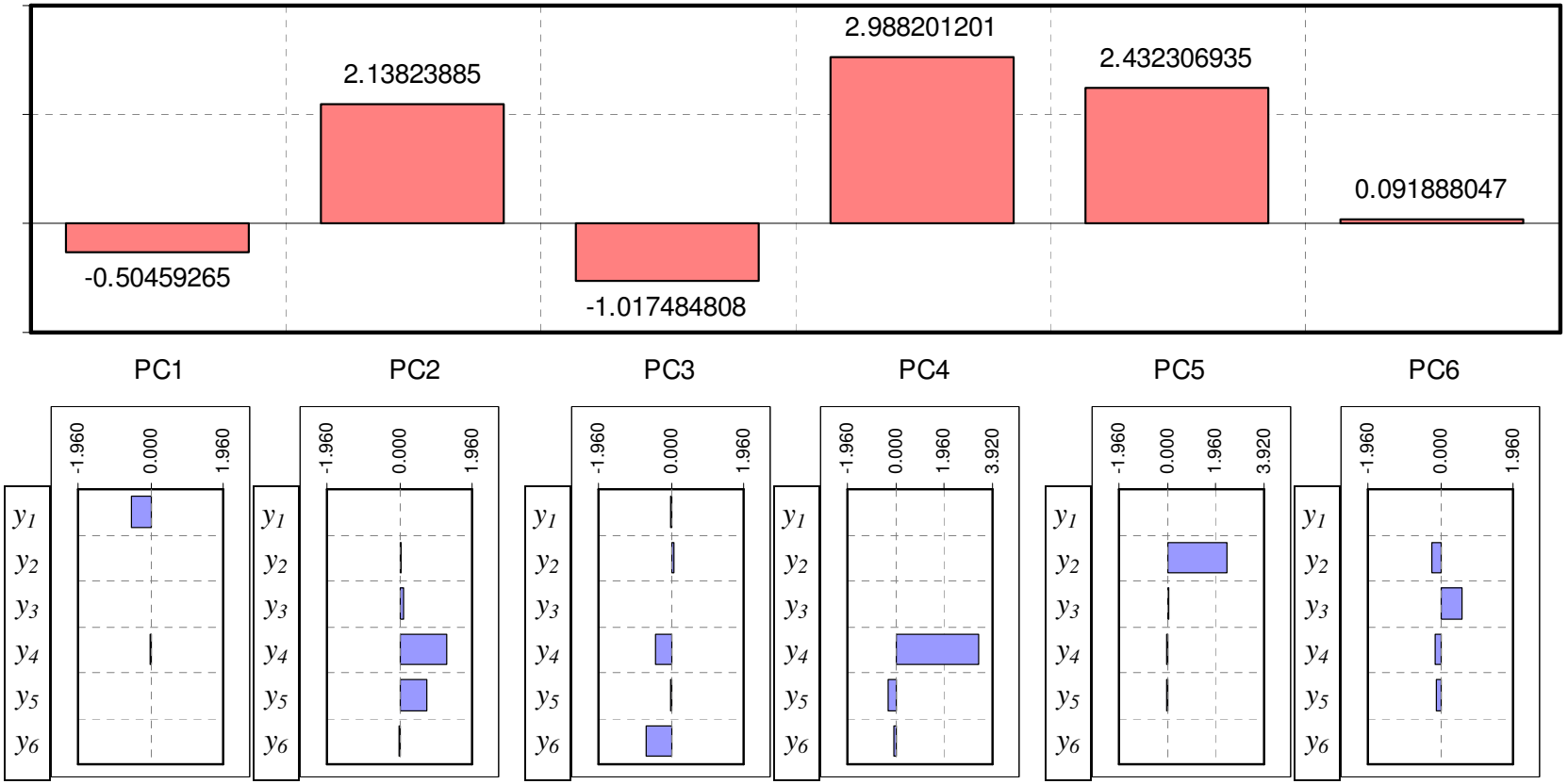

NOMENCLATURE

y_1 : Generator Output
y_2 : Fuel Flow
y_3 : Compressor Discharge Pressure
y_4 : Compressor Discharge Temperature
y_5 : Compressor Airflow
y_6 : Turbine Exhaust Temperature

Figure 6-44: Principal component analysis for the 2nd data set with three gross errors imposed

Figure 6-45: PCA for the 3rd, 4th, and 5th data sets with three gross errors imposed

Table 6-24: Measurement corrections by smeared data reconciliation subject to three gross errors

Measurements/System Outputs	Unit	Data Set 1	Data Set 2	Data Set 3	Data Set 4	Data Set 5
Generator Output	Sigma	0.73	1.06	0.23	-0.45	-1.58
Fuel Flow	Sigma	**-5.18**	**-5.21**	**3.06**	**3.43**	**3.93**
Compressor Discharge Pressure	Sigma	-1.20	-0.67	0.15	-0.32	2.02
Compressor Discharge Temperature	Sigma	**-4.63**	**-5.05**	**3.27**	**2.32**	**4.12**
Compressor Airflow	Sigma	0.44	-0.50	0.19	-0.29	0.35
Exhaust Temperature	Sigma	**3.98**	**3.16**	**-3.49**	**-2.17**	**-1.45**

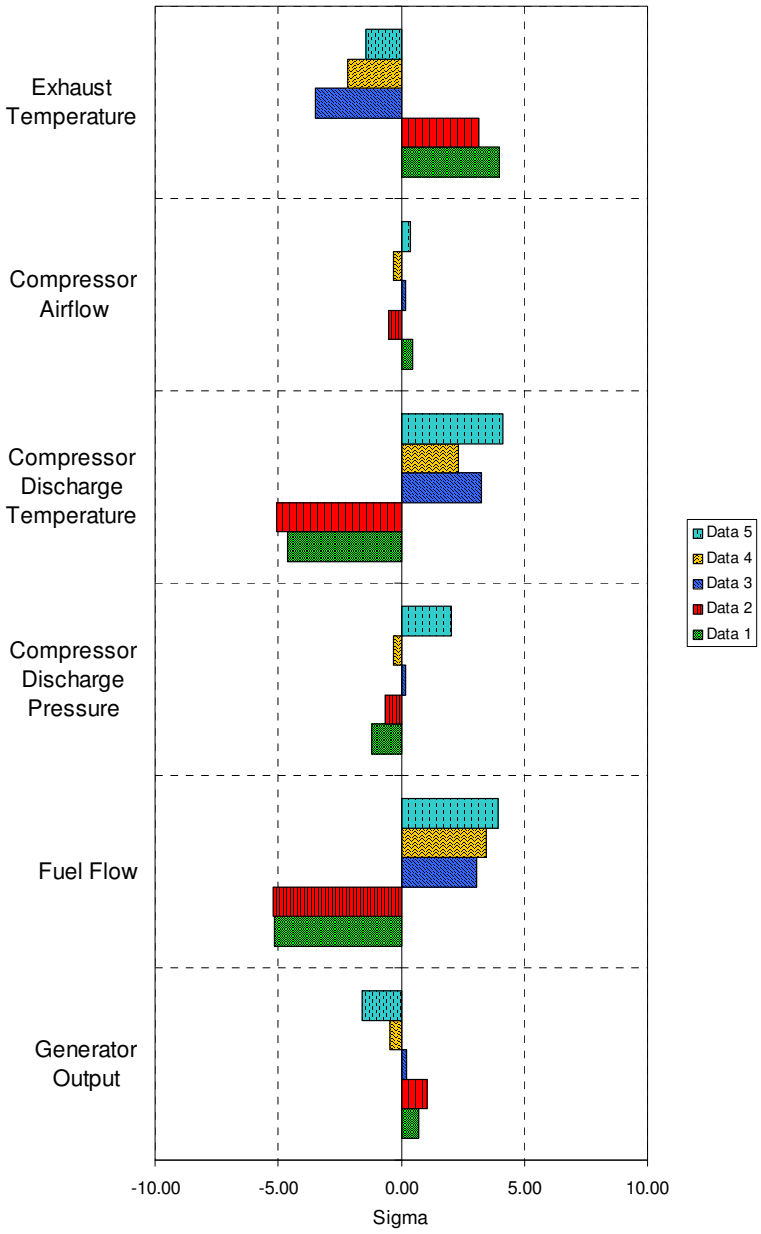

Figure 6-46: Bar chart of measurement corrections by smeared data reconciliation

Table 6-25: Measurement corrections by using robust *M*-estimator subject to three gross errors

Measurements/System Outputs	Unit	Data Set 1	Data Set 2	Data Set 3	Data Set 4	Data Set 5
Generator Output	Sigma	0.04	0.03	0.04	0.02	-0.25
Fuel Flow	Sigma	**-8.39**	**-8.54**	0.08	0.71	1.60
Compressor Discharge Pressure	Sigma	-1.11	-0.62	0.36	0.01	2.54
Compressor Discharge Temperature	Sigma	**-6.97**	**-7.36**	0.99	0.06	1.93
Compressor Airflow	Sigma	0.33	-0.61	0.07	-0.41	0.24
Exhaust Temperature	Sigma	**4.36**	**3.43**	-2.82	-1.20	-0.02

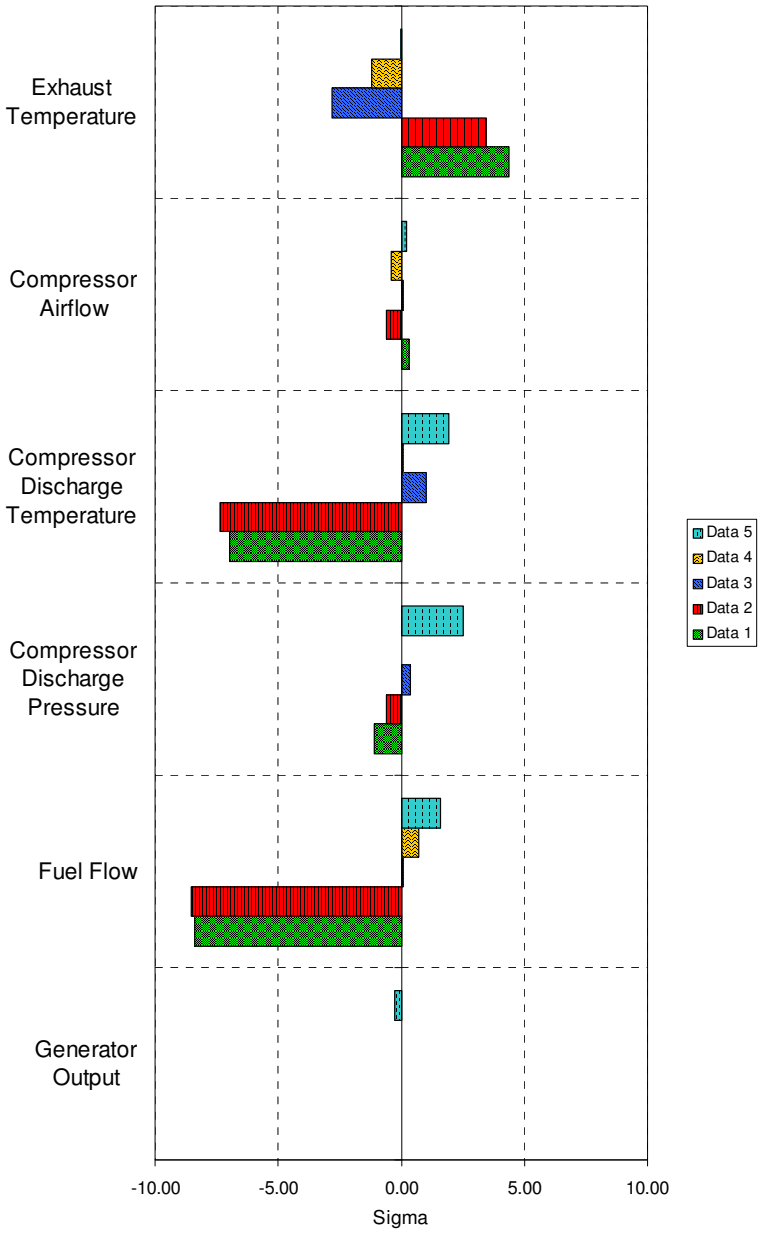

Figure 6-47: Bar chart of measurement corrections using robust *M*-estimator with three gross errors

Table 6-26: Measurement corrections by using serial bias compensation with three gross errors

Measurements/System Outputs	Unit	Data Set 1	Data Set 2	Data Set 3	Data Set 4	Data Set 5
Generator Output	Sigma	0.08	0.35	0.68	0.03	-1.14
Fuel Flow	Sigma	**-9.16**	**-9.16**	-0.41	-0.05	0.46
Compressor Discharge Pressure	Sigma	-1.36	-0.79	0.25	-0.24	2.12
Compressor Discharge Temperature	Sigma	**-7.97**	**-8.33**	0.03	-0.94	0.90
Compressor Airflow	Sigma	0.41	-0.53	0.15	-0.33	0.32
Exhaust Temperature	Sigma	**5.70**	**5.00**	-1.10	0.18	0.93

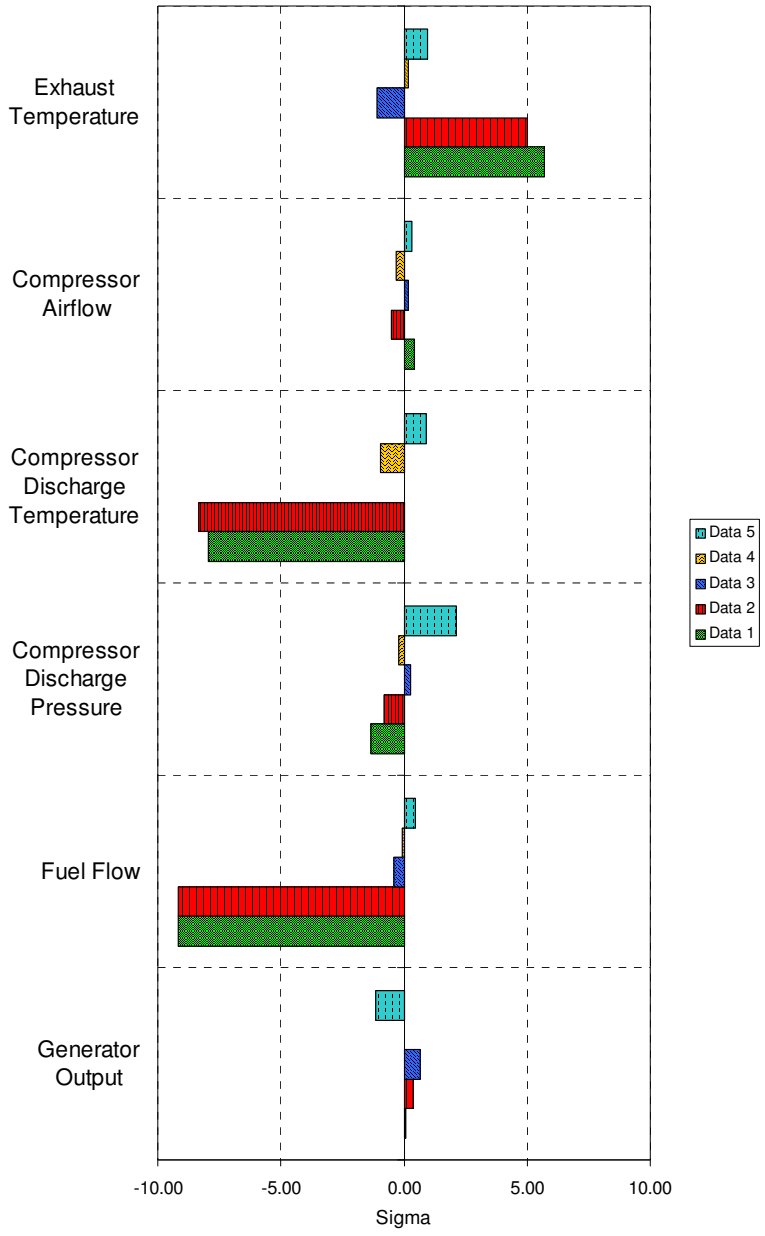

Figure 6-48: Bar chart of measurement corrections by using serial bias compensation with three gross errors

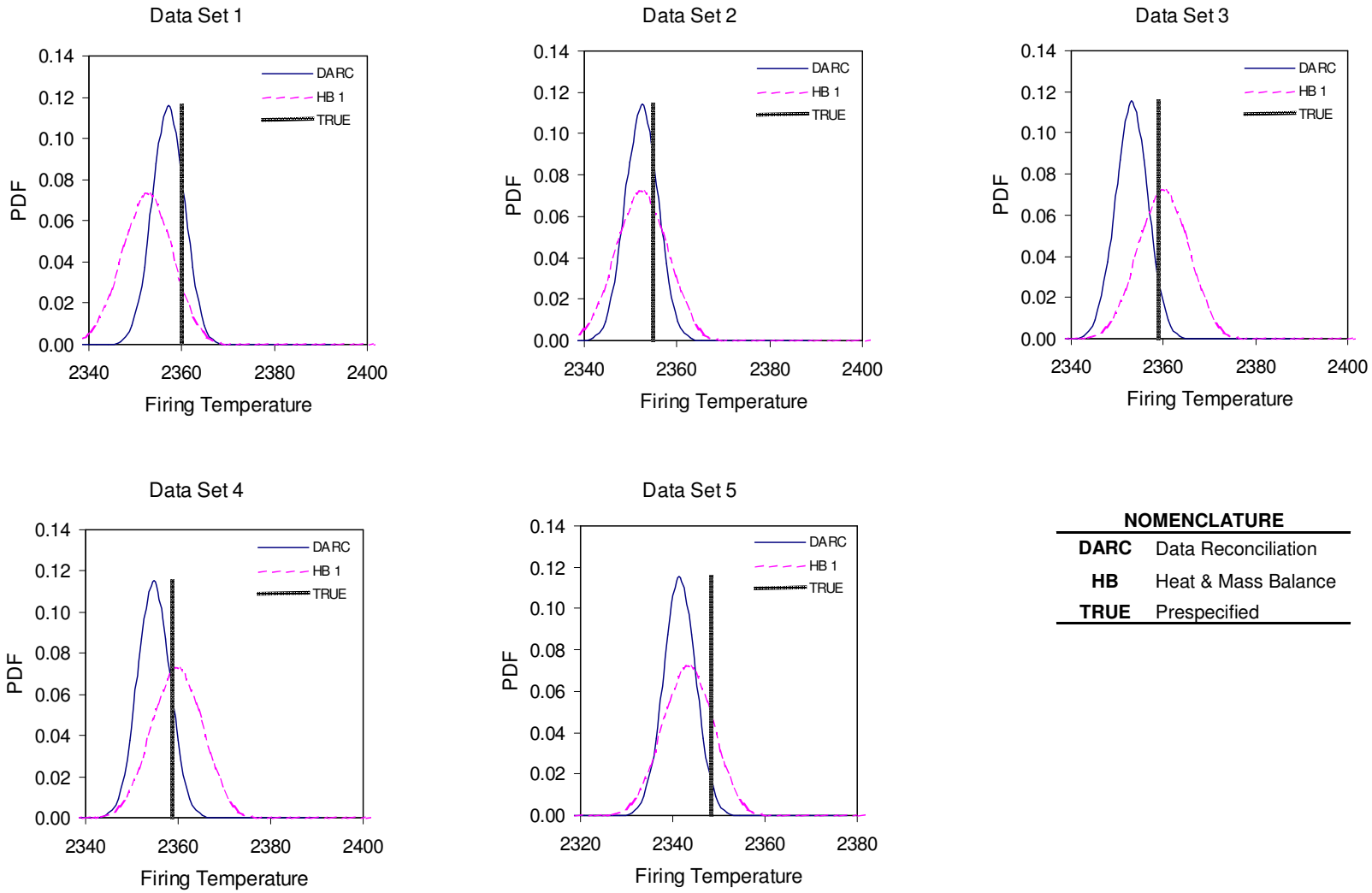

NOMENCLATURE

DARC	Data Reconciliation
HB	Heat & Mass Balance
TRUE	Prespecified

Figure 6-49: Estimated firing temperatures and estimate uncertainties by smeared data reconciliation subject to three gross errors

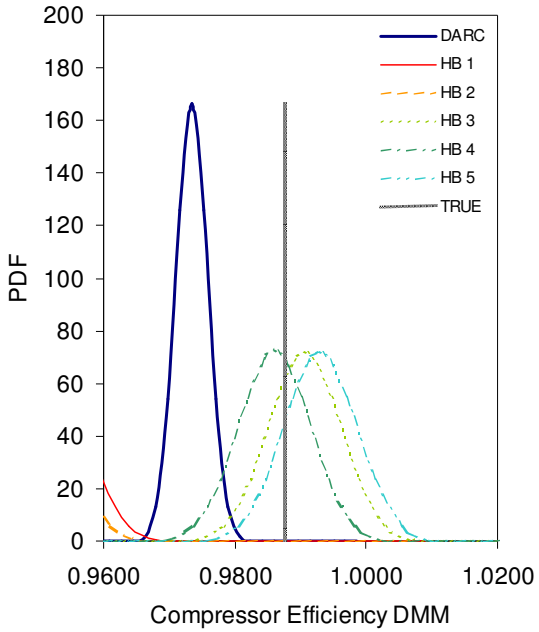

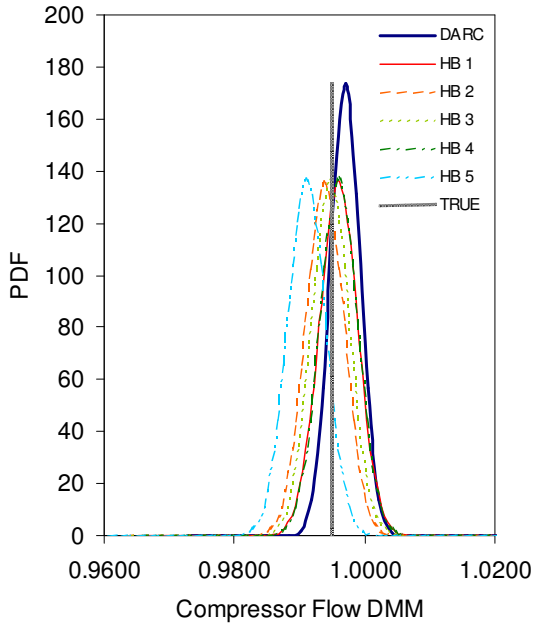

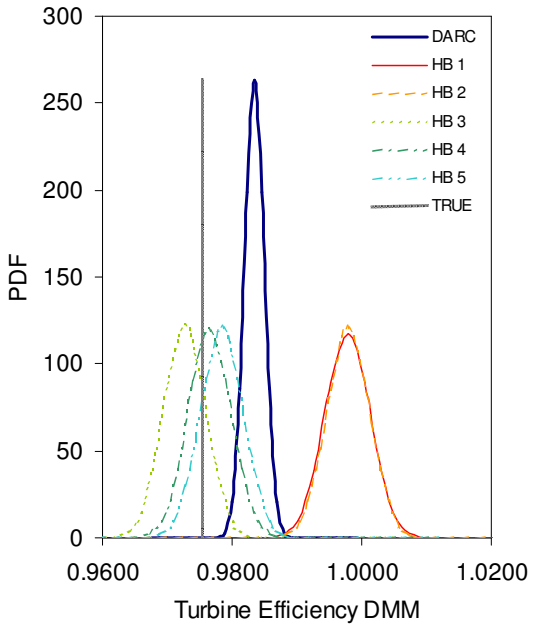

NOMENCLATURE	
DARC	Data Reconciliation
HB 1~5	Heat & Mass Balance for Data Set 1 ~5
TRUE	Prespecified

Figure 6-50: Estimated performance multipliers and estimate uncertainties by smeared data reconciliation subject to three gross errors

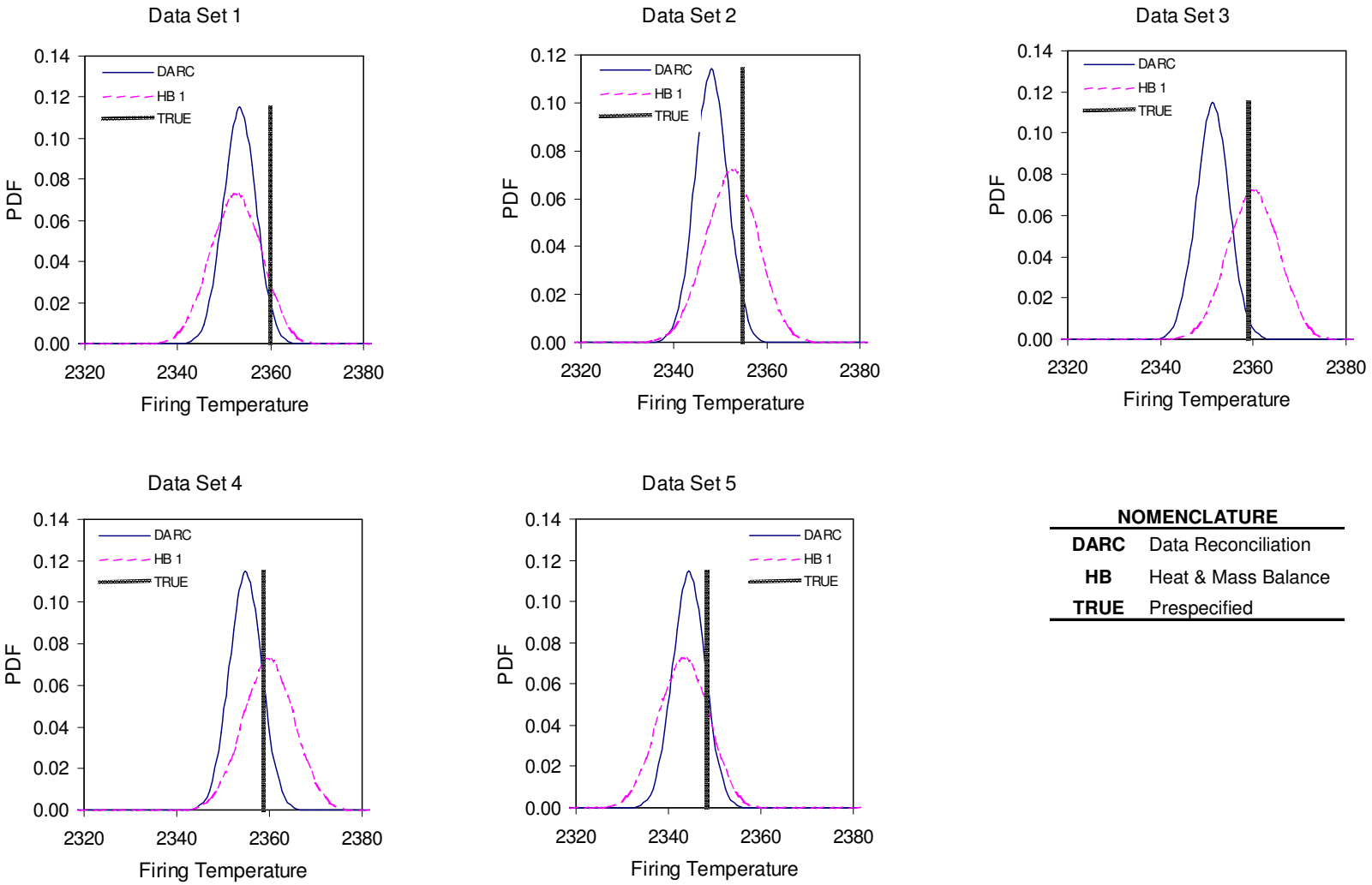

NOMENCLATURE	
DARC	Data Reconciliation
HB	Heat & Mass Balance
TRUE	Prespecified

Figure 6-51: Estimated firing temperatures and estimate uncertainties by using robust *M*-estimator subject to three gross errors

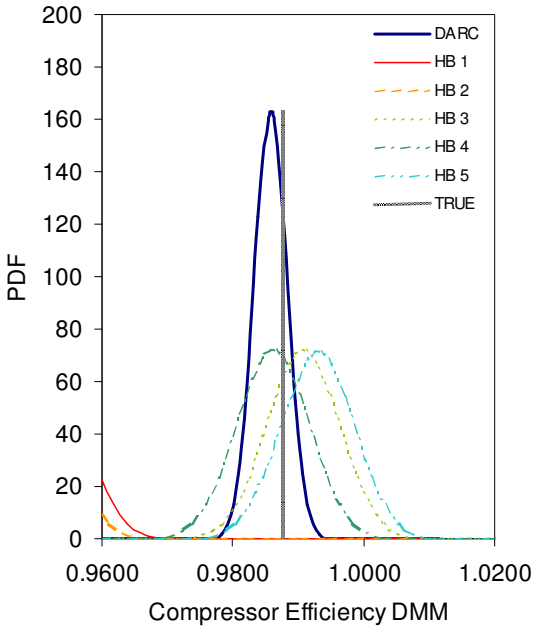

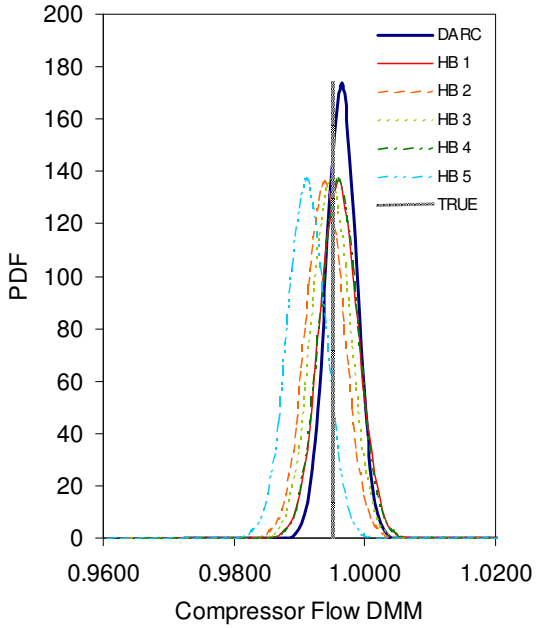

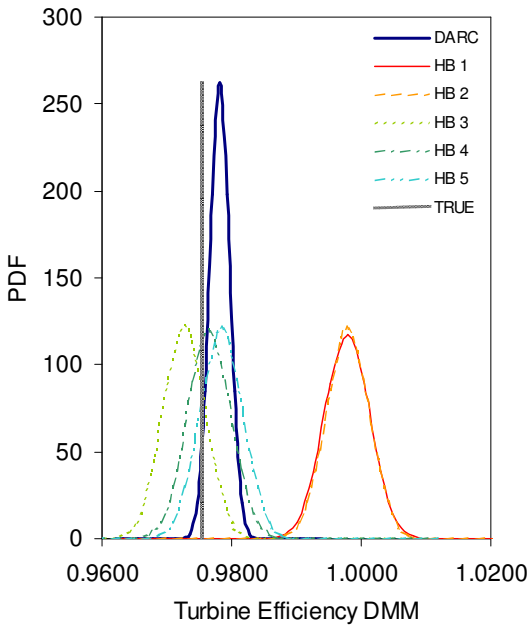

NOMENCLATURE	
DARC	Data Reconciliation
HB 1~5	Heat & Mass Balance for Data Set 1 ~5
TRUE	Prespecified

Figure 6-52: Estimated performance multipliers and estimate uncertainties by using robust *M*-estimator subject to three gross errors

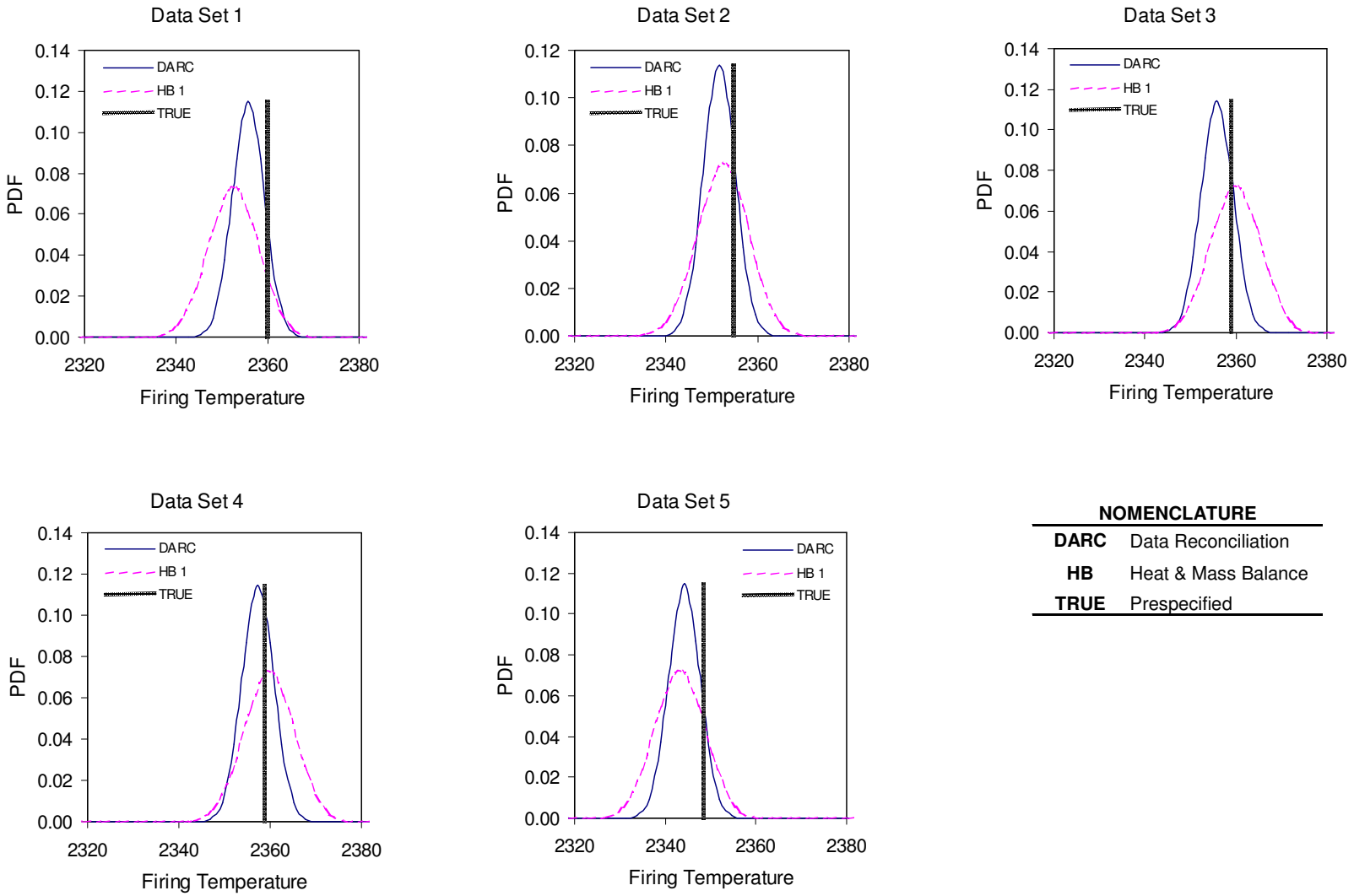

NOMENCLATURE

DARC	Data Reconciliation
HB	Heat & Mass Balance
TRUE	Prespecified

Figure 6-53: Estimated firing temperatures and estimate uncertainties by using serial bias compensation subject to three gross errors

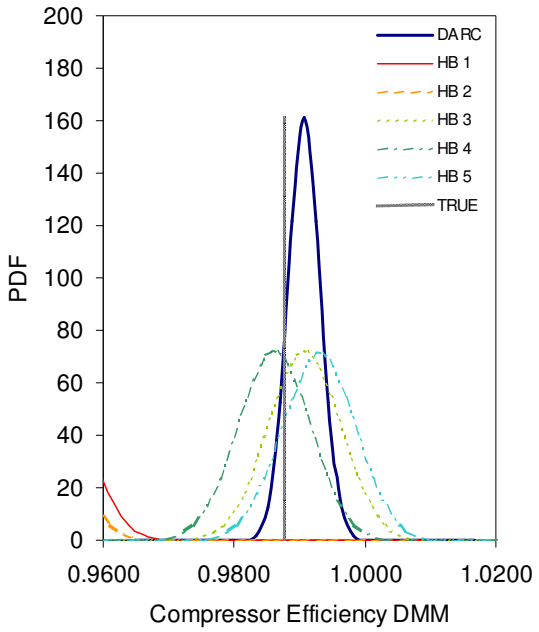

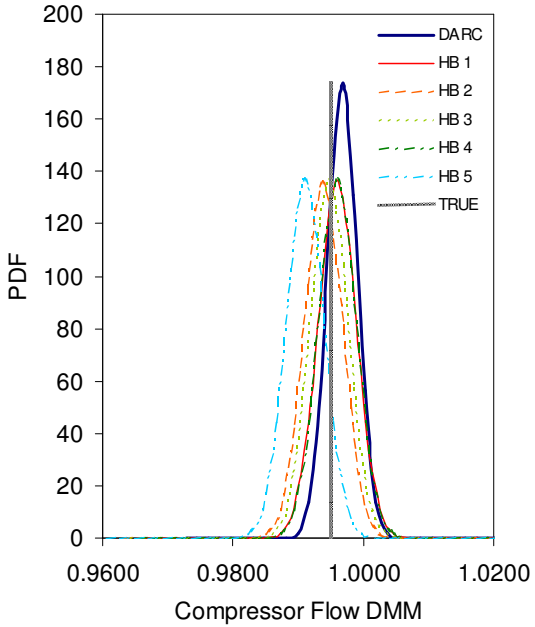

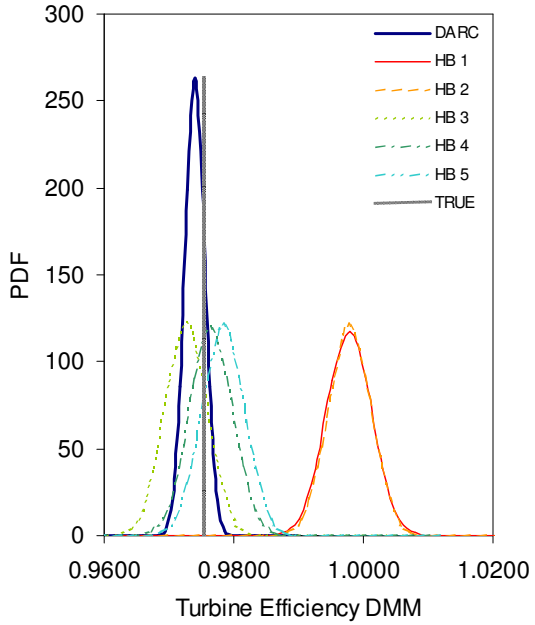

NOMENCLATURE	
DARC	Data Reconciliation
HB 1~5	Heat & Mass Balance for Data Set 1 ~5
TRUE	Prespecified

Figure 6-54: Estimated performance multipliers and estimate uncertainties by using serial bias compensation subject to three gross errors

In this case of one measurement bias artificially imposed on the compressor discharge temperature, two gross error detection techniques were applied: the robust *M*-estimator method and the serial bias compensation method. The Hampel's redescending function was used in the robust *M*-estimator method, whereas the three tuning constants were given by a_H =1.3, b_H =2.6, and c_H =5.2, determined based on the AIC criteria.

In the serial bias compensation method, the hypotheses tests were carried out on all of the one-bias gross error models applied in each corresponding simultaneous data reconciliation & parameter estimation, in which the least squares objective function was used.

6.4. Case Study III: Heat Recovery Steam Generator (HRSG) - SDRMC

A generic single-train heat recovery steam generator (HRSG) with two pressure sections was chosen for the demonstration of simultaneous data reconciliation and degradation status estimation (*SDRDE*). Commercial heat balance software, GateCycle™, was utilized for the HRSG heat balance modeling, which also serves as a transfer function in the *SDRDE* process. Figure 6-55 shows the GateCycle™ heat balance model for this specific two-pressure HRSG configuration. It includes seven major components: high-pressure superheater, high-pressure evaporator, first high-pressure economizer, low-pressure superheater, low-pressure evaporator, second high-pressure economizer (on the top), and low-pressure economizer. These major HRSG components are actually a series of counter-flow heat exchangers that utilize the hot exhaust gas to heat steam/water inside the tubes.

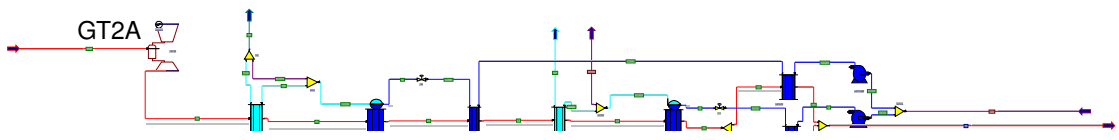

Figure 6-55: GateCycle™ heat balance model of a single train two-pressure HRSG

In the phase of heat balance modeling, the system configuration and detailed heat exchanger geometries of each HRSG component are used to size the HRSG at the design mode. In the off-design running mode, its performance is determined by gas turbine exhaust flow conditions, drum pressures, and degradation effects of the HRSG itself. In this demonstrative work it is assumed that the gas turbine flow parameters had been through the *SDRDE* process, and the reconciled values were taken directly as inputs to the HRSG heat balance model. On the other hand, HRSG drum pressures, which have significant impacts on the HRSG steam production, are determined from the steam turbine throttle in the case of no control valve at the turbine entrance. The values used for the model inputs of drum pressures can either be obtained from an independent data reduction or taken directly from measurements since measurements of steam pressures are quite accurate in the saturation conditions that exist in the evaporator drums. These values can also be validated by the measurements of the saturation temperature. By introducing the state equation of saturated steam, independent data reconciliation for both measured pressure and measured temperature can be carried out.

Except for taking the gas turbine exhaust conditions and HRSG drum pressures as known inputs to the HRSG heat balance model, there is, however, another option, which treats all of these parameters as unknown variables to be reconciled in the local *SDRDE* for the HRSG. The major drawback of doing this is increasing the number of variables to the local *SDRDE* optimizer. In addition, without reconciling these values in advance, uncertainties contributed from these variables would be propagated through the *SDRDE* process and cause larger uncertainties in the estimates. In the demonstration it is assumed that the gas turbine exhaust conditions and HRSG drum pressures had been through reconciliation process, and they are used as fixed model inputs.

6.4.1. Degradation Modeling

Once the gas turbine exhaust conditions and HRSG drum pressures are determined, either through a data reconciliation process or by the direct use of accurate measurements, the HRSG off-design performance only depends on the degradation status of the HRSG itself. Degradation occurs due to different reasons. One of them results from the gas turbine exhaust gas, which contains some chemicals in a form of ash and soot that can deposit on the outer surfaces of the heat exchangers in the major HRSG components. In addition, the impurities of the water will also deposit on the inner surfaces of the heat exchanger pipes. These represent major HRSG degradation effects called outer and inner surfaces fouling, and they lead to degradation in heat exchanger performance (effectiveness) and increased internal and external pressure drops.

The degradation effect of each HRSG component is modeled by adjusting its heat transfer correction factor. A heat transfer correction factor (HTC factor) is a performance multiplier used to adjust the overall heat transfer coefficient of a heat exchanger. In the modeling phase, the heat transfer coefficient of a HRSG heat exchanger is determined from the inputs of tube configuration and geometry. The need for adjustments of HTC factors comes when the off-design performance deviates from the measured data. Ideally, without any adjustment the heat balance model should give an off-design performance result that matches the precision test data measured at a new & clean status. But in reality, there is always a certain amount of deviation between the model-estimated heat transfer coefficient and the real heat transfer coefficient at the new and clean status. To calibrate the model at the new & clean status, the HTC factors are tuned until the model-estimated performance matches the precision test data. A calibration of the heat balance model to its new & clean precision test data is crucial because it provides the prior information of the heat transfer correction factors. In addition, a model calibration can tell whether the modeling is appropriate or not. A bad modeling (i.e. incorrect inputs of tube configuration and geometry) could cause a matching problem during the calibration

and force a recheck of the modeling process. After determining the new & clean HTC factors, these calibrated values are used to set the upper bounds in the data reconciliation of a degraded HRSG. Table 6-27 shows the calibrated values of HRSG heat transfer correction factors to the new & clean precision test data. The corresponding flow parameters affected by the HTC factors are listed as well. Since actual precision test data obtained from actual tests are proprietary and not allowed for disclosure, "pseudo-data" were used in the demonstration.

Table 6-27: Calibrated heat transfer correction factors

Heat Transfer Correction Factors	New & Clean HTC Values	Correspondant Flow parameters
HP Superheater HTC	1.054	HPSHT Steam Outlet Temperature
HP Evaporator HTC	0.94	HPEVP Steam Production
1st HP Economizer HTC	0.805	HPECO1 Water Outlet Temperature
2nd HP Economizer HTC	1.097	HPECO2 Water Outlet Temperature
LP Superheater HTC	0.72	LPSHT Steam Outlet Temperature
LP Evaporator HTC	1.112	LPEVP Steam Production
LP Economizer HTC	1.035	LPECO Water Outlet Temperature

6.4.2. Sensitive Studies of The HRSG Degradation Effects

The objective of performing sensitivity studies on the heat transfer correction factors is to provide a clear view of how the degradation of each HRSG component has an impact on the major flow parameters in the bottoming cycle and on the whole plant performance. In the sensitivity study, a design of experiment (DOE) was carried out. The DOE was run for over one hundred of cases with different combinations of HTC factors. Several flow parameters and performance factors were investigated. These metrics included combined cycle efficiency (CC EFF), heat rate (CC HR), steam turbine power (ST POWER), high-pressure steam flow rate (HP STEAM FLOW), low-pressure steam flow rate (LP STEAM FLOW), and stack temperature (STACK TEMP). The results were analyzed by the commercial statistical software, JMP 5.0™, and given in a form of "prediction profilers" presented in Fig. 6-56. Prediction profilers present the trends of metric variations subject to the change of each independent variable. In a prediction profiler the impact of an independent variable on the dependent output can be identified

by the gradient of the curve: a large gradient suggests a significant impact and vice versa. From the results shown in Fig. 6-56, significant impacts can be recognized for 1st high-pressure economizer degradation and high-pressure evaporator degradation on the overall plant performance and the major bottoming cycle flow parameters. The results can be interpreted in two different ways. One is that, with a limited budget, upgrading the components that have larger impacts on overall performance will give a bigger performance benefit. The other is that the uncertainty of the estimated HTC factor that has larger impacts on model-calculated flow parameters during the data reconciliation process is smaller compared to others. Figure 6-57~6-59 give closer views of how the degradations of some HRSG components affect the model-estimated flow parameters. These results disclose a crucial fact that the model-estimated plant performance and flow parameters will change when the degradation status of HRSG components change as well.

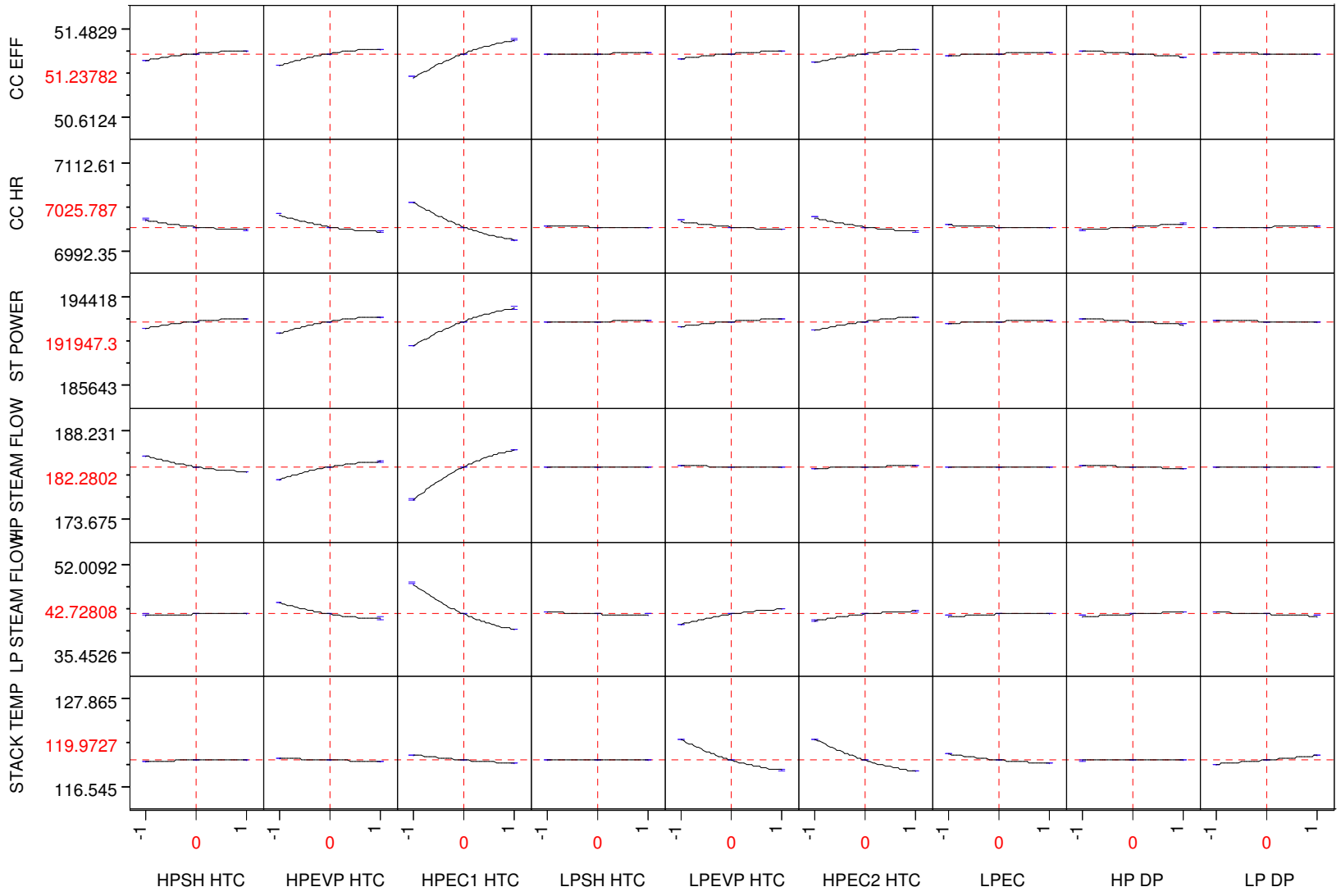

Figure 6-56: Prediction profilers for HRSG degradation effects

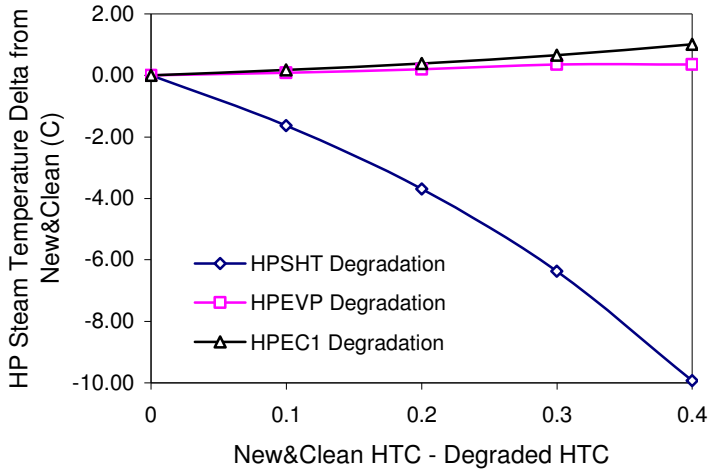

Figure 6-57: HRSG degradation effects on high-pressure steam outlet temperature

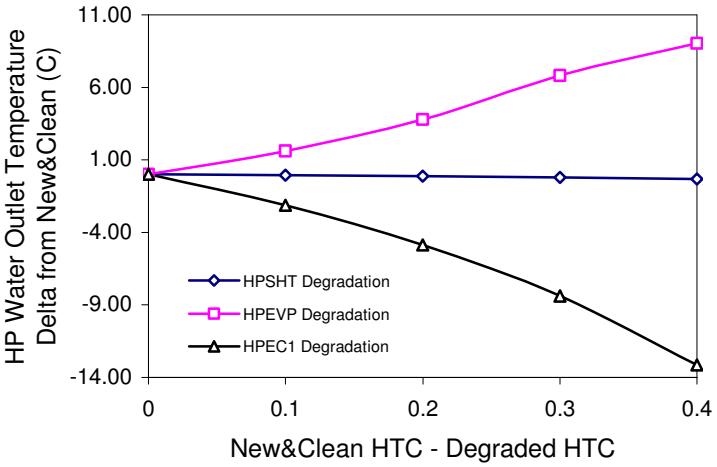

Figure 6-58: HRSG degradation effects on high-pressure water outlet temperature

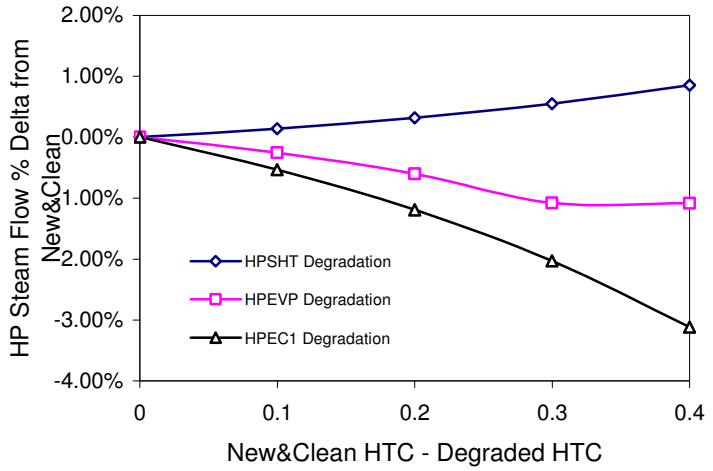

Figure 6-59: HRSG degradation effects on high-pressure steam production

6.4.3. Simultaneous Data Reconciliation and Degradation Status Estimation

The task is to perform *SDRDE* to reconcile the measurements and obtain a set of heat transfer correction factors for a degraded HRSG. A conclusion from the previous section states that the model-predicted performance changes if a different degradation status is applied. For example, when the HRSG has a certain degree of degradation, it produces less high-pressure steam, but the low-pressure steam production increases, with the assumption that gas turbine exhaust conditions remain the same. This is due to the fact that the degradation effect in the high-pressure section reduces the utilization of hot exhaust gas, and lets the gas with higher enthalpy passing through the following low-pressure section. Unless the low-pressure section degrades so badly, the positive impact from the higher energy gas will surpass the negative impact of the low-pressure section degradation. Thus, if a new & clean HRSG heat balance model is used to rectify the flow measurements obtained from a degraded plant during data reconciliation, the reconciled data will not be valid. On the other hand, we cannot have a clear idea of the current HRSG degradation level until its measured data is analyzed. Since the measurements are from the degraded HRSG, they are the only sources that can be used to evaluate the current HRSG degradation level. There are, however, measurement uncertainties and biases that could corrupt the estimation of the current status. Thus, in order to reconcile the measurements by a heat balance model with unknown degradation status, data reconciliation and degradation estimation must be carried out simultaneously. Before knowing the actual degradation, there are infinite degradation statuses (i.e., infinite sets of HRSG HTC factors) that can be applied to close the heat balance. There is, however, one that gives the model-estimated flow parameters that have the least deviations from the measurements. The deviations are evaluated by the maximum likelihood function constructed by the probability distribution functions assumed for the measurements. The objective of simultaneous data reconciliation and degradation estimation (*SDRDE*) is to

maximize the likelihood function by varying the HTC factors, which represent the degradation status of each HRSG component.

In this demonstration, pseudo data were utilized. To generate pseudo data for a degraded HRSG, a set of HRSG HTC factors was assigned artificially in the heat balance model to simulate a certain degree of degradation. A set of "perfect measurements" was first generated from running the heat balance model. By applying typical measurement uncertainties to the "perfect data" with the assumption of normal distributions, a set of "pseudo measurements" can be generated by means of a random number generator. The calibrated new & clean HRSG HTC factors were used as initial values as the *SDRDE* process started. During *SDRDE*, the optimizer searched for the optimum set of HTC factors that minimized the deviations of reconciled flow parameters from the pseudo measurements.

Before *SDRDE* can be carried out, redundancy availability needs to be checked in advance. Measurement redundancy occurs when more data than necessary is available to do the heat balance analysis. In the example of a two-pressure HRSG with seven components, the HTC factors can be uniquely determined from the measurements of those seven corresponding flow parameters listed in table 6-27. If there are no redundant measurements available, it becomes a pure data matching process. In this situation, the uncertainties of the measurements are propagated without any mitigation (or damping effect) through the matching process to the estimated HTC factors. Especially when a gross error occurs, the estimation of heat transfer correction factors is biased because the grosser are propagated directly through the matching process.

On the other hand, if the redundant measurements are available, the *SDRDE* process can be introduced. The uncertainty propagations can be mitigated by the redundant measurements as well. For example, the measurement of steam flow has a direct impact on determining the HTC factor of an evaporator. The steam flow can be measured either at the evaporator outlet or at the superheater exit. Or, the feed water flow

can be measured at the exit of the feed water pump. By assuming there are no leakages from the pipelines or any type of blow down at the evaporator, all these measurements indicate the steam production of the evaporator, and theoretically they should all give the same values. But due to the measurement uncertainties and/or gross errors, there are always inconsistencies among these measured values. The *SDRDE* is, therefore, carried out to reconcile the least deviations from all these three measured values. The process is very similar to a curve fit problem – obtaining a set of curve parameters (coefficients) and using them to estimate the means. In the case when one of these measurements has a gross error during the *SDRDE* process, the contamination effect can be mitigated by the other two measurements without gross errors. Thus, to make the data reconciliation and degradation estimation less sensitive to the gross errors, redundant measurements are necessary for each of these HRSG components. The redundant measurements could be at the steam side or gas side as long as they are directly affected by the degradation status of the HRSG.

Once the gas turbine exhaust conditions, drum pressures, and other operation conditions (depending on how detailed the HRSG is modeled) are decided, the HRSG heat balance model should be able to give the model-calculated values of those flow parameters listed in table 6-27, which could have the same values as other redundant measurements. For those redundant measurements made for the same flow parameter at different locations, their model-calculated values share the same function of HRSG heat transfer correction factors. For example, if the leakages and blow-down flows are ignored, the superheater and evaporator should have the same steam flows, and have the same function for the degradation factors,

$$\overline{w}_{sph} = \overline{w}_{evp} = \overline{w}_{fdw} = \overline{f}\,(c_1, c_2, c_3 \ldots\ldots\ldots\ldots, c_n) \tag{6-31}$$

SDRDE is a probabilistic data matching technique. It accounts for the measurement uncertainties. The uncertainty of a measurement is usually assumed to have a normal

distribution. As we repeatedly measure a flow parameter whose value is also a function of degradation factors, the measured value is normally is found distributed about a mean with a probability of ~68% that any single measurement of the flow parameter would be within one standard deviation of the mean. By making a number of measurements for a certain flow parameter at a certain location, an estimate can be made of its mean value with any desired precision. *The task is to determine the mean value of the flow parameter with an uncertainty characterized by the standard deviation of the Normal distribution of the measured data.* This determined mean value represents the same mother population from which the measured value comes. As mentioned above, this type of problem is similar to the curve-fitting problem. *SDRDE* is actually a process to find the values of the HRSG degradation factors (HTC factors) that minimize the discrepancy between the measured value, f_i, and the estimated mean value, $\overline{f_i}$, which is calculated by the heat balance model and is a function of the HTC factors.

Since the HRSG heat balance model is utilized to perform *SDRDE*, heat and mass balances are always satisfied during the iteration process. In *SDRDE*, it is desired to extract the most probable estimates for the degradation factors, and before proceeding, the criteria of the minimal discrepancy between the measured and model-calculated values needs to be defined. For any set of the HTC factors, the differences between the measured and model-calculated flow parameters being reconciled can be calculated. With well-chosen HTC factors, the discrepancies should be relatively small.

In *SDRDE*, the method of maximum likelihood, or M-estimator, is used to search for the optimum set of HTC factors that gives the minimum discrepancies. It is assumed that each measured value, f_i, is from a Normal distribution with a mean, $\overline{f_i}(c_1, c_2, c_3 \ldots\ldots\ldots, c_n)$, and a standard deviation σ_i, where $\overline{f_i}(c_1, c_2, c_3 \ldots\ldots\ldots, c_n)$ represents the model-calculated value as a function of HTC factors, $c_1, c_2, c_3 \ldots\ldots\ldots, c_n$.

By assuming the Normal distribution, the probability p_i of making the measurement f_i with a standard deviation σ_i about the mean $\overline{f}_i(c_1,c_2,c_3.....,c_n)$ is given by

$$p_i = \frac{1}{\sigma_i\sqrt{2\pi}} exp\left\{-\frac{1}{2}\left[\frac{f_i-\overline{f}_i(c_1,c_2,c_3.....,c_n)}{\sigma_i}\right]^2\right\} \tag{6-32}$$

The probability of making all measurements at different measuring points (including the redundant measurements) is the product of the probabilities for each observation at its measuring point:

$$p = \prod\left(\frac{1}{\sigma_i\sqrt{2\pi}}\right) exp\left\{-\frac{1}{2}\sum\left[\frac{f_i-\overline{f}_i(c_1,c_2,c_3.....,c_n)}{\sigma_i}\right]^2\right\} \tag{6-33}$$

Equation (6-33) is defined as a likelihood function. The objective of *SDRDE* is to find the optimum set of HRSG HTC factors, $c_1,c_2,c_3.....,c_n$, that maximizes the likelihood function given in Equation (6-33). Maximizing Equation (6-33) is equivalent to minimizing the sum in the exponential. The sum can be defined as the goodness-of-fit parameter χ^2:

$$\chi^2 = \sum\left[\frac{f_i-\overline{f}_i(c_1,c_2,c_3.....,c_n)}{\sigma_i}\right]^2 \tag{6-34}$$

Now the task is to find out a set of HRSG HTC factors that minimizes χ^2. The magnitude of χ^2 is determined by the measurement uncertainties, σ_i, and the differences between measured data and model-calculated values. The optimum values of HTC factors, c_j^*, are obtained by minimizing χ^2 simultaneously with respect to each HTC factor, c_j:

$$\begin{aligned}\frac{\partial\chi^2}{\partial c_j} &= \frac{\partial}{\partial c_j}\sum\left[\frac{f_i-\overline{f}_i(c_1,c_2,c_3.....,c_n)}{\sigma_i}\right]^2 = 0\\ &= -2\sum\left[\frac{1}{\sigma_i^2}\left[f_i-\overline{f}_i(c_1,c_2,c_3.....,c_n)\right]\frac{\partial\overline{f}_i(c_1,c_2,c_3.....,c_n)}{\partial c_j}\right]\end{aligned} \tag{6-35}$$

Taking partial derivatives of χ^2 with respect to each HTC factor gives *n* coupled equations for *n* unknown HTC factors. Since these equations are nonlinear, linearization techniques or nonlinear programming methods are needed to solve the problem. The *SDRDE* process can then be expressed by a typical nonlinear unconstrained optimization problem with upper bounds on the variables:

$$\textbf{\textit{Minimize}}: \sum \left[\frac{f_i - \overline{f_i}(c_1, c_2, c_3 \ldots\ldots\ldots, c_n)}{\sigma_i} \right]^2$$

$$\textbf{\textit{Subject to:}}\ c_j < c_{j(New\ \&\ Clean)}$$

(Upper bounds set by calibrated new & clean HTC factors)

$$\textbf{\textit{By varying:}}\ c_j$$

$f_i = [f_1, f_2, f_3 \ldots, f_n]$: *Measured flow parameters*

$\overline{f_i} = [\overline{f_1}, \overline{f_2}, \overline{f_3} \ldots, \overline{f_n}]$: *Model-calculated flow parameters*

To keep the HTC factors within physically allowable ranges during the *SDRDE* process, upper bounds set by calibrated new & clean HTC factors are imposed.

To deal with correlations among the HRSG HTC factors, a conjugate-gradient search was chosen to perform the optimization. The algorism was coded by the VB scripts and built in the user-defined optimization component in Model Center 4.0™, which is a commercial software product that wraps up the simulation tools and optimization drivers. A Model Center ™ module was built by connecting the HRSG heat balance model built from GateCycle™ to a local optimizer performing a conjugate-gradient search. A screenshot of the *SDRDE* Model Center ™ module of the HRSG is given in Fig. 6-60.

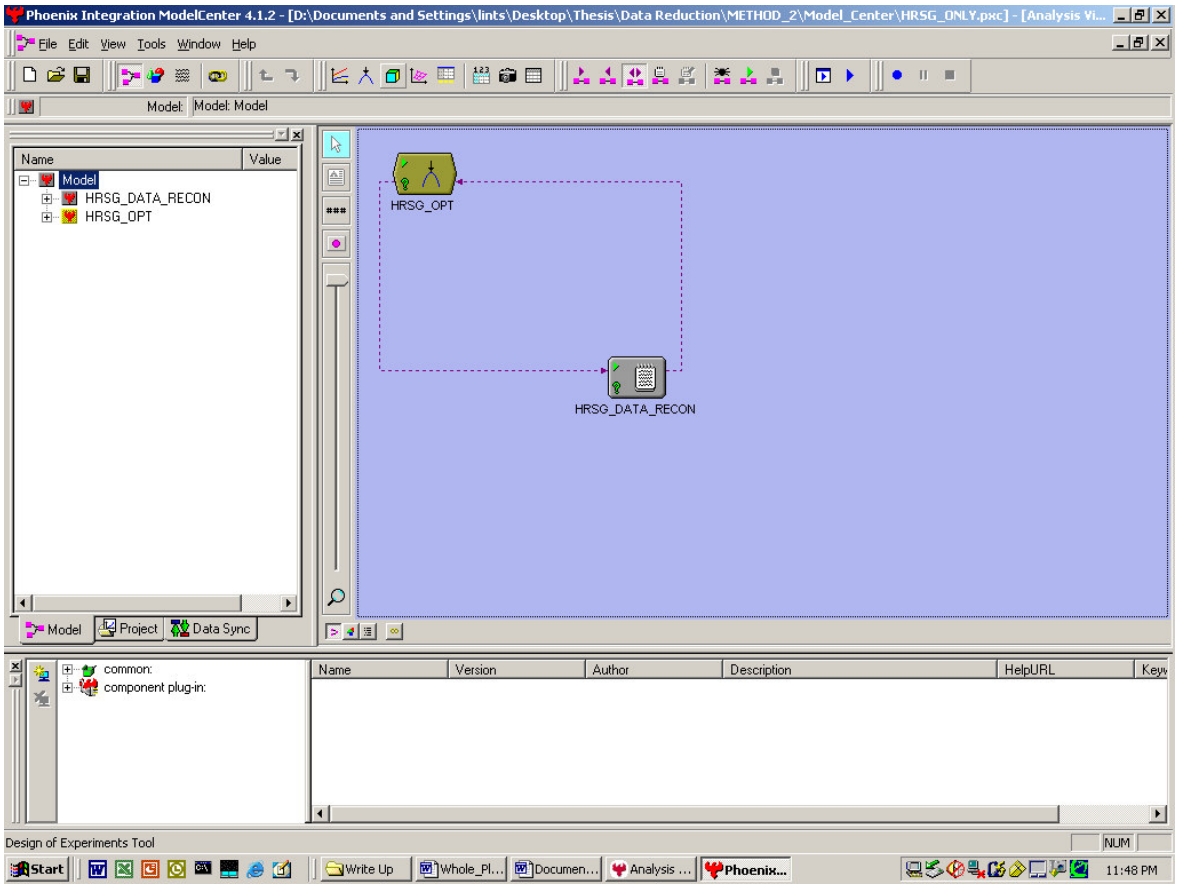

Figure 6-60: *SDRDE* Model Center ™ model for HRSG

As mentioned earlier, in this demonstration gas turbine exhaust conditions are assumed to have been reconciled. In addition, it was assumed that measurements of the HRSG drum pressures were very accurate. Therefore, these values were treated as known values and used as fixed inputs to the HRSG heat balance model during *SDRDE*. Figures 6-61 and 6-62 show variations of the goodness-of-fit parameter χ^2, and the HRSG HTC factors during the iterations in the *SDRDE* process. The HRSG HTC factors varied from their initial new & clean calibrated values to the final estimated results, which were very close to the specified degraded values. Due to the uncertainties imposed to the "perfect measurements", the final estimated values did not exactly match the specified values, but the deviations were within the estimation uncertainties.

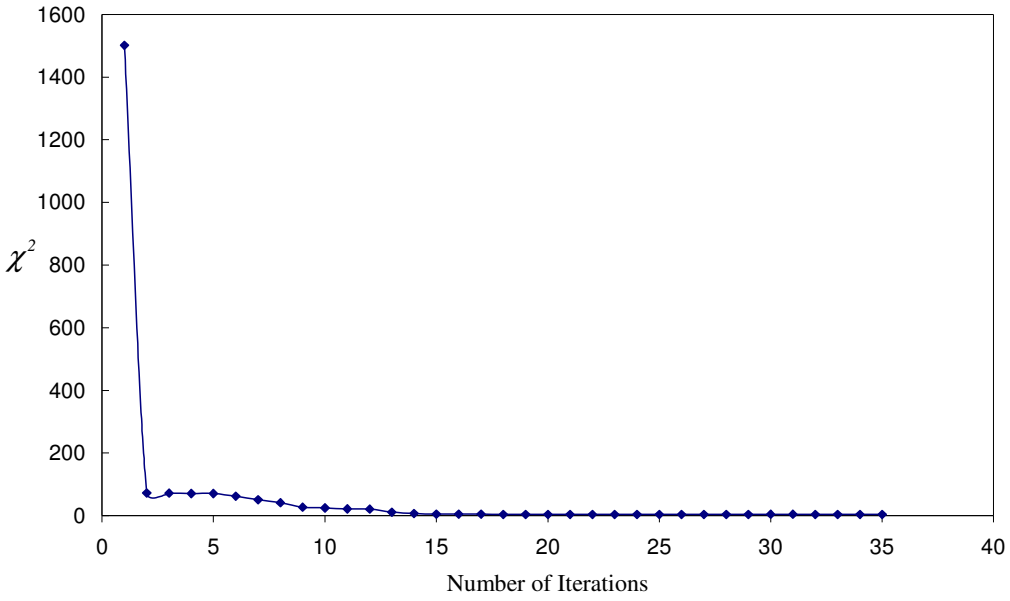

Figure 6-61: Variation of χ^2 during data reconciliation

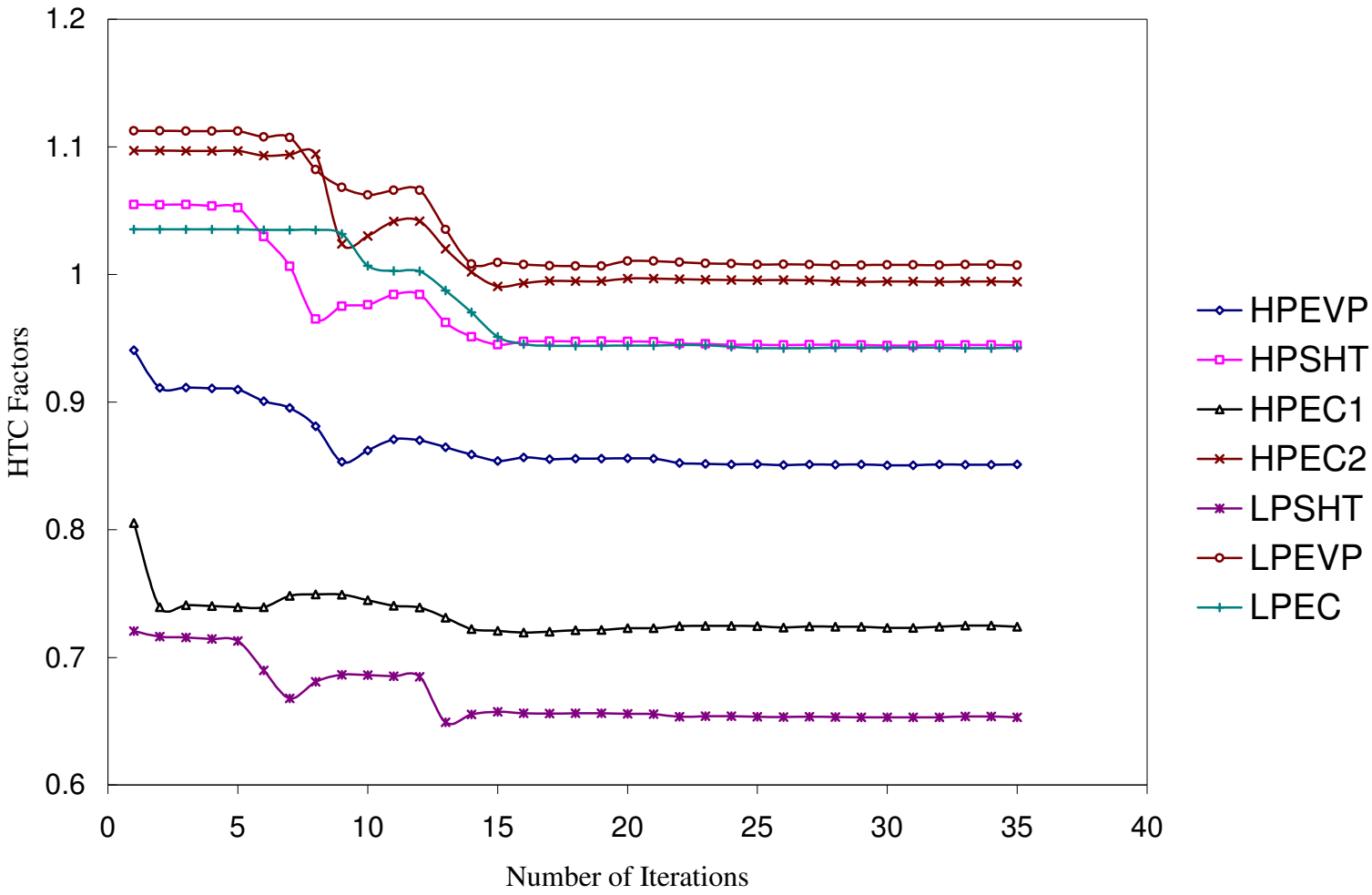

Figure 6-62: Variations of the HTC factors during data reconciliation

6.4.4. Uncertainties of Estimates

Through the SDRDE process, propagations of uncertainties were mitigated. By utilizing the error propagation principle, the uncertainties of estimated HRSG HTC factors were investigated as well. During *SDRDE*, each of the measured data was used to estimate HRSG HTC factors and contributed its own uncertainty in the process. For a sufficiently large event sample, the likelihood function becomes a Normal function of each HTC factor centered on its value that minimizes χ^2 :

$$P(c_j) = A e^{-(c_j - c'_j)^2 / 2\sigma_i^2} \tag{6-36}$$

In Equation (6-36), "*A*" is a function of the other HTC factors c_m for $m \neq j$. The function of goodness-of-fit parameter, χ^2 (Equation (6-34)) can be rewritten as:

$$\chi^2 = -2\,ln\left[P(c_1, c_2, c_3, \ldots c_n)\right] + 2\sum ln(\sigma_i \sqrt{2\pi}) \tag{6-37}$$

From Equation (6-36), Equation (6-37) can be rewritten as:

$$\chi^2 = \frac{\left(c_j - c'_j\right)^2}{\sigma_j^2} + K \tag{6-38}$$

Equation (6-38) gives the variation of χ^2 with respect to the HTC factor c_j in the vicinity of its minimum. The constant K is a function of measurement uncertainties σ_i and the HTC factor c_m for $m \neq j$. The uncertainties of the estimated HTC factors can be then calculated by taking the second derivative of χ^2 in Equation (6-38) and inversing it:

$$\sigma_j^2 = 2\left(\frac{\partial^2 \chi^2}{\partial c_j^2}\right)^{-1} \tag{6-39}$$

Since the estimated HTC factors are correlated, the second derivative of χ^2 with respect to c_j in Equation (6-39) must be under the condition that other HTC factors c_m for $m \neq j$ must be at their optimum values that minimize χ^2. Under this condition the

variation of χ^2 near its minimum value with respect to c_j can be approximated by a parabola passing through three points including the optimum point:

$$\chi^2 = d_1 + d_2 c_j + d_3 c_j^2 \tag{6-40}$$

Once the values of χ^2, $\chi_1^2 = \chi(c_{j1})$, $\chi_2^2 = \chi(c_{j2})$, and $\chi_0^2 = \chi(c_j^{*'})$ are obtained, where $c_{j1} = c_j^* + \Delta c_j$, $c_{j2} = c_j^* + 2\Delta c_j$ and χ_0^2 is the minimum value of χ^2 at the optimum $c_j = c_j^*$, the three coefficients, d_1, d_2 and d_3 can be obtained. To calculate the uncertainty of the estimated HTC factor from Equation (6-39) only the coefficient d_3 needs to be known:

$$\sigma_j^2 = 2\left(\frac{\partial^2 \chi^2}{\partial c_j^2}\right)^{-1} = d_3^{-1} = \left(\frac{\chi_0^2 - 2\chi_1^2 + \chi_2^2}{2\Delta c_j{}^2}\right)^{-1} \tag{6-41}$$

Table 6-28 shows values of the HTC factors during the iterations and the uncertainties of estimated values. In table 6-29, values of the new & clean, specified degraded, and *SDRDE* estimated HRSG HTC factors with two-sigma uncertainties are compared.

Table 6-28: Convergence history and uncertainties of the HTC factors

Gas Turbine Exhaust Flow	839	lb/sec
Gas Turbine Exhaust Temperature	1040	F
HP Drum Pressure	72.35	barg
LP Drum Pressure	3.92	barg

		Heat Transfer Correction Factors (HTC Factors)						
Iteration		HPSHT	HPEVP	HPEC1	HPEC2	LPSHT	LPEVP	LPEC
1		1.0549	0.9406	0.8053	1.0971	0.7206	1.1126	1.0353
2		1.0547	0.9111	0.7395	1.0971	0.7165	1.1126	1.0353
3		1.0549	0.9114	0.7409	1.0970	0.7156	1.1124	1.0353
4		1.0537	0.9108	0.7403	1.0970	0.7146	1.1124	1.0353
5		1.0524	0.9098	0.7394	1.0970	0.7130	1.1124	1.0353
6		1.0295	0.9007	0.7395	1.0933	0.6900	1.1079	1.0348
7		1.0062	0.8954	0.7484	1.0939	0.6679	1.1073	1.0348
8		0.9650	0.8811	0.7495	1.0945	0.6809	1.0823	1.0348
9		0.9751	0.8533	0.7493	1.0239	0.6864	1.0683	1.0316
10		0.9761	0.8622	0.7448	1.0301	0.6863	1.0625	1.0068
11		0.9842	0.8709	0.7406	1.0418	0.6852	1.0660	1.0026
12		0.9841	0.8702	0.7392	1.0419	0.6848	1.0661	1.0025
13		0.9623	0.8645	0.7312	1.0199	0.6490	1.0352	0.9873
14		0.9511	0.8590	0.7222	1.0019	0.6553	1.0082	0.9702
15		0.9449	0.8540	0.7209	0.9906	0.6572	1.0093	0.9511
16		0.9475	0.8566	0.7196	0.9930	0.6562	1.0077	0.9455
17		0.9477	0.8552	0.7203	0.9950	0.6560	1.0068	0.9440
18		0.9475	0.8557	0.7213	0.9948	0.6560	1.0066	0.9440
19		0.9477	0.8558	0.7215	0.9947	0.6560	1.0065	0.9439
20		0.9474	0.8560	0.7229	0.9967	0.6556	1.0103	0.9442
21		0.9473	0.8557	0.7229	0.9967	0.6555	1.0103	0.9443
22		0.9459	0.8524	0.7246	0.9962	0.6533	1.0096	0.9448
23		0.9456	0.8515	0.7247	0.9958	0.6538	1.0086	0.9446
24		0.9449	0.8513	0.7247	0.9955	0.6539	1.0084	0.9434
25		0.9450	0.8513	0.7245	0.9954	0.6533	1.0076	0.9422
26		0.9448	0.8508	0.7235	0.9955	0.6532	1.0079	0.9423
27		0.9450	0.8513	0.7243	0.9954	0.6533	1.0077	0.9422
28		0.9449	0.8510	0.7242	0.9946	0.6532	1.0072	0.9426
29		0.9447	0.8511	0.7241	0.9943	0.6530	1.0072	0.9426
30		0.9443	0.8505	0.7231	0.9944	0.6530	1.0074	0.9426
31		0.9443	0.8505	0.7231	0.9944	0.6530	1.0074	0.9426
32		0.9447	0.8511	0.7241	0.9943	0.6530	1.0072	0.9426
33		0.9446	0.8509	0.7251	0.9944	0.6535	1.0076	0.9422
34		0.9446	0.8509	0.7251	0.9944	0.6535	1.0076	0.9422
35	**Optimum**	0.9445	0.8511	0.7241	0.9943	0.6530	1.0072	0.9426
Uncertainty		***0.0163***	***0.0037***	***0.0019***	***0.0087***	***0.0103***	***0.0065***	***0.0161***

Table 6-29: HRSG HTC factors for new & clean, specified degraded, and estimated values

Heat Transfer Correction Factors (HTC factors)

	New & Clean	Specified Degraded	Estimated	Uncertainties (2 Standard Deviations)
HPSPHT	1.05490005	0.949410045	0.944462917	0.032673133
HPEVAP	0.940559983	0.846503985	0.85106728	0.007416576
HPEC1	0.805339992	0.724805993	0.724113394	0.003784673
HPEC2	1.097100019	0.987390018	0.994289302	0.017477995
LPSPHT	0.720589995	0.648530996	0.652967073	0.020681705
LPEVAP	1.112599969	1.001339972	1.007226434	0.013043567
LPEC	1.035300016	0.931770015	0.942630512	0.032268709

Once the uncertainties of *SDRDE* estimated HRSG HTC factors are obtained, two-sigma uncertainty spans centered at their estimated values can be constructed. Figure 6-63 shows that all the specified degraded values of HRSG HTC factors are located within these two-sigma spans. This indicates that *SDRDE* makes a good estimation of the HRSG degradation status. Figure 6-63 also shows that the uncertainty of the estimated HTC factor of 1st high-pressure economizer has the smallest uncertainty. This matches the result of the sensitivity study presented by the prediction profiler. In the prediction profiler given in Fig 6-56, the 1st high-pressure economizer has the highest impact on its corresponding flow parameters, which suggests a wide range of measurement variation causes the least change in its heat transfer correction factor. The magnitudes of uncertainties for other HRSG HTC factors can be compared with their impact on flow parameters presented in the prediction profiler as well. The comparisons between the measured and reconciled values of major flow parameters are given in Fig. 6-64.

After the uncertainties of the estimated heat transfer correction factors (HTC factors) were obtained, these uncertainties to the estimated values were applied and carried out in a Monte Carlo Simulation. The objective is to determine the uncertainties of the reconciled flow parameters. By assuming the Normal distribution for each of the HTC factors, the resultant distributions of selected reconciled flow parameters,

obtained by the Monte Carlo Simulation with 500 trials, are given in Fig. 6-65. The results show significant reductions in uncertainties of the reconciled flow parameters. This validates the expectation for the significant uncertainty mitigations by *SDRDE*.

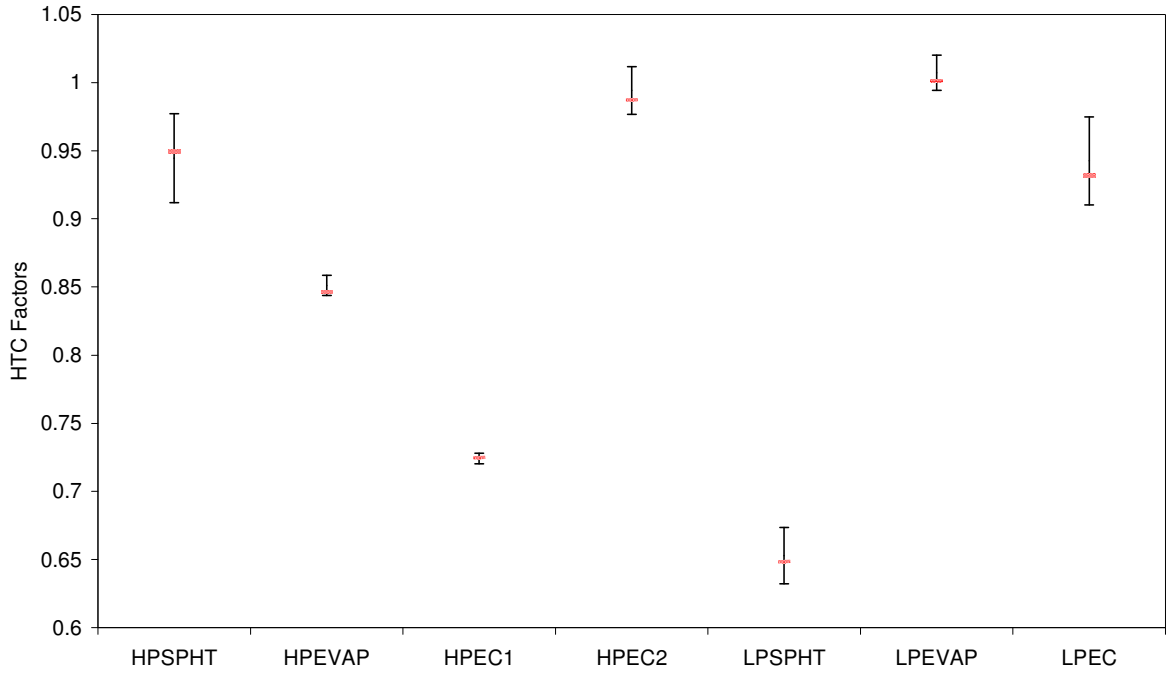

Figure 6-63: Specified HTC factors within ranges of uncertainties

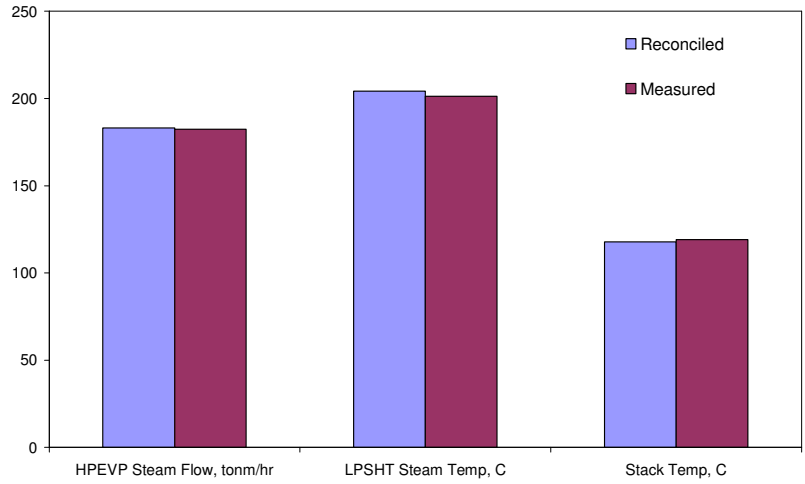

Figure 6-64: Comparisons of measured and reconciled values

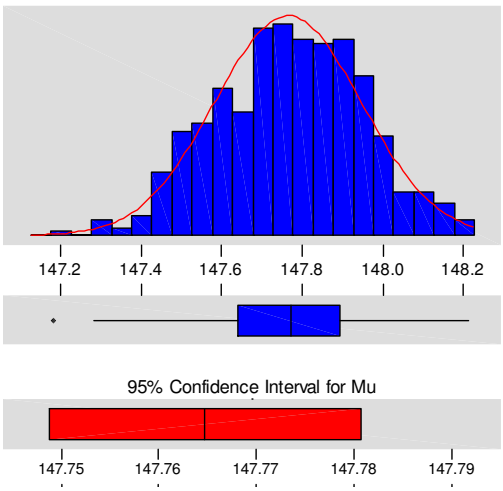

Variable: LPEC TEMP

Anderson-Darling Normality Test

A-Squared:	0.748
P-Value:	0.051
Mean	147.765
StDev	0.182
Variance	3.31E-02
Skewness	-1.2E-01
Kurtosis	-2.5E-01
N	500
Minimum	147.180
1st Quartile	147.640
Median	147.770
3rd Quartile	147.890
Maximum	148.210

95% Confidence Interval for Mu

147.749	147.781

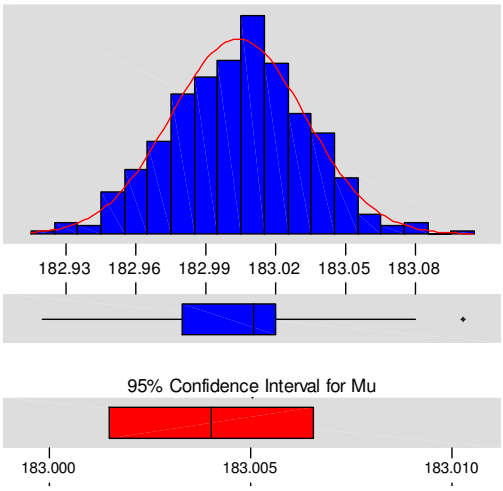

Variable: HPEVP FLOW

Anderson-Darling Normality Test

A-Squared:	2.627
P-Value:	0.000
Mean	183.004
StDev	0.029
Variance	8.26E-04
Skewness	-1.1E-02
Kurtosis	-2.9E-03
N	500
Minimum	182.920
1st Quartile	182.980
Median	183.010
3rd Quartile	183.020
Maximum	183.100

95% Confidence Interval for Mu

183.002	183.007

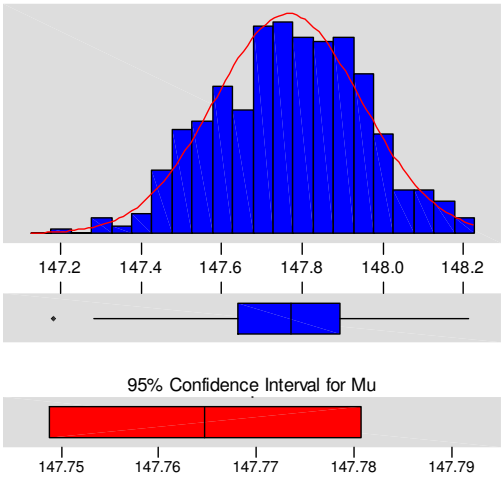

Variable: LPEC TEMP

Anderson-Darling Normality Test

A-Squared:	0.748
P-Value:	0.051
Mean	147.765
StDev	0.182
Variance	3.31E-02
Skewness	-1.2E-01
Kurtosis	-2.5E-01
N	500
Minimum	147.180
1st Quartile	147.640
Median	147.770
3rd Quartile	147.890
Maximum	148.210

95% Confidence Interval for Mu

147.749	147.781

Figure 6-65: Uncertainties of selected reconciled flow parameters

6.5. A Combined Strategy for Gross Error Detection

A comparison between two gross error detection techniques – robust *M*-estimator and serial bias compensation shows: with sufficient measurement redundancy and healthy data sets, both techniques are able to identify the locations of gross errors and estimate the corresponding magnitudes. The differences between estimated and designated bias magnitudes are less than 2-sigma of measurement uncertainties, which are caused mainly by random errors. Once subtracting the magnitudes of simulated random errors from the total adjustments, one can obtain the estimated gross error magnitudes very close to the designated values.

The *Hampel's Redescending M*-estimator outperforms the serial bias compensation technique in requiring less computation time. Unlike the serial hypotheses testing techniques, the robust *M*-estimator does not require a sequential scheme to detect multiple gross errors. In the robust *M*-estimator data reconciliation, the gross error effects are suppressed by the likelihood function itself as the measurements with gross errors fall into the flat zone in the influence function characterized by the robust *M*- estimator. Due to the fact that gross errors have very minor influence on the fitting function formed by the robust *M*-estimator, during data reconciliation the system optimizer moves the solutions toward the healthy data that fall into the steep zone of the influence function while doing very little adjustments to the data with gross errors that are being reconciled. In the end of the reconciliation process, the locations and magnitudes of all gross errors can be identified by comparing the reconciled data to he measured data directly. Therefore, only a single execution of data reconciliation is needed to detect all hidden gross errors when utilizing the robust *M*-estimator data reconciliation. The robust *M*-estimator, however, needs majority of healthy data to make the biased data fall in the flat region of the influence function. Sufficient measurement redundancy and healthy data sets are, therefore, required to

avoid false detections when using the robust *M*-estimator. If the number of faulty data sets outnumbers the healthy data sets, the healthy data will likely fall into the flat region of the influence function, and the biased data that fall in the steep region will drive the reconciliation toward the biased results. As the measurement redundancy and number of healthy data sets decrease, the robust *M*-estimator commits more false detections, and, as a result, the reconciliation results also become more sensitive to the initial values.

When using the serial bias compensation technique, a sequential process is required for hypothesis testing. In the case where multiple gross errors occur, the technique identifies each gross error in a series manner. At each round of hypotheses testing, the gross error model with the highest testing score goes to the next round of hypotheses testing for all scenarios with one more bias added. The process stops when no more gross error needs to be added to obtain a better testing score. Since each hypothesis testing needs a single execution of data reconciliation using the least squares objective function, which is insensitive to the initial values of reconciled data, it is expected the initial values of reconciled data have very little impacts on the reconciliation results in the serial bias compensation technique. In previous case study it was shown that even with very few healthy data sets, the serial bias compensation techniques still identified the locations of gross errors correctly although the estimated gross error magnitudes had errors in the ranges of more than 2-sigma. The main advantages of using the serial bias compensation technique are, therefore, its insensitivity to the initial values and the capability of identifying the locations of biases with insufficient healthy data sets and measurement redundancy. The biggest disadvantage is more computation time required.

The fast execution of robust *M*-estimator makes it suitable for the on-line performance monitoring system that is equipped with well-arranged instruments for measurement redundancy and has healthy data as majority. As the measurement

redundancy and number of healthy data sets are sufficient, the gross error detection rate of robust *M*-estimator is as good as the serial bias compensation technique. Most importantly, it requires less computation time as compared to the serial bias compensation technique, since only one single execution of data reconciliation is required.

On the other hand, the serial bias compensation technique is adequate to the off-line performance modeling and simulation especially when there are not sufficient redundancy and healthy instruments in the measurement system. Due to its insensitivity to initial values, the serial bias compensation technique commits less false detection than the robust *M*-estimator when lacking redundancy and healthy data sets.

One can combine these two GED techniques to form an integrated environment for model calibration and data reconciliation. In this integrated environment the robust *M*-estimator along with the system model serve as on-line performance monitoring package, which carries out model based data reconciliation and degradation monitoring. The drifted sensors that occur in a short time basis can be detected by the robust *M*-estimator as long as the measurement redundancy and number of healthy data sets are sufficient. After a period of time, during which significant degradation takes place and the number of healthy data sets deteriorates, the off-line model calibration and gross error detection are engaged to calibrate the model and detect the measurement biases. The serial bias compensation technique is less sensitive to the lack of healthy data sets and to the deviation from the original status due to degradation. It can be, therefore, utilized to perform simultaneous data reconciliation and model calibration off-line. Once the model has been recalibrated to reflect the current degradation status and the biased instruments have also been detected and calibrated, the robust *M*-estimator and the calibrated model are re-engaged to the on-line performance monitoring system. Figure 6-66 shows the process map of the integrated environment.

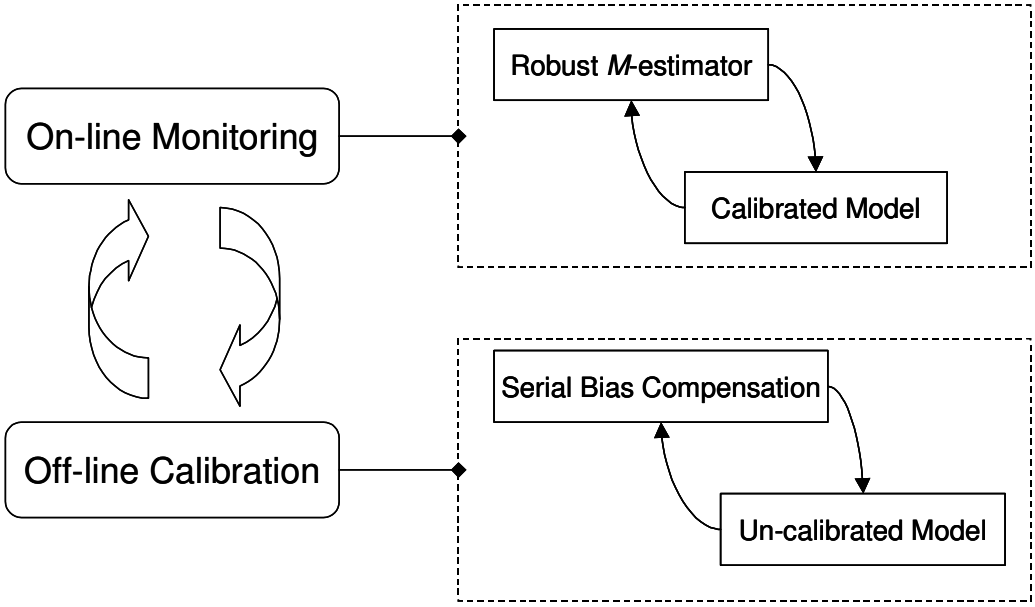

Figure 6-66: Integrated environment for on-line performance monitoring and model calibration

Figure 6-67 shows a generic long-term schedule for on-line performance monitoring and off-line model calibration, in which the two GED techniques are switched accordingly. In this long-term schedule the robust *M*-estimator is carried out continuously until the periodic off-line calibration executed by serial bias compensation is engaged. Once the off-line calibration is completed, the robust *M*-estimator is reengaged to the system again.

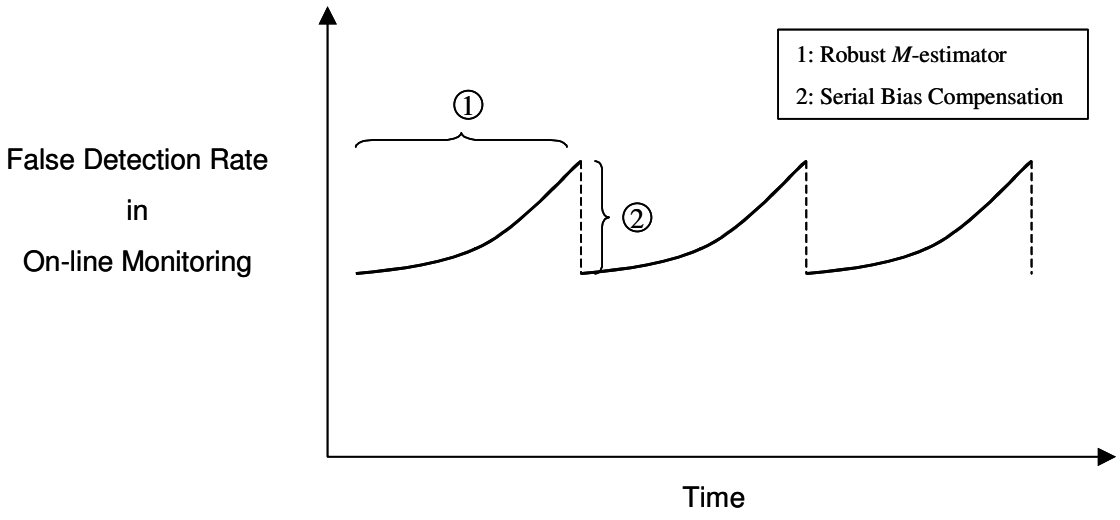

Figure 6-67: Generic long-term schedule for on-line performance monitoring and off-line model calibration

In summary, the robust M-estimator technique can be utilized in the on-line performance monitoring system due to its advantage of fast execution in handling the abrupt instrument drifting. The implementation of robust *M*-estimator is a long-term continuous activity. After a period of time as significant system degradation and instrument deterioration take place, the serial bias compensation technique is engaged to recalibrate the model and identify the gross errors in measurements. This integrated scheme of data reconciliation and model calibration is expected to enhance the performance of on-line performance monitoring system by combining two GED techniques. In the off-line model calibration and gross error detection, the MDA (multivariate data analysis) technique can also be engaged to improve the performance of gross error detection.

CHAPTER 7

STRATEGIES OF DATA RECONCILIATION AND MODEL CALIBRATION FOR A COMPLEX SYSTEM

For a complex thermo system that has multiple subsystems connected and interacting with one another, simultaneous data reconciliation and model calibration (SDRMC) faces major challenges of increasing problem dimensionality and computation time. The increase in dimensionality arises from the fact that more measured data and calibration parameters from subsystems are involved in the simultaneous scheme. The computation time, on the other hand, increases because more system level iterations are required to reach convergence on the interactions between subsystems. Solving the maximum-likelihood- based data reconciliation by a single optimizer, which handle all the variables at the same time has the following difficulties:

- Some independent variables from one subsystem could have dominant impacts on the objective function over others. This could cause the optimizer to make most of the adjustments to those dominant variables from one subsystem while doing very little to those variables with relatively minor influences from others. The over-adjustment situation often happens when measurement redundancy is not sufficient and the presumed measurement uncertainties for those dominant variables are relatively small.
- As more variables are involved in the simultaneous scheme, construction of Jacobian matrix and its inversion become extremely time consuming. If the second order approximation is utilized in the optimization process, the number of function evaluation increases tremendously, making the computational budget even worse. The function evaluation is directly related to the model execution. Model execution for a complex thermo system often takes long,

especially for the type of model running as the performance simulator. The size of the optimization problem and the complexity of the model all together lead to large time consumption in simultaneous data reconciliation and model calibration.

In this research, system decomposition and process decomposition are proposed to tackle these two issues. In system decomposition, the thermo system is decomposed into several subsystems, for each of which the local maximum likelihood data reconciliation is carried out. In process decomposition, the model calibration for subsystems are decomposed from the simultaneous scheme such that data reconciliation is carried out first and the reconciled data is used for model calibration thereafter.

7.1. System Decomposition

For a complex system that has physically interconnected subsystems, the internal solver often takes significant time in iterating the solutions among subsystems to eliminate discrepancies. As a result, when putting a complex system model into the simultaneous scheme for data reconciliation and model calibration, it becomes extremely time consuming due to large amount of model runs requested by the system level optimizer. If a complex system can be decomposed into subsystems and the simultaneous data reconciliation & model calibration is carried out locally, it will save significant time caused by the dimensionality of problem solving.

A complex system can be decomposed into several subsystems in such a way that the number of fed-back variables among subsystems is minimized or eliminated. For instance, in the combined cycle power system the gas turbine and HRSG can be isolated as two subsystems because the only fed-back variable from the HRSG to gas turbine is the pressure drop across the HRSG, which does affect the calculation of gas turbine exhaust energy. This fed-back information of pressure drop is often calculated by the HRSG module, which takes the gas turbine exhaust energy as the input for the

calculation. When running these two modules as an integrated model, the internal solver needs to iterate on the guessing and calculated values of HRSG pressure drop to reach consistency. One can decomposed the model by ignoring the pressure drop calculation from the HRSG module but, instead, believing in the measured data to eliminate the fed-back data stream.

System decomposition eases the computational cost by distributing the total system dimensionality into local optimizers. Figure 7-1 shows two architectures of carrying out simultaneous data reconciliation and model calibration- the architecture without system decomposition is given in Fig. 7-1(a), while the Fig. 7-1(b) shows the architecture with system decomposition.

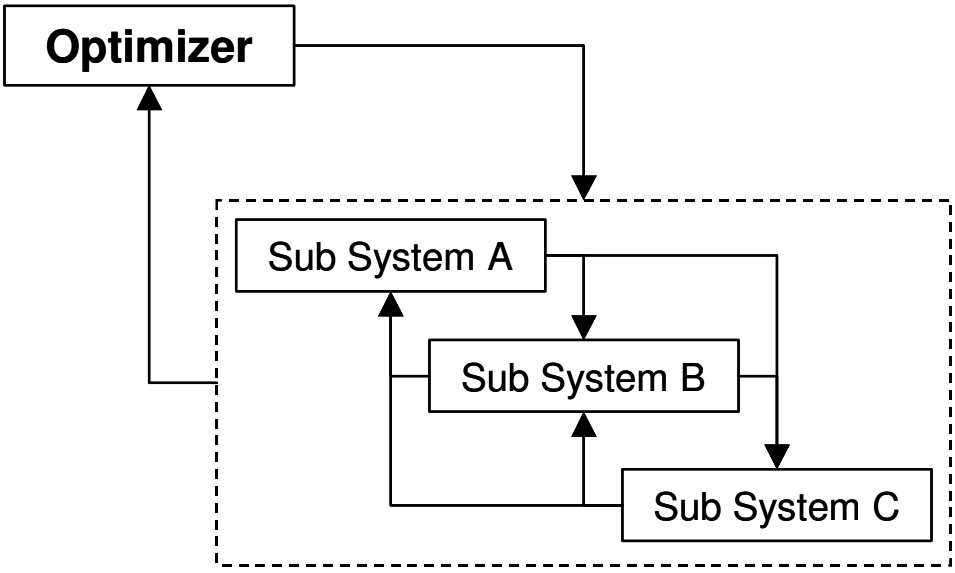

(a)

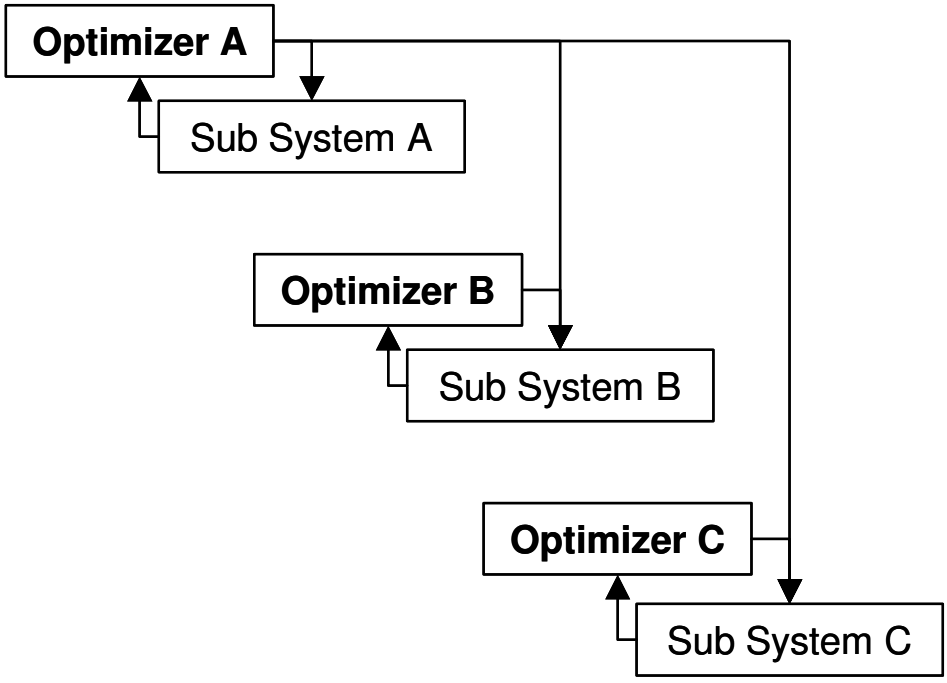

(b)

Figure 7-1: Architectures of SDRMC- System Decomposition

7.2. Process Decomposition

The purpose of process decomposition is to reduce the computation time of data reconciliation by decoupling the model calibration from the simultaneous scheme. In the simultaneous scheme the model is running at performance simulation mode, through which the measured data are reconciled by tuning the performance factors to minimize the objective function. Running the thermo system model in the simulation mode i.e. off-design, however, requires more computation time due to extra iterations of heat and mass balances on the values predicted by the model.

In order to decouple the model calibration from the process, the performance simulators of subsystems need to be replaced by the models based on heat and mass balances. As the heat-and-mass-balance type model is introduced, the problem of maximum likelihood data reconciliation also needs to change. Instead of searching the optimum solutions for the calibration factors, the optimizer should be set to solve for the reconciled data directly. Since the heat and mass balance model is built for taking input data to calculate the others, depending on the way of closing heat and mass balances, the problem solving becomes: finding the optimum set of input data such that the likelihood function is maximized. The computation time is significantly reduced through introducing the heat-and-mass-balance type model, which does not require internal iteration and, therefore, needs much less execution time.

Model calibration is carried out after data have been reconciled. The reconciled data serve as target values to be matched by tuning the calibration factors in the performance simulator. By process decomposition, model calibration becomes an iteration process and one can use the technique such as fast point iteration for exact data matching. Figure 7-2 shows two architectures of data reconciliation and model calibration for a complex system. Figure 7-2(a) shows the simultaneous scheme and Fig. 7-2(b) shows the serial scheme from process decomposition.

Process decomposition can be done partially in such a way that simultaneous data reconciliation and model calibration is implemented to some subsystems and the heat-and-mass-balance type data reconciliation is carried out for the others. This hybrid scheme is highly recommended for the situation when obtaining surrogate models is difficult for those subsystems that are highly nonlinear and running the performance simulation type model becomes inevitable. In the hybrid scheme, the variables to be solved for maximizing the likelihood function are mixed with performance factors and measured data. The subsystem implemented with the simultaneous scheme can be replaced with the surrogate model such as the RSE to further reduce the computation time.

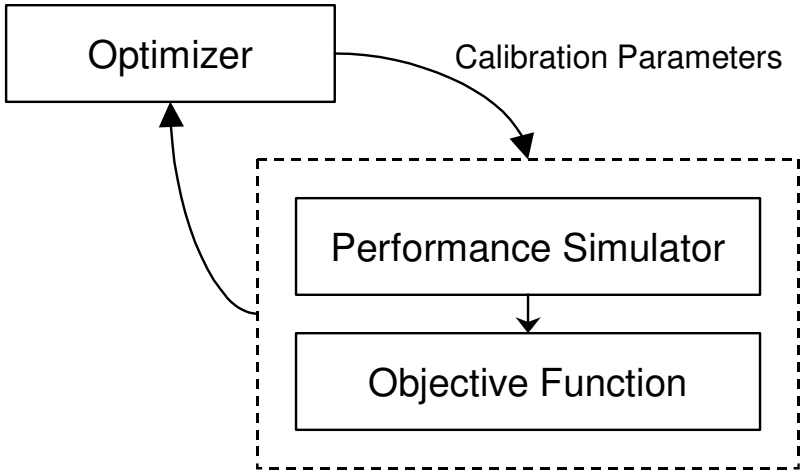

(a)

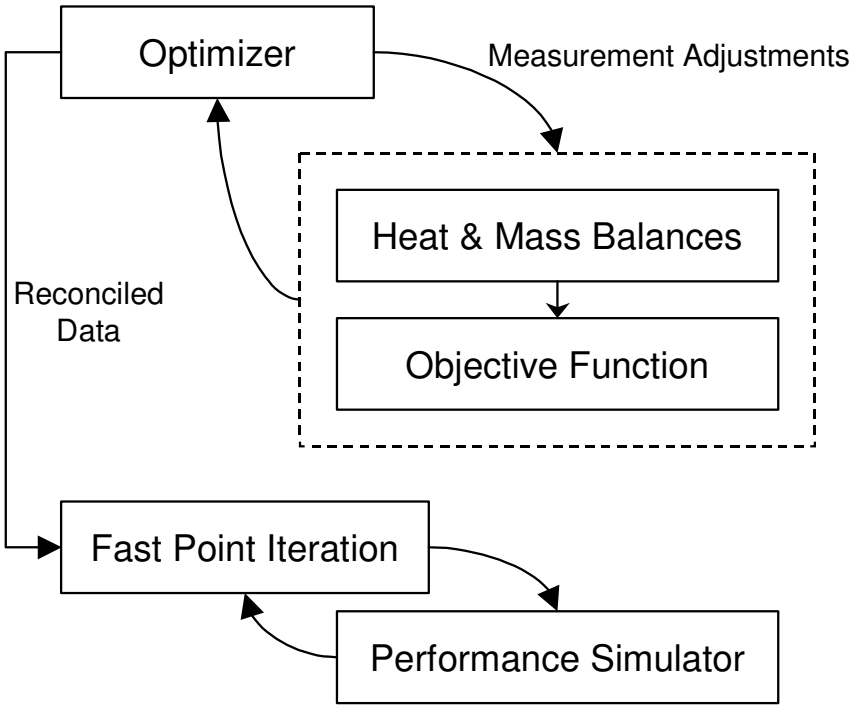

(b)

Figure 7-2: Architectures of SDRMC- Process Decomposition

7.3. Combined Cycle Application

A combined cycle power plant is composed of three major subsystems – gas turbine, HRSG and steam turbine. Each subsystem can also be subdivided into a series of components, each of which contributes to the overall plant performance degradation or improvement. When measurement redundancy and a high fidelity tool for performance simulation are available, one can perform both data reconciliation and model calibration for the whole combined cycle system i.e. the whole plant *SDRMC* with a high fidelity performance simulation code. For a complex combined cycle system having multiple pressure levels and HRSG trains, the number of variables, including the measurement data to be reconciled and the performance factors to be estimated, is usually overwhelmingly large, which suggests the need for evaluating high-dimensional Jacobian and Hessian matrixes in the NLP least squares minimization scheme. On the other hand, as the whole system is modeled with interconnected subsystems- gas turbine, HRSG, and steam turbine, each of which has the capability of performance simulation (size and geometry oriented), it usually takes significant time for model convergence. The combination of a high-dimensional design space for independent variables and the time-consuming system simulation can cause extremely high computational expense. In addition, if the gross error detection technique such as hypotheses testing with serial compensation strategy is to be employed, using the high fidelity performance simulation code for the whole combined cycle system can lead to tremendous time consumption in model evaluation.

Two strategies are proposed in this study for the combined cycle whole plant data reconciliation and model calibration. The first strategy is system decomposition where the whole combined cycle system is decomposed into major subsystems, for each of which one can perform SDRMC with a smaller design space for the independent

variables. The second is process decomposition- decomposing the once-through SDRMC process into two serial steps – data reconciliation followed by model calibration.

7.4. SDRMC for Combined Cycle System Using System Decomposition

When applying system decomposition to a combined cycle system, the SDRMC with smaller dimensionality is carried out locally for each decomposed heat balance model. Each of these models represents one of the major subsystems in the combined cycle. In this framework, the SDRMC is performed locally for each subsystem (i.e. gas turbine, HRSG, or steam turbine). These modules with local SDRMC are then linked together with iterations on pressure and mass balances.

7.4.1. Subsystem Interactions in Combined Cycle

In a combined cycle power plant, the gas turbine provides the HRSG with hot exhaust gas to generate steam at different pressure levels, and the steam turbine is then driven by these high-pressure steam sources from the HRSG to produce power. The gas and steam flows inside the HRSG are flowing in a subsonic regime where disturbances propagate to upstream. Therefore nature forces pressure balances in both steam side and gas path. In the gas path, in order to achieve the ambient pressure at the stack while there is a pressure drop across the HRSG due to turbulence, friction, and heat transfer, nature forces a higher pressure at the gas turbine exhaust, which causes a power loss in the gas turbine. The steam turbine, which is usually operated in a sliding pressure mode in a combined cycle system, produces a pressure signal, based on the amount of steam going through the throttle valve. This signal is passed upstream to the HRSG steam ports, and this will determine the HRSG drum pressure levels. Nature forced pressure balances on both the top cycle (the gas turbine) and the bottom cycle (the HRSG and steam turbine) have crucial impacts on plant performance. For example, an increase in gas turbine

exhaust pressure degrades the gas turbine performance while higher drum pressures cause lower steam productions in the HRSG.

7.4.2. System Decomposition for Combined Cycle

Thus, to carry out a SDRMC locally for each decomposed heat balance model while a whole combined cycle system is being considered, nature forced features must be taken into account during data reconciliation. The advantage of a whole plant model where all major parts are connected together is that the mass and pressure balances are achieved automatically through the internal solver of the model itself. The use of a whole plant model is suitable for the case when degradation estimations are not required and only data reconciliation is pursued. In this situation knowledge about the current plant degradation status is known or a new and clean status is assumed. However, in this proposed method, the whole combined cycle system is decomposed into three major parts – gas turbine, HRSG, and steam turbine, and three heat balance models are built separately for each. The SDRMC process is carried out locally for each of these models, and an outside loop driver that utilizes fast point iteration (FPI) makes connections between these SDRMC modules and iterates on the pressure and mass balances among these models. Through the FPI driver, the deviations between guessed and reconciled pressures and mass flow rates reduce, and the iteration continues until a specified tolerance is reached. Each SDRMC module, which contains a local optimizer and a decomposed heat balance model, generates reconciled values of pressures and mass flow rates that may not match the initial guessed values, which have been used as inputs for other modules. Thus, a system level optimizer or convergence driver is needed to iterate on these pressure and mass differentiations. A local SDRMC module can be shown in Fig. 7-3, and the integration of these modules by a system level convergence driver is given in Fig. 7-4.

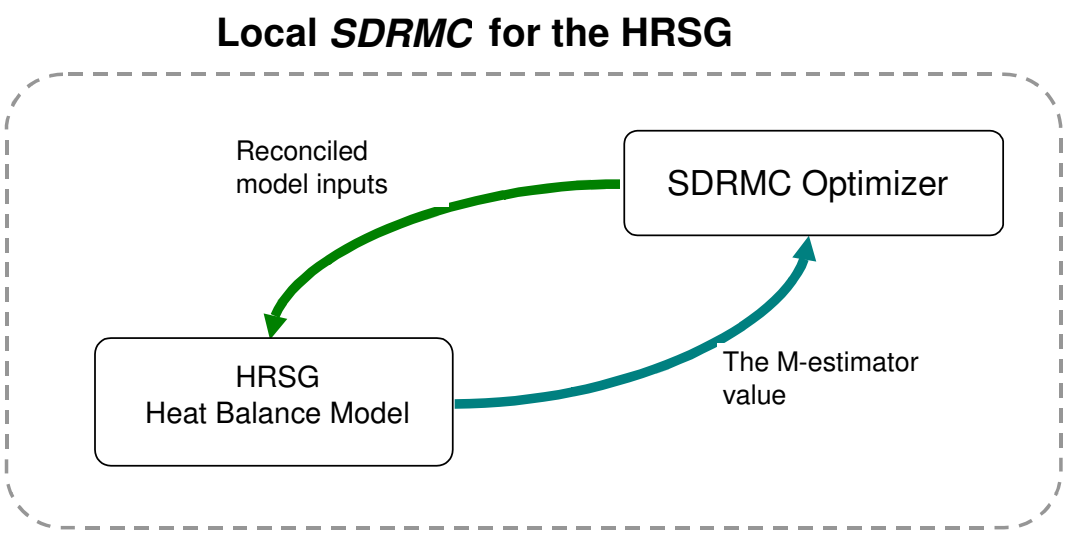

Figure 7-3: Local SDRMC module

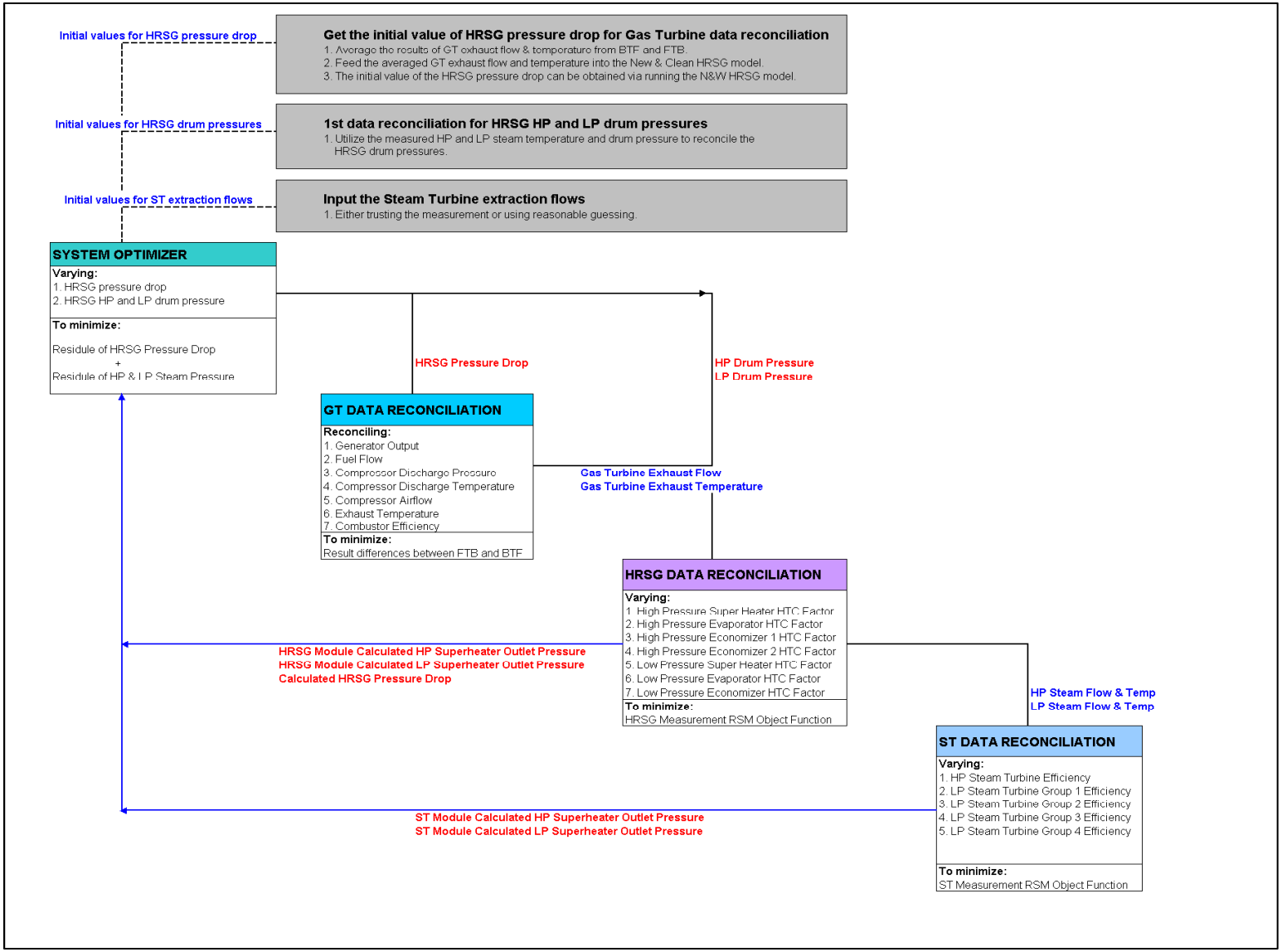

Figure 7-4: Integrated SDRMC for the whole combined cycle system

7.4.3. Implementation of System Decomposition to Combined Cycle

SDRDE Using a Decomposed Combined Cycle Model

In this study, three decomposed heat balance models including the gas turbine, HRSG, and steam turbine are used to perform simultaneous data reconciliation and degradation estimations (*SDRDE*). The main advantage of this method is the significant reduction in number of system level variables. The reduced size of the *SDRDE* problem at the local module level makes the optimization process more robust and efficient. While each local optimizer carries out its *SDRDE*, the system level optimizer or convergence driver performs iterations on the pressure and mass balances. The entire process is very similar to a multidisciplinary optimization (MDO) problem, and can be described in detail as follows.

Initial Values

A local gas turbine module needs the HRSG pressure drop as an input to carry out *SDRDE*. A reasonable initial value of the HRSG pressure drop can be obtained by substituting the averaged values of gas turbine exhaust flow and temperature from two methods of gas turbine heat balance analysis into the new & clean HRSG model. The initial value of the HRSG pressure drop can then be obtained by running the new & clean HRSG model. On the other hand, the HRSG module needs drum pressures at different sections as inputs to carry out the *SDRDE*. The initial values of drum pressures can be estimated by performing data reconciliation on measurements of drum pressures and temperatures. Usually, measurements of drum pressures are very accurate and can be utilized directly without a reconciliation process in advance. After setting up the initial values in the system level, they are fed into the local *SDRDE* modules for the first system level iteration.

Local SDRDE Module

In the gas turbine *SDRDE* module, the HRSG pressure drop is taken as an input and the local optimizer manipulates the values of major gas turbine heat balance model inputs to minimize the value of the *M*-estimator. The reconciled gas turbine exhaust flow and exhaust temperature along with values of drum pressures from the system level are then taken into the HRSG *SDRDE* module as inputs. The HRSG local optimizer then carries out *SDRDE* by varying HRSG heat transfer correction factors to minimize the value of the *M*-estimator. After the optimization process is completed, the model-calculated HRSG pressure drop is fed back to the system module and compared with the initial value of the HRSG pressure drop. At the same time, the reconciled values of steam flows and temperatures are fed into the steam turbine module. Also, the reconciled values of steam pressures at superheater outlets are also fed back into the system module. In the steam turbine module, the local optimizer takes the reconciled values of steam conditions from the HRSG as inputs and performs the *SDRDE* by varying the design point steam turbine stage group efficiencies to minimize the value of the *M*-estimator. The reconciled values of superheater outlet steam pressures from the steam turbine *SDRDE* module are then fed back to the system module and compared with those reconciled values from the HRSG module.

System Level Convergence Driver

After each local module completes its own *SDRDE*, the system module receives the feedbacks from the local modules. These feedbacks include the HRSG pressure drop reconciled in the HRSG module, reconciled superheater outlet steam pressures from the HRSG module, and those obtained in the steam turbine module. The task of the system optimizer is to minimize the difference between the guessed and reconciled HRSG pressure drop, and minimize the difference of superheater outlet steam pressures reconciled by the HRSG model and by those computed in the steam turbine module. In

this study, a fast point iteration (FPI) method is chosen to carry out the iteration by updating the guessed values of HRSG pressure drop and drum pressures.

The combined cycle *SDRDE* using decomposed models is implemented by using Model Center 4.0 for the linkages among three major *SDRDE* modules. A generic two-pressure combined cycle system with a single train is used for the implementation. Figure 7-5 shows the screen shot of the decomposed *SDRDE* using Model Center 4.0^{TM}.

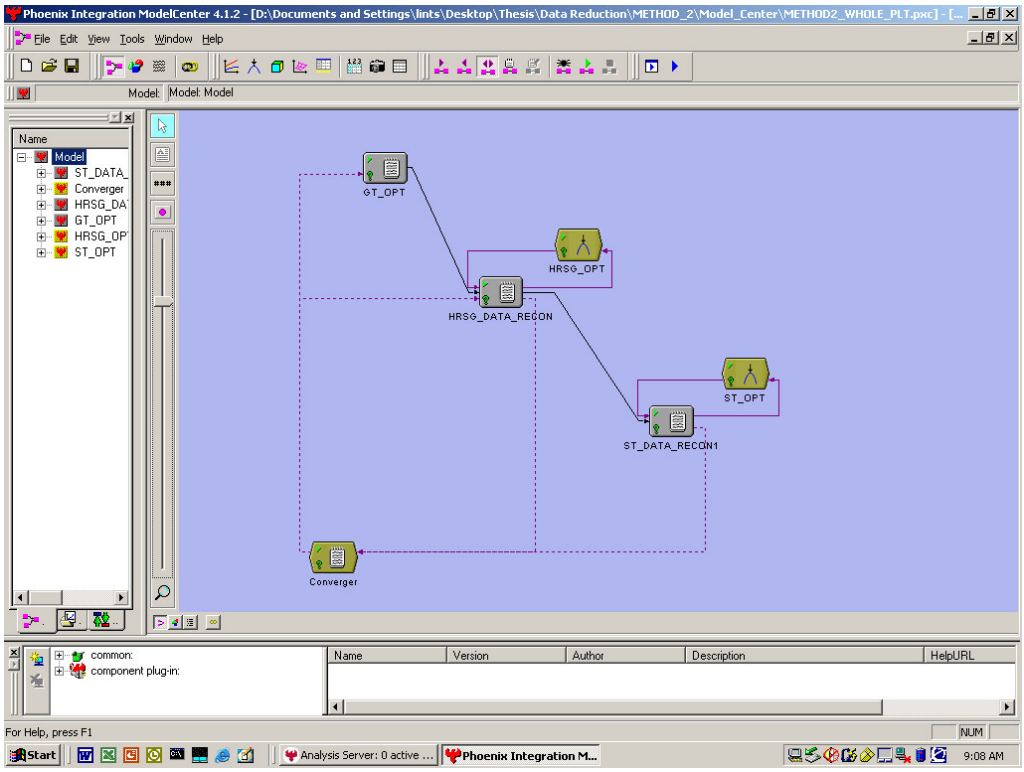

Figure 7-5: ModelCenter model for decomposed SDRMC

The mass and pressure balancing among each SDRDE module is taken into account by using the fast point iteration (FPI) as the system level driver. Figure 7-6 shows the reduced balancing error during the FPI.

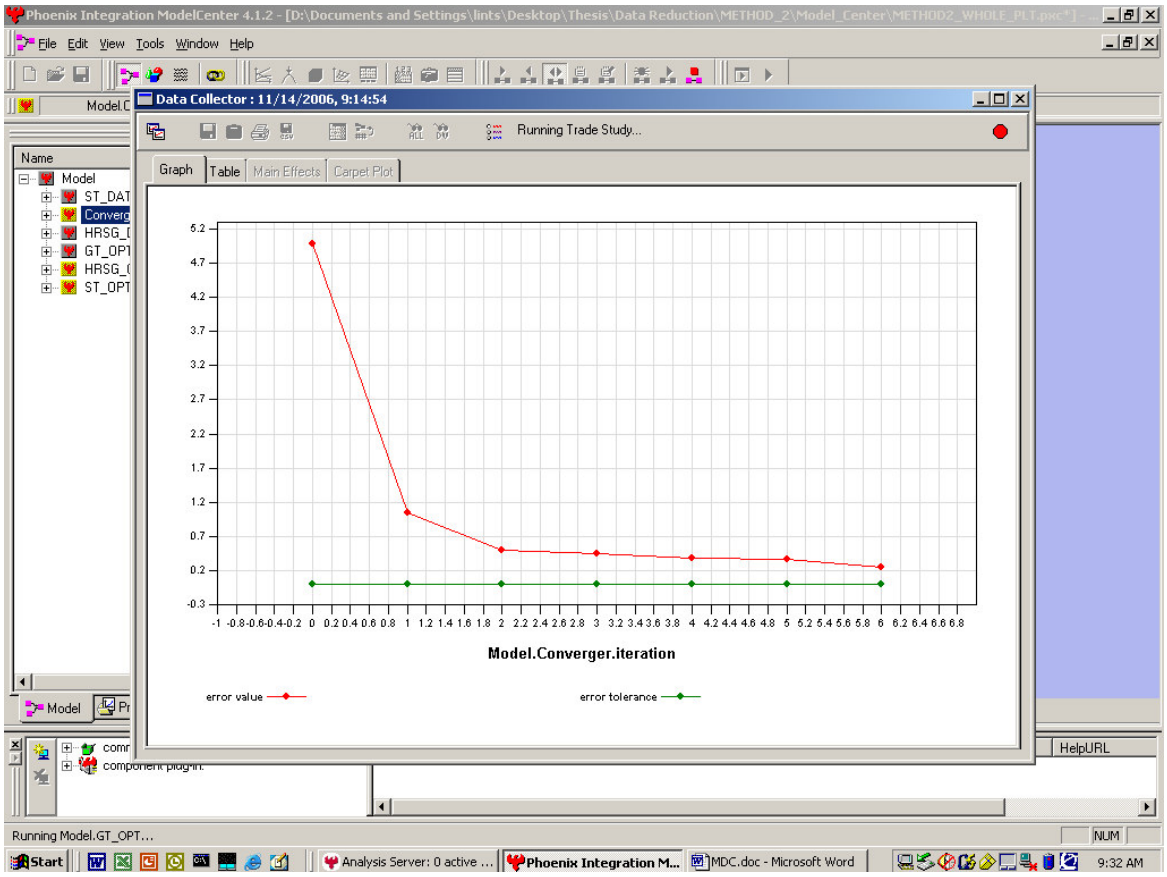

Figure 7-6: Reduced balancing error during FPI in whole plant SDRMC

7.5. SDRMC for Combined Cycle System Using Process Decomposition

Process decomposition is implemented to simultaneous data reconciliation and model calibration (SDRMC) for a tree-pressure-reheat combined cycle system that contains multiple trains. As recommended in previous section, a hybrid scheme is utilized, where the SDRMC is applied to gas turbines whereas the model calibration for bottoming cycle is decoupled from the simultaneous scheme. In this hybrid scheme a gas turbine performance simulator is used for gas turbine model calibration and data reconciliation, whereas the heat and mass balances for bottoming cycle i.e. HRSG and steam turbine is utilized for bottoming cycle data reconciliation. Model calibration for the bottoming cycle is performed after completing the hybrid SDRMC.

7.5.1. Gas Turbine

Gas turbine modeling is carried out by GTP ^{TM}, a gas turbine performance simulation tool developed by GE. When running the gas turbine simulation code in its prediction mode, the gas turbine performance is dependent on the performance multipliers, firing temperature, and the ambient conditions. In this application, it is assumed the measurement data of ambient conditions and the operational parameters such as inlet pressure loss, exit pressure loss, and IGV angle are not included in the reconciliation process, and, therefore, are treated as constants. Based on this assumption, the gas turbine characteristic performance parameters – power, fuel flow, compressor discharge pressure, compressor discharge temperature, compressor airflow, and turbine exhaust temperature, are functions of performance multipliers and firing temperature, which are indicators of current machine degradation status. One can refer section 6-5 for more detail description. Measurement data of these characteristic performance parameters are to be reconciled while, at the same time, the performance multipliers are to be calibrated in the SDRMC scheme for gas turbine. Table 7-1 lists the measurement data being reconciled and the calibration parameters in gas turbine SDRMC.

Table 7-1: Measurement data to be reconciled and the calibration parameters in gas turbine SDRMC

Measured Data to be Reconciled	*Calibration Parameters*
Power	Compressor Efficiency DMM
Fuel Flow	Compressor Flow DMM
Compressor Discharge Pressure	Combustor Efficiency DMM
Compressor Discharge Temperature	Turbine Stage 1 Nozzle Area DMM
Compressor Air Flow	Turbine Efficiency DMM
Turbine Exhaust Temperature	Firing Temperature

Figure 7-7 shows the screenshot of the gas turbine module in the developed tool which performs SDRMC for gas turbines while providing only data reconciliation to the bottoming cycle (hybrid process decomposition) for a typical combined cycle system. Variables listed in the column "Optimal Values" are the calibration parameters to be optimized for obtaining the minimized least squares of the whole system. The least squares of the gas turbine (not including other gas turbines and bottoming cycle components) are shown in the last cell of column "*M*-ESTIMATOR").

Model Performance Factors	Unit	Optimal Values	Lower Bound	Upper Bound	Standard Deviation
Compressor Efficiency (DMM)		0.982635989	0.9	1.03	0.002462612
Compressor Flow (DMM)		0.974178622	0.97	1.03	0.002294312
Combustor Efficiency (DMM)		1	1	1	0.003191258
Turbine Efficiency (DMM)		1.015794422	0.97	1.02	0.001517585
Turbine CQ (DMM)		1.025	1.025	1.025	0.003094987
Tfire Data GT 1	F	2297.060479	2260	2310	3.456958009

GT Measurements (To be reconciled)	Unit	Reconciled	Measured (User Input)	Uncertainty	STD	*M*-ESTIMATOR
Generator Output	kW	201800.8997	☑ 201786.58	0.50%	514.7616791	0.000387019
Fuel Flow	lb/sec	28.29232896	☑ 28.33	1.00%	0.144527937	0.029568854
Compressor Discharge Pressure	psia	195.0810489	☑ 194.96	0.50%	0.497350617	0.028917302
Compressor Discharge Temperature	F	709.2305561	☑ 709.50	7.00	3.571428571	0.002861173
Compressor Airflow	lb/sec	1292.936675	☐	1.00%	0	0
Exhaust Temperature	F	1088.283177	☑ 1087.12	7.00	3.571428571	0.05260501
Exhaust Flow	lb/sec	1337.364664				
						0.114339358

Figure 7-7: Gas turbine SDRMC module

7.5.2. Bottoming Cycle

The bottoming cycle contains HRSGs and a steam turbine. In this hybrid scheme, these bottoming cycle components are represented by their heat and mass balances. Unlike the performance simulator such as GateCycle™, the heat-and-mass-balance type model does not have the capability of performance prediction based on the operational conditions and degradation status. Instead, the model takes part of the data as inputs and calculates the others by closing the heat and mass balances. The major advantage of using

heat-and-mass-balance type model is its rapid execution. But since it only provides a measure of reconciling the data, model calibration need s to be carried out thereafter. In this application, the closure of heat and mass balances is done in the following way:

1. The high- pressure superheater steam flow and reheat steam flow are calculated by closure of the mass balance.
2. The HRSG stack temperature is calculated by closing the HRSG energy balance.
3. The exit enthalpy of low-pressure steam turbine section is calculated based on the energy balances of the steam turbine and condenser.

The screenshot of the HRSG module in the developed tool for combined cycle data reconciliation and model calibration is given in Fig. 8-8. Since, the high- pressure superheater steam flow, reheat steam flow, and stack temperature are calculated, these variables are dependent on the heat & mass balance input variables, optimized by the system level solver in order to minimize the overall least squares. The HRSG module is fed with the gas turbine exhaust conditions by the gas turbine module. Figure 7-9 shows the heat and mass balance of the HRSG used in this developed tool.

HRSG Measurements (To be reconciled)	Unit	Reconciled		Measured	Uncertainty	STD	*M*-ESTIMATOR
IPSH Steam Flow	lb/sec	23.05747712	☑	23.04420007	1.00%	0.117572449	0.006376204
LPSH Steam Flow	lb/sec	24.08984526	☑	24.07387493	1.00%	0.122825892	0.008453139
Hot Reheat Spray Flow	lb/sec	4.469632411	☑	4.469134799	1.00%	0.022801708	0.000238132
Total Feed Water Flow	lb/sec	203.0632208	☑	204.2506272	1.00%	1.042095037	0.64916355
Cold Reheat Steam Flow	lb/sec	146.5560333	☑	146.5001689	1.00%	0.747449841	0.002793036
HPSH Exit Steam Pressure	psia	1558.933577	☑	1558.929077	0.50%	3.976859889	6.40177E-07
HPSH Exit Steam Temperature	F	1000.875946	☑	1001.098856	7	3.571428571	0.001947797
IPSH Exit Steam Pressure	psia	436.5274814	☑	436.5276997	0.50%	1.113591071	1.9208E-08
IPSH Exit Steam Temperature	F	597.5318912	☑	597.5321899	7	3.571428571	3.49904E-09
LPSH Exit Steam Pressure	psia	64.44322473	☑	64.44325519	0.50%	0.164396059	1.71631E-08
LPSH Exit Steam Temperature	F	506.2284097	☑	506.2552883	7	3.571428571	2.83203E-05
Cold Reheat Inlet Steam Pressure	psia	418.8035634	☑	418.8037728	0.50%	1.068376971	1.9208E-08
Cold Reheat Inlet Steam Temperature	F	666.8971336	☑	666.897467	7	3.571428571	4.35856E-09
Hot Reheat Exit Steam Pressure	psia	415.0258785	☑	415.0190118	0.50%	1.058721969	2.10329E-05
Hot Reheat Exit Steam Temperature	F	991.2138136	☑	991.432598	7	3.571428571	0.001876372
Feed Water Inlet Pressure	psia	194.3494391	☑	194.3495822	0.50%	0.495789751	4.16631E-08
Feed Water Inlet Temperature	F	104.4004466	☑	100.3369548	7	3.571428571	0.647269038
Fuel Heating Hot Side Water Flow	lb/sec	2.84724E-05	☐	0	0.01	0	0
Fuel Heating Hot Side Water Pressure	psia	628.7276483	☐	628.7276483	0.005	1.603897062	0
Fuel Heating Hot Side Water Temperature	F	431.7247608	☐	431.7247609	7	3.571428571	0
HPSH Steam Flow	lb/s	151.4462375	☑	150.9446689	1.00%	0.770125862	0.212083693
Hot Reheat Steam Flow	lb/s	174.0831429	☑	174.0135038	1.00%	0.887823999	0.003076255
Stack Temperature	F	216.9674459	☑	202.3365231	7	3.571428571	8.391304957
							9.924632271

Figure 7-8: HRSG data reconciliation module

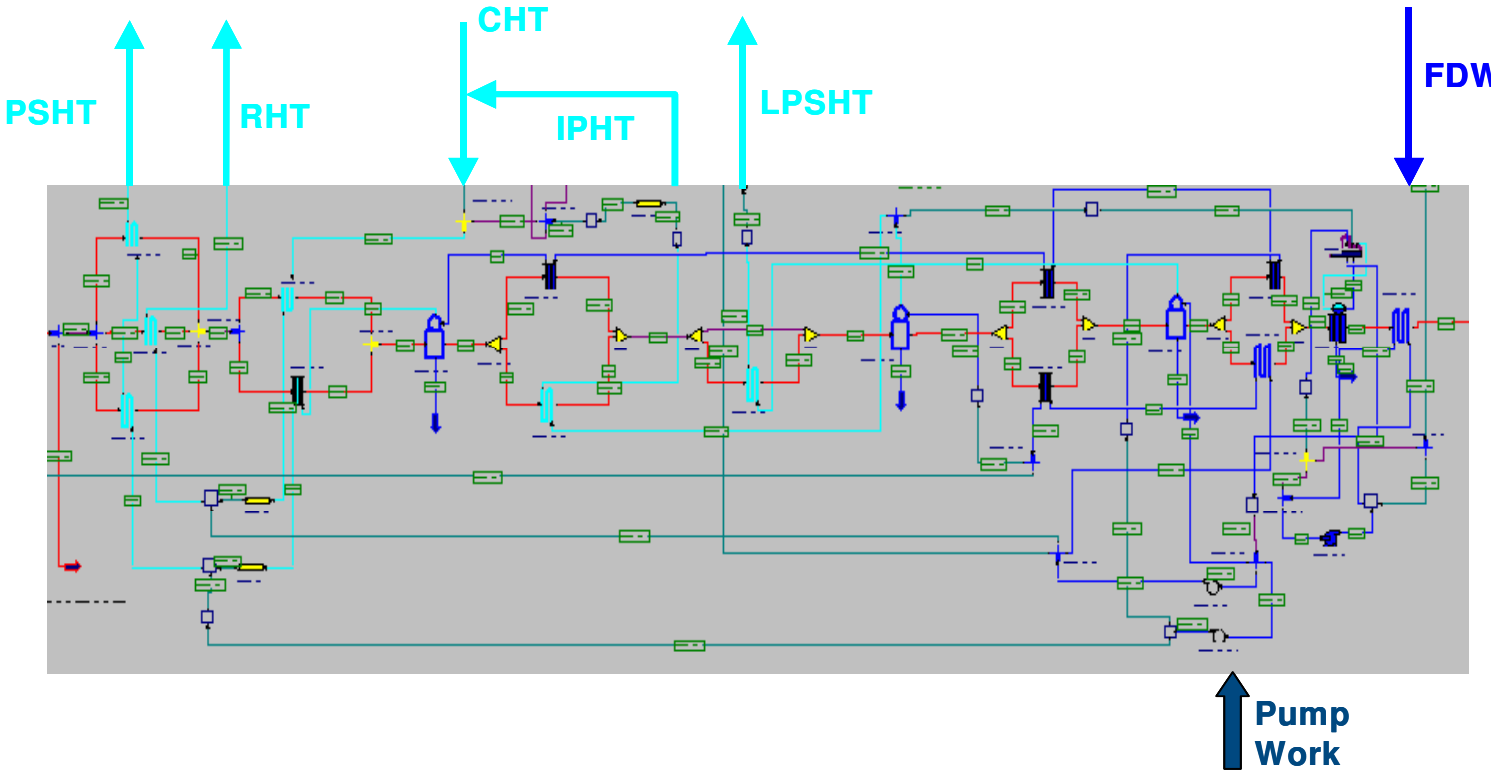

Figure 7-9: HRSG heat and mass balance

In the steam turbine module, the steam flows across each turbine section are calculated based on mass balances of the reconciled steam flows from the HRSG modules. The calculated flows are compared to the corresponding measured values, from which the least squares can be obtained. The enthalpy of the saturated steam at the exhaust of low-pressure steam turbine section is calculated based on the combined heat and mass balances of steam turbine and condenser. Therefore, the cooling water flow becomes one of the independent variables in the system level.

In this application, the steam pressures and temperatures of each turbine section at both inlet and outlet port are treated as independent variables being optimized by the system level optimizer. However, one can exclude these variables from the independent variables by introducing presumed pressure drops and enthalpy changes across the pipelines from the HRSG exit to the steam turbine admission ports. By doing so, one can estimate the steam properties (pressures and temperatures) based on the HRSG steam properties and the specified pressure drops and enthalpy changes. These estimated values along with their corresponding measured data are then used to obtain the least squares.

The screenshot of the steam turbine module in the developed tool for combined cycle data reconciliation and model calibration is given in Fig. 7-10. Figure 7-11 shows the combined heat and mass balance of the steam turbine and condenser used in this developed tool. In this developed tool the isentropic efficiency of each section is also calculated according to the reconciled steam properties. These calculated sectional efficiencies can be included as the problem constraints i.e. the sectional efficiency cannot be greater than one.

ST Measurements (To be reconciled)	Unit	Reconciled		Measured	Uncertainty	STD	*M*-ESTIMATOR
Cooling Water In/Out - Flow	lb/s	24514.02364	☑	25627.94762	5%	653.7741741	1.451528585
HP ST Throttle Pressure	psia	1508.079037	☑	1508.102812	0.50%	3.847201051	1.90948E-05
HP ST Throttle Temp	F	996.5128895	☑	996.1476658	7.00	3.571428571	0.005228821
HP ST Outlet Pressure	psia	454.5353331	☑	454.5313742	0.50%	1.159518812	5.82865E-06
HP ST Outlet Temp	F	666.1207107	☑	666.4645482	7.00	3.571428571	0.004634389
IP ST Admission Pressure	psia	402.8328464	☑	402.8348332	0.50%	1.027639881	1.86889E-06
IP ST Admission Temp	F	992.9470522	☑	992.5698556	7.00	3.571428571	0.005577269
IP ST Outlet Pressure	psia	54.83548994	☑	54.83551714	0.50%	0.139886523	1.89139E-08
IP ST Outlet Temp	F	521.007791	☑	521.0088296	7.00	3.571428571	4.22853E-08
LP ST Admission Pressure	psia	57.83547279	☑	57.83551714	0.50%	0.147539585	4.51876E-08
LP ST Admission Temp	F	522.3971613	☑	522.3467943	7.00	3.571428571	9.94439E-05
HP ST Throttle Flow	lb/s	304.6473319	☐	307.0269997	1.00%	1.566464284	0
HP ST Outlet Flow	lb/s	300.2693851	☐	298.1380997	1.00%	1.521112753	0
IP ST Admission Flow	lb/s	352.7029303	☐	352.9558973	1.00%	1.800795394	0
IP ST Outlet Flow	lb/s	357.0808771	☐	351.8458973	1.00%	1.795132129	0
LP ST Admission Inlet Flow	lb/s	50.80884128	☐	50.8628814	1.00%	0.259504497	0
LP ST Bowl Inlet Flow	lb/s	408.9393164	☐	403.8187787	1.00%	2.060299891	0
LP ST Outlet Flow	lb/s	408.9393164	☐	403.8187787	7.00	3.571428571	0
ST Generator Power	kW	235815.6314	☑	235870.4791	0.50%	601.710406	0.00415444
							1.471249848

Constraint	Calculated	Lower Bound	Upper Bound
HP ST Isentropic Efficiency	0.932916795	0.70	1.00
IP ST Isentropic Efficiency	0.897321795	0.70	1.00
LP ST Isentropic Efficiency	0.854791936	0.70	1.00

HPSH Throttle P- Calculated	HPST Throttle P- Reconciled
1558.933577	1508.079037

IPSH Admission P- Calculated	IPST Admission P- Reconciled
436.5274814	402.8328464

LPST Admission P- Calculated	LPST Admission P- Reconciled
64.44322473	57.83547279

Figure 7-10: Steam turbine data reconciliation module

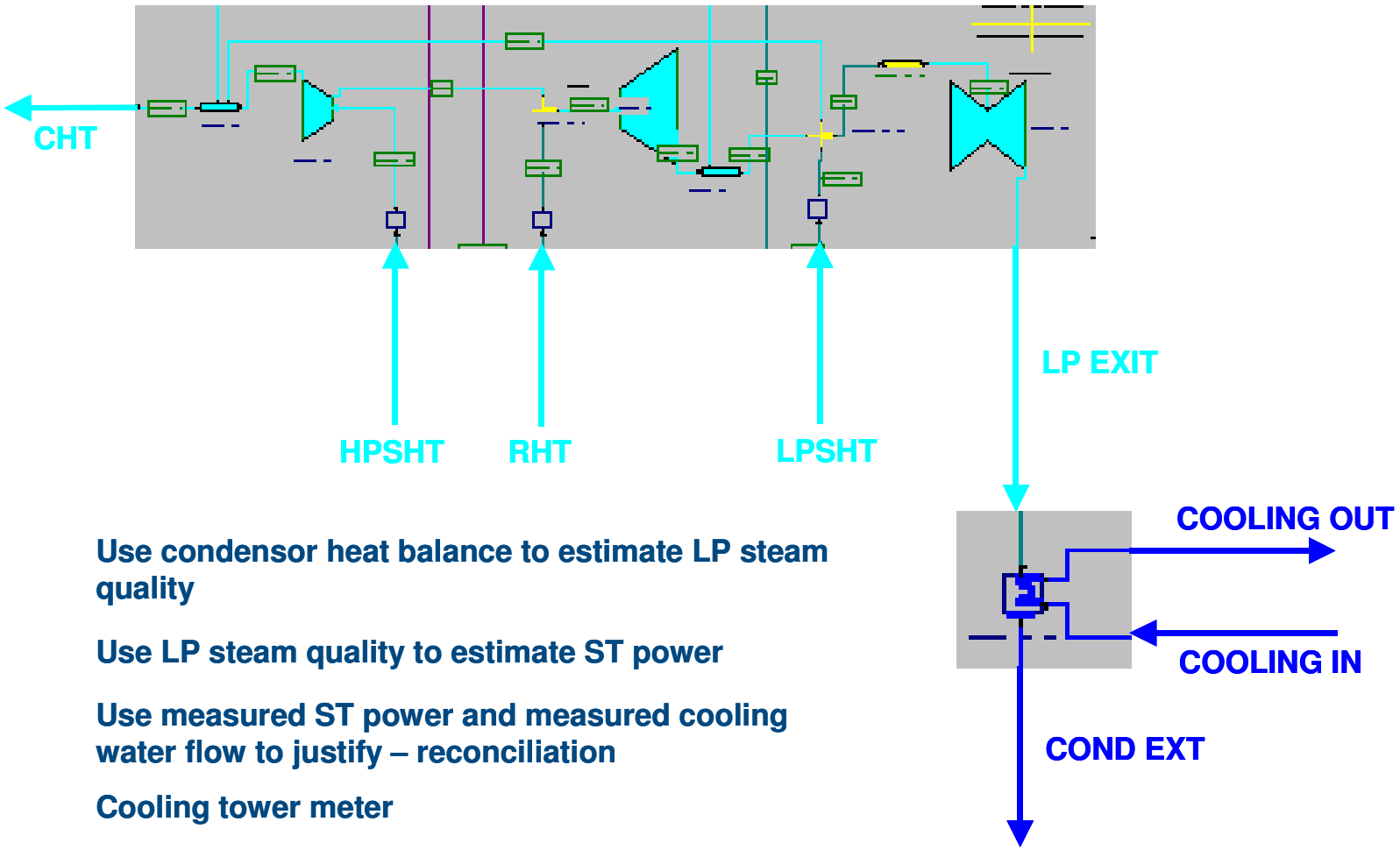

Figure 7-11: Combined heat and mass balances for the steam turbine and condenser

7.5.3. Implementation of the Hybrid Process Decomposition to Combined Cycle Data Reconciliation and Model Calibration

When performing the hybrid process decomposition for combined cycle data reconciliation and model calibration, the simulated gas turbine exhaust flow and temperature are fed into the HRSG modules, while the calculated steam flows and properties from HRSG heat & mass balances are populated to the steam turbine module where the steam turbine power is calculated. During the process of data reconciliation and model calibration, the system optimizer searches the optimum solutions for the independent variables identified in all modules from the combined cycle system to minimize the overall least squares objective function. The independent variables in the gas turbine module are the performance multipliers and firing temperature. For the bottoming cycle, the independent variables are those used to close the heat and mass balances. A list of all independent variables manipulated by the system solver is given in table 7-2.

Table 7-2: System level independent variables

Gas Turbine	HRSG	Steam Turbine
Compressor Efficiency (DMM)	IPSH Steam Flow	Cooling Water In/Out - Flow
Compressor Flow (DMM)	LPSH Steam Flow	HP ST Throttle Pressure
Combustor Efficiency (DMM)	Hot Reheat Spray Flow	HP ST Throttle Temp
Turbine Efficiency (DMM)	Total Feed Water Flow	HP ST Outlet Pressure
Turbine CQ (DMM)	Cold Reheat Steam Flow	HP ST Outlet Temp
Tfire Data GT 1	HPSH Exit Steam Pressure	IP ST Admission Pressure
	HPSH Exit Steam Temperature	IP ST Admission Temp
	IPSH Exit Steam Pressure	IP ST Outlet Pressure
	IPSH Exit Steam Temperature	IP ST Outlet Temp
	LPSH Exit Steam Pressure	LP ST Admission Pressure
	LPSH Exit Steam Temperature	LP ST Admission Temp
	Cold Reheat Inlet Steam Pressure	
	Cold Reheat Inlet Steam Temperature	
	Hot Reheat Exit Steam Pressure	
	Hot Reheat Exit Steam Temperature	
	Feed Water Inlet Pressure	
	Feed Water Inlet Temperature	
	Fuel Heating Hot Side Water Flow	
	Fuel Heating Hot Side Water Pressure	
	Fuel Heating Hot Side Water Temperature	

The value of overall least squares objective function is obtained by the summation of all least squares terms from different modules. The maximum-likelihood based data reconciliation and model calibration for the combined cycle system is then given by:

$$\min_{X_{GT},\, X_{HRSG},\, X_{ST}} \left[LSQ_{GT}(X_{GT}) + LSQ_{HRSG}(X_{HRSG}) + LSQ_{ST}(X_{ST}) \right]$$

where X_{GT} and LSQ_{GT} represent the set of independent variables and the least squares function in the gas turbine module; X_{HRSG} and LSQ_{HRSG} represent for the HRSG; X_{ST} and LSQ_{ST} for the steam turbine. Some constrains such as the steam turbine isentropic efficiencies and the HRSG heat utilization factors can be added to the minimization problem to insure the results make physical sense.

The occurrence of gross errors is indicated by the value of the overall least squares objective function. The threshold value for the indicator is based on the overall system degree of freedom, defined as:

number of total least squares terms – number of total independent variables

If the indicator manifests the occurrence of gross errors, one should carry out the serial elimination strategy for gross error detection. For a complex system, the serial elimination often costs large computation time. One can choose to use the robust *M*-estimator for gross error detection, especially when the measurement redundancy is sufficient. The developed tool provides the options of different *M*-estimator including the least squares to choose. Figure 7-12 shows the data streams in the decomposed combined cycle data reconciliation and model calibration. The screenshot of the developed tool for combined cycle data reconciliation and model calibration is given in Fig. 7-13.

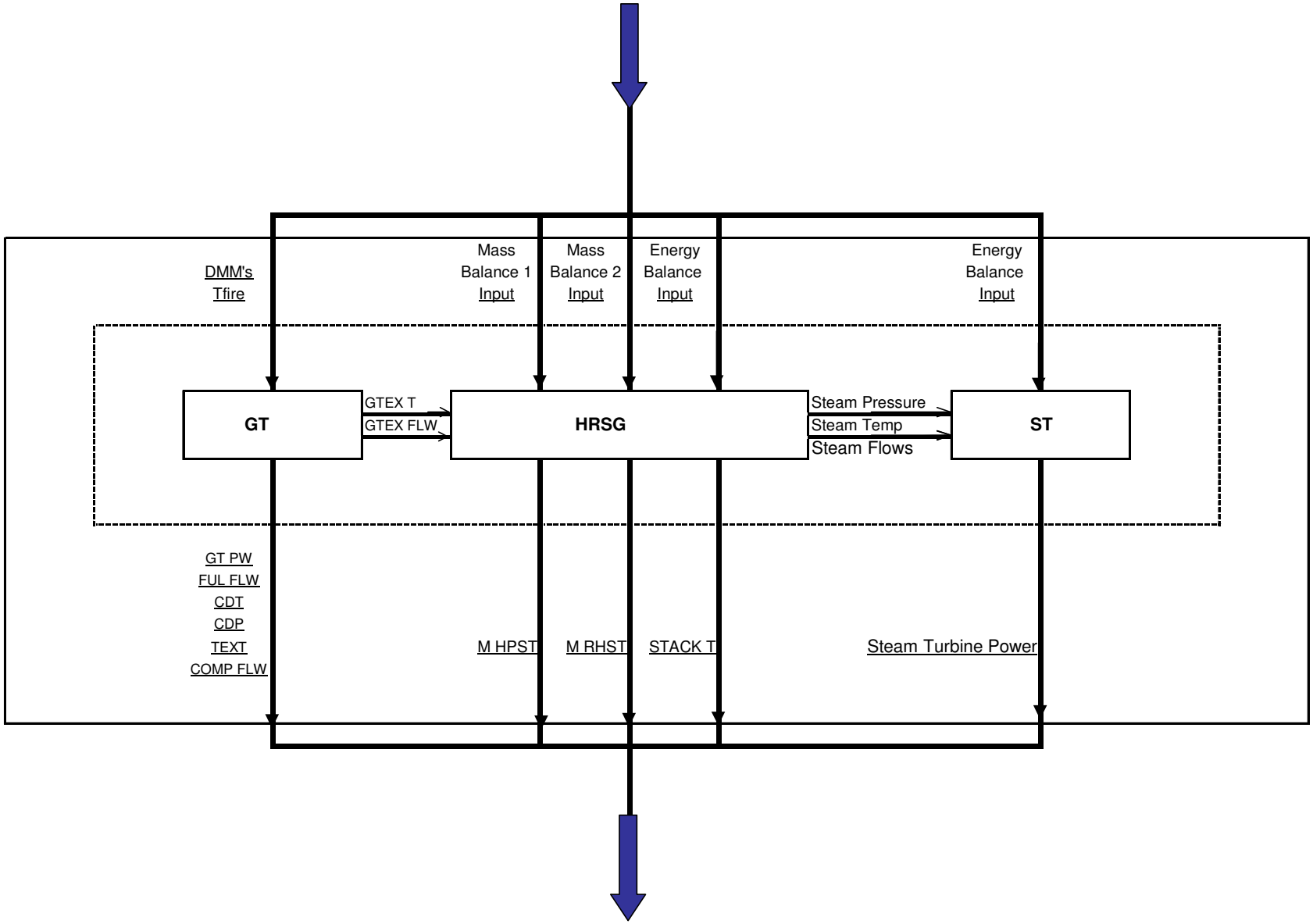

Figure 7-12: Data streams in decomposed combined cycle data reconciliation and model calibration

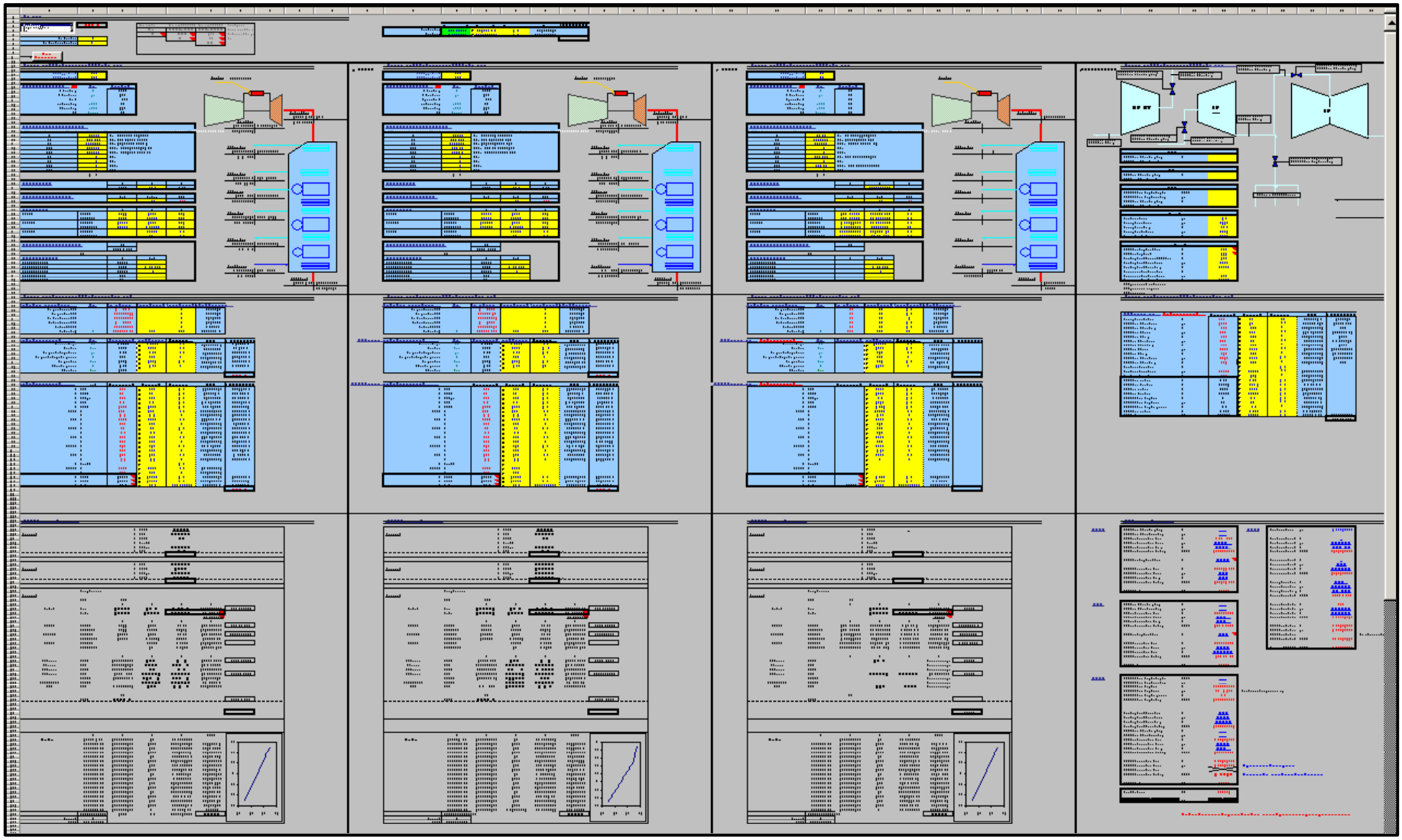

Figure 7-13: Screenshot of developed tool for combined cycle data reconciliation and model calibration

CHAPTER 8

CONCLUSION

Modeling and simulation (M&S) for the after-market power system faces the major challenge of estimating the system degradation based on the data that are subject to measurement errors. Performance engineers often have to rely on data from the on-site monitoring system. These data have larger uncertainties and more biases than the precision test, which has been used to carry out model calibration and performance simulation. Currently, the majority in the power generation industry utilizes the deterministic data matching method to calibrate the model and to estimate system degradation. This causes significant calibration uncertainties and, therefore, increases the risk of issuing performance guarantees due to the lack of a suppression mechanism for error propagation.

In this research work it has been shown that by using the probabilistic data reconciliation method to calibrate the model, one can reduce the calibration uncertainty and mitigate error propagation to performance simulation (Section 6.3). An M&S environment where one can carry out model calibration and data reconciliation for a complex power system with degradation has been developed. In this environment the performance engineer can import multiple data sets to improve the calibration quality when carrying out simultaneous data reconciliation and model calibration (SDRMC). System degradation is then quantified by a performance comparison between the calibrated model and its expected new and clean (N&C) status.

Examination of the difficulties in M&S for the after-market power systems and the awareness of a need for a probabilistic calibration methodology give rise to the motivating research question addressed in Chapter 2 and repeated below.

Research Question 1: *How can the performance engineer estimate system degradation based on the measurement data that are subject to errors?*

In response to this motivating question, an M&S environment where one can carry out SDRMC based on multiple measurement data sets has been developed. This M&S environment was demonstrated through an EXCEL-based tool implemented to data reconciliation problems for a simple cycle gas turbine power plant and for a combined cycle power plant. In this environment, calibration uncertainties are estimated via the error analysis module, a programmed functionality based on the error propagation principle discussed in Section 4.5. The calibration uncertainties are then populated to the uncertainties in performance simulation by using the error propagation principle, which is carried out either by the random sampling technique, such as Monte Carlo simulation, or by the Variance-Covariance method discussed in Chapter 4. Demonstrations of both of these processes are shown in Section 6.2.4.

Once completing model calibration, one can obtain the corrected performance by executing the calibrated model at a reference condition. By comparing with the expected N&C performance, the system degradation, which is defined as the performance downfall from its N&C status, can be quantified. Since the calibrated model is run as a performance simulator, one can examine the individual contribution to the overall system degradation from each subsystem component. This is done by replacing the degraded component with its N&C performance correction factor, from which the degradation cascades are illustrated. Therefore, the first hypothesis given in Chapter 2 and repeated below can be verified.

Hypothesis 1: *By performing data reconciliation and model calibration simultaneously, i.e., simultaneous data reconciliation and model calibration (SDRMC), one can estimate system degradation based on the error-free data, i.e., the reconciled data, while the measurement uncertainties are taken into account.*

In the SDRMC scheme, all measurement data are subject to rectifications. The magnitudes and signs are determined by the optimizer based on their measurement uncertainties and the sensitivities of system responses. The subjective decision making on what data to match and what to ignore can be avoided in this probabilistic calibration methodology. Instead, the model is calibrated through data reconciliation based on the maximum likelihood principle where all measurement data are taken into account (Section 4.3). Calibration uncertainty is reduced when using maximum-likelihood based data reconciliation as compared to the deterministic data matching method. The reduction of estimate uncertainties from the deterministic data reduction method to SDRMC is shown in Section 6.2~6.4. If more data sets are imported to the simultaneous scheme, the calibration uncertainty can be further reduced. This confirms a fact of regression statistics that increasing system degree of freedom in the regression problem by introducing more data sets makes the regressed model more robust in reducing errors in measurements.

The maximum-likelihood based data reconciliation and model calibration is discussed in-depth in Chapter 4. Additionally, two types of data reconciliation are suggested, i.e., heat-and-mass-balance based data reconciliation and performance-simulation based data reconciliation. When applying the heat-and-mass-balance type reconciliation, it is suggested to transform the conventional constrained optimization problem to the unconstrained problem solving by deciding the direction of balance closure in advance. The direction of balance closure can be determined by the measurement uncertainties in such a way that the uncertainties of calculated parameters in the balancing equations are the least among the options of balancing closure (Section 6.2.2). For the performance-simulation type data reconciliation, on the other hand, it already fits to the NLP (nonlinear programming) scheme where data reconciliation and model calibration are carried out simultaneously.

The second hypothesis, repeated below, is therefore verified.

Hypothesis 2: *If one carries out SDRMC instead of utilizing data reduction for model calibration, the calibration uncertainties and, therefore, the uncertainties of performance simulation can be reduced.*

This hypothesis is also used to answer the second research question, repeated below:

Research Question 2: *What is the major benefit that the performance engineer can get by using SDRMC instead of a deterministic data reduction method which needs less computation time?*

The maximum-likelihood based data reconciliation and model calibration is essentially a nonlinear optimization problem, in which the optimizer performance has a direct impact on the results. At the end of Chapter 4, an optimization scheme based on the Levenberg-Marquardt (LM) algorithm is suggested (Section 4.4). This algorithm has been programmed into the M&S tool, which has been developed to solve the least squares based data reconciliation problem. The Levenberg-Marquardt (LM) algorithm is a nonlinear optimization technique most suitable for solving the type of objective function expressed as the sum of squares of a nonlinear function. Performing as a combination of steepest descent and Gauss-Newton expansion methods, the LM algorithm significantly outperforms gradient descent and conjugate gradient methods in a wide range of problems. Because the Levenberg Marquardt algorithm combines the two methods of analytical expansion and gradient search, it works efficiently in the path toward the valley of the objective function just like the gradient search, and it converges rapidly like the expansion method when the true solution is nearby. This feature is especially powerful in applying hypotheses testing for gross error detections when using the least squares based data reconciliation and model calibration.

In SDRMC, "smearing effects" occur during the reconciliation process when the least square is used as the objective function and there are gross errors in measurement data (Section 5.2). The smearing effects drive the optimizer to make "biased"

measurement adjustments over the ranges of presumed measurement uncertainties, which violates the assumption that only random errors are allowed. This leads to the third research question:

Research Question 3: *How can one perform SDRMC properly when the measurement data are subject to gross errors?*

In this research work, the gross error detection techniques are applied to the simultaneous scheme for data reconciliation and model calibration in the M&S environment. The gross error detection (GED) scheme is carried out in two stages. The first stage is a screening stage, in which serious gross errors, i.e., gross errors with large magnitudes, are eliminated in advance. The GED techniques used in the screening stage are based on multivariate data analysis (MDA), including multivariate data visualization and principal component analysis (PCA). The multivariate data visualization (Section 5.4.1) provides the visual environment for the user to identify and remove the measurement data with serious biases from the data reconciliation process. These measurement data with biases present themselves as outliers in the scatter plot matrix. A scatter plot illustrates the population for possible outcomes of correlated system responses generated by the random sampling technique such as a Monte Carlo simulation.

The principal component analysis (Section 5.4.2) is the type of multivariate data analysis that provides test statistics for one to justify the occurrence of gross errors. One of the major properties of PCA is being able to break down the contribution of different errors, and this makes PCA an effective tool in identifying serious gross errors from multi-dimensional data sets. Also, PCA is an efficient way of identifying patterns in data sets and expressing the data in a way as to highlight their similarities and differences. Like multivariate data visualization, PCA relies on the correlated system responses generated by the random sampling technique, which is based on the presumed ranges of model parameters. As a matter of fact, the decision on the ranges of the model parameters

is often based on the historical data or engineering judgment, which itself is sometimes subjective. Therefore, the GED techniques that rely on MDA are suitable for detecting large gross errors since justification of subtle gross errors is sensitive to the ranges of model parameters. The implementation of the MDA techniques is shown in Section 6.3~6.4.

At the second stage of GED dealing with subtle gross errors, two GED techniques are provided in the developed modeling & simulation environment - serial bias compensation and robust *M*-estimator. In the serial bias compensation scheme (Section 5.6), hypothesis testing is carried out iteratively for the gross error model that is updated with one gross error at each round. At each round of hypotheses testing, the gross error model with the highest testing score goes to the next round of hypotheses testing with one gross error added for all possible scenarios. The process continues until no more gross errors can be added to obtain a better testing score. Each hypothesis testing requires a complete execution of least-square based data reconciliation with extra variables of bias magnitudes added. The optimization process is carried out through the Levenberg Marquardt algorithm, whose performance is superior than any of the other algorithms considered in this research work for the hypotheses testing for gross errors.

For GED based on the robust *M*-estimator (Section 5.5), the gross error effects are suppressed by the likelihood function itself. Due to the robustness of the objective function, the solver updates solutions in the way toward the healthy data while making very little adjustments to the data with gross errors. Therefore, unlike serial bias compensation, the robust *M*-estimator does not require a sequential scheme, but instead a single execution of data reconciliation is required to detect all hidden gross errors. Sufficient measurement redundancy and healthy data are, however, required by the robust *M*-estimator to obtain the results which are less sensitive to the initial points.

The two-staged GED scheme was implemented to the simple cycle gas turbine data reconciliation and model calibration, discussed in Section 6.3~6.4. It has been shown

that the simulated gross errors can be identified and isolated, by which data reconciliation and model calibration can be carried out with least amount of smearing effects. The mitigation of smearing effects is shown in Fig. 6-46~6-48 for the case study of multiple gross errors in the gas turbine measurements. The robust *M*-estimator technique is also implemented to the combined cycle system, which is discussed in Chapter 7.

These verification experiments were conducted to demonstrate the third hypothesis repeated below:

Hypothesis 3: *The occurrence of gross errors can be tested. Once it is confirmed, one can apply gross error detection techniques to mitigate the smearing effects and identify locations and magnitude of gross errors while performing SDRMC.*

For a complex system, running the model usually takes significant time, especially in the case where the performance simulator is utilized. Additionally, when implementing the GED technique based on hypotheses testing, such as the serial bias compensation, a large amount of model runs are required during data reconciliation. A combination of the high fidelity performance simulation code and the hypotheses-testing based GED scheme could, therefore, lead to tremendous computation costs for a complex system. This leads to the fourth research question:

Research Question 4: *How can one reduce the computation time in SDRMC for a complex system?*

Meta-modeling, due to its rapid execution, can be used to replace the high fidelity simulation code to save the model running time. In this research work, meta-modeling using the response surface equation (RSE) technique is applied to the combined cycle subsystems – gas turbine and HRSG. In the developed modeling and simulation tool, the performance engineer can use the design of experiment (DOE) or the Monte Carlo simulation to generate the experiment cases by running the high fidelity performance simulator. The functionality of creating response surface equations based on the Levenberg Marquardt algorithm has also been programmed into the tool. A

demonstration of the functionality is shown in Chapter 6 for the gas turbine application. It is shown that by applying meta-models to model calibration and gross error detection the computation time for a complex system is reduced significantly in the simultaneous scheme of data reconciliation. Therefore, the fourth hypothesis, repeated below, can be verified by the verification experiments conducted in this research work.

Hypothesis 4: *For a complex system, one can incorporate the meta-modeling for the whole system or its components in the simultaneous scheme of data reconciliation and model calibration.*

8.1. Contributions

The formulation and development of the modeling and simulation environment where the performance engineer can carry out simultaneous data reconciliation and model calibration (SDRMC) for a complex thermodynamic system is the primary contribution of this research. Several secondary contributions, which form the foundations of this developed environment, are also summarized below.

A unique methodology that integrates the gross error detection scheme into the simultaneous data reconciliation and model calibration has been developed, programmed, and embedded into the developed environment as functional codes. In this environment, it is allowed to select different gross error detection techniques, i.e., serial bias compensation and several robust *M*-estimators, to engage with the simultaneous scheme for data reconciliation and model calibration. The need for GED techniques depends on the test statistics, i.e., the least squares obtained from the first run of SDRMC. In this adaptive environment, it provides the test statistics as an indicator for the performance engineer to decide the engagement of the GED scheme.

This developed M&S environment also provides the functionality of two multivariate data analysis (MDA) methods – multivariate data visualization and principal component (PCA). These MDA techniques serve as the screening process for serious

gross errors, by which one can visualize the biased measurements through the pair-wise scatter plot matrix or the bar charts from the PCA. The implementation of multivariate data visualization and principal component analysis to the gross error detections is a new and novel approach in the power generation engineering.

The Levenberg Marquardt algorithm has been programmed and embedded into this M&S environment. The algorithm was tailored to fit the combined GED and SDRMC problem solving, making the implementation of the LM algorithm to the integrated GED and SDRMC problem unique. The LM algorithm, with modifications, has also been applied to create the response surface equations (RSE) to build the meta-models in the developed tool. At the user interface in this M&S environment, the performance engineer can create the experimental cases for the high fidelity simulation tool by running a Monte Carlo simulation. These randomly generated experimental cases are then used for fitting the response surface equations. Once the meta-model is built, it is allowed to switch between the meta-model and the original performance simulation code such that the performance engineer can decide whether or not to engage the meta-model. The way the M&S environment is designed and built makes it an adaptive and pragmatic tool for the performance engineer to create meta-models, carry out SDRMC, and engage the two-staged GED scheme for a complex thermodynamic system. The use of Levenberg Marquardt algorithm in both integrated SDRMC & GED and RSE regression is also a novel application.

Finally, the system decomposition and process decomposition are implemented to a complex combined cycle system. The architecture of system decomposition has been developed via using ModeCenter^{TM} for a generic combined cycle system. The hybrid process decomposition has also been implemented to the combined cycle SDRMC and GED, in which the robust *M*-estimator is utilized. The implementation is completed through the developed EXCEL based tool, which is now used and tested in the combined cycle studies conducted by the service engineers in the General Electric Company.

8.2. Future Work

The M&S environment developed in this research work for data reconciliation and model calibration still has room for improving and expanding its functionalities. Recommendations on future works for extending this research task are given below.

- Incorporate a trade-off study on calibration uncertainty and computation budget

Measurement redundancy has a crucial impact on the results of data reconciliation and model calibration. Introducing more redundancy can improve the calibration quality, i.e., reduce calibration uncertainty, but it can also increase the computation time during the reconciliation process. The demonstrated methodology currently allows unlimited data sets to be imported. It can be expanded, however, by incorporating a trade-off analysis on the balance between calibration quality and computation time.

- Optimize the sensor network

In the maximum-likelihood based data reconciliation, measurement uncertainties and system sensitivities to the reconciled variables have direct impacts on the solutions. There is a need for a trade-off study to manage the instrument budget based on the system sensitivities. For instance, the precision of an instrument should be increased if the derivative of the likelihood function with respect to the measured variable is a large number. The sensor network should also be arranged properly so that measurement redundancy is sufficient. Therefore, the arrangement of sensor network can also be optimized.

- Incorporate analytical derivatives to reduce computation time

When the response surface equations are utilized in the SDRMC scheme, the analytical derivatives are available. These analytical derivatives can be used to construct the Jacobian and Hessian matrix in advance such that the finite differences are not needed. This can save significant time in the reconciliation process, in which the Jacobian and Hessian matrices are calculated numerically.

- Incorporate the Bayesian approach to enhance the power of GED

The major challenge in GED is how to improve the power and selectivity of the test without increasing the frequency of Type I error. By incorporating historical information on measuring instruments, such as the frequency of past failures on sensors, one can enhance the power and selectivity of GED. The information of past data can be taken into account by using Bayesian theorem in statistics [91]. A GED algorithm based on the Bayesian approach for steady state processes has been developed by Tamhane et al. [92,93]. However, it hasn't been applied to the combined cycle applications. The Bayesian approach is not a one-time application, but rather a sequential procedure that collects and updates historical data over time [94]. The sequential approach raises the following questions:

- How often are the measuring instruments inspected and identified with gross errors?
- How soon are the failed sensors repaired and how good are they after being repaired?
- Should the aging of instruments be taken into account?

These issues make the Bayesian algorithm a challenging task. In addition, results obtained from the Bayesian approach highly depends on the prior estimates. The dependence of prior probability can be reduced by increasing the weight of current data. More works are required to make the Bayesian approach competitive with other GED techniques. The sequential Bayesian algorithm is similar to the proposed serial bias compensation method, but takes more computational time. It is therefore suitable for the off-line model calibration.

APPENDIX A

THERMO SYSTEM DATA RECONCILIATION AND MODEL CALIBRATION ENVIRONMENT

GUI DEMONSTRATION

A.1. Module Function

Executable Process Map (Fig. A-1)

Each functional module is embedded to the process map, which the user can flow to carry out the simultaneous data reconciliation and model calibration (SDRMC)

- Monte Carlo Simulation

Perform Monte Carlo simulation based on user defined parameter distributions to explore the degradation space of the thermo system, from which one can create the response surface equation and perform multivariate data analysis.

- Response Surface Equation

Perform the multidimensional regression by the Levenberg Marquardt algorithm to create response surface equations.

- Multivariate Visualization (Fig. A-2)

Provide the pair-wise scatter plot matrix to identify the outliers. This function is utilized for gross error prescreening

- PCA (Fig. A-3)

Perform principal component analysis (PCA) to obtain and visualize the test statistics for gross errors.

- Mode Slection

Two radio buttons allowing the user to switch between the high fidelity model and the metamodel of response surface equation (RSE)

- Robust M-estimator

A drop-down list with different types of robust *M*-estimators including the least squares objective function. Usually, the first execution is carried out on the least squares. Then, either one of the robust *M*-estimators or the hypothesis testing technique is selected by the user to carry out the gross error detection.

- Hypothesis testing [Stepwise]

Perform the serial bias compensation for gross error detection. This function must be run with the selection of least squares objective function from the drop-down list.

- Hypothesis testing [All Bias Model]

Perform the hypothesis testing for all possible gross error models based on the number of gross errors presumed by the user. This function must also be run with the selection of least squares objective function from the drop-down list.

A.2. Plotting Area

Three major plots are provided in this integrated environment:

- Status Watch

A radar plot showing the current model degradation status

- Bias Watch

A bar chart showing the gross errors of measurement data

- Calibration Uncertainty (Fig. A-4)

Several plots showing uncertainties of the estimated model parameters

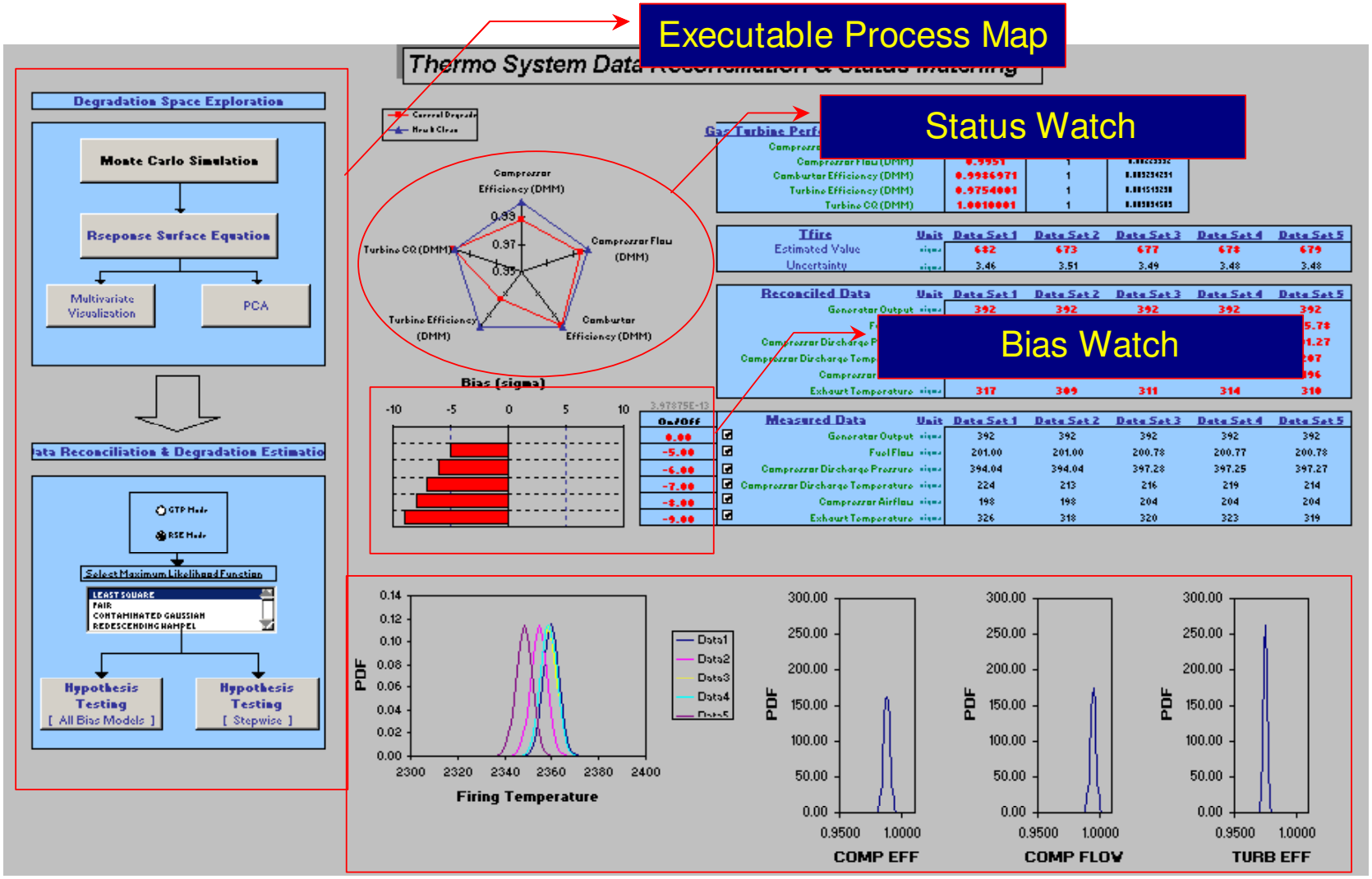

Figure A-1: Screenshot of the Thermo System Data Reconciliation and Model Calibration Environment

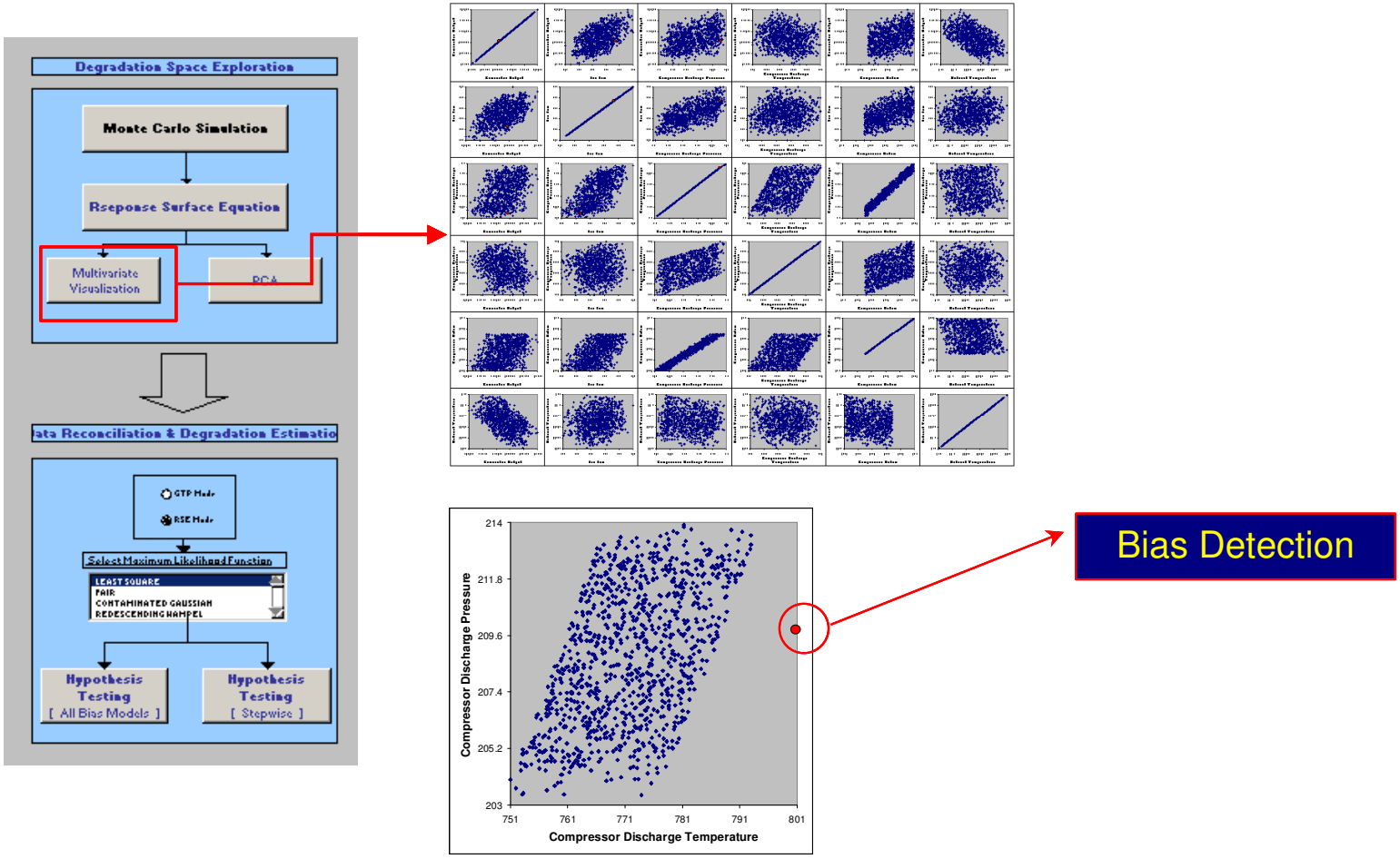

Figure A-2: Multivariate data analysis – pair-wise scatter plot

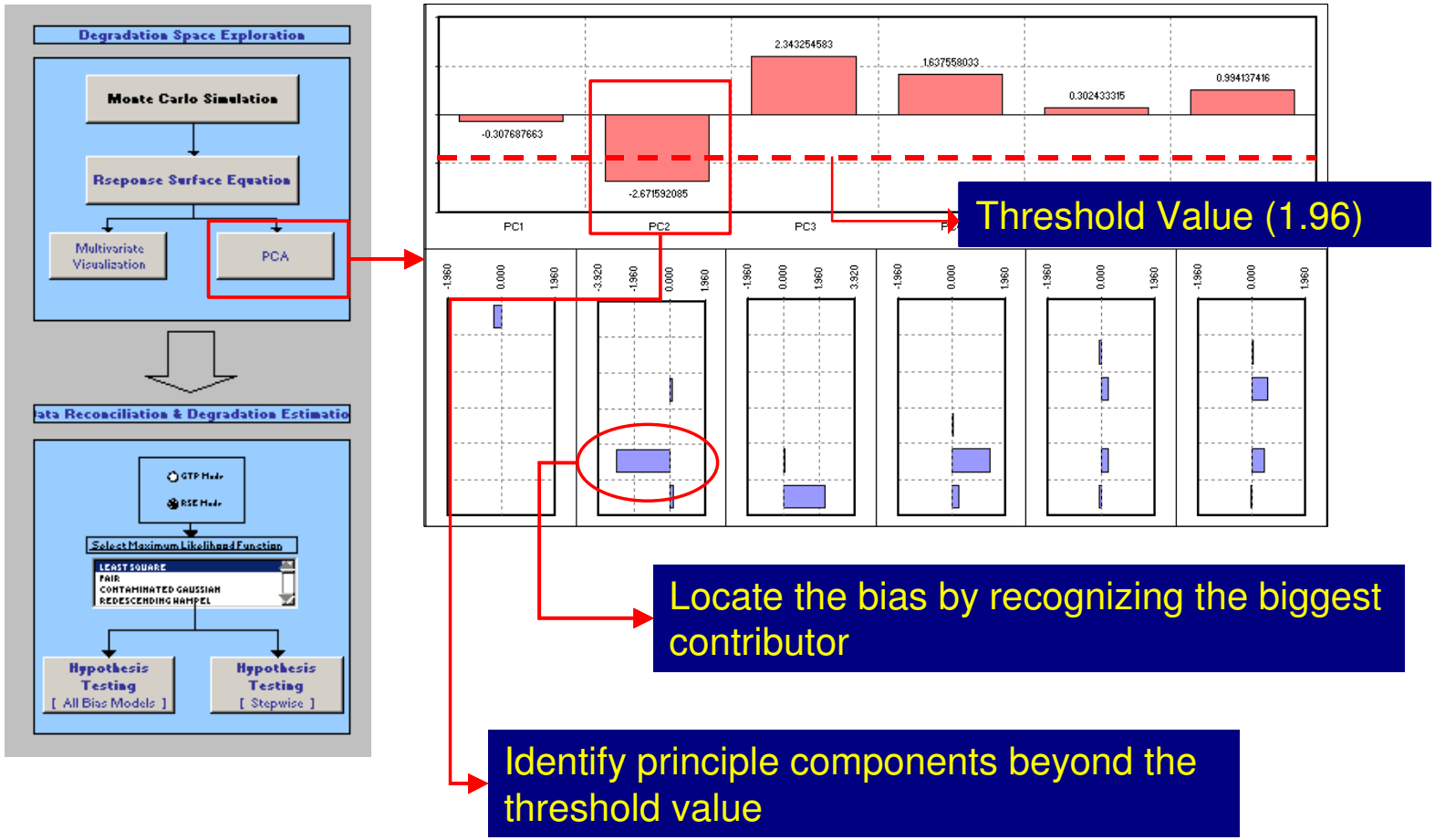

Figure A-3: Principal component analysis (PCA)

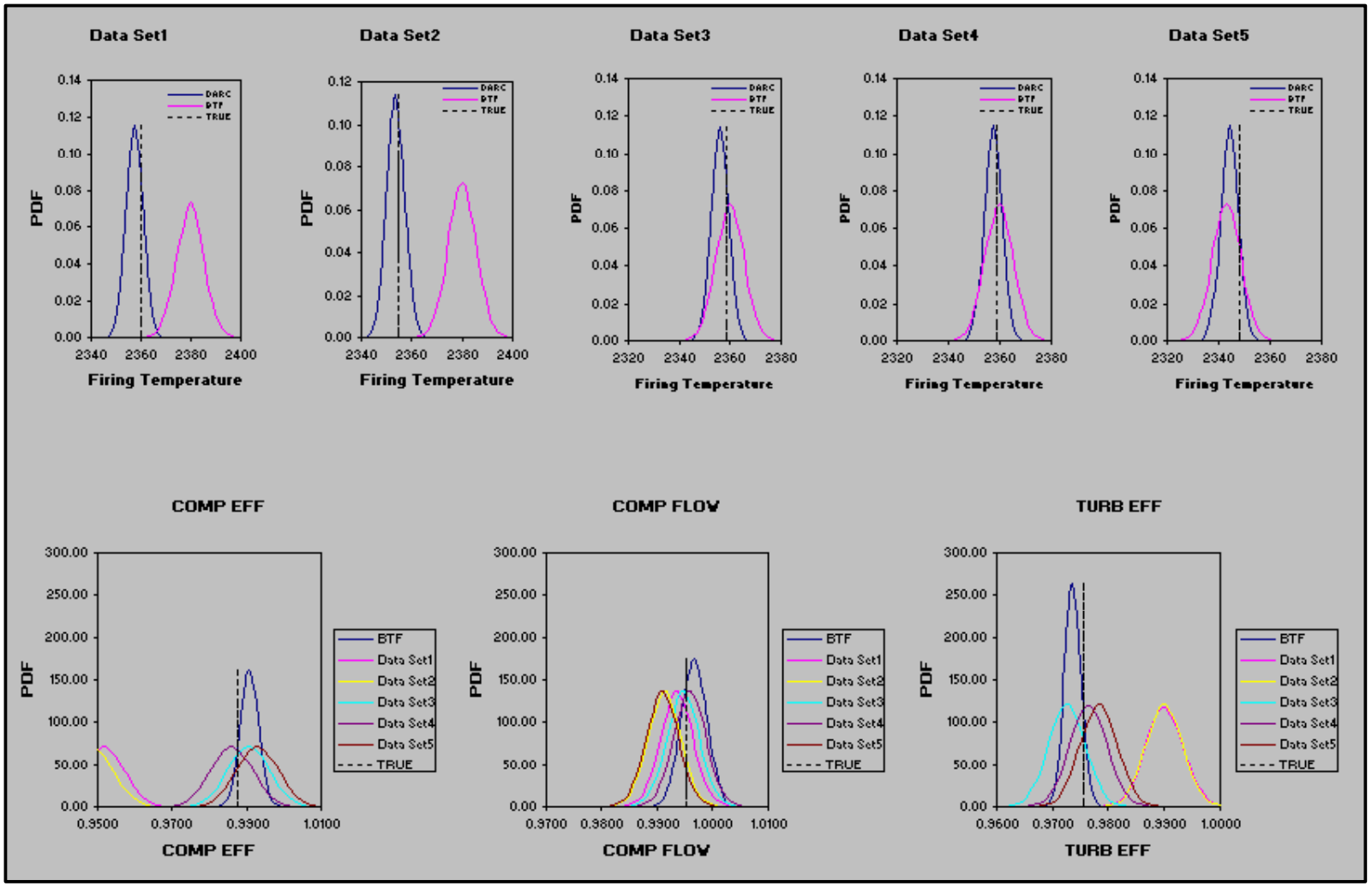

Figure A-4: Estimate uncertainties for model parameters

REFERENCES

[1]. ASME PTC 46-1996, Performance Test Code on Overall Plant Performance, The American Society of Mechanical Engineers

[2]. Gay, R. R., C. A. Palmer, and M. R. Erbes, *Power Plant Performance Monitoring*, R-Squared Publishing, CA, USA, 2004

[3]. ASME PTC 19.1-1998, Measurement Uncertainty, The American Society of Mechanical Engineers

[4]. GE Enter Software, LLC, GateCycle manual, Version 5.61, 2005

[5]. Narasimhan, S., & Jordache, C., *Data reconciliation and gross error detection: An intelligent use of process data*, Houston, TX: Gulf Publishing Company, 2000.

[6]. Snachez, M., and J. Romahnoli. "Use of Orthogonal Transformations in Data Classification-Reconciliation." *Computers Chem. Engng.* 20 (1996): 483-493

[7]. Horlock, J. H, *Combined Power Plants*, Pergamon Press, Oxford, UK, 1992.

[8]. Crane, R. I., *Combined Cycle for Power Plants: Thermodynamics of Combined Cycle Plants*, Von Karman Institute, Lecture Series 1993-08, 1993.

[9]. Kehlhofer, R., *Combined Cycle Gas and Steam Turbine Power Plants*, 2nd Ed., PennWell, Tulsa, OK, Aug, 1999.

[10]. Horlock, J. H., "Combined Power Plants-Past, Present, and Future," ASME J. Eng. Gas Turbines Power, **117**, pp. 608-616, 1995.

[11]. Frutschi, H. U., "Highest Efficiencies for Electrical Power Generation With Combined Cycle Plants," ABB Rev., **3**, pp. 12-18, 1999.

[12]. Fantozi, F., and Desideri, U., "Simulation of Power Plant Transients With Artificial Neural Networks: Application to an Existing Combined Cycle," Proc. Inst. Mech. Eng. A, J. Power, **212**, pp. 299-313, 1998.

[13]. Haub, G. L., Hauhe, W. E., Jr., Myers, C. O., "Real Time Performance Analysis and Condition Monitoring of a Gas Turbine Based 300 MW Base Load Cogeneration Plant," ASME paper 89-GT-28, 1989.

[14]. Rickli, J. P., *Combined Cycles for Power Plants: Controls, Monitoring and Performance Measurements*, Von Karman Institute, Lecture Series 1993-08, 1993.

[15]. Lozano, M. A.; Bartolome, J.L.; Valero A.; Reini, M., "Thermoeconomic Diagnosis of Energy System," Flowers 94, Florence World Energy Research Symposium. July 6-8, Florence, Italy, 1994.

[16]. Torres, C., Varlo, A., Serra, L., "Structural Theory and Thermoeconomic Diagnosis. Part I: Om Malfunctions and Dysfunction Analysis," ECOS'99, 1999.

[17]. Valero, A., Correas, L., Serra, L., "On-Line Thermoeconomic Diagnosis Of Thermal Power Plants. NATO ASI on Thermodynamics and Optimization of Complex Energy Systems," July 1998, Constantza, Rumania, 1998.

[18]. Valero, A., Lozano, M. A., Munoz M., " A General Theory of Exergy Saving: Part I, On Exergy Cost, Part II, On the Thermoeconomic Cost, Part III, Exergy Saving and Thermoeconomics in Computer-Aided Engineering of Energy Systems," Vol. 3 – Second Law Analysis and Modeling, pp. 1-22, R. A. Gaggioli ed., ASME, New York, 1986.

[19]. Varlo, A., Serra, L., Lozano, M. A., "Structural Theory of Thermoeconomics," ASME Winter Annual Meeting Symposium on thermodynamics and the design, analysis and improvement of energy systems. November 28-December 3, Session II General Thermodynamics & Energy Systems, 1993.

[20]. Correas, L.; Martinez, A.; Valero, A, "Operation Diagnosis of a Combined Cycle Based on the Structural Theory of Thermoeconomics,"

[21]. Stoppato, A., and Lazzaretto, A., "The Exergy Analysis for Energy System Diagnosis," *ASME Engineering Systems Design and Analysis Conference*, Vol. 1, July 1-4, Montpelier, France, ASME, New York, pp. 191-198, 1996.

[22]. Arena, A. P., and Borchielini, R., "Application of Different Productive Structures for Thermoeconomic Diagnosis of a Combined Cycle Power Plant," Int. J. Thermal Sci., 38, pp. 601-602, 1999.

[23]. Lerch, F., Roys, J., Serra, L., "Structural Theory and Thermoeconomic Diagnosis. Part II: Application on an Actual Power Plant, ECOS'99, June 8-10, Tokyo, pp. 374-379, 1999.

[24]. Lazzaretto, A., Macor, A., Mirandola, A., and Stoppato, A., *Proceedings of the ASME Advanced Energy Systems Division,* AES-Vol 39, ASME, New York, pp. 611-619, 1999.

[25]. Zaleta, A., Munoz, A. G., Hernandez, V. R., and Valero, A., "A Reconciliation Method Based on a Module Simulator: An Approach to the Diagnosis of Energy System Malfunctions," Int. J. Thermodynamics, Vol. 7, (No.2), pp. 51-60, June, 2004.

[26]. Saunders, E. A. D., *Heat Exchangers: Selection, Design and Construction*, Longman Group, London, UK, 1988.

[27]. Von Nostrand, W. L., et al., *Fouling of Heat Transfer Equipment*, Hemisphere, Washington, DC, 1981.

[28]. Tabakoff, W., "Compressor Erosion and Performance Deterioration," AIAA/ASME 4th Joint Fluid Mechanics, Plasma Dynamics, and Laser Conference, Atlanta, GA, May 12-14, 1986.

[29]. Escher, P. C., "Pythia: An Object-Oriented Gas Path Analysis Computer Program for General Applications," Ph. D. thesis, Granfield University, School of Mechanical Engineering, UK, 1995.

[30]. Daikunchak, I. S., "Performance Deterioration in Industrial Gas Turbines," ASME J. Eng. Gas Turbines Power, 114(2), 1992.

[31]. Tabakoff, W., Lakshminarasimha, A. N., and pasin, M., "Simulation of Compressor Performance Deterioration Due to Erosion," ASME J. Eng. Gas Turbines Power, 112(1), 1990.

[32]. Lakshminarasimha, A. N., Boyce, M. P., and Meher-Homji, C. B., "Modeling and Analysis of Gas Turbine Performance Deterioration," ASME J. Eng. Gas Turbines Power, 116(1), 1994.

[33]. Bevington, P. R., and Robinson, D. K., *Data Reduction and Error Analysis- for the Physical Sciences*, McGraw-Hill Higher Education, New York, NY, 2003.

[34]. Romagnoli, J. A., Sanchez, M. C., 2000, Data Processing and Reconciliation for Chemical Process Operations: Volume Two (Process System Engineering, 1st Ed., Academic Press, New York.

[35]. Crowe C. M., Y. A. G. Campos and A. Hrymak, Reconciliation of process flow rates by matrix projection. Part I: linear case. *AIChE Jl* 29, 881 (1983).

[36]. Pai C. C. D. and G. D. Fisher, Application of Broyden's method to reconciliation of nonlinearly constrained data. AIChE Jl 34, 873 (1988).

[37]. Swartz C. L. E., Data reconciliation for generalized flow-sheet applications. Paper presented at American Chem Soc. National Mtg, Dallas, TX (1989).

[38]. Tjoa I. B. and L. T. Biegler, Simultaneous solution and optimization strategies for parameter estimation of differential-algebraic equation systems. Ind. Engng Chem. Res. 30, 376 (1991)

[39]. Tjoa I. B. and L. T. Biegler, Simultaneous strategies for data reconciliation and gross error detection of nonlinear systems. Computers Chem. Engng, Vol. 15, No. 10, pp. 679-690 (1991)

[40]. Ozyurt, D. B. and R. W. Pike, Theory and practice of simultaneous data reconciliation and gross error detection for chemical process. Computers & Chemical Engineering, 28, 381-402 (2003)

[41]. Tamhane A. C. and R. H. S. Mah, Data reconciliation and gross error detection in chemical process networks. Technometrics 27, 409 (1985).

[42]. Rosenberg J., R. S. H. Mah and C. Jordache, Evaluation of schemes for detecting and identifying gross errors in process data. Ind. Engng. Chem. Res. 26, 555 (1987).

[43]. Narasimhan S. and R. H. S. Mah, Treatment of general steady state process models in gross error identification. Computers chem.. Engng 13, 851 (1989)

[44]. Duever, T. A., S. E. Keeler and P. M. Reilly, "An Application of the Eror-in-Variables Model-Parameter Estimation from Van Ness-Type Vapor-Liquid Equilibrium Experiments," *Chem. Eng. Sci.*, 42, 403-412 (1987).

[45]. Esposito, W. R. and C. A. Floudas, "Global Optimization in Parameter Estimation of Nonlinear Algebraic Models via the Error-in-Variables Approach," *Ind. Eng. Chem. Res., 37,* 1841-1858 (1998).

[46]. Cheng, P. C., Andersen, H., The Implementation of the Data Validation Process in a Gas Turbine Performance Monitoring System, ASME Paper GT-2005-68429 (2005).

[47]. Harter, P., J. Petek, and P. Pechtl, Model-Based Data Reconciliation to Improve Accuracy and Reliability of Performance Evaluation of Thermal Power Plants, ASME Paper GT2005-68937 (2005).

[48]. Gotz, W., and S. Reisacher, Data Validation Improves Reliability and Accuracy of Performance Monitoring and Field Acceptance Tests, 3rd European Conference on Turbo Machinery (1998).

[49]. Gulen, S. C., and R. W. Smith, A Simple Mathematical Approach to Data Reconciliation in a Single-Shaft Combined-Cycle System, ASME Paper GT2006-90145, 2006.

[50]. http://lmhwww.epfl.ch/Services/ModelTesting/modeltesting.htm, (2006)

[51]. Crowe, C. M., "Data Reconciliation – Progress and Challenges", *J. Proc. Cont.* Vol. 6, No. 2/3, pp. 89-98, 1996.

[52]. Kuehn, D. R. and Davidson, H., *Chem. Eng. Prog.* 1961, 57 (6), 44.

[53]. Reilly, P. M. and Carpani, R. E., "Application of Statistical Theory of Adjustment to Material Balances", 13th Can. Chem. Eng. Conf., Montreal, Que., 1963

[54]. Grauf E., Jansky, J., Langenstein, M., "Reconciliation of Process Data in Nuclear Power Plant (NPPs)", 8th International Conference on Nuclear Engineering (ICONE) April 2-8, 2000 Baltimore, MD USA.

[55]. H. Eitschberger, M. Neuhauser, "10 Years Experience with Process Data Reconciliation at KKL, EPRI Nuclear Power Performance Improvement Seminar", July 15-16, 2002, Saratoga Springs

[56]. G. R. Stephenson and C. F. Shewchuk, "Reconciliation of Process Data with Process Simulation", *AIChE Journal, Vol. 32, No. 2,* (1986).

[57]. Kim, I. W., Liebman, M. J., and T. F. Edgar, "Robust Error-in-Variables Estimation Using Nonlinear Programming Techniques", *AIChE Journal, Vol. 36, No. 7,* (1990).

[58]. MacDonald, R. J., and C. S. Howat, "Data Reconciliation and Parameter Estimation in Plant Performance Analysis", *AIChE Journal, Vol. 34, No. 1,* (1988).

[59]. Schwetlick, H., and V. Tiller, "Numerical Method for Estimating Parameters in Nonlinear Models with Error in the Variables", *Technometrics*, 27(1), 17 (1985).

[60]. Fisher, R.A., "On the Mathematical Foundations of Theoretical Statistics", *Phil. Trans. Royal Soc. London*, A222, 309 (1922)

[61]. Britt, H. I., and R. H. Luecke, "The Estimation of Parameters in Nonlinear, Implicit Models," *Technometrics*, **5**, No. 2, 233 (1973).

[62]. M. Lampton. “Damping-Undamping Strategies for the Levenberg-Marquardt Nonlinear Least-Squares Method,” *Computers in Physics Journal*, 11(1): 110-115, Jan./Feb. 1997

[63]. C.T. Kelly. “Iterative Methods for Optimization,” SIAM Press, Philadelphia, 1999.

[64]. S. Bellavia, M. Macconi and B. Morini, “An affine scaling trust-region approach to bound-constrained nonlinear systems,” Technical Report, Dipartimento di Energetica, University of Floerence, Italy, 2001

[65]. H. Dan, N. Yamashita and M. Fukushima, “Convergence properties of the inexact Levenberg-Marquardt method under local error bound conditions,” Technical Report 2001-001, Department of Applied Mathematics and Physics, Kyoto University (January 2001).

[66]. J. Nocedal and S.J. Wright. “Numerical Optimization,” Springer, New York, 1999.

[67]. T.F. Anderson, D.S. Abrams, and E.A. Grens II, “Evaluation of Parameter for Nonlinear Thermodynamic Models”, *AIChE Journal* (Vol. 24, No 1), January, 1978

[68]. Kirby, M., “A Methodology for Technology Identification, Evaluation, and Selection in Conceptual and Preliminary Aircraft Design,” PhD dissertation, Georgia Institute of Technology, March, 2001

[69]. Mavris, D.N., Kirby, M.R., “Technology Identification, Evaluation, and Selection for Commercial Transport Aircraft,” SAWE Paper No. 2456

[70]. Roth, B.A., Mavris, D.N., “Evaluation and Selection of Technology Concepts for a Hypersonic High Speed Standoff Missile,” Presented at the AIAA 2000 Missile Sciences Conference, Monterey, CA, November 7-9, 2000

[71]. Khaled Labib and V. Rao Vemuri, “Application of Exploratory Multivariate Analysis for Network Security,” Department of Applied Science, University of California, One Shields Avenue, Davis, California 95616, U.S.A.

[72]. Hotelling H., “Analysis of a Complex of Statistical Variables into Principal Components”. *Journal of Educational Psychology*, 24:417–441, 1933

[73]. Duda R., Hart P., Stork D., "Pattern Classification," Second Edition, John Wiley & Sons, Inc., 2001

[74]. Haykin S., Neural Networks: "A Comprehensive Foundation," Second Edition. Prentice Hall Inc., 1999

[75]. Huber, P.J. 1981, "Robust Statistics" (New York: Wiley).

[76]. Launer, R.L., and Wilkinson, G.N. (eds.) 1979, "Robustness in Statistics", (New York: Academic Press).

[77]. Fair, R. C. (1974). On the robust estimation of economic models. Annals of Economic and Social Measurement, 3, 667-677

[78]. Johnston, L. P. M., & Kramer, M. A. (1995). Maximum likelihood data rectification: Steady-state systems. AIChE Journal, 41(11), 2415-2426

[79]. Andrews, D. F., Bickel, P. J., Hampel, F. R., Huber, P. J., Rogers, W. H., & Tukey, J. W. (1972). Robust estimates of location: Survey and advances. Princeton, NJ: Princeton University Press.

[80]. Nikhil Arora, Lorenz T. Biegler, "Redescending estimators for data reconciliation and parameter estimation," *Computers & Chemical Engineering* 25 (2001) 1585-1599

[81]. Farris, R. H., & Law, V. J. (1979), "An efficient computational technique for generalized application of maximum likelihood to improve correlation of experimental data," *Computers and Chemical Engineering*, 3, 95–104.

[82]. Derrick K. Rollins, Yisun Cheng, and Sriam Devanathan, "Intelligent Selection of Hypothesis Tests To Enhance Gross Error Identification", *Computers chem. Engng* Vol. 20, No 5, pp. 517-530, 1996

[83]. Narasimhan S. and R. S. H. Mah, "Generalized likelihood ratio methods for gross error identification," *AIChE J.* 33, 1514 (1987)

[84]. Narasimhan S. and R. S. H. Mah, "Generalized likelihood ratio methods for gross error identification in dynamic processes," *AIChE J.* 34, 1321 (1988)

[85]. Terry, P. A. and Himmelblau, D. M., "Data Rectification and Gross error Detection in a Steady-State Process via Artificial Neural Networks," *Ind. Eng. Chem. Res.* 1993, 32, 3020

[86]. Kim, I.; et al. "Robust Data Reconciliation and Gross Error Detection: The Modified IMT using NLP," *Comput. Chem. Eng.* 1997, 21, 775

[87]. T. Renganathan and Shankar Narasimhan, "A Strategy for Detection of Gross Errors in Nonlinear Processes", *Ind. Eng. Chem. Res.* 1999, 38, 2391-2399

[88]. Roth, B A., Doel, D. L., Mavris, D, "Estimation of Turbofan Engine Performance Model Accuracy and Confidence Bounds", ISABE 2003-1208, Presented at the 2003 ISABE Conference, Sept. 1-4, Cleveland, OH.

[89]. Roth, B A., Doel, D. L., and Cissell, J. J., "Probabilistic Matching of Turbofan Engine Performance Models to Test Data", GT2005-68201, Proceedings of ASME Turbo Expo 2005

[90]. Roth, B., Doel, D., Mavris, D., Beeson, D., "High Accuracy Matching of Engine Performance Models to Test Data," ASME Turbo Expo, Atlanta, June 16-19 2003, GT-2002-38784

[91]. Box, G.E.P., and G.C. Tiao, "Bayesian Inference in Statistical Analysis", Reading, Mass.: Addison-Wesley, 1973.

[92]. Tamhane, A. C., C. Iordache, and R.S.H. Mah, "A Bayesian Approach to Gross Error Detection in Chemical Process Data. Part I: Model Development", *Chemometrics and Intel. Lab. Sys.* 4 (1988): 33-45.

[93]. Tamhane, A. C., C. Iordache, and R.S.H. Mah, "A Bayesian Approach to Gross Error Detection in Chemical Process Data. Part II: Simulation Results", *Chemometrics and Intel. Lab. Sys.* 4 (1988): 131-146.

[94]. Iordache, C. A, "Bayesian Approach to Gross Error Detection in Process Data", Ph.D. Dissertation, Northwestern University, Evanston, Ill., 1987.

VITA

TSUNG-PO LIN

Tsung-Po Lin was born on May 21, 1974 in Taipei, Taiwan. He attended junior high school in Miaoli, living with his parents and younger brother. Tsung-Po graduated from Senior High School of National Taiwan Normal University (HSNU) in 1992 in Taipei, where his grandmother nurtured him. He then attended National Chiao Tung University, graduating in 1998 with a MS of Mechanical Engineering. Tsung-Po completed his two-year mandatory military service as an artillery lieutenant. He is very proud of serving for his country. Tsung-Po then attended the Georgia Institute of Technology, obtaining a MS in Aerospace Engineering in 2003 continuing to obtain his Ph.D. in 2008. When he is not working on his research, Tsung-Po enjoys watching movie with his best friend, Ana.